INVESTIGATION OF THE TOXICITY OF SILVER AND GOLD NANOPARTICLES

WANG CHUNYAN

(B.Sc., Soochow University)

A THESIS SUBMITTED

FOR THE DEGREE OF DOCTOR OF PHILOSOPHY

DEPARTMENT OF CHEMISTRY

NATIONAL UNIVERSITY OF SINGAPORE

2013

DECLARATION

I hereby declare that this thesis is my original work and it has been written by me in its entirety, under the supervision of Assoc Prof. Suresh Valiyaveettil, Chemistry Department, National University of Singapore, between 2009 and 2013.

I have duly acknowledged all the sources of information which have been used in the thesis. This thesis has also not been submitted for any degree in any university previously.

The content of the thesis has been partly published in:

1) **Chunyan Wang** and Suresh Valiyaveettil, "Environmental and health concerns of nanomaterials", In: Applications of Nanomaterials for Water Quality, Future Science Ltd, 2013 Pages 100-123 eBook ISBN: 978-1-909453-07-4
2) **Wang Chunyan** and Suresh Valiyaveettil, "Correlation of biocapping agents and cytotoxic effects of silver nanoparticles on human tumor cells", RSC Advances, 2013, 3, 14329-14338

Wang Chunyan	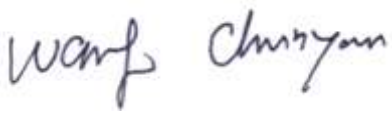	25 July 2014
Name	Signature	Date

ACKNOWLEDGEMENTS

I would like to express my sincere gratitude to the following people, for if not them, the thesis would not have been possible. First of all, I would like to express my deepest gratitude to my supervisors, Assoc Prof. Suresh Valiyaveettil, who has been instrumental in guiding this research and providing useful advice throughout the long period of this research work. His assistance and supervision are great treasures to me and this thesis work.

I would like to extend my sincere thanks to Dr Mark Richard, for his enormous trust, support during the work. His critical comments and suggestions helped a lot in the progress of this thesis. Special thanks to Dr. Saji George for his discussions and constructive comments. I greatly appreciate the help from Gwendoline Goh and the training she provided.

I am thankful to my lab mates and colleagues Teow Yiwei, Ramakrishna, Ashok, Jitendra, Kalidhasan, Brahatheeswaran, Lekha, Vanga Devendar Goud, Mithun, Daisy, Evelyn, Roshan, Ping Sen, Sriramulu Deepa, Syed Abdulrahim Syed Nizar.

Finally, a special thanks to my parents for their unconditional love and support in every way possible throughout the process of my PhD course.

TABLE OF CONTENTS

SUMMARY

Many nanomaterials have been synthesized and explored for potential use in consumer and medical products. Majority of the commercial products incorporated with nanomaterials exist in the areas of skin care and cosmetics, but interests of using nanomaterials in various applications related to electronics, food additives and biomedical products are increasing. The prevalent of nanomaterials applications has attracted researchers' attention on their health and environmental safety concerns. Previous studies in nanotoxicology demonstrated adverse health effects of many nanomaterials. The toxicity of new nanomaterials could not be deduced from earlier knowledge and results, as small differences in composition and properties of nanomaterials could induce large changes in toxicity. Thus detailed studies of toxicity of all nanomaterials need to be carefully investigated and documented.

In this thesis, we are focusing on the toxicity studies of two nanomaterials: silver (Ag) and gold (Au) nanoparticles. Particularly, Ag nanoparticles are incorporated in many commercial products such as sunscreens, cosmetics, wound dressings, surgical tools, detergents and automotive paints because of their antibacterial effects. Au nanoparticles have attracted significant scientific and technological interest owing to their ease of synthesis, chemical

stability and unique optical properties.

In Chapter 1, a brief introduction is given to discuss the development of nanotechnology and its potential impact on health and environmental safety. In Chapter 2, the materials and methods used were discussed in detail. Nanomaterials used in this thesis were characterized with multiple different techniques.

In Chapter 3, the cytotoxicity of Ag nanoparticles with plant extracts as capping agents was examined using human tumor cells. The results demonstrated that Ag nanoparticles with different capping agents induced different toxicities. In Chapter 4, shape-dependent toxicity of Ag nanoparticles in human skin fibroblast cells is discussed in detail. Ag nanocube, Ag truncated nanocube and Ag nanowire were used for the investigation. Among the three Ag nanomaterials, Ag nanocubes were the most toxic as compared to other particles, which could be attributed to their relatively sharp angles and high instability. The confocal microscope images showed that Ag nanomaterials penetrated inside the cytoplasm but not entered the nucleus of cells. In Chapter 5, shape-dependent toxicity of Au nanoplates (Au hexagon, Au pentagon and Au triangle) is discussed with details. Among three Au nanoplates investigated, Au triangle nanoplates were the most toxic. The relatively sharp angles and high surface potential energy

of Au triangle nanoplates enabled them to penetrate cell membrane more easily. Transmission electron microscope images of the thin section of cells indicated that Au nanomaterials were distributed in both cytoplasm and nucleus of cells.

In Chapter 6, the cytotoxicity and genotoxicity of Ag and Au nanoparticles were explored using human colon cancer stem cells and embryonic stem cells. The results showed that Ag and Au nanoparticles did not cause cytotoxicity to colon cancer stem cells at low concentrations. Similarly, Ag nanoparticles did not cause adverse effect to both undifferentiated cells and differentiated cells at low concentrations. In conclusion, the toxicity of nanomaterials is influenced by composition, surface functional group, size, shape and the colloidal stability of the nanomaterials.

LIST OF TABLES

LIST OF FIGURES

ABBREVIATIONS

a.r.	aspect ratio
A-431	human epithelial cells
A549	human carcinoma lung cells
AAS	atomic absorption spectroscopy
AFM	atomic force microscopy
Ag	silver
Ag NMs	silver nanomaterials
Ag nps	silver nanoparticles
Ag_2O	silver oxide
Ag-coffee	coffee capped silver nanoparticles
Ag-ginger	ginger capped silver nanoparticles
Ag-mint	mint capped silver nanoparticles
$AgNO_3$	silver nitrate
Ag-PVP	PVP capped silver nanoparticles
AK	adenylate kinase
ATP	adenosine-5'-triphosphate
Au	gold
Au NMs	gold nanomaterials
Au nps	gold nanoparticles
AuNPs	gold nanoplates
Au-PVP	PVP capped gold nanoparticles

BET	Brunauer, Emmett and Teller
BHK21	baby hamster kidney cells
BPEI	branched polyethyl-eneimine
$CaCl_2$ $2H_2O$	calcium chloride dihydrate
CBMN	cytokinesis-blocked micronucleus assay
cDNA	complementary DNA
CO2	carbon dioxide
CSCs	cancer stem cells
CTAB	cetyltrimethylammoniumbromide
cube 1	nanocubes
cube 2	truncated nanocubes
DAPI	4', 6-diamidino-2-phenylindole
DCF	2′-, 7′- dichlorodihydrofluorescein
DCF-DA	2', 7' - dichlorohydrofluorescein diacetate
DCFH	2’, 7’-diclorfluorescein
DEPC	diethylpyrocarbonate
DLS	dynamic light scattering
DMEM	Dulbecco’s modified eagles medium
DMEM / F-12	Dulbecco's modified eagle medium: nutrient mixture
DNA	deoxyribonucleic acid
DPBS	dulbecco’s phosphate buffered saline
EB	embryonic stem cells

EC_{50}	half maximal effective concentration
EDS/EDX	energy dispersive X-ray spectroscopy
EG	ethylene glycol
EGFR	epidermal growth factor receptor
EHS	Environmental, Health, and Safety
ESCs	embryonic stem cells
FBS	fetal bovine serum
fcc	face centered cubic
FITC	Fluorescein isothiocyanate
FTIR	Fourier transform infrared spectroscopy
G1	gap1
G2/M	gap2/mitosis
GAPDH	glyceraldehyde-3-phosphate dehydro-genase
GI	gastro-intestinal
h	hour(s)
H_2O	water
H_2O_2	hydrogen peroxide
HaCaT	human keratinocyte cells
HAP	hydroxyapatite
HAuNPs	gold hexagon nanoplates
HDF	human dermal fibroblast
HeLa	human cervical cancer cells

HepG2	hepatocellular liver carcinoma cells
HESCs	human embryonic stem cells
IC_{50}	half maximal inhibitory concentration
ICP	Inductively-coupled plasma
ICP-MS	inductively coupled plasma-mass spectrometry
ICP-OES	inductively coupled plasma optical emission spectroscopy
ICP-RIE	inductively coupled plasma reactive ion etching
IMR90	lung fibroblast cells
JNK	c-Jun NH2-terminal kinase
$KAuCl_4$	potassium gold (III) chloride
LD_{50}	lethal dose fifty
LDH	lactate dehydrogenase
MAPK	mitogen activate protein kinase
MCF7	breast cancer cells
MEF	mouse embryonic fibroblasts
MEM	minimum essential medium
MHDA	mercaptohexadecanoic acid
MSNs	mesoporous silica nanoparticles
MTS	3-(4,5-dimethylthiazol-2-yl)-5-(3-carboxymethoxyphenyl)-2-(4-sulfophenyl)-2H-tetrazolium
MTT	3-(4,5-dimethylthiazol-2-yl)-2,5-diphenyltetrazolium

	bromide
MWCNTs	multiwalled carbon nanotubes
NEAA	non-essential amino acids
NIR	near-infrared region
NLS	nuclear location sequence
NMR	nuclear magnetic resonance
NNI	National Nanotechnology Initiative
OA	oleic acid
PAuNPs	gold pentagon nanoplates
PBS	phosphate buffered saline
PCR	polymerase chain reaction
PEDT	Poly(3,4-ethylenedioxythiophene)
PEG	polyethylene glycol
PI	propidium iodide
PMAA	poly(methacrylic acid)
PS	phosphotidyl serine
PVP	polyvinylpyrrolidone
R&D	research and development
RGD	arginine-glycine-aspartic acid
ROS	reactive oxygen species
RPA	ribonuclease protection assay
RT-PCR	reverse transcriptase- polymerase chain reaction

S	DNA synthesis
SAXS	small-angle X-ray scattering
SCI	science citation index
SEM	scanning electron microscopy
SGC-7901	human stomach cancer cells
siRNA	small interfering RNA
SPR	surface plasmon resonance
TAuNPs	triangle nanoplates
TEM	transmission electron microscope
TGA	ultraviolet–visible
TiO_2	titanium dioxide
UV-Vis	ultraviolet–visible
XAS	X-ray absorption spectroscopy
XPS	X-ray photoemission spectroscopy
XRD	X-ray diffraction
XTT	2,3-bis-(2-methoxy-4-nitro-5-sulfophenyl)-2H-tetrazolium-5-carboxanilide
ZnO	zinc oxide
ZP	zeta potential

LIST OF PUBLICATIONS

1. **Chunyan Wang** and Suresh Valiyaveettil, "Environmental and health concerns of nanomaterials", In: Applications of Nanomaterials for Water Quality, Future Science Ltd, 2013, 100-123, eBook ISBN: 978-1-909453-07-4
2. **Wang Chunyan** and Suresh Valiyaveettil, "Correlation of biocapping agents and cytotoxic effects of silver nanoparticles on human tumor cells", RSC Advances, 2013, 3, 14329-14338
3. Saji George, Hannah Gardner, Eng Khuan Seng, Hengky Chang, **Chunyan Wang**, Crystal Hay Yu Fang, Mark Richards, Suresh Valiyaveettil and Woon Khiong Chan, "Differential effect of solar light in increasing the toxicity of silver and titanium dioxide nanoparticles to a fish cell line and zebrafish embryos", **Environmental Science & Technology**, 2014, 48, 6374-6382
4. **Chunyan Wang**, Jitendra Kumar, Thang Toan Pham and Suresh Valiyaveettil, "Shape Selective Toxicity of Silver Nanomaterials on Human Skin Fibroblast Cells", submitted
5. **Chunyan Wang,** Yoshikazu Ito, Bindu Pradeep and Suresh Valiyaveettil, "Shape sensitivity of gold nanoplates on human breast cancer cells", submitted
6. **Chunyan Wang,** Gwendoline Goh, Mark Richard and Suresh Valiyaveettil, "Investigation of nanotoxicity on stem cells

exposed to silver and gold nanoparticles", under preparation

7. **Chunyan Wang,** Gwendoline Goh, Mark Richard and Suresh Valiyaveettil, "Molecular mechanisms of toxicity of silver nanoparticles in human embryonic stem cells", under preparation

LIST OF CONFERENCE TALKS AND PRESENTATIONS

Oral presentation

1. **Chunyan Wang,** Mark Richard, Suresh Valiyaveettil, "Investigation of nanotoxicity on stem cells exposed to silver and gold nanoparticles", ***ICMAT***, Singapore, 2013
2. **Chunyan Wang,** Mark Richard and Suresh Valiyaveettil, "Genotoxicity of silver nanoparticles in human embryonic stem cells", ***MRS Spring***, San Francisco, 2013
3. **Chunyan Wang** and Suresh Valiyaveettil, "Study of cytotoxic effects of green synthesized silver nanoparticles with mint ginger and coffee extracts on tumor cells", The 7th Mathematics and Physical Sciences Graduate Congress, ***NUS***, Singapore, 2011
4. **Chunyan Wang** and Suresh Valiyaveettil, "Investigation of cytotoxic effects of water soluble silver nanoparticles on tumor cells", ***MRS Fall***, Boston USA, 2011

Poster presentation

1. Yong Fatt Pui, **Chunyan Wang** and Suresh Valiyaveettil, "The interaction of functional nanomaterials with living cells

and the recovery effect on these cells using plant extracts", ***SICC7***, NUS, Singapore, 2012

2. **Chunyan Wang** and Suresh Valiyaveettil, "Nanoparticle shape sensitive cytotoxicity in human skin cells", ***MRS Fall***, Boston USA, 2012.
3. **Chunyan Wang** and Suresh Valiyaveettil, "Investigation of cytotoxic effects of au nanoparticles with different morphologies on human tumor cells", ***ICYRAM***, Biopolis, Singapore, 2012
4. **Chunyan Wang** and Suresh Valiyaveettil, "Study of cytotoxic effects of green synthesized silver nanoparticles with different capping agents on tumor cells", ***5th MRS-S Conference on Advanced Materials***, NUS, Singapore, 2012

CHAPTER 1

INTRODUCTION

Publication from this chapter:

Chunyan Wang and Suresh Valiyaveettil, "Environmental and health concerns of nanomaterials", In: Applications of Nanomaterials for Water Quality, Future Science Ltd, 2013, 100-123, eBook ISBN: 978-1-909453-07-4

1.1 Overview of nanotechnology

Nano, originated from Greek words, means "one billionth" (10^{-9}). Nanoscale is normally defined as smaller than 100 nanometers in at least one dimension, although sometimes it may be used to describe even smaller materials. Nanotechnology is the term used to describe areas of science and engineering of design, characterization, production and application of materials, structures, devices and systems at nanoscale dimensions. Nanomaterials which have at least one dimension in the range 1 - 100 nm, exhibit interesting properties that differ from the bulk materials. Early example of use of nanostructured materials can be back dated to 4th century, the Lycurgus Cup (Rome), made of colloidal gold and silver, looks opaque green when lit from outside but translucent red when light shines from inside.[1] During the 9th and 17th century, glowing and glittering polychrome lustreware bowl which was used in the Islamic world and later in Europe, contained either silver or copper or other metallic nanoparticles.[2]

Concepts of nanotechnology became more popular after the talk given by physicist Richard Feynman at an American Physical Society meeting in 1959.[3] Feynman suggested that a process to manipulate individual atoms and molecules might be developed, using one set of precise tools to build and operate another proportionally smaller set, down to the needed scale. The term "nanotechnology" was first used in 1974 by Norio Taniguchi,[4] and defined as follows: "Nanotechnology mainly consists of the processing of, separation, consolidation, and deformation of materials by one atom or by one molecule." The book 'Engines of Creation: The Coming Era of Nanotechnology' written by Dr. K. Eric Drexler (1986),[5] is considered as the first book on the topic of nanotechnology. Nanotechnology and nanoscience started in the early 1980s with two major developments. One major development is the birth of cluster science and the invention of the scanning tunneling microscope (1981)[6] while the other is the synthesis and properties of semiconductor nanocrystals (1981,

1985).[7,8] Later, Don Eigler and Erhard Schweizer of the IBM's Almaden Research Center, manipulated 35 individual xenon atoms to spell out the IBM logo in 1989.[6] In 1990s, early nanotechnology companies began to operate, e.g. Nanophase Technologies in 1989, Helix Energy Solutions Group in 1990, Zyvex in 1997, and Nano-Tex in 1998. Consumer products making use of nanotechnology, such as nano-silver antibacterial socks, clear sunscreens and deep-penetrating therapeutic cosmetics, began appearing in the marketplace in 1999–early 2000's.

The world's first national nanotechnology program – the U.S.'s National Nanotechnology Initiative (NNI) – was launched by President Clinton in 2000. From 2001 through 2012, the U.S. government invested approximately $15.6 billion in nanoscience, engineering and technology through NNI and $1.8 billion in NNI funding has requested by President Obama for 2013.[9] In 2004, the European Commission adopted the Communication "Towards a European Strategy for Nanotechnology," COM (2004) 338, which proposed an integrated and responsible approach to institutionalize European nanoscience and nanotechnology research and development (R&D).

Inventions related to nanotechnology are reflected by the number of patent applications filed in the top 15 repositories, which increased from 1,200 in 2000 (of which 405 were filed at the US Patent and Trade Office, USPTO)[10,11] to about 13,000 in 2008 (of which 3,729 were filed at USPTO), with an annual growth rate of about 35%, as shown in **Figure 1.1**.[12,13] As products incorporating nanotechnology commercialized, investments in nanotechnology have already begun to yield economic benefits. The value of these products reached about $200 billion worldwide in 2008.[12] The estimation made by Roco and Bainbridge[14] for a product value of $1 trillion by 2015 still appears to hold (**Figure 1.2**).[12] Owing to successive introduction of new products, the market increase with an annual speed 25% and nearly double in every 3 years.

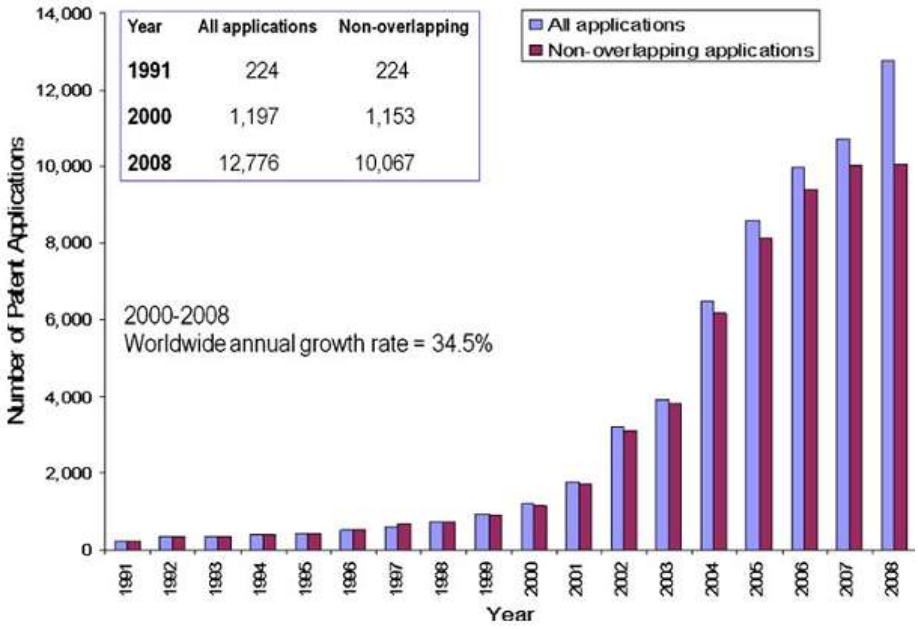

Figure 1.1: Longitudinal evolution of the total number of nanotechnology patent applications in the 15 repositories per year ("title abstract," 1991–2008). (Adapted from Ref[12, 13])

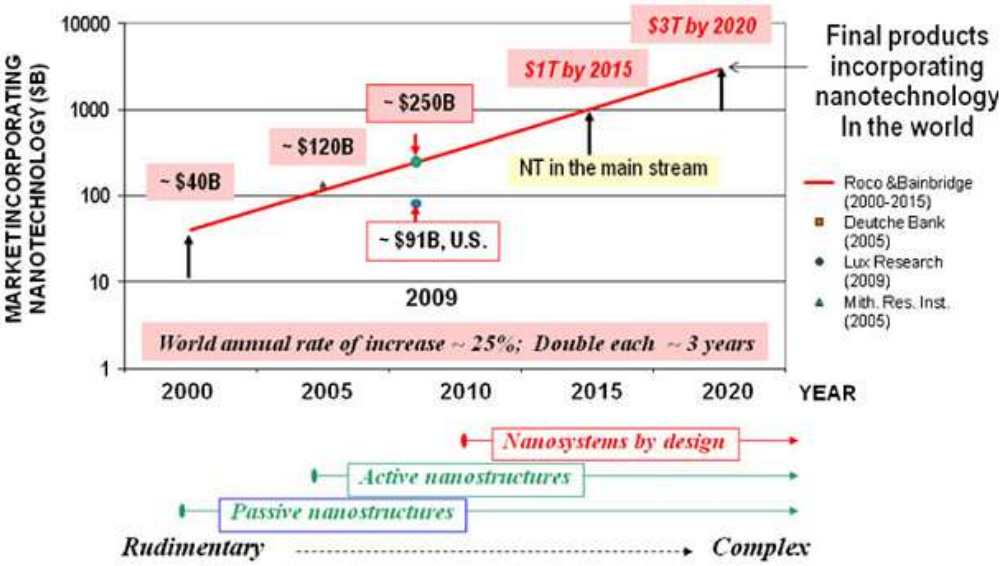

Figure 1.2: Market timeline: projection for the worldwide market of final products that incorporate nanotechnology. (Adapted from Ref [12])

1.2 Classification of nanoparticles

There are various approaches for classification of nanoparticles. Generally nanoparticles can be classified by their composition and morphology.[15]

As to compositions, nanoparticles can be composed of a single constituent

material or be a composite of several materials. The nanoparticles found in nature are often agglomerations with various compositions, while pure single-composition materials are normally synthesized in labs. In detail, nanoparticles can be further divided into metals (gold, silver, platinum), metal oxides (zinc oxide, titanium dioxide, iron oxide, aluminium oxide), carbon-based nanoparticles (fullerenes, carbon nanotubes) nanomaterials, organic (e.g. dendrimer, micelle) and hybrid structures such as quantum dots, core-shell structures.

Based on the shape of particles, nanoparticles could be classified into different groups, such as, nanosphere, nanocube, hexagon, pentagon, triangle, nanoflower, nanowire and octahedral structures. Different morphological variants of nanoparticles are represented in **Figure 1.3**.

1.3 Synthesis of nanomaterials

In general, nanomaterials may be separated into two classes based on the method of fabrication: bottom up or top down methods.[16,17] Top-down methods seek to create smaller devices by slicing or successive cutting of a bulk material, on the other hand, bottom up methods refer to building up of a material from the bottom: atom by atom or molecule by molecule (**Figure 1.4**). Attrition or milling is a typical top down method in making nanomaterials, whereas synthesis of colloidal dispersion via reducing of metal salts is a good example of bottom up approach for the synthesis of nanomaterials.

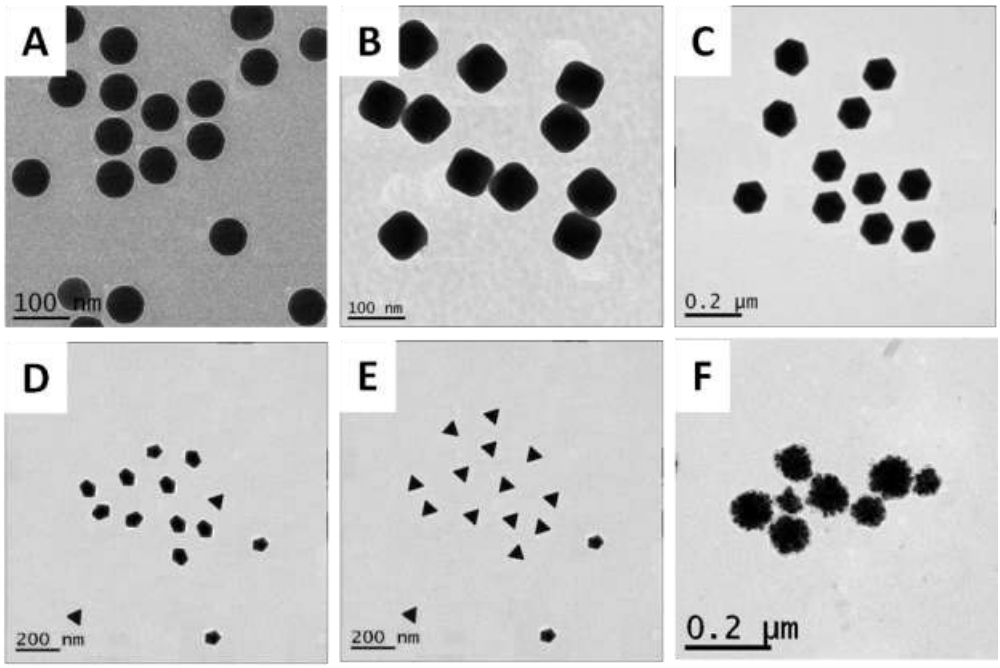

Figure 1.3: Morphological variant of inorganic Au nps: sperical (A), cube (B), hexagon (C), pentagon (D), triangle (E) and nanoflower (F).

In the top-down approaches, large starting material is reduced to small size by using mechanical or chemical methods. The most commonly used top down fabrication techniques include silicon micro-fabrication and photolithography.[18] Advantages of this method are the possibility of mass production in the industrial setting and place different materials next to each other.[19] The major disadvantages of the top-down approach include time consuming processes, high deployment costs, low impact to overall organization, generation of a broad feature size distribution and imperfections or defects of the surface morphology generated. The production of monodispersed spherical colloids from metals with relatively low melting points such as bismuth, lead, indium, tin and cadmium, can be realized by emulsifying molten drops of bismuth in boiling di(ethylene glycol), followed by quenching with cold ethanol.[16] ZnO nanowire devices could be fabricated by using optical lithography[20] and semiconductor nanowires such as InP and InGaAsP/InP nanowires could be fabricated by using inductively coupled plasma reactive ion etching from their respective wafers.[21] Surface

deformations were reported to have a significant impact on its physical properties and surface chemistry of the nanoparticles.[22] In pyrolysis, an organic precursor was burnt after forcing through an orifice at high pressure and the resulting ash was processed to recover the oxidized nanoparticles with a wide particle size distribution.[22] This process consumed enormous amounts of energy to sustain the high pressure and temperature. On the contrary, the bottom-up approaches normally operate under ambient conditions which leads to high energy savings.

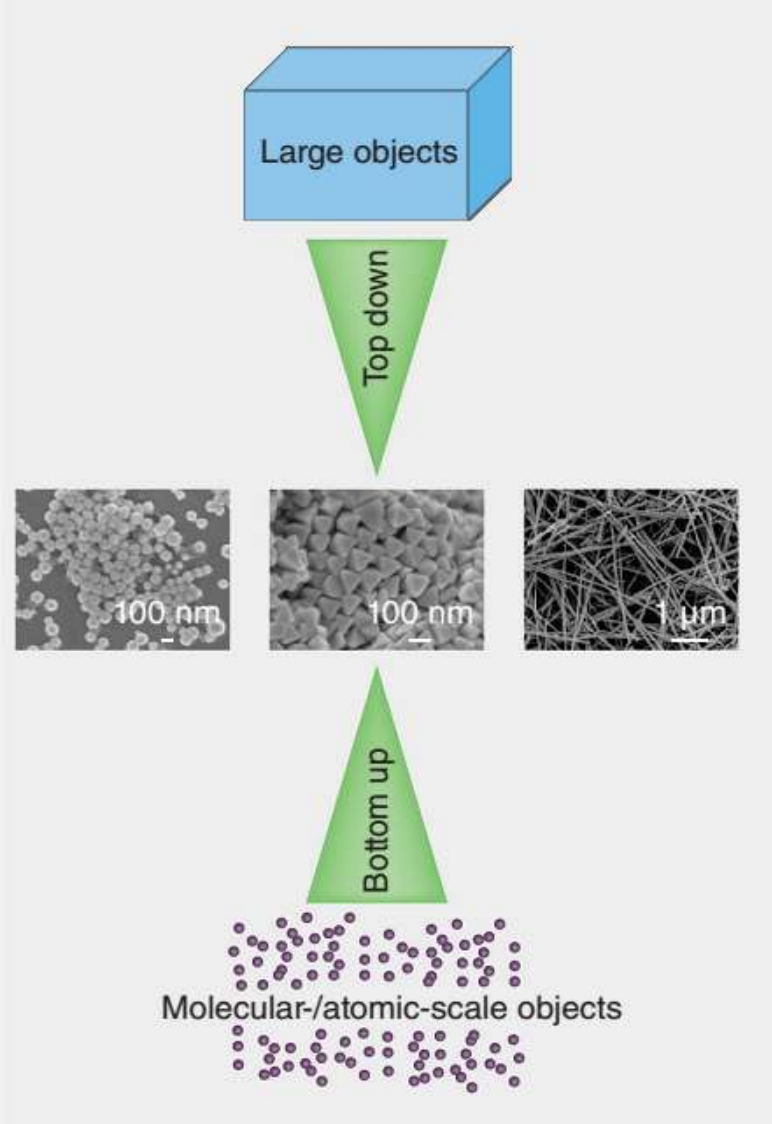

Figure 1.4: Nanomaterials of different sizes and morphologies (such as nanosphere, nanopyramid and nanowire) can be fabricated via either top-down mechanical methods or bottom-up approaches.

A variety of bottom-up approaches exist, comprising precipitation from solution, co-precipitation, complex coacervation of two oppositely-charged polyelectrolytes, salting-out from an aqueous–organic mixture, nanoprecipitation or solvent displacement, chemical vapor deposition, gas condensation, solvent emulsification–diffusion using an oil–water emulsion, high-temperature decomposition of organic precursors, laser ablation, radiolytic methods, vacuum evaporation of metal, the Svedberg method of electrocondensation and using supercritical fluids.[23-25] These techniques can be used to generate a variety of nanomaterials which include metal nanoparticles (magnetic or Ag nps), liposomes, nanoemulsions, polymeric micelles, polymeric nanoparticles, protein nanoparticles, solid lipid nanoparticles and carbohydrate (chitosan, alginate, hyaluronic acid, dextran) nanoparticles.[25-27] The most commonly employed method is wet chemical synthesis method, where metal ions were reduced to yield the corresponding metal particles by a suitable reducing agent in the presence of capping agent(s). The growth of the metal particle is controlled by the addition of capping agents, which works either by conferring a charge (carboxylic acids for negative charge and amines for positive charge) on the surface to help repel neighbouring nanoparticles, or by sterically preventing the agglomeration of two nanoparticles.[28] Apart from preventing nanoparticles from precipitation, capping agents also serve other important functions such as controlling particle size, shape, surface charge, solubility and surface functionality which can confer special properties.[29]

Recently, there has been a growing interest in biological synthesis of metallic nanoparticles using bacteria,[30] yeast,[31] fungi, plants and algae.[22] As compared to conventional chemical methods, these methods offer advantages such as avoiding the use of toxic organic solvents and reagents, generation of hazardous side-products, high cost and energy consumption as well as producing nanoparticles which are relatively non-toxic and biocompatible.

During the synthesis, biomaterials extracts can be used as both reducing agents and capping agents.[32] Extracts from biomaterials such as coffee,[33] tea,[33] garlic, jatropha seeds,[34] plant leaf,[35] rosa rugosa leaf,[36] lemongrass,[37] aloevera,[38] alfalfa,[39] neem,[40] tamarind[41] have been used for the synthesis of nanomaterials. Different nanoparticles from Ag, Au, CdS, magnetite and uranium were reported to be synthesized through biological processes.[42] A similar method for synthesis of Ag nps using fungal cell filtrate was also reported.[43]

1.4 Characterization of nanoparticles

Nanoparticles exhibit entirely different properties from their bulk materials, which offer them special advantages in many commercial products such as fillers, catalysts, semiconductors, cosmetics, microelectronics, and drug carriers.[44] Important factors such as size, morphology, composition, surface area, surface chemistry and aggregation of nanoparticles in solution affect their properties.[44] The need to characterize nanomaterials before incorporating them into applications is a high priority. Many techniques are often complementary and used together to fully characterize nanomaterials. For example, the transmission electron microscope (TEM) is used to image nanomaterials, which provides the information of nanomaterials morphology and size distribution. However, this technique is limited to materials with high electron density, organic capping agents or uncrystallized surface matter cannot be seen clearly. Dynamic light scattering (DLS), which could detect the hydrodynamic size of nanoparticles including the contribution from the ligands and the hydration shell in a solvent, can be used in conjunction with TEM to support the data obtained from each other. A systematic characterization for nanomaterials has been recommended by Sayeset al.:[45]

Primary characterization is performed on dry nanomaterials to get the basic characterization parameters of nanomaterials. These parameters include chemical composition, crystal structure, size and morphology, which can be measured with multiple techniques (**Table 1.1**).[46,47] For example, the size and

morphology of nanomaterials can be detected by TEM,[48] scanning electron microscopy (SEM)[49] and atomic force microscopy (AFM).[50] The chemical composition of nanomaterials can be analyzed by both elemental analysis (ICP-MS) and X-ray photoemission spectroscopy (XPS).[51] Moreover, XPS is a surface chemical analysis technique which can be used to analyze the surface chemistry of nanomaterials.[52] Crystal structure of nanomaterials is detected by X-ray diffraction (XRD)[53] and specific surface area evaluation of nanomaterials is measured by Brunauer, Emmett and Teller (BET) method.[54] Fourier transform infrared spectroscopy (FTIR) is used to detect infrared spectrum of nanomaterials.[55]

Secondary characterization of nanomaterials is done in solution or suspension form. Parameters such as size distribution, concentration, purity, solubility, stability, agglomeration/aggregation, surface charge, surface activity and presence of other reactive species are investigated.[56] Additional experiments which could be carried out are DLS, zeta potential and nuclear magnetic resonance (NMR) (**Table 1.1**).

Table 1.1: Nanomaterials characterization experiment *vs* sensitivity[a]

Experiment *vs* information	**Size**	**Chemical ID**	**Organic/inorganic hybrid structures**	**Organic impurities**	**Sample state**
TEM	bulk to <1 nm	*via* EDX/EELS	poor contrast	no	ultra-high vacuum
SEM	bulk to ~2 nm	*via* EDX	poor contrast	no	ultra-high vacuum
AFM	bulk to ~2 nm	–	intermediate contrast	yes	interface
UV–vis–IR	varies, nanoscale via material dependent	limited to IR fingerprint matching	functional groups	–	solution

Experiment *vs* information	**Size**	**Chemical ID**	**Organic/inorganic hybrid structures**	**Organic impurities**	**Sample state**
	absorption; sensitive to aggregation				
H NMR	–	fingerprint matching	functional groups	yes	solution
XPS	indirect determination by density distribution	elemental and chemical state	quantitative	yes	ultra-high vacuum
TGA	–	*via* mass spectroscopy	core–shell mass ratio	–	solid
BET	surface area	–		yes	solid
DLS	10–3000 nm sensitive to aggregation	–		–	solution
XRD	bulk to 1 nm	lattice parameter	crystal only	–	solid
SAXS	1–100 nm	–	intermediate contrast	–	solid or solution

[a] TGA: thermal gravimetric analysis and SAXS: small-angle X-ray scattering. Hybrid structures are those with a significant organic and inorganic structure that need differentiation. Organic impurities are low *Z* small molecules that need detection or purification. Sample state is the necessary condition for measurement. No experiment captures the entire description of the particle, and many aspects require more than one experiment. (Adapted from Ref[47])

Generally, primary and secondary characterization should be used together to fully characterize nanomaterials. Typically, only a fraction of these techniques are accessible or usable. Moreover, multiple techniques required for characterization may slow down or limit complete execution progress. For example, purified Au nps can be fully characterized by using a reduced set of

techniques:[57] ^{1}H NMR to identify ligands and organic impurities; UV−Vis spectroscopy to verify the optical properties and estimate sizes from the plasmon spectral shifts; TEM/EDX to determine geometry, core size and elemental composition. In addition, some concerns involving nanomaterials purity, equipment sensitivity and sample state associated with current available methods are also highlighted in **Table 1.1**.[47]

1.5 Silver and gold nanoparticles

Nanomaterials with different characteristics are designed and manufactured for specific applications; metallic nanoparticles especially silver and gold are largely used in multidisciplinary areas.

1.5.1 Silver nanoparticles (Ag nps)

Silver metal has been used by mankind for thousands of years in the area such as coins, jewelry or dental alloy. Silver is well known by its antibacterial property. In ancient time as early as 1000 BC, the Greeks and others used silver containers for the conservation of water and food to prevent bacterial overgrowth.[58] In 8th century, the first medicinal record was using silver as a treatment to cure blood-related disorders and heart palpitations.[58] Silver nitrate was used to treat ulcers in 17th and 18th century and further used in the standard surgical operation in the 19th century.[59] In addition, silver has also been used for treating burn infections for a long time.[60-64] After the emergence of nanotechnology, commercialized products incorporated with nanosilver have invaded the market, owing to the antimicrobial activity of silver. These products include wide ranges such as wound and burn dressings, cosmetics, household detergents, refrigerators, mobile phones or clothes. Sometimes Ag nps have also been proposed for medical applications such as imaging, drug delivery, disinfection and tissue repair.[65-67]

It is estimated that today about 320 tons/year of Ag nps are produced for use in commercial or industrial products[68] and the number is expected to reach

1,120 tons by 2015.[69] Further, the number of nanosilver-containing products has increased from less than 30 in 2006 to over 300 at the beginning of 2011.[69] Lem et al.[70] conducted a market based intellectual property study to examine the current global patent landscape of companies using Ag nps in their consumer product development and production from 1980 to 2010. As shown in **Figure 1.5A,** a growing patent publication trend in commercial products was observed, especially for the last decade from 2001 to 2010, the number reached 1199 in 2010. **Figure 1.5B** gives an overall patent publication of the consumer products that contains Ag nps. Similar to the patent publication numbers in commercial products, the patent publication in consumer products peaked at 162 in 2010. Moreover, among 932 publications in consumer products, cosmetics, personal care, medical and health care were reported to occupy more than 70% of the application areas as shown in **Figure 1.6**.[70]

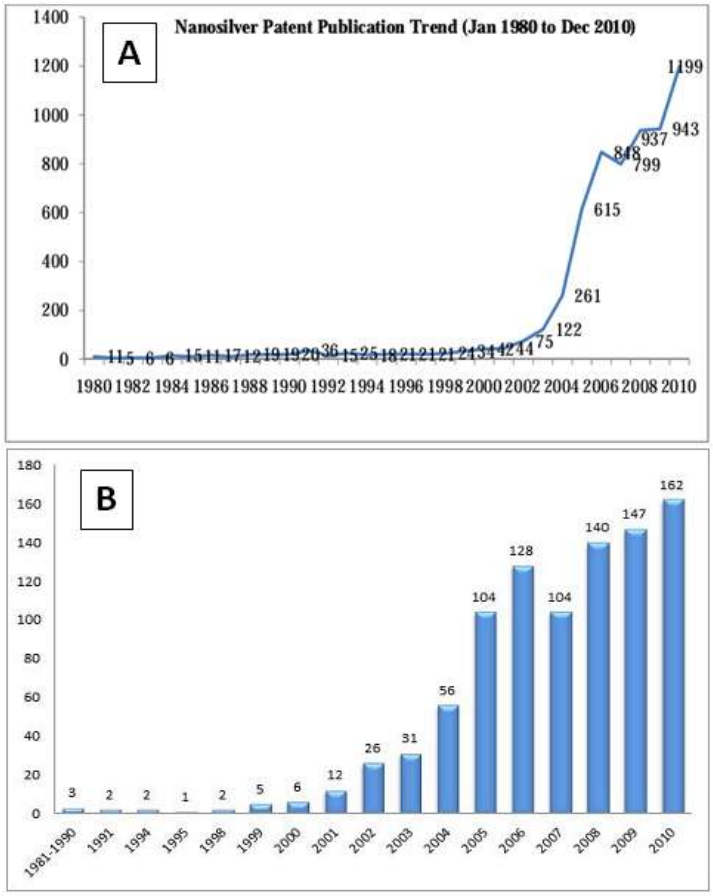

Figure 1.5: Patent publication trend of nanosilver-containing commercial products (A) and the consumer products that contains Ag nps (B) from January

1, 1980 to December 31, 2010. (Adapted from Ref[70])

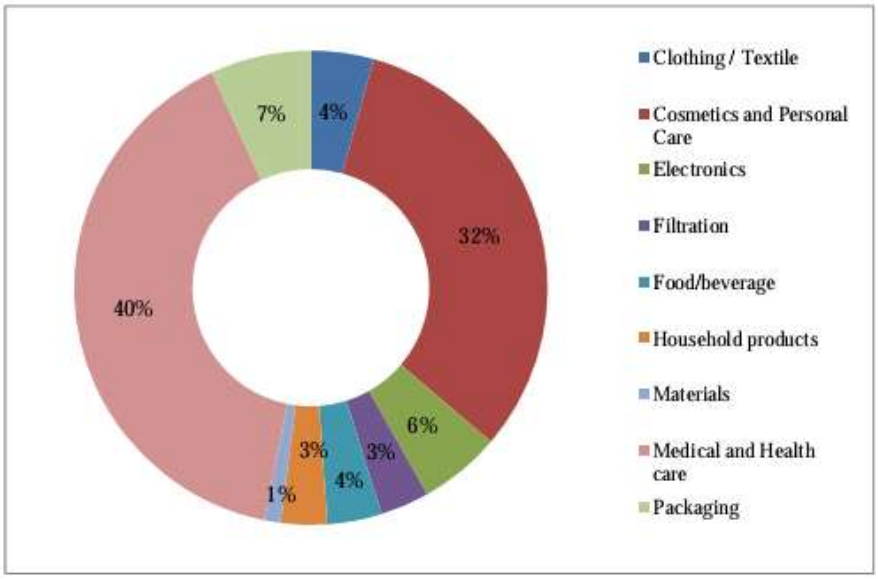

Figure 1.6: Nanosilver in various application of consumer products. (Adapted from Ref[70])

1.5.2 Gold nanoparticles (Au nps)

Gold was used in decorative objects in Eastern Europe in 4000 BC and gold jewelries were found in the tomb of Djer, King of the first Egyptian Dynasty (2500 BC).[71] The earliest records of the use of gold for medicinal and healing purposes can be traced back to the Chinese in 2500 BC.[72] Over 5000 years ago the Egyptians ingested gold for mental and bodily purification. Gold was mainly used in medicine for its magico-religious powers throughout the ancient world from Egypt to India.[73] For a long time, gold was used as a drug called "nervin" for the revitalization of people suffering from nervous disorders.[74] In the beginning of the 19th century, gold was used to treat syphilis[75] and later gold complexes were introduced for the treatment for rheumatoid arthritis.[72] However, the modern scientific study of colloidal gold commenced in 1857, when Michael Faraday proved that the color of gold solutions was attributed to the small size of gold particles.[76] Due to their unique properties, Au nps have been used as an additive to various drugs. In 1971, Au nps used as labels in immunostaining considered as the beginning of their biological applications.[77] Over the past decades, Au nps have been

extensively studied for biological and medical applications such as colorimetric biosensors,[78,79] drug delivery,[80,81] cancer imaging[82-84] and cancer therapies,[85-87] due to their good biocompatibility, monodispersity, easy synthesis and ready functionalization. For example, Au NMs can resonantly absorb and scatter incident light upon excitation of their surface plasmon oscillations typically in the near-infrared region (NIR)[88] and photon energies that are absorbed by Au NMs can be efficiently converted into heat on a picosecond time scale, as a result of electron-phonon and phonon-phonon processes. Therefore, Au NMs can be a highly potent photothermal therapeutic agent, by exploiting their strong absorptions and efficient heat conversions.[88-90] In addition, Guo et al.[81] first developed charge-reversal functional Au nps prepared by layer-by-layer technique to deliver small interfering RNA (siRNA) and plasmid DNA into cancer cells.

1.6 Safety concern of nanoparticles

Nanotechnology may be able to create many new functional materials and devices with a vast range of applications; however, it also raises important issues on living systems, environmental adverse impact of nanomaterials and their potential negative effects on global economy. As nanomaterials are increasingly prevalent, the chance of human exposure to nanoparticles has increased. In 2004, "Nanoscience and Nanotechnologies: Opportunities and Uncertainties" published Britain's Royal Society and the Royal Academy of Engineering, which advocate the need to address potential health and environmental effects of nanoparticles. It also makes recommendations on regulatory issues associated with nanotechnology. In 2008, the first official NNI Strategy for Nanotechnology-Related Environmental, Health, and Safety (EHS) Research was published, which was updated in 2011.

Earlier studies have shown the association of air pollution with lung diseases such as asthma, lung cancer and cardiovascular diseases such as myocardial infarction.[91-93] Evidences suggest that exposure to the

nanoparticles induced adverse effects to human health.[94] More research must be done to provide a complete understanding of biological responses of nanoparticles at the cellular level. The current pool of data available in the literature was gathered from the bioactivity studies of nanoparticles such as titanium dioxide (TiO_2),[95,96] zinc oxide (ZnO)[97] or silver (Ag)[98,99] nanoparticles, several of the earliest commercialised nanomaterials. The data obtained from such studies offers much valuable information and sheds light to the mechanisms of nanoparticle toxicity.

1.7 Exposure of nanoparticles to living systems

Many factors such as manufacturing conditions, volume of production, industrial applications, usage of consumer products, distribution, stability, behavior and environmental fate could affect the outcome of human exposure to nanomaterials. Living organisms are exposed to nanomaterials through active routes which include work and lifestyle related activities or passive exposure through living in contaminated areas or ingesting of contaminated water or food. External exposure routes for humans comprise inhalation (e.g. as aerosols), absorption through the skin and gastrointestinal tract. After the entry, absorption, distribution, metabolism and excretion of particles inside the body will depend on the size, chemical nature and stability of the nanomaterials. Nanomaterials could reach various organs through blood circulation and may accumulate inside the body as well.[100] Detailed information of portals of nanoparticle entry into living systems is summarized in the following sections.

1.7.1 Inhalation

The lungs are the most likely route of exposure to nanomaterials. Particle deposition and retention in the different pulmonary compartments is determined by many factors such as respiratory tract anatomy, breathing pattern, the exposure time and concentration, method of particle administration, particle size and agglomeration state.[101,102] Ultrafine particles

with size less than 100 nm were the crucial cause of respiratory disorders; these particles were more toxic and caused greater inflammation than larger particles.[103] Small particles were found to penetrate deeper as compared to larger ones.[104] Multiwalled carbon nanotubes reach the subpleura in mice after a single inhalation exposure of 30 mg/L for 6 h.[105] Nanoparticles can enter in the lung-epithelium and depth translocate beyond the epithelial barrier[106] or be cleared by macrophages.[107] This process is influenced by the size and shape of nanomaterials.[108] Nanoparticles with size below 400 nm have a high chance to cross the epithelial barrier, enter the blood or lymphatic systems and subsequently transport to different organs.[109] Inhalation experiments of Au[107,110] and Ag[111] nanoparticles in animal models resulted in systemic distribution and subsequent deposition in various organs.

1.7.2 Skin absorption

The human skin is one of the major entry routes for external substances,[112] owing to its large surface area and accessibility to environmental exposure. Nanomaterials contact with human skin may happen not only accidentally but also intentionally due to their presence in clothing, drugs, cosmetics, and other skin care products. Healthy skin is an efficient barrier to nanoparticles and other chemicals. The strongly keratinized stratum corneum (10 mm) is the main skin barrier which expels foreign bodies effectively.[113] However, the sweat glands and hair follicles on the skin could make this barrier vulnerable and facilitate nanoparticles entry. Most of the studies assessing the skin penetration of nanoparticles (such as titanium dioxide (TiO_2),[114] ZnO,[115,116] Ag nps[117] or quantum dots[118]) have shown penetration of particles into upper layers of the stratum corneum, occasionally reaching the viable epidermis.[119] Smaller iron nanoparticles (10 nm) accumulated in hair follicle orifices and penetrated through the lipid matrix of the stratum corneum but not deeper than the uppermost strata of the epidermis.[119] Ag nps exhibited low penetration through intact and damaged human skin, but in the case of damaged skin, an

increased absorption of Ag nps was observed.[117] Rancan et al.[120] reported that the skin penetration and cellular uptake of amorphous silica nanoparticles were size-dependent. These nanoparticles (42, 75 to 290 nm) partially disrupted stratum corneum, only small nanoparticles (42 ± 3 nm) were found to be associated with epidermal cells and especially dendritic cells, independent of their surface charge.[120]

1.7.3 Ingestion

Absorption of nanoparticles through the gastro-intestinal (GI) tract is one of the potential exposure routes for the entry of nanoparticles into human body owing to their use in food additives and drugs. Multiple parameters such as size, shape, composition, surface charge or surface functionalization could affect their targeting and absorption in GI tract.[121] Ingested nanomaterials may agglomerate inside the intestinal tract due to pH changes. These agglomerates can get expelled through feces if they are small enough or induced obstruction of GI tract and death if they are too big.[122] Au nps with size of 15 nm showed higher penetration rates in rat intestinal models as compared to larger ones (102 and 198 nm).[123] Internal diffusion and absorption of TiO_2 nanoparticles in the digestive system of mice explored by Abe et al.[124] described that TiO_2 fed to mice was detected in the lung, liver, and spleen after 10 days of exposure. TiO_2 nanoparticles were also reported to migrate into other tissues and organs (include brain) and induce significant lesions to the liver and kidneys.[125] These reports indicate that nanomaterials could penetrate the GI tract and result in translocation to other organs.

1.7.4 Translocation

From the site of entry, nanoparticles can enter multiple organs such as brain, spleen, liver, kidney and muscles through the circulatory system.[109,126] Intratracheal-instilled iron oxide nanoparticles passed through the alveolar-capillary barrier into systemic circulation within 10 min.[127] The pulmonary deposition and the translocation to secondary target organs in

Wistar rats intratracheally instilled with ceria nanoparticles showed that ceria nanoparticles could penetrate through the alveolar wall into the systemic circulation and accumulate in the extra-pulmonary organs.[128] Nanoparticle characteristics such as size and composition, surface charge and surface structures are vital factors to influence nanoparticle biokinetics, as they determined the interactions of nanoparticles with proteins and cellular components and thereby the mechanisms for particle translocation and accumulation in extra-pulmonary organs.[126] Nanoparticles with hydrodynamic diameter less than 30 nm and a noncationic surface charge translocate rapidly from the lung to mediastinal lymph nodes.[129] The individual health status is also an important determinant of the response to nanomaterials exposure. Significantly higher concentrations of Au were detected in heart and thymus of healthy animals, whereas higher concentrations of Au nps were observed in spleen in animals with prior lung inflammation.[130]

1.7.5 Excretion of nanoparticles

Excretion of nanomaterials are proposed to be through various routes such as urine, feces, sweat, breast milk and saliva.[104] Expulsion of nanoparticles is dependent on various parameters such as size, agglomeration, surface functionality and aspect ratio.[122,129] Nanoparticles (< 6 nm) can traffic rapidly from the lungs to lymph nodes and the bloodstream, and then be subsequently cleared by the kidneys.[129] Quantum dots with size less than 5.5 nm were rapidly eliminated in the rat model while renal excretion was prevented when the hydrodynamic diameter of quantum dots increased to larger than 15 nm owing to proteins adsorption on their surface.[131] Highly-charged mesoporous silica nanoparticles (+34.4 mV at pH 7.4) were rapidly excreted from the liver into the gastrointestinal tract as compared to lesser charged particles (+17.6 mV at pH 7.4), suggesting that charge-dependent adsorption of serum proteins greatly facilitates the hepatobiliary excretion of silica nanoparticles.[132] Carbon nanotubes (with high aspect ratios) that are well individualized and soluble in

biological milieu can also cross the kidney barrier and be excreted in urine.[133]

1.8 Nanotoxicity

The toxicity of nanomaterials was studied both in vivo and in vitro. In vitro studies are usually done with commercially available cell lines while in vivo studies are typically performed on rats[134] and mice,[135,136] some other models include zebrafish,[137] zebrafish embryos,[138] mosquito larvae,[139] guinea pig,[140] fruit fly[141] and fruit fly eggs.[142]

1.8.1 In vitro and in vivo toxicity testing

For in vitro studies, cytotoxicity of nanomaterials is performed using viability/proliferation assays (MTT/MTS or ATP), cytotoxicity assay (lactate dehydrogenase, glyceraldehyde-3-phosphate dehydro-genase (GAPDH), adenylate kinase), and necrosis and apoptosis assay.[143-146] Genotoxicity of nanomaterials were studied using the reverse mutation (Ames) assay,[147] cytokinesis-blocked micronucleus assay (CBMN) and alkaline single-cell gel electrophoresis (comet assay)[148] while alteration in gene expression were examined by northern blot analyses, ribonuclease protection assay (RPA), polymerase chain reaction (PCR) and microarray analyses.[147] However, physicochemical properties of nanomaterials which include high adsorption capacity, optical properties, catalytic activity, acidity/alkalinity, magnetic properties and dissolution, often limit the use of *in vitro* toxicity assays.[146] Studies designed to determine nanomaterial toxicity should be performed using test systems that cannot be influenced by nanospecific properties.[44,146] In addition, cellular uptake of nanomaterials can be monitored by confocal microscopy[149-151] and their exact distribution can be observed by imaging the ultrathin cells section using TEM.[152-154] Moreover, the quantitative analysis of the amount of nanomaterials inside cells is generally detected by ICP-MS.[154]

In vivo systems are extremely complicated and the interactions of nanomaterials with biological components, such as proteins and cells, could

lead to unique biodistribution, clearance, immune response, and metabolism.[155] In vivo studies were generally used to gather information on short/long-term effects, tissue localization, biodistribution and retention/excretion.[156] NM exposure via different pathways such as inhalation (lung), dermal (skin), ingestion (GI tract) and intravenous injection can provide useful information on toxicity and accumulation of nanomaterials in target organs.[157] The content of nanomaterials in tissue or blood samples can be analyzed by using neutron activation methods (INAA or NAA), inductively coupled plasma-mass spectrometry (ICP-MS), and atomic absorption spectroscopy (AAS).[158,159] In addition, the commonly used methods for identification and localization of nanomaterials in tissues include autometallography, SEM, and TEM techniques.[159,160] Elemental data of nanomaterials in tissues could be obtained by combining SEM or TEM analysis with energy dispersive X-ray spectroscopy (EDX). Furthermore, X-ray absorption spectroscopy (XAS) can be used to obtain structural information of nanomaterials in samples under examination.[159]

1.8.2 Nanotoxicity - In vitro

In vitro study suggests that nanomaterials could affect cellular functions at molecular levels[161] indicated by the depletion of intracellular glutathione.[162] Ag NMs showed significant damages to mammalian germ line stem cells through apoptosis,[163] anti-platelet properties[164] and caused severe damage to erythrocytes via lysis, membrane damage, hemagglutination and cytoskeletal distortions at a high concentration of 100 μg/mL.[165] Nanomaterials are reported to have the capability of penetrating the physiological barriers to reach vital areas or organs due to their small size. Cellular uptake studies showed that nanomaterials could penetrate cell membrane into cytoplasm of the cells, sometime even to the nucleus area (**Figure 1.7**). The toxicity of nanomaterials was believed to be caused by oxidative stress resulting from the generation of reactive oxygen species (ROS) inside the cells.[166] ROS was

responsible for DNA damage and chromosomal aberrations, which further induced cell cycle arrest at G2/M or S stage and caused cell death through apoptosis.

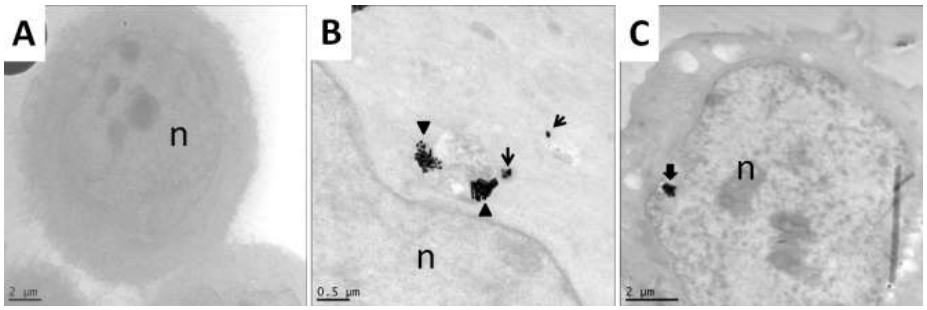

Figure 1.7: TEM images of ultrathin section of MCF7 cells treated with Au NMs. Untreated cells showed no abnormality (A) while cells treated with Au NMs showed aggregate nanomaterials in lysosomes (thick arrows) or scattered Au NMs in the cytoplasm (open arrow) inside cells (B). Image also showed Au NMs aggregate in the nucleus (diamond arrow) through penetrating the nuclear membrane (C).

Cancer growth is dictated by a small cell population called cancer stem cells (CSCs),[167] which have been isolated from a variety of tumor types.[168] CSCs have the ability to generate more differentiated tumor cells, the majority of a tumor mass.[169] Due to this reason, CSCs commonly show resistance to conventional cancer therapies and are responsible for tumor maintenance.[170,171] Since CSCs are the cell populations responsible for the development of tumor and have important role in cancer recurrence, these cells are of particular importance to explore innovative cancer therapies. Multiwalled carbon nanotubes (MWCNTs) were injected into breast tumors, followed by heated with a quick, 30-second laser treatment killed breast cancer stem cells.[172] In addition, Wang et al.[173] reported that aptamer-conjugated Au nanorods can be used to target and kill both prostate cancer cells and cancer stem cells by near-infrared (NIR) laser irradiation. However, until recently no studies were reported on cellular responses of Ag and Au nps on cancer stem cells.

Stem cells have attracted particular attention in the field of regenerative

medicine because of their pluripotency. Directed differentiation of stem cells into certain types of cells is one of the most important issues in embryonic stem cells (ESCs) research, which represent not only theoretical interest, but also show potential application on cell or tissue therapy for curing serious human diseases.[174] Several groups have explored the possibilities of using embryonic and fetal stem cells to produce dopaminergic cells for curing Parkinson's disease.[175] Mesenchymal stem cells could be implanted locally to promote or augment repair or regeneration of a fractured or osteoporotic bone.[176] Skin stem cells can not only provide hope for the functional repair of the skin itself but also offer a potential source of adult stem cells for the cell-based therapy of injuries and diseases throughout the body.[177] Yi et al.[178] reported that Au nps can promote the differentiation of mesenchymal stem cells toward osteoblast cells over adipocyte cells through p38 MAPK Pathway. Smith et al.[179] proposed that nano-fibrous architecture could enhance the osteogenic differentiation of the human ESCs compared to more traditional scaffolding architectures. In addition, Greulich et al. found that Ag nps exerted cytotoxic effects on human mesenchymal stem cells at high concentrations and induced cell activation (as analyzed by the release of IL-8) at high but nontoxic concentrations of nanosilver.[180] However, cytotoxicity and genotoxicity of Ag nps on human ESCs were not fully investigated, especially their cellular responses at nontoxic doses.

1.8.3 Nanotoxicity - In vivo

Animal study showed that nano-anatase TiO_2 at a relative high dose could cause serious damage to liver, kidney, and myocardium of mice by disturbing the balance of blood sugar and lipid in mice.[181] In addition, no pulmonary inflammation, DNA damage or hepatic histopathology were observed in mice instilled with NanoTiO_2 dust from paint while pure NanoTiO_2 caused the inflammation.[182] Research report showed that multiwalled carbon nanotubes could easily reach the subpleura tissue in mice after a single inhalation

exposure and get embedded in the subpleural wall and within subpleural macrophages.[105] Moreover, it is reported that nanomaterials transferred from pregnant mice to their offspring can damage genital and cranial nerve systems.[100] The biodistribution of Au NMs in vital organs after injected intravenously to 6–8-week-old female nu/nu mice bearing orthotopic ovarian tumors showed that Au nanorods were taken up to a lesser extent by the liver, had longer circulation time in the blood, and higher accumulation in the tumors, as compared with their spherical counterparts.[183] Huang et al.[184] reported that organ distributions of intravenously administrated mesoporous silica nanoparticles (MSNs) were mainly present in the liver, spleen and lung (>80%) in mice and there is obvious shape effects on their in vivo behaviors. Short-rod MSNs were easily trapped in the liver, while long-rod MSNs distributed in the spleen.[184] Various routes for excretion of nanomaterials (such as through urine, feces, sweat, breast milk and saliva) have been suggested in the literature. However, only a few (through urine and feces[185]) have been proven experimentally. Excretion of nano-sized latex particles from medaka (Oryzias latipes) embryos and larvae was size-dependent; the smaller particles (50 nm) were removed slower than the larger particles (500 nm).[186] MSNs are found to be mainly excreted by urine and feces, and their clearance rate was primarily shape-dependent, where short-rod MSNs showed a more rapid clearance rate than long-rod MSNs in both excretion routes.[184] Although MSNs did not cause significant toxicity in vivo as indicated by hematology, serum biochemistry, and histopathology results, MSNs have the potential to induce of biliary excretion and glomerular filtration dysfunction in mice.[184] Special design of nanomaterials structure (clustering design of nanorose) could enhance the excretion of nanomaterials, which could help to limit the potential toxicity of nanomaterials in clinical applications.[187]

Recently, use of zebrafish as the animal model has attracted interest owing to high degree of homology to the human genome, and the transparency of the

eggs for easy visualization of embryogenesis.[137,188] Zebrafish have become a popular organism for the study of vertebrate gene function, and it is reported that approximately 70% of human genes have at least one obvious zebrafish orthologue.[189,190] Further, zebrafish is also proving to be a quick, cheap, and facile model to conservatively assess toxicity of nanomaterials.[191] Adverse effects of nanomaterials exposure on zebrafish embryo can be observed in the development of notochord, eye, heart, tail, brain and fish size.[192]

1.9 Factors affecting cellular uptake and nanotoxicity

The cellular uptake and cytotoxicity of nanomaterials can be influenced by a few characteristics such as shape, size, stability and surface functionalities. Such a high number of variable make the nanoparticles to behavior differently from small molecular pollutants.[193] The small size of nanomaterials (< 100 nm) enables them to interact with biological entities such as bacteria, cells, cellular proteins and viruses. Cellular uptake, cytotoxicity and innate immune response of nanomaterials depend on size, shape, compositions, surface functionalities, chemical nature and cell types.[194-200]

1.9.1 Size effect

Earlier reports showed that nanomatrials exhibited size-dependent toxicity (**Table 1.2**).[138,201-205] Nanomatrials with smaller size are reported to be more toxic than those with the larger size owing to their higher reactive surface area for interaction with biomolecules and easy uptake into cells via varied mechanisms such as diffusion or endocytosis.[138,206-210] Au nps of 1 - 2 nm in size were highly toxic and induce cell death via both apoptosis and necrosis,[194,211] while larger 50 – 100 nm Au particles were comparatively nontoxic.[194]. Cui et al.[212] reported that small Au nps could be endocytosed by cells resulting in cytotoxicity while large aggregates adhered onto the cell surface and increased the growth rate of HeLa cells. In addition, the ultimate intracellular destination of Au nps is also determined by the size. The smaller

Au nps penetrate nucleus and cytoplasm, and some particles remain at the membrane, while the larger ones did not enter the cells and were located at the cellular periphery.[205]

Table 1.2: Summary of literature of nanomaterials with size-dependent cellular uptake and toxicity[a]

Species	**Cellular uptake and toxicity**	**Sources**
Au nps	2.4 nm: localize in the nucleus 5.5 and 8.2 nm: partially delivered into the cytoplasm; 16 nm or larger: not enter the cells and located at the cellular periphery	205
Au nps	1 - 2 nm: highly toxic > 15 nm: comparatively nontoxic	206
Au nps	IC_{50} 0.8 nm: 200 μM 1.2 nm: 100 μM 1.4 nm: 80 μM 1.8 nm: 200-500 μM 15 nm: > 6300 μM	194
Au nanosphere	the cell had 1.5 – 2.4-times higher uptake for the 15 nm than for the 45 nm samples	209
Au nanocages	the 33 nm sample showed 1.5 – 4.4-times higher uptake than the 45 nm sample	209
Ag nps	Human lung adenocarcinoma epithelial (A549) cells: EC_{50} 5 nm: 1 μg/mL 20 nm: 10 μg/mL 50 nm: 14 μg/mL	207
Ag nps	30 – 50 nm: mitochondrial function was reduced at 10 – 20 μg/mL,	

Species	**Cellular uptake and toxicity**	**Sources**
	necrosis/apoptosis at 2.5 – 15 μg/mL	
Ag nps	79 ± 1 nm, toxic at 15 and 30 μg/mL; 82 ± 1 nm, toxic at 7.5 and 15 μg/mL (after 4 days); toxic at 30 μg/mL (after 2 days); 88 ± 1 nm, toxic at 7.5 μg/mL (after 4 days), toxic at 15 and 30 μg/mL (after 2 days), toxic at 15 μg/mL (after 4 days); 94 ± 1 nm, toxic at 7.5 and 15 μg/mL (after 4 days), toxic at 30 μg/mL (after 4 days); 95 ± 1 nm, toxic at 7.5, 15 and 30 μg/mL (after 4 days); 99 ± 1 nm, toxic at 7.5, 15 and 30 μg/mL (after 4 days)	[204]
Ag nps	20 nm, EC_{20} (WST test)=21 μg/mL; EC_{20} (LDH assay)=3 μg/mL; 80 nm, EC_{20} (WST test)=31 μg/mL; EC_{20} (LDH assay)=33 μg/mL; 113 nm, EC_{20} (WST test)=29 μg/mL; EC_{20} (LDH assay)=43 μg/mL	[203]
Ag nps	10 nm, cytotoxicity ca. 40% at 25 μg/mL; 20 nm, cytotoxicity ca. 20% at 25 μg/mL; 32nm, cytotoxicity ca. 50% at 12.5 μg/mL, ca. 70%at 25 μg/mL; 40 nm, not toxic at 25 μg/mL	[138]
Ag nps	25 nm, toxic at 62.5 μg/mL; 35 nm, toxic at 62.5 μg/mL; 45 nm, toxic at 62.5 μg/mL; 60 nm, toxic at 125 μg/mL; 70 nm, toxic at 125 μg/mL	[201]
Ag nps	4 nm, cell viability 36% at 3.12 μg/mL; 20 nm, cell viability 6% at 25 μg/mL;	[202]

Species	**Cellular uptake and toxicity**	**Sources**
	70 nm, cell viability 100% at 50 μg/mL	
Ag nps	5 nm, cell viability 50% at 6.25 μg/mL, 0% at > 12.5 μg/mL; 100 nm, cell viability 100% at 25 μg/mL	[210]
Silica titania hollow nps	Viability at 500 μg/mL: 25 nm: 68% 50 nm: 65% 75 nm:72% 100 nm: 78%	[213]
SiO_2	Human kidney cells (HK-2) at 100 μg/mL 20 nm, 12% colony formation; 100 nm, 80% colony formation	[214]

[a] IC_{50} = half maximal inhibitory concentration, EC_{50} = half maximal effective concentration

1.9.2 Shape effect

Shape is another important factor which affects the responses in living and environment.[138,215-218] The shape anisotropy and initial orientation of nanomaterials play a complicated role in their physical translocation,[219] and biological outcome depends on the differences in the surface reactivity, cellular uptake, biocompatibility of nanomaterials and retention at various tissues or organs.[220,221] For instance, a recent study showed that dendrimer shaped nickel nanoparticles exhibited higher toxicity than spherical nanoparticles in zebrafish embryos.[222] The shape effect of nanomaterials was also observed in bacteria,[221,223] human cancer cell lines[224] and zebrafish embryos.[138] Ag nanoplates showed a higher degree of toxicity than Ag sphere nanoparticles, owing to surface reactivity resulting from crystal defects.[138] However, until now, no comparison study was reported on Ag NMs with different shapes such as Ag nanocubes and truncated nanocubes. Au nanorods

induced cell apoptosis while Au nanosphere did not induce any such detrimental effects to cells.[225] In addition, spherical Au nps displayed high biocompatibility in mice models, and rod-shaped Au nps were more toxic than cube-shaped Au nps.[217] Au nanoplates (AuNPs) have attracted great interests as they could exhibit a strong plasmon band in the near-infrared region (NIR). However, no comparison studies on their shape sensitive effects on cellular responses in human cells were reported.

Table 1.3: Summary of literature on shape-dependent cellular uptake and toxicity of nanomaterials [a]

Species	**Shape dependent effects**	**Sources**
Ag NMs	Toxicity: Ag nanoplates > spheres or wires	138
Ag_2O NMs	*E. coli* at 5 μg/mL: octahedral particles, 80% viability; cubic particles, 10% viabilty	226
Au NMs	Au nanorods caused significant ROS production and up-regulated several genes involved in cellular stress and toxicity as compares to Au nanospheres	225
Au NMs	Cellular uptake on human breast cancer cells (SK-BR-3): spherical particles > cubic particles (capped with PEG or anti-HER2)	209
ZnO NMs	EC_{50}: Nanorod, 8.5 μg/mL Nanosphere, 12.1 μg/mL	227
PEDT NMs	Toxicity: PEDT-1 (aspect ratio = 1.3) > PEDT-2 (aspect ratio = 4.5) or PEDT-3(aspect ratio = 25.0).	215
PANI	Toxicity increased with decreasing aspect ratio of PANI nanomaterials	228
Multiwalled carbon nanotubes	the length of carbon nanotubes greatly affected their toxicity in zebrafish embryos: long nanotubes did not induce any obvious toxicity, short nanotubes	229

Species	**Shape dependent effects**	**Sources**
	caused severe developmental toxicity	
Silica nanowires	Zebrafish embryo: aspect ratios > 1, highly toxic (LD_{50} = 110 pg/g embryo) and cause embryo deformities; aspect ratio = 1 neither toxic nor teratogenic at the same concentrations	[230]
TiO_2 NMs	Long nanobelts, highly toxic, initiates inflammatory responses; nanospheres and Short nanobelts, not significantly cytotoxic	[231]

[a] Ag_2O = silver oxide, PEDT = Poly(3,4-ethylenedioxythiophene), a.r. = aspect ratio

Aspect ratio is also a vital factor to impact the toxicity of nanomaterials. Toxicity of nanowires, nanotubes or nanobelts with high aspect ratio was summarized here (**Table 1.3**). As for the polymer nanomaterials such as PEDT or polyaniline, the toxicity of nanomaterials increased as decreasing their aspect ratios.[215,228] Similar results was also reported for multiwalled carbon nanotubes, short nanotubes caused severe developmental toxicity whereas long nanotubes did not induce any obvious toxicity in the tested developing zebrafish embryos.[229] On the contrary, silica nanowires with aspect ratios > 1 showed high toxicity and caused embryo deformities whereas nanowires with aspect ratio = 1 were neither toxic nor teratogenic at the same concentrations.[230] As for TiO_2 nanomaterials, long TiO_2 nanobelts (> 15 μm) interact with lung macrophages while nanospheres (200 nm) and short nanobelts (< 5 μm) were not significantly cytotoxic.[231]

1.9.3 Surface functionalization effect

Surface functionalization of nanomaterials cause interesting properties such as changes in stability, solubility, surface charge, hydrophilicity or

hydrophobicity of nanomaterials, which could affect nanomaterials biocompatibility, subsequent uptake and downstream processing by cells. Various molecules (e.g. polyethylene glycol, polyvinylpyrrolidone (PVP)) have been used as capping agents to improve solubility of nanoparticles in water. Cetyltrimethylammoniumbromide (CTAB) coated Au nanorods were highly toxic while nanorods coated with polymers[232] such as poly(styrenesulfonate),[233] polyethylene glycol (PEG),[234,235] phosphatidylcholine[236] or small molecules such as mercaptohexadecanoic acid (MHDA)[235] could reduce cytotoxicity (**Table 1.4**). It is reported that surface charge plays important roles in nanomaterials toxicity; positively charged nanomaterials were much more toxic as compared to negatively charged or neutral nanomaterials (**Table 1.4**).[213,237-244] Polymer-coated cerium oxide nanoparticles with different surface charges (positive, negative, and neutral) showed a surface-charge-dependent cell localization and cytotoxicity in normal and cancer cells.[244] Similarly, Ag nps also exhibited surface charge-dependent toxicity on the bacillus species.[241] Charged Au nps induced cell death through apoptosis while neutral Au nps led to necrosis.[245] Surface functionalization of nanomaterials which normally covered the nanomaterials surface can influence their intracellular solubility, which further affects their cytotoxicity. Copper oxide were reported to be highly cytotoxic, while carbon stabilized copper nanoparticles were less cytotoxic and showed no adverse effect.[246] In addition, cationic and hydrophobic Au nps could penetrate into the circulatory system of the fish, leading to widespread distribution in the organs of the fish and cause fish mortality in less than 24 h while the hydrophilic surface of nanoparticles prevents their accumulation, facilitates clearance and minimizes environmental impacts.[239]

Cell type is considered as another variable to influence the intracellular fate and toxic response to nanomaterials.[166] Platinum nanoparticles capped with PVP showed higher cellular uptake in human cervical cancer cells (HeLa)

than in breast cancer cells (MCF7) and lung fibroblast cells (IMR90).[247] Au sphere nanoparticles induced death response in human carcinoma lung cells (A549) but nontoxic to baby hamster kidney cells (BHK21) and human liver carcinoma (HepG2).[248] In addition, Ag nps also showed different toxicities to different cell lines: EC_{50} of Ag nps (50 nm) in A549 cells is 14 μg/mL, in HepG2 34 μg/mL, in MCF7 48 μg/mL and in human stomach cancer cells (SGC-7901) 112 μg/mL.[207]

Table 1.4: Summary of literature on surface functionalization-dependent cellular uptake and toxicity of nanomaterials[a]

Species	**Functionalization dependent effects**	**Sources**
Au nanorods	CTAB coated nanorods are toxic, nanorods coated with polymer reduce cytotoxicty	232
Au nanorods	Toxicity: CTAB coated nanorods more toxic than poly(styrenesulfonate) coated	233
Au nanorods	HeLa cells treated with 0.05 mM: CTAB-coated, 80% cell death PEG-coated: 10% cell death	234
Au nanorods	Au-PEG and Au-MHDA nanorods exhibited minimal effects on cell proliferation, Au-CTAB reduced cell proliferation significantly, low cellular uptake for Au-PEG, high uptake for Au-MHDA	235
Au nanorods	Toxicity to HeLa cells: phosphatidylcholine-modified nanorods < CTAB-coated nanorods	236
Au nanorods	Cellular uptake of Au nanorods can be truned from very high to very low by manipulating the surface charge and functional groups of the polyelectrolyte.	237
Au nanosphere	Cationic nanoparticles are much more toxic than anionic particles of the same size	238

Species	**Functionalization dependent effects**	**Sources**
Au nps	Cationic and hydrophobic Au nps: penetrate into the circulatory system of the fish, lead to widespread distribution in the organs of the fish and cause fish mortality in less than 24 h; Hydrophilic surface: prevents accumulation, facilitates clearance and minimize environmental impact	239
Au nps	The acute cytotoxicity and genotoxicity of positively charged Au nps depend on the hydrophobicity of the ligands attached on their surface. Increasing the hydrophobicity of the particles increased their cytotoxicity.	240
Ag nps	Ag nps exhibited surface charge-dependent toxicity on the bacillus species: the more negative citrate coated Ag nps were the least toxic, whereas the positively charged BPEI coated Ag nps were the most toxic.	241
silica nps	Surface charge-dependent cellular uptake, positive surface charge enhances the uptake of nanoparticles	242
silica-titania hollow nps	Cationic nanoparticles are the most toxic as compared to anionic and neutral nanoparticles.	213
HAP nps	Positively charged HAP nanoparticles are easily penetrated the cells as compared to negatively charged nanoparticles; Neutral HAP nanoparticles could not penetrate the cell membrane due to their larger size	243
cerium oxide nps	Nanoceria with a positive or neutral charge enters most of the cell lines studied, while nanoceria with a negative charge internalizes mostly in the cancer cell lines.	244
ZnO nps	The ability to reduce the cytotoxicity of ZnO nanoparticles: medium-soaked ≈ PMAA > OA; PMAA-coated ZnO had significant genotoxicity compared to uncoated ZnO and the other coated	249

Species	**Functionalization dependent effects**	**Sources**
	nanoparticles	
Ag NMs	Human skin keratinocyte cells (HaCaT): Citrate coated silver nanopowder, toxic; PVP-coated nanoprism or nanopowder, nontoxic	250
Au nps	Au nps cellular uptake is directly dependent on the surface display of the cell-penetrating peptide	205
Au nanosphere, nanocages	uptake by the SK-BR-3 cells decreased in the following order: PAA > anti-HER2 > PEG	209

[a] PMAA = poly(methacrylic acid) , HAP = hydroxyapatite, OA = oleic acid, CTAB = cetyltrimethylammoniumbromide, PEG = polyethylene glycol , MHDA = mercaptohexadecanoic acid, BPEI = branched polyethyl-eneimine

Moreover, the behavior and fate of nanomaterials in environment have attracted much concern due to the discard or run-off of nanomaterials into water sources, which may further contaminate our drinking water. The stability of nanoparticles in water can be heavily influenced by surface coatings.[251] A dramatic difference between the behaviour of coated and uncoated nanoparticles in wastewater have been reported:[251] surfactant-coated nanoparticles rapidly aggregated and sedimentated out to form part of the solid sewage sludge while uncoated nanoparticles remained dispersed in the sewage and therefore simply continue through the effluent stream.[251] The aggregation of surfactant-coated nanoparticles could be attributed to interactions between the adsorbed surfactant molecules and organic matter in the sewage. Furthermore, dissolution and presence of other impurities could also affect the behavior and the fate of nanomaterials in living organism and environment.[252] The primary mechanism of Ag nanoparticle toxicity in aquatic lifeforms could be attributed to the release of silver ions in the exposure medium, as Ag nps have been reported to dissolve in a biological environment or in acidic

pH.[253,254]

1.10 Rationale and scope of the thesis

As summarized in the earlier sections, the cytotoxicity of nanomaterials is dependent on several factors, such as surface functional groups, nanomaterial morphology and cell types. Ag and Au are two most commonly used metallic nanomaterials; however, no systematic study on their toxicity was done so far. Research reports on the adverse effects of Ag and Au NMs have focused mainly on spherical nanoparticles, but very few of these reports touch upon the cytotoxicity of nanomaterials with different shapes, especially for Ag and Au NMs. It should be noted that the toxicity of Ag and Au NMs with different shapes cannot simply be deduced from the existing data of the spherical nanoparticles as slight differences in physical and chemical properties, such as surface functional group, particle size, surface charge and shapes, would largely affect the toxicity of such nanomaterials. This is important as more and more commercial products are available on the market, which may cause potential damage to human.

Stem cells, either cancer stem cells or normal stem cells, which have the capability to self-renew and differentiated into different cell lines, have attracted much attention due to their vital roles in cancer therapy or tissue implanting. However, very few researches have reported on cytotoxic and genotoxic effects of metallic nanoparticles on these stem cells. Therefore, cytotoxicity of Ag and Au NMs on stem cells was investigated in detail here.

The specific objectives of this study were to:

1. Compare the toxicity of Ag nps with different functional groups, especially for those extracted from natural materials, some of which can even be used as traditional drugs;
2. Investigate the cellular responses towards Ag NMs with different morphologies;

3. Study the cytotoxicity of AuNPs with different shapes, such as triangle, hexagon, pentagon nanoplates; and
4. Explore cytotoxicity and genotoxicity of Ag and Au nps on human stem cells.

In this study, the cytotoxicity of Ag nps with different functional groups and that of Ag and Au NMs with different morphologies were investigated on human cells. The cellular responses were evaluated by cell viability, reactive oxygen species generation and alternation in cell cycle. The results in this project could provide guidelines for the use of nanomaterials in biomedical applications.

To achieve the above objectives, the thesis will be divided into several sections accordingly. Chapter 2 of the thesis describes the materials and methods used in the present study. Cytotoxicity of Ag nps synthesized with different natural material extracts as both reducing agents and capping agents was explored in human cancer cells and the results were presented in chapter 3. Synthesis of Ag NMs with different morphologies such as nanocubes, truncated nanocubes or nanowires and their shape-dependent toxicity to human skin fibroblast cells are summarized in chapter 4. Chapter 5 describes cellular responses of AuNPs with different structures (hexagon, pentagon and triangle) in human breast cancer cells while chapter 6 discusses cytotoxicity and genotoxicity of Ag and Au nps on human colon cancer stem cells and embryonic stem cells at low doses.

1.11 References

(1) Freestone, I.; Meeks, N.; Sax, M.; Higgitt, C. *Gold bulletin* **2007**, *40*, 270.

(2) Rio, A. P. d.; Roehrs, S.; Aucouturier, M.; Castaing, J.; Bouquillon, A. *The Arabian J. Sci. and Eng.* **2010**, *35*, 157.

(3) Feynman, R. P. *Engineering Sci.* **1960**, 22. (Talk)

(4) Taniguchi, N. In *Proc. Intl. Conf. Prod. Part II, British Society of Precision Engineering* London, 1974.
http://en.wikipedia.org/wiki/Norio_Taniguchi

(5) Drexler, K. E. Engines of Creation The Coming Era of Nanotechnology, *New York: Anchor Press/Doubleday* **1986**. (Book)

(6) Toumey, C. *Nat. Nano* **2007**, *2*, 9.

(7) Ekimov, A. I.; Onushchenko, A. A. *JETP Lett.* **1981**, *34*, 345.

(8) Ekimov, A. I.; Efros, A. L.; Onushchenko, A. A. *Solid State Communications* **1985**, *56*, 921.

(9) The nonal nanotechnology initiative: overview, reauthorization, and appropriations issues; *CRS Report for Congress*, Sargent, J. F., Ed., 2012. (CRS Report for Congress)

(10) Huang, Z.; Chen, H.; Che, Z.; Roco, M. *J. Nanopart. Res.* **2004**, *6*, 325.

(11) Huang, Z.; Chen, H.; Yan, L.; Roco, M. *J. Nanopart. Res.* **2005**, *7*, 343.

(12) Roco, M. *J. Nanopart. Res.* **2011**, *13*, 427.

(13) Dang, Y.; Zhang, Y.; Fan, L.; Chen, H.; Roco, M. *J. Nanopart. Res.* **2010**, *12*, 687.

(14) Roco, M.; Bainbridge, W.; Societal implications of nanoscience and nanotechnology, Springer, Ed. Boston, 2001.(Book)

(15) Buzea, C.; Blandino, I. I. P.; Robbie, K. *Biointerphases* **2007**, *2*, MR17

(16) Wang, Y.; Xia, Y. *Nano Lett.* **2004**, *4*, 2047.

(17) Wong, T.-S.; Brough, B.; Ho, C.-M. *Mol. Cell Biomech.* **2009**, *6*, 1.

(18) Mishra, B.; Patel, B. B.; Tiwari, S. *Nanomed. Nanotech. Biol. Med.* **2010**, *6*, 9.

(19) Li, C.; Solomon, V.; Wang, L. *Microsc. Microanal.* **2011**, *17*, 1832.

(20) Sultan, S. M.; Sun, K.; Partridge, J.; Allen, M.; Ashburn, P.; Chong, H. M. H. In *Ultimate Integration on Silicon (ULIS), 2011 12th International*

Conference on 2011, p 1.

(21) Wang, H.; Sun, M.; Ding, K.; Hill, M. T.; Ning, C.-Z. *Nano Letters* **2011**, *11*, 1646.

(22) Thakkar, K. N.; Mhatre, S. S.; Parikh, R. Y. *Nanomed. Nanotech. Biol. Med.* **2010**, *6*, 257.

(23) Tartaj, P.; Morales, M. ı. d. P.; Veintemillas-Verdaguer, S.; no, T. G. a.-C.; Serna, C. J. *J. Phys. D: Appl. Phys.* **2003**, *36*, 182.

(24) Krutyakov, Y. A.; Kudrinskiy, A. A.; Olenin, A. Y.; Lisichkin, G. V. *Russian Chem. Rev.* **2008**, *77*, 233.

(25) Cuenya, B. R. *Thin Solid Films* **2010**, *518*, 3127.

(26) Liu, Z. H.; Jiao, Y. P.; Wang, Y. F.; Zhou, C. R.; Zhang, Z. Y. *Adv. Drug Deliv. Rev.* **2008**, *60*, 1650.

(27) Szarpak, A.; Cui, D.; Dubreuil, F.; De Geest, B. G.; De Cock, L. J.; Picart, C.; Auzely-Velty, R. *Biomacromolecules* **2010**, *11*, 713.

(28) Thanh, N. T. K.; Green, L. A. W. *Nano Today* **2010**, *5*, 213.

(29) Liang, M.; Lin, I. C.; Whittaker, M. R.; Minchin, R. F.; Monteiro, M. J.; Toth, I. *ACS Nano* **2010**, *4*, 403.

(30) Reddy, A. S.; Chen, C. Y.; Chen, C. C.; Jean, J. S.; Chen, H. R.; Tseng, M. J.; Fan, C. W.; Wang, J. C. *J. Nanosci. Nanotechnol.* **2010**, *10*, 6567.

(31) Kowshik, M.; Ashtaputre, S.; Kharrazi, S.; Vogel, W.; Urban, J.; Kulkarni, S. K.; Paknikar, K. M. *Nanotechnology* **2003**, *14*, 95.

(32) Kumar, K. P.; Paul, W.; Sharma, C. P. *Process Biochem.* **2011**, *46*, 2007.

(33) Nadagouda, M. N.; Varma, R. S. *Green Chem.* **2008**, *10*, 859.

(34) Bar, H.; Bhui, D. K.; Sahoo, G. P.; Sarkar, P.; Pyne, S.; Misra, A. *Colloid Surface A* **2009**, *348*, 212.

(35) Song, J.; Kim, B. *Bioprocess Biosyst. Eng.* **2009**, *32*, 79.

(36) Dubey, S. P.; Lahtinen, M.; Sillanpää, M. *Colloids and Surfaces A* **2010**, *364*, 34.

(37) Shankar, S. S.; Rai, A.; Ankamwar, B.; Singh, A.; Ahmad, A.; Sastry, M. *Nat Mater* **2004**, *3*, 482.

(38) Chandran, S. P.; Chaudhary, M.; Pasricha, R.; Ahmad, A.; Sastry, M. *Biotech. Progress* **2006**, *22*, 577.

(39) Gardea-Torresdey, J. L.; Parsons, J. G.; Gomez, E.; Peralta-Videa, J.; Troiani, H. E.; Santiago, P.; Yacaman, M. J. *Nano Lett.* **2002**, *2*, 397.

(40) Shankar, S. S.; Rai, A.; Ahmad, A.; Sastry, M. *J. Colloid Interf. Sci.* **2004**, *275*, 496.

(41) Ankamwar, B.; Chaudhary, M.; Sastry, M. *Synth. React. Inorganic Metal-Organic Nano-Metal Chem.***2005**, *35*, 19.

(42) Nanda, A.; Saravanan, M. *Nanomed. Nanotech. Biol. Med.* **2009**, *5*, 452.

(43) Gajbhiye, M.; Kesharwani, J.; Ingle, A.; Gade, A.; Rai, M. *Nanomed.Nanotech. Biol. Med.* **2009**, *5*, 382.

(44) Nel, A.; Xia, T.; Mädler, L.; Li, N. *Science* **2006**, *311*, 622.

(45) Sayes, C. M.; Warheit, D. B. *Wiley Interdisciplinary Rev. Nanomed. Nanobiotech.* **2009**, *1*, 660.

(46) Grassian, V. H.; O'Shaughnessy, P. T.; Adamcakova-Dodd, A.; Pettibone, J. M.; Thorne, P. S. *Environ Health Perspect* **2007**, *115*, 397.

(47) Richman, E. K.; Hutchison, J. E. *ACS Nano* **2009**, *3*, 2441.

(48) Truong, L.; Tilton, S. C.; Zaikova, T.; Richman, E.; Waters, K. M.; Hutchison, J. E.; Tanguay, R. L. *Nanotoxicology* **2013**, *7*, 192.

(49) He, G.; Zeng, J.; Jin, M.; Zhang, H.; Lu, N.; Wang, J.; Kim, M. J.; Xia, Y. *ChemCatChem* **2012**, *4*, 1668.

(50) Gu, Y.; Xie, H.; Gao, J.; Liu, D.; Williams, C. T.; Murphy, C. J.; Ploehn, H. J. *Langmuir* **2005**, *21*, 3122.

(51) Artyushkova, K.; Levendosky, S.; Atanassov, P.; Fulghum, J. *Top Catal* **2007**, *46*, 263.

(52) Okpalugo, T. I. T.; Papakonstantinou, P.; Murphy, H.; McLaughlin, J.; Brown, N. M. D. *Carbon* **2005**, *43*, 153.

(53) Mourdikoudis, S.; Simeonidis, K.; Vilalta-Clemente, A.; Tuna, F.; Tsiaoussis, I.; Angelakeris, M.; Dendrinou-Samara, C.; Kalogirou, O. *J. Magn. Magn. Mater.* **2009**, *321*, 2723.

(54) Esswein, A. J.; McMurdo, M. J.; Ross, P. N.; Bell, A. T.; Tilley, T. D. *J. Phys. Chem. C* **2009**, *113*, 15068.

(55) Markova-Deneva, I. *J. University Chem. Tech. Metallurgy* **2010**, *45*, 351.

(56) Murdock, R. C.; Braydich-Stolle, L.; Schrand, A. M.; Schlager, J. J.; Hussain, S. M. *Toxicol. Sci.* **2008**, *101*, 239.

(57) Sweeney, S. F.; Woehrle, G. H.; Hutchison, J. E. *J. Am. Chem. Soc.* **2006**, *128*, 3190.

(58) Wadhera, A.; Fung, M. *Dermatol. Online.J* **2005**, *11*.

(59) Bhattacharya, R.; Mukherjee, P. *Adv. Drug Deliver. Rev.* **2008**, *60*, 1289.

(60) Klasen, H. J. *Burns* **2000**, *26*, 117.

(61) Klasen, H. J. *Burns* **2000**, *26*, 131.

(62) Moyer, C. A. *Trans. Stud. Coll. Physicians Philadelphia* **1965**, *33*, 53.

(63) Moyer, C. A. *J. Natl. Med. Assoc.* **1965**, *57*, 95.

(64) Moyer, C. A.; Brentano, L.; Gravens, D. L.; Margraf, H. W.; Jr., W. W. M. *Arch. Surg.* **1965**, *90*.

(65) Jain, P. K.; Huang, X.; El-Sayed, I. H.; El-Sayed, M. A. *Accounts Chem. Res.* **2008**, *41*, 1578.

(66) Koh, A. L.; Shachaf, C. M.; Elchuri, S.; Nolan, G. P.; Sinclair, R. *Ultramicroscopy* **2008**, *109*, 111.

(67) Schrand, A. M.; Braydich-Stolle, L. K.; Schlager, J. J.; Dai, L.; Hussain1, S. M. *Nanotechnology* **2008**, 19, 235104.

(68) Nowack, B.; Krug, H. F.; Height, M. *Environ. Sci. Tech.* **2011**, *45*, 1177.

(69) Stensberg, M. C.; Wei, Q.; McLamore, E. S.; Porterfield, D. M.; Wei,

A.; Sep úlveda, M. S. *Nanomed.* **2011**, *6*, 879.

(70) Lem, K. W.; Choudhury, A.; Lakhani, A. A.; Kuyate, P.; Haw, J. R.; Lee, D. S.; Iqbal, Z.; Brumlik, C. J. *Recent Pat Nanotechnol* **2012**, *6*, 60.

(71) *The old kingdom in Egypt and the beginning of the first intermediate period*; Nsmith, W. S., Ed.; The syndics of the Cambridge University press: London, 1962; Vol. 1.

(72) Fricker, S. P. *Gold Bulletin* **1996**, *29*, 53.

(73) Higby, G. J. *Gold Bulletin* **1982**, *15*, 130.

(74) SP, F.; RG, B. *Anticancer Res.* **1996**, *16*, 3755.

(75) MC, D.; D, A. *Chem. Rev.* **2004**, *104*, 293.

(76) Panyala, N. R.; Pe ña-M éndez, E. M.; Havel, J. *J. Appl. Biomed.* **2009**, *7*, 75.

(77) Faulk, W. P.; Taylor, G. M. *Immunochem.* **1971**, *8*, 1081.

(78) Wu, S.-H.; Wu, Y.-S.; Chen, C.-h. *Analy. Chem.* **2008**, *80*, 6560.

(79) Wang, J.; Shao, Y.; Jin, Y.; Wang, F.; Dong, S. *Analy. Chem.* **2005**, *77*, 5760.

(80) Wang, F.; Wang, Y.-C.; Dou, S.; Xiong, M.-H.; Sun, T.-M.; Wang, J. *ACS Nano* **2011**, *5*, 3679.

(81) Guo, S.; Huang, Y.; Jiang, Q.; Sun, Y.; Deng, L.; Liang, Z.; Du, Q.; Xing, J.; Zhao, Y.; Wang, P. C.; Dong, A.; Liang, X.-J. *ACS Nano* **2010**, *4*, 5505.

(82) Boisselier, E.; Astruc, D. *Chem. Soc. Rev.* **2009**, *38*, 1759.

(83) Javier, D. J.; Nitin, N.; Levy, M.; Ellington, A.; Richards-Kortum, R. *Biocon. Chem.***2008**, *19*, 1309.

(84) Shi, X.; Wang, S. H.; Van Antwerp, M. E.; Chen, X.; Baker, J. J. R. *Analyst* **2009**, *134*, 1373.

(85) Wu, X.; Ming, T.; Wang, X.; Wang, P.; Wang, J.; Chen, J. *ACS Nano* **2009**, *4*, 113.

(86) Sun, L.; Liu, D.; Wang, Z. *Langmuir* **2008**, *24*, 10293.

(87) Nam, J.; Won, N.; Jin, H.; Chung, H.; Kim, S. *J. Am. Chem. Soc.*

2009, *131*, 13639.

(88) Kuo, W.-S.; Chang, C.-N.; Chang, Y.-T.; Yang, M.-H.; Chien, Y.-H.; Chen, S.-J.; Yeh, C.-S. *Angew. Chem*. **2010**, *122*, 2771.

(89) Liu, H.; Chen, D.; Li, L.; Liu, T.; Tan, L.; Wu, X.; Tang, F. *Angew.Chem*. **2011**, *123*, 921.

(90) Van de Broek, B.; Devoogdt, N.; D'Hollander, A.; Gijs, H.-L.; Jans, K.; Lagae, L.; Muyldermans, S.; Maes, G.; Borghs, G. *ACS Nano* **2011**, *5*, 4319.

(91) Brook, R. D.; Franklin, B.; Cascio, W.; Hong, Y.; Howard, G.; Lipsett, M.; Luepker, R.; Mittleman, M.; Samet, J.; Smith, S. C.; Tager, I. *Circulation* **2004**, *109*, 2655.

(92) Abelsohn, A.; Stieb, D. M. *Canadian Family Physician* **2011**, *57*, 881.

(93) Rylance, J.; Gordon, S. B.; Naeher, L. P.; Patel, A.; Balmes, J. R.; Adetona, O.; Rogalsky, D. K.; Martin, W. J. *American J. Physi. Lung Cell. Mole. Physi.* **2013**.

(94) Hoet, P.; Bruske-Hohlfeld, I.; Salata, O. *J. Nanobiotech*. **2004**, *2*, 12.

(95) Chang, X.; Zhang, Y.; Tang, M.; Wang, B. *Nanoscale Res. Lett*. **2013**, *8*, 51.

(96) Rossi, E.; Pylkkanen, L.; Koivisto, A.; Nykasenoja, H.; Wolff, H.; Savolainen, K.; Alenius, H. *Part. Fibre Toxic*. **2010**, *7*, 35.

(97) Raemy, D.; Grass, R.; Stark, W.; Schumacher, C.; Clift, M.; Gehr, P.; Rothen-Rutishauser, B. *Part. Fibre Toxic*. **2012**, *9*, 33.

(98) Drake, P. L.; Hazelwood, K. J. *Ann. Occu. Hyg*. **2005**, *49*, 575.

(99) Panyala, N. R.; Pena-Mendez, E. M.; Havel, J. *J. Appl. Biomed* **2008**, *6*, 117.

(100) Takeda, K.; Suzuki, K. I.; Ishihara, A.; Kubo-Irie, M.; Fujimoto, R.; Tabata, M.; Oshio, S.; Nihei, Y.; Ihara, T.; Sugamata, M. *J. Health Sci.* **2009**, *55*, 95.

(101) Geiser, M.; Quaile, O.; Wenk, A.; Wigge, C.; Eigeldinger-Berthou,

S.; Hirn, S.; Schäffler, M.; Schleh, C.; Möller, W.; Mall, M. A.; Kreyling, W. G. *Part. Fibre Toxic.* **2013**, *10*.

(102) Johnston, H. J.; Hutchison, G.; Christensen, F. M.; Peters, S.; Hankin, S.; Stone, V. *Crit. Rev. Toxic.***2010**, *40*, 328.

(103) Wang, B.; Feng, W.; Wang, M.; Wang, T.; Gu, Y.; Zhu, M.; Ouyang, H.; Shi, J.; Zhang, F.; Zhao, Y.; Chai, Z.; Wang, H.; Wang, J. *J. Nanopart. Res.* **2008**, *10*, 263.

(104) Oberdörster, G.; Oberdörster, E.; Oberdörster, J. *Environ Health Perspect* **2005**, *113*, 823.

(105) Ryman-Rasmussen, J. P.; Cesta, M. F.; Brody, A. R.; Shipley-Phillips, J. K.; Everitt, J. I.; Tewksbury, E. W.; Moss, O. R.; Wong, B. A.; Dodd, D. E.; Andersen, M. E.; Bonner, J. C. *Nat. Nano* **2009**, *4*, 747.

(106) Geiser, M. *J Aerosol Med Pulm Drug Deliv* **2010**, *23*, 207.

(107) Semmler-Behnke, M.; Kreyling, W. G.; Lipka, J.; Fertsch, S.; Wenk, A.; Takenaka, S.; Schmid, G.; Brandau, W. *Small* **2008**, *4*, 2108.

(108) Elder, A.; Yang, H.; Gwiazda, R.; Teng, X.; Thurston, S.; He, H.; Oberdörster, G. *Adv. Mat.* **2007**, *19*, 3124.

(109) Furuyama, A.; Kanno, S.; Kobayashi, T.; Hirano, S. *Arch. Toxic.* **2009**, *83*, 429.

(110) Balasubramanian, S. K.; Poh, K.-W.; Ong, C.-N.; Kreyling, W. G.; Ong, W.-Y.; Yu, L. E. *Biomaterials* **2013**, *34*, 5439.

(111) Kim, W.-Y.; Kim, J.; Park, J. D.; Ryu, H. Y.; Yu, I. J. *J. Toxic. Environ. Health Part A* **2009**, *72*, 1279.

(112) Kim, S.; Jeong, S.; Lee, E.; Park, Y.-H.; Bae, H.; Jang, Y.; Maeng, E.; Kim, M.-K.; Son, S. *Toxicol. Environ. Health Sci.* **2011**, *3*, 258.

(113) Schneider, M.; Stracke, F.; Hansen, S.; Schaefer, U. F. *Dermato-Endocrinology* **2009**, *1*, 197.

(114) Senzui, M.; Tamura, T.; Miura, K.; Ikarashi, Y.; Watanabe, Y.; Fujii, M. *J. Toxic. Sci.* **2010**, *35*, 107.

(115) Cross, S.; Innes, B.; Roberts, M.; Tsuzuki, T.; Robertson, T.;

McCormick, P. *Skin Pharmacol Physiol* **2007**, *20*, 148.

(116) Zvyagin, A. V.; Zhao, X.; Gierden, A.; Sanchez, W.; Ross, J. A.; Roberts, M. S. *J. Biomed. Optics* **2008**, *13*, 064031.

(117) Larese, F. F.; D'Agostin, F.; Crosera, M.; Adami, G.; Renzi, N.; Bovenzi, M.; Maina, G. *Toxicology* **2009**, *255*, 33.

(118) Zhang, L. W.; Yu, W. W.; Colvin, V. L.; Monteiro-Riviere, N. A. *Toxic. Appl. Pharma.* **2008**, *228*, 200.

(119) Baroli, B.; Ennas, M. G.; Loffredo, F.; Isola, M.; Pinna, R.; Lopez-Quintela, M. A. *J. Invest. Derma.* **2007**, *127*, 1701.

(120) Rancan, F.; Gao, Q.; Graf, C.; Troppens, S.; Hadam, S.; Hackbarth, S.; Kembuan, C.; Blume-Peytavi, U.; Rühl, E.; Lademann, J.; Vogt, A. *ACS Nano* **2012**, *6*, 6829.

(121) Teow, Y.; Asharani, P. V.; Hande, M. P.; Valiyaveettil, S. *Chem. Commun.* **2011**, *47*, 7025.

(122) Wang, B.; Feng, W.-Y.; Wang, T.-C.; Jia, G.; Wang, M.; Shi, J.-W.; Zhang, F.; Zhao, Y.-L.; Chai, Z.-F. *Toxic. Lett.* **2006**, *161*, 115.

(123) Sonavane, G.; Tomoda, K.; Sano, A.; Ohshima, H.; Terada, H.; Makino, K. *Colloids and Surfaces B* **2008**, *65*, 1.

(124) Abe, S.; Koyama, C.; Esaki, M.; Akasaka, T.; Uo, M.; Kuboki, Y.; Morita, M.; Watari, F. *Bio-Med. Mat. Eng.* **2009**, *19*, 221.

(125) Wang, J. J.; Sanderson, B. J. S.; Wang, H. *Mutation Research/Genetic Toxic. Envir. Mutagene.* **2007**, *628*, 99.

(126) Geiser, M.; Kreyling, W. G. *Particle and Fibre Toxic.* **2010**, *7*, 1.

(127) Zhu, M.-T.; Feng, W.-Y.; Wang, Y.; Wang, B.; Wang, M.; Ouyang, H.; Zhao, Y.-L.; Chai, Z.-F. *Toxicol. Sci.* **2009**, *107*, 342.

(128) He, X.; Zhang, H.; Ma, Y.; WeiBai; Zhang, Z.; Lu, K.; Ding, Y.; Zhao, Y.; Chai, Z. *Nanotechnology* **2010**, *21*, 285103.

(129) Choi, H. S.; Ashitate, Y.; Lee, J. H.; Kim, S. H.; Matsui, A.; Insin, N.; Bawendi, M. G.; Semmler-Behnke, M.; Frangioni, J. V.; Tsuda, A. *Nat Biotech* **2010**, *28*, 1300.

(130) Hussain, S.; Vanoirbeek, J. A. J.; Haenen, S.; Haufroid, V.; Boland, S.; Marano, F.; Nemery, B.; Hoet, P. H. M. *Bio. Med. Res. Int*. **2013**, *2013*, 923475.

(131) Choi, H. S.; Liu, W.; Misra, P.; Tanaka, E.; Zimmer, J. P.; Ipe, B. I.; Bawendi, M. G.; Frangioni, J. V. *Nat. Biotechnol* **2007**, *25*, 1165.

(132) Souris, J. S.; Lee, C.-H.; Cheng, S.-H.; Chen, C.-T.; Yang, C.-S.; Ho, J.-a. A.; Mou, C.-Y.; Lo, L.-W. *Biomaterials* **2010**, *31*, 5564.

(133) Lacerda, L.; Herrero, M. A.; Venner, K.; Bianco, A.; Prato, M.; Kostarelos, K. *Small* **2008**, *4*, 1130.

(134) Abdelhalim, M.; Jarrar, B. *J. Nanobiotech.* **2012**, *10*, 5.

(135) Shin, S.-H.; Ye, M.-K. *Clin. Exp. Otorhinolaryngol* **2012**, *5*, 222.

(136) Stebounova, L.; Adamcakova-Dodd, A.; Kim, J.; Park, H.; O'Shaughnessy, P.; Grassian, V.; Thorne, P. *Part. Fibre Toxic.* **2011**, *8*, 5.

(137) Lin, S.; Zhao, Y.; Nel, A. E.; Lin, S. *Small* **2013**, *9*, 1608.

(138) George, S.; Lin, S.; Ji, Z.; Thomas, C. R.; Li, L.; Mecklenburg, M.; Meng, H.; Wang, X.; Zhang, H.; Xia, T.; Hohman, J. N.; Lin, S.; Zink, J. I.; Weiss, P. S.; Nel, A. E. *ACS Nano* **2012**, *6*, 3745.

(139) Salunkhe, R.; Patil, S.; Patil, C.; Salunke, B. *Parasitol Res.* **2011**, *109*, 823.

(140) Korani, M.; Rezayat, S.; Gilani, K.; Bidgoli, S. A.; Adeli, S. *Int J Nanomedicine* **2011**, *6*, 855.

(141) Panacek, A.; Prucek, R.; Safarova, D.; Dittrich, M.; Richtrova, J.; Benickova, K.; Zboril, R.; Kvitek, L. *Envir. Sci. Tech.* **2011**, *45*, 4974.

(142) Gorth, D. J.; Rand, D. M.; Webster, T. J. *Int. J. Nanomedicine* **2011**, *6*, 343.

(143) Niles, A. L.; Moravec, R. A.; Riss, T. L. *Curr. Chem. Genomics* **2009**, *3*, 33.

(144) Crouch S, K. R., Slater K *J. Immunol. Methods* **1993**, *160*, 81.

(145) Niles, A. L.; Moravec, R. A.; Riss, T. L. *Expert Opin. Drug Discov.* **2008**, *3*, 655.

(146) Kroll, A.; Pillukat, M. H.; Hahn, D.; Schnekenburger, J. *European J. Pharma. Biopharma.* **2009**, *72*, 370.

(147) Hillegass, J. M.; Shukla, A.; Lathrop, S. A.; MacPherson, M. B.; Fukagawa, N. K.; Mossman, B. T. *Wiley Interdiscip. Rev. Nanomed. Nanobiotechnol* **2010**, *2*, 219.

(148) AshaRani, P. V.; Low Kah Mun, G.; Hande, M. P.; Valiyaveettil, S. *ACS Nano* **2008**, *3*, 279.

(149) Wang, T.; Bai, J.; Jiang, X.; Nienhaus, G. U. *ACS Nano* **2012**, *6*, 1251.

(150) Estrela-Lopis, I.; Romero, G.; Rojas, E.; Moya, S. E.; Donath1, E. *J Physics* **2011**, *304*, 012017.

(151) Davda, J.; Labhasetwar, V. *Int. J. Pharma.* **2002**, *233*, 51.

(152) Mu, Q.; Hondow, N.; Krzeminski, L.; Brown, A.; Jeuken, L.; Routledge, M. *Part. Fibre Toxic.* **2012**, *9*, 29.

(153) Zhang, L. W.; Monteiro-Riviere, N. A. *Toxicol. Sci.* **2009**, *110*, 138.

(154) Zhu, Z.-J.; Ghosh, P. S.; Miranda, O. R.; Vachet, R. W.; Rotello, V. M. *J. Am. Chem. Soc.* **2008**, *130*, 14139.

(155) Fischer, H. C.; Chan, W. C. W. *Curr. Op. Biotech.* **2007**, *18*, 565.

(156) Marquis, B. J.; Love, S. A.; Braun, K. L.; Haynes, C. L. *Analyst* **2009**, *134*, 425.

(157) Maurer-Jones, M. A.; Haynes, C. L. *J. Law, Med. Ethics* **2012**, *40*, 795.

(158) Khlebtsov, N.; Dykman, L. *Chem. Soc. Rev.* **2011**, *40*, 1647.

(159) Wang, L.; Li, Y.-F.; Zhou, L.; Liu, Y.; Meng, L.; Zhang, K.; Wu, X.; Zhang, L.; Li, B.; Chen, C. *Analy. Bioanaly. Chem.* **2010**, *396*, 1105.

(160) Darien, B. J.; Sims, P. A.; Kruse-Elliott, K. T.; Homan, T. S.; Cashwell, R. J.; Albrecht, R. M. *Scanning Microsc* **1995**, *9*, 773.

(161) Fujita, K.; Morimoto, Y.; Ogami, A.; Myojyo, T.; Tanaka, I.; Shimada, M.; Wang, W.-N.; Endoh, S.; Uchida, K.; Nakazato, T.; Yamamoto, K.; Fukui, H.; Horie, M.; Yoshida, Y.; Iwahashi, H.; Nakanishi, J. *Toxicology*

2009, *258*, 47.

(162) Hussain, S. M.; Hess, K. L.; Gearhart, J. M.; Geiss, K. T.; Schlager, J. J. *Toxicol. in Vitro* **2005**, *19*, 975.

(163) Braydich-Stolle, L.; Hussain, S.; Schlager, J. J.; Hofmann, M.-C. *Toxicol Sci.* **2005**, *88*, 412.

(164) Shrivastava, S.; Bera, T.; Singh, S. K.; Singh, G.; Ramachandrarao, P.; Dash, D. *ACS Nano* **2009**, *3*, 1357.

(165) Asharani, P. V.; Sethu, S.; Vadukumpully, S.; Zhong, S.; Lim, C. T.; Hande, M. P.; Valiyaveettil, S. *Adv. Fun. Mat.* **2010**, *20*, 1233.

(166) Mahmoudi, M.; Hofmann, H.; Rothen-Rutishauser, B.; Petri-Fink, A. *Chem. Rev.* **2011**, *112*, 2323.

(167) Di Franco, S.; Mancuso, P.; Benfante, A.; Spina, M.; Iovino, F.; Dieli, F.; Stassi, G.; Todaro, M. *Cancers* **2011**, *3*, 1957.

(168) Todaro, M.; Francipane, M. G.; Medema, J. P.; Stassi, G. *Gastroenterology* **2010**, *138*, 2151.

(169) Botchkina, G. *Cancer Lett.* **2012**, 137, 3489.

(170) Neuzil, J.; Stantic, M.; Zobalova, R.; Chladova, J.; Wang, X.; Prochazka, L.; Dong, L.; Andera, L.; Ralph, S. J. *Biochem. Biophy. Res. Comm.* **2007**, *355*, 855.

(171) Vinogradov, S.; Wei, X. *Nanomedicine* **2012**, *7*, 597.

(172) Burke, A. R.; Singh, R. N.; Carroll, D. L.; Wood, J. C. S.; D'Agostino Jr, R. B.; Ajayan, P. M.; Torti, F. M.; Torti, S. V. *Biomaterials* **2012**, *33*, 2961.

(173) Wang, J.; Sefah, K.; Altman, M. B.; Chen, T.; You, M.; Zhao, Z.; Huang, C. Z.; Tan, W. *Chemistry – An Asian Journal* **2013**, *10*, 2417.

(174) Grivennikov, I. A. *Biochemistry Moscow.* **2008**, *73*, 1438.

(175) Brodhun, M.; Bauer, R.; Patt, S. *Exper. Toxicol. Pathology* **2004**, *56*, 103.

(176) Tarantino, U.; Cerocchi, I.; Celi, M.; Scialdoni, A.; Saturnino, L.; Gasbarra, E. *Clin. Cases Miner Bone Metab.* **2009**, *6*, 144.

(177) Shi, C.; Zhu, Y.; Su, Y.; Cheng, T. *Trends in biotech*. **2006**, *24*, 48.

(178) Yi, C.; Liu, D.; Fong, C.-C.; Zhang, J.; Yang, M. *ACS Nano* **2010**, *4*, 6439.

(179) Smith, L. A.; Liu, X.; Hu, J.; Ma, P. X. *Biomaterials* **2010**, *31*, 5526.

(180) Greulich, C.; Kittler, S.; Epple, M.; Muhr, G.; Köller, M. *Langenbecks Arch Surg* **2009**, *394*, 495.

(181) Liu, H.; Ma, L.; Liu, J.; Zhao, J.; Yan, J.; Hong, F. *Toxicol. Envir. Chem*. **2010**, *92*, 175.

(182) Saber, A.; Jacobsen, N.; Mortensen, A.; Szarek, J.; Jackson, P.; Madsen, A.; Jensen, K.; Koponen, I.; Brunborg, G.; Gutzkow, K.; Vogel, U.; Wallin, H. *Part. Fibre Toxic.* **2012**, *9*, 4.

(183) Arnida; Janát-Amsbury, M. M.; Ray, A.; Peterson, C. M.; Ghandehari, H. *European J. Pharma. Biopharm*. **2011**, *77*, 417.

(184) Huang, X.; Li, L.; Liu, T.; Hao, N.; Liu, H.; Chen, D.; Tang, F. *ACS Nano* **2011**, *5*, 5390.

(185) Baek M, C. H., Yu J, Lee JA, Kim TH, Oh JM, Lee WJ, Paek SM, Lee JK, Jeong J, Choy JH, Choi SJ *Int. J. Nanomed.* **2012**, *2012*, 3081.

(186) Manabe, M.; Tatarazako, N.; Kinoshita, M. *Aquatic Toxico.* **2011**, *105*, 576.

(187) Jenkins, J. T.; Halaney, D. L.; Sokolov, K. V.; Ma, L. L.; Shipley, H. J.; Mahajan, S.; Louden, C. L.; Asmis, R.; Milner, T. E.; Johnston, K. P.; Feldman, M. D. *Nanomed. Nanotech. Bio. Med.* **2013**, *9*, 356.

(188) Bar-Ilan, O.; Albrecht, R. M.; Fako, V. E.; Furgeson, D. Y. *Small* **2009**, *5*, 1897.

(189) Howe, K.; Clark, M. D.; Torroja, C. F.; Torrance, J.; Berthelot, C.; Muffato, M.; Collins, J. E.; Humphray, S.; McLaren, K.; Matthews, L.; McLaren, S.; Sealy, I.; Caccamo, M.; Churcher, C.; Scott, C.; Barrett, J. C.; Koch, R.; Rauch, G.-J.; White, S.; Chow, W.; Kilian, B.; Quintais, L. T.; Guerra-Assuncao, J. A.; Zhou, Y.; Gu, Y.; Yen, J.; Vogel, J.-H.; Eyre, T.; Redmond, S.; Banerjee, R.; Chi, J.; Fu, B.; Langley, E.; Maguire, S. F.; Laird,

G. K.; Lloyd, D.; Kenyon, E.; Donaldson, S.; Sehra, H.; Almeida-King, J.; Loveland, J.; Trevanion, S.; Jones, M.; Quail, M.; Willey, D.; Hunt, A.; Burton, J.; Sims, S.; McLay, K.; Plumb, B.; Davis, J.; Clee, C.; Oliver, K.; Clark, R.; Riddle, C.; Eliott, D.; Threadgold, G.; Harden, G.; Ware, D.; Mortimer, B.; Kerry, G.; Heath, P.; Phillimore, B.; Tracey, A.; Corby, N.; Dunn, M.; Johnson, C.; Wood, J.; Clark, S.; Pelan, S.; Griffiths, G.; Smith, M.; Glithero, R.; Howden, P.; Barker, N.; Stevens, C.; Harley, J.; Holt, K.; Panagiotidis, G.; Lovell, J.; Beasley, H.; Henderson, C.; Gordon, D.; Auger, K.; Wright, D.; Collins, J.; Raisen, C.; Dyer, L.; Leung, K.; Robertson, L.; Ambridge, K.; Leongamornlert, D.; McGuire, S.; Gilderthorp, R.; Griffiths, C.; Manthravadi, D.; Nichol, S.; Barker, G.; Whitehead, S.; Kay, M. *Nature* **2013**, *496*, 498.

(190) Schier, A. F. *Nature* **2013**, *496*, 443.

(191) Fako, V. E.; Furgeson, D. Y. *Adv. Drug Del. Rev.* **2009**, *61*, 478.

(192) Hill, A. J.; Teraoka, H.; Heideman, W.; Peterson, R. E. *Toxicol. Sci.* **2005**, *86*, 6.

(193) Mackay, C. E. H., K.M. *Boca raton: CRC Press Taylor & Francis.* **2009**, *Chapter 7*.

(194) Pan, Y.; Neuss, S.; Leifert, A.; Fischler, M.; Wen, F.; Simon, U.; Schmid, G.; Brandau, W.; Jahnen-Dechent, W. *Small* **2007**, *3*, 1941.

(195) Akhavan, O.; Ghaderi, E.; Akhavan, A. *Biomaterials* **2012**, *33*, 8017.

(196) Park, M.; Neigh, A. M.; Vermeulen, J. P.; de la Fonteyne, L. J. J.; Verharen, H. W.; Briede, J. J.; van Loveren, H.; de Jong, W. H. *Biomaterials* **2011**, *32*, 9810.

(197) Zhang, L.; Bai, R.; Li, B.; Ge, C.; Du, J.; Liu, Y.; Le Guyader, L.; Zhao, Y.; Wu, Y.; He, S.; Ma, Y.; Chen, C. *Toxic. Lett.* **2011**, *207*, 73.

(198) Maupas, C.; Moulari, B.; Béduneau, A.; Lamprecht, A.; Pellequer, Y. *Int. J. Pharma.* **2011**, *411*, 136.

(199) Yu, T.; Malugin, A.; Ghandehari, H. *ACS Nano* **2011**, *5*, 5717.

(200) Elbakry, A.; Wurster, E.-C.; Zaky, A.; Liebl, R.; Schindler, E.;

Bauer-Kreisel, P.; Blunk, T.; Rachel, R.; Goepferich, A.; Breunig, M. *Small* **2012**, *8*, 3847.

(201) Li, L.; Sun, J.; Li, X.; Zhang, Y.; Wang, Z.; Wang, C.; Dai, J.; Wang, Q. *Biomaterials* **2012**, *33*, 1714.

(202) Park, J.; Lim, D.-H.; Lim, H.-J.; Kwon, T.; Choi, J.-s.; Jeong, S.; Choi, I.-H.; Cheon, J. *Chem. Commun.* **2011**, *47*, 4382.

(203) Park, M. V. D. Z.; Neigh, A. M.; Vermeulen, J. P.; de la Fonteyne, L. J. J.; Verharen, H. W.; Briedé, J. J.; van Loveren, H.; de Jong, W. H. *Biomaterials* **2011**, *32*, 9810.

(204) Sur, I.; Cam, D.; Kahraman, M.; Baysal, A.; Culha, M. *Nanotechnology* **2010,** *21*,175104.

(205) Oh, E.; Delehanty, J. B.; Sapsford, K. E.; Susumu, K.; Goswami, R.; Blanco-Canosa, J. B.; Dawson, P. E.; Granek, J.; Shoff, M.; Zhang, Q.; Goering, P. L.; Huston, A.; Medintz, I. L. *ACS Nano* **2011**, *5*, 6434.

(206) Yen, H. J.; Hsu, S. H.; Tsai, C. L. *Small* **2009**, *5*, 1553.

(207) Liu, W.; Wu, Y.; Wang, C.; Li, H. C.; Wang, T.; Liao, C. Y.; Cui, L.; Zhou, Q. F.; Yan, B.; Jiang, G. B. *Nanotoxicology* **2010**, *4*, 319.

(208) Peng, H.; Zhang, X.; Wei, Y.; Liu, W.; Li, S.; Yu, G.; Fu, X.; Cao, T.; Deng, X. *J. Nano Mat.* **2012**, *2012*, 9.

(209) Cho, E. C.; Au, L.; Zhang, Q.; Xia, Y. *Small* **2010**, *6*, 517.

(210) Lim, D.-H.; Jang, J.; Kim, S.; Kang, T.; Lee, K.; Choi, I.-H. *Biomaterials* **2012**, *33*, 4690.

(211) Yen, H.-J.; Hsu, S.-h.; Tsai, C.-L. *Small* **2009**, *5*, 1553.

(212) Cui, W.; Li, J.; Zhang, Y.; Rong, H.; Lu, W.; Jiang, L. *Nanomed. Nanotech. Bio. Med.* **2012**, *8*, 46.

(213) Oh, W. K.; Kim, S.; Choi, M.; Kim, C.; Jeong, Y. S.; Cho, B. R.; Hahn, J. S.; Jang, J. *ACS Nano* **2010**, *4*, 5301.

(214) Passagne, I.; Morille, M.; Rousset, M.; Pujalté, I.; L'Azou, B. *Toxicology* **2012**, *299*, 112.

(215) Oh, W. K.; Kim, S.; Yoon, H.; Jang, J. *Small* **2010**, *6*, 872.

(216) Simon-Deckers, A.; Loo, S.; Mayne-L'Hermite, M.; Herlin-Boime, N.; Menguy, N.; Reynaud, C.; Gouget, B.; Carriere, M. *Envir. Sci. Tech.* **2009**, *43*, 8423.

(217) Liu, W.; Yeh, Y. C.; Lipner, J.; Xie, J.; Sung, H. W.; Thomopoulos, S.; Xia, Y. *Langmuir* **2011**, *27*, 9088.

(218) Peng, X.; Palma, S.; Fisher, N. S.; Wong, S. S. *Aquatic Toxico.* **2011**, *102*, 186.

(219) Yang, K.; Ma, Y.-Q. *Nat. Nano* **2010**, *5*, 579.

(220) George, S.; Lin, S. J.; Jo, Z. X.; Thomas, C. R.; Li, L. J.; Mecklenburg, M.; Meng, H.; Wang, X.; Zhang, H. Y.; Xia, T.; Hohman, J. N.; Lin, S.; Zink, J. I.; Weiss, P. S.; Nel, A. E. *ACS Nano* **2012**, *6*, 3745.

(221) Pal, S.; Tak, Y. K.; Song, J. M. *Appl. Environ. Microbio.* **2007**, *73*, 1712.

(222) Ispas, C.; Andreescu, D.; Patel, A.; Goia, D. V.; Andreescu, S.; Wallace, K. N. *Environ. Sci. Technol.* **2009**, *43*, 6349.

(223) Morones, J. R.; Elechiguerra, J. L.; Camacho, A.; Holt, K.; Kouri, J. B.; Ramirez, J. T.; Yacaman, M. J. *Nanotechnology* **2005**, *16*, 2346.

(224) Huang, X. L.; Li, L. L.; Liu, T. L.; Hao, N. J.; Liu, H. Y.; Chen, D.; Tang, F. Q. *ACS Nano* **2011**, *5*, 5390.

(225) Schaeublin, N. M.; Braydich-Stolle, L. K.; Maurer, E. I.; Park, K.; MacCuspie, R. I.; Afrooz, A. R. M. N.; Vaia, R. A.; Saleh, N. B.; Hussain, S. M. *Langmuir* **2012**, *28*, 3248.

(226) Wang, X.; Wu, H.-F.; Kuang, Q.; Huang, R.-B.; Xie, Z.-X.; Zheng, L.-S. *Langmuir* **2009**, *26*, 2774.

(227) Hsiao, I. L.; Huang, Y.-J. *Sci. Total Envir.* **2011**, *409*, 1219.

(228) Oh, W.-K.; Kim, S.; Kwon, O.; Jang, J. *J. Nanosci. Nanotech.* **2011**, *11*, 4254.

(229) Cheng, J.; Cheng, S. H. *Int. J. Nanomed.* **2012**, *7*, 3731.

(230) Nelson, S. M.; Mahmoud, T.; Beaux, M.; Shapiro, P.; McIlroy, D. N.; Stenkamp, D. L. *Nanomed. Nanotech. Biol. Med.* **2010**, *6*, 93.

(231) Hamilton, R.; Wu, N.; Porter, D.; Buford, M.; Wolfarth, M.; Holian, A. *Part. Fibre Toxic.* **2009**, *6*, 35.

(232) Alkilany, A. M.; Nagaria, P. K.; Hexel, C. R.; Shaw, T. J.; Murphy, C. J.; Wyatt, M. D. *Small* **2009**, *5*, 701.

(233) Parab, H. J.; Chen, H. M.; Lai, T.-C.; Huang, J. H.; Chen, P. H.; Liu, R.-S.; Hsiao, M.; Chen, C.-H.; Tsai, D.-P.; Hwu, Y.-K. *J. Physic. Chem. C* **2009**, *113*, 7574.

(234) Niidome, T.; Yamagata, M.; Okamoto, Y.; Akiyama, Y.; Takahashi, H.; Kawano, T.; Katayama, Y.; Niidome, Y. *J. Contro. Release* **2006**, *114*, 343.

(235) Grabinski, C.; Schaeublin, N.; Wijaya, A.; D'Couto, H.; Baxamusa, S. H.; Hamad-Schifferli, K.; Hussain, S. M. *ACS Nano* **2011**, *5*, 2870.

(236) Takahashi, H.; Niidome, Y.; Niidome, T.; Kaneko, K.; Kawasaki, H.; Yamada, S. *Langmuir* **2005**, *22*, 2.

(237) Hauck, T. S.; Ghazani, A. A.; Chan, W. C. W. *Small* **2008**, *4*, 153.

(238) Goodman, C. M.; McCusker, C. D.; Yilmaz, T.; Rotello, V. M. *Biocon. Chem.* **2004**, *15*, 897.

(239) Zhu, Z.-J.; Carboni, R.; Quercio, M. J.; Yan, B.; Oscar R. Miranda; Anderton, D. L.; Arcaro, K. F.; Rotello, V. M.; Vachet, R. W. *Small* **2010**, *6*, 2261.

(240) Chompoosor, A.; Saha, K.; Ghosh, P. S.; Macarthy, D. J.; Miranda, O. R.; Zhu, Z.-J.; Arcaro, K. F.; Rotello, V. M. *Small* **2010**, *6*, 2246.

(241) El Badawy, A. M.; Silva, R. G.; Morris, B.; Scheckel, K. G.; Suidan, M. T.; Tolaymat, T. M. *Environ. Sci. Tech.* **2010**, *45*, 283.

(242) Chung, T.-H.; Wu, S.-H.; Yao, M.; Lu, C.-W.; Lin, Y.-S.; Hung, Y.; Mou, C.-Y.; Chen, Y.-C.; Huang, D.-M. *Biomaterials* **2007**, *28*, 2959.

(243) Chen, L.; Mccrate, J. M.; Lee, J. C-M.; Li, H. *Nanotechnology* **2011**, *22*, 105708.

(244) Asati, A.; Santra, S.; Kaittanis, C.; Perez, J. M. *ACS Nano* **2010**, *4*, 5321.

(245) Schaeublin, N. M.; Braydich-Stolle, L. K.; Schrand, A. M.; Miller, J.

M.; Hutchison, J.; Schlager, J. J.; Hussain, S. M. *Nanoscale* **2011**, *3*, 410.

(246) Studer, A. M.; Limbach, L. K.; Van Duc, L.; Krumeich, F.; Athanassiou, E. K.; Gerber, L. C.; Moch, H.; Stark, W. J. *Toxic. Lett*. **2010**, *197*, 169.

(247) Teow, Y.; Valiyaveettil, S. *Nanoscale* **2010**, *2*, 2607.

(248) Patra, H. K.; Banerjee, S.; Chaudhuri, U.; Lahiri, P.; Dasgupta, A. K. *Nanomed. Nanotech. Bio. Med.* **2007**, *3*, 111.

(249) Yin, H.; Casey, P. S.; McCall, M. J.; Fenech, M. *Langmuir* **2010**, *26*, 15399.

(250) Lu, W.; Senapati, D.; Wang, S.; Tovmachenko, O.; Singh, A. K.; Yu, H.; Ray, P. C. *Chem. Physics Lett*. **2010**, *487*, 92.

(251) Jarvie, H. P.; King, S. M. *Nano Today* **2010**, *5*, 248.

(252) Wong, S. W. Y.; Leung, P. T. Y.; Djurisic, A. B.; Leung, K. M. Y. *Anal. Bioanal. Chem*. **2010**, *396*, 609.

(253) Glover, R. D.; Miller, J. M.; Hutchison, J. E. *ACS Nano* **2011**, *5*, 8950.

(254) Liu, J. Y.; Sonshine, D. A.; Shervani, S.; Hurt, R. H. *ACS Nano* **2010**, *4*, 6903.

CHAPTER 2

MATERIALS AND METHODS

2.1 Chemicals

Nanoparticle synthesis was carried out using a standard procedure through reduction of silver or gold salt.[1] All glasswares used for the synthesis were treated with piranha solution [30% hydrogen peroxide/concentrated sulphuric acid in 3:1 ratio] and washed thoroughly in ultrapure water (Millipore Corporation).

The following chemicals were used as received from commercial suppliers. Silver nitrate ($AgNO_3$), potassium gold (III) chloride ($KAuCl_4$), ethylene glycol (EG, 99.8%) and polyvinylpyrrolidone (PVP, Mw = 40 000) were purchased from Sigma Ardrich. 1, 6-Hexanediol (+97%) were purchased from Tokyo Chemical Industry Company. Calcium chloride dihydrate ($CaCl_2$ $2H_2O$) was purchased from MERCK. All chemicals were used without further purification.

Dry mint leaves and ginger rhizome were purchased from local Chinese traditional medicine shops, while pure soluble coffee (NESCAFE Gold), 100% freeze-dried soluble coffee (Nestle Korea Ltd.) was purchased from local supermarket in Singapore. Millipore water was used in all the preparations.

2.2 Synthesis of nanomaterials

2.2.1 Synthesis of Ag-mint, Ag-ginger and Ag-coffee nps

The plant material extracts were used as both reducing agents and capping agents in this project and their selection was done based on their effects for enhancing the solubility and stability of Ag nps. The extracts could reduce silver nitrate into Ag nps at room temperature without adding other reducing agents.[2,3]

Dried mint leaves (5 g) were washed triplicates with 200 mL Millipore water before boiling in 350 mL water until volume reduced to 150 mL, the final solution was filtered with filter paper. The dry powder of extracts was

obtained by freeze drying process. The extracts were freeze at -20 ℃ overnight before dried with a vacuum pump for 2-3 days. No attempt was made to purify or isolate compounds in the extracts. Finally, the appropriate amount of mint extract powder was weighed and dissolved in millipore water to obtain a standard mint extract solution. Ag-mint nanoparticles were synthesized by reducing silver nitrate solution with mint extracts solution at the ratio of m_{Ag}/m_{mint} = 1/5 under constant stirring at room temperature. The color of the solution was changed to yellowish brown with time, indicating nanoparticle formation. The mixture was stirred for an additional 2 h. Ag nps were purified using repeated centrifuging and washing with water to remove any traces of unbound mint extracts, dispersed in pure water and used for structural characterization.

Ginger extracts was generated from dried ginger rhizome following the above procedures while pure soluble coffee (NESCAFE Gold) were used directly for coffee extracts. Ag-ginger nanoparticles and Ag-coffee nanoparticles were synthesized as described above for Ag-mint nanoparticles. All three Ag nps showed high dispersion and solubility at high concentrations during the cell viability studies.

2.2.2 Synthesis of Ag nanocubes - Ag cube 1

The silver nanocubes were synthesized by adopting a reported procedure.[4] Briefly, 5 ml of anhydrous ethylene glycol was heated at 160 ℃ for 1 h under nitrogen atmosphere. $AgNO_3$ (0.127 g, 0.75 mmol) and PVP (0.125 g, 1.13 mmol) were dissolved separately in ethylene glycol (each 3 mL) and simultaneously injected to the reaction flask by using two syringes at a rate of 0.2 mL in 30 second interval. The reaction mixture was further heated at 160 ℃ for another 45 min which showed the formation of gray color suspension, cooled to room temperature and diluted with Millipore water (50 mL). SEM images of the reaction mixture showed nanocubes formation along with a few rods. The nanocubes were purified by centrifuging the solution and

then washing with water for three times. At the last stage, the pellet was washed with acetone and dried under vacuum oven.

2.2.3 Synthesis of Ag nanowires

Synthesis of Ag nanowires was achieved using similar procedures as that of Ag nanocubes, however the $AgNO_3$ and PVP were mixed together prior to addition in the reaction flask. Briefly, $AgNO_3$ (0.127 g, 0.75 mmol) and PVP (0.125 g, 1.13 mmol) were dissolved separately in ethylene glycol (each 3 mL) and mixed together at room temperature and kept for 45 min, after which the solution turned light yellow. A combined solution of PVP/$AgNO_3$ (6 mL) was injected to the reaction flask, containing ethylene glycol (5 mL) preheated at 160 ℃ for 1h, at a rate of 0.4 mL with 30 second interval. After the addition, the reaction was stirred for 45 min and the temperature was slowly raised to 180 ℃. A gray colored precipitate appeared and the reaction was stirred for 45 min, cooled to room temperature and diluted with Millipore water (50 mL). The Ag nanowires were separated using centrifugation, washed and dried under vacuum.

2.2.4 Synthesis of Ag truncated nanocubes - Ag cube 2

The procedure of synthesis of Ag truncated nanocubes was through modifying the reported procedure for synthesis of silver nanocubes.[5] In a typical synthesis, anhydrous ethylene glycol (5 mL) was heated at 160 ℃ for 1.5 h; then separate solutions of $AgNO_3$ (0.425 g, 2.50 mmol) and PVP (0.383 g, 3.45 mmol) in ethylene glycol (each 3 mL) were simultaneously injected into the reaction flask by using a two-channel syringe pump at a rate of 500 μL/min. The color of the reaction mixture was changed from colorless to reddish yellow, and to gray. The mixture was stirred at 160 ℃ for another 45 minutes. Truncated cubes were purified by repeated centrifuge and filtration. The pellet obtained after the lyophilization (Freeze Dryer, Alpha 2-4 LD plus, Christ) was redispersed in ultrapure water through sonication to prepare the

stock solutions.

2.2.5 General procedure for the synthesis of shape-controlled Au nanoplates (AuNPs)

Hexagon (HAuNPs), pentagon (PAuNPs) and triangle AuNPs (TAuNPs) were prepared using a modified alkanediol process.[6] Stock solution of PVP (1.24 g) and $KAuCl_4$ (0.075 mmol, 28.3 mg) were dissolved in 3 mL 1, 6-HEXANEDIOL solution at 80 ℃, separately, and kept warming until injection. Different concentrations of $CaCl_2$ solutions were employed for controlling shape formation of AuNPs. Stock solutions of calcium chloride dihydrate at various concentrations of Au were prepared with Au/Ca ratio of 200/1 (Au:Ca = 200:1), 400/1 and 800/1 in 1, 6-HEXANEDIOL solution. Solution of $CaCl_2$ (0.15 mL) was added to 5.0 mL 1, 6-HEXANEDIOL solution at 220 ℃. PVP (3.0 mL) and $KAuCl_4$ (3.0 mL) stock solutions were alternatively injected every 30 seconds over 9 min under vigorous stirring. Note that simultaneous injection of both solutions or injection of $KAuCl_4$ stock solution to 8 mL PVP 1, 6-HEXANEDIOL solution changed the shape formation. After the injection, the resulting mixture was kept for 1 hour and cooled to room temperature. The nanoplates formed were washed with ethanol and water three times to remove excess amount of PVP and collected by centrifugation. All nanoplates were dried using lypholization and resuspended in an appropriate amount of ultrapure water to prepare a stock solution.

2.2.6 Synthesis of Ag-PVP and Au-PVP nps

Briefly, 2 ml of $AgNO_3$ stock solution (0.1 M) and 400 mg PVP dissolved in 8 ml of ultrapure water were added to 188 ml of ultrapure water in a flask. Further, 40 mg of $NaBH_4$ dissolved in 2 ml of ultrapure water were added dropwise to the resulting mixture while stirring. The color of the solution immediately changed to reddish-brown. The solution continued stirring for 24 hours at room temperature to react completely. A similar procedure was

carried out to synthesize Au nps by replacing 2 mL of $AgNO_3$ stock solution (0.1 M) with 2mL of $HAuCl_4$ stock solution (0.1 M) during the reaction.

After synthesis, the nanoparticles solution was centrifuged and washed with ultrapure water several times to remove any unreacted or excess reagents. The pellet obtained was resuspended in ultrapure water and filtered through a 0.2 μm filter to remove any aggregates. The nanoparticles solution was freeze-dried and the resulting powder was resuspended in ultrapure water for preparation of nanoparticles stock solution.

2.3 Characterization of nanomaterials

2.3.1 Transmission electron microscopy (TEM)

The size and morphology of Ag-mint, Ag-coffee, Ag-ginger nanoparticles, Ag-PVP nanoparticles, Au-PVP nanoparticles and AuNPs were observed with JEOL 2010-F Field Emission Transmission Electron Microscope (FETEM). Briefly, aqueous solution of Ag NMs (10 μL) was dropped on the copper grids and left dried in air. Then the samples were imaged using TEM.

2.3.2 Scanning electron microscope (SEM)

The morphology of Ag cube1, cube 2 and nanowires were observed with JEOL JSM-6701F field emission scanning electron microscope (FESEM). For sample preparation, a dilute solution of Ag NMs was dispersed in ultrapure water, placed onto 12 mm cover glass (Marlenfeld GmbH) and left to dry in oven (70 ℃) for overnight and used for SEM.

2.3.3 Elemental analysis

Elemental analysis of freeze-dried Ag-mint, Ag-ginger, Ag-coffee, Ag-PVP and Au-PVP nanoparticles was analyzed for their respective elemental composition. Presence of carbon, hydrogen and nitrogen content was detected using Elementar Vario Micro Cube. Inductively-coupled plasma (ICP) analysis (Dual-view Optima 5300 DV ICP-OES) was used for the

determination silver level in digested solutions of Ag nps.

2.3.4 X-ray diffraction

X-ray diffraction (XRD) pattern of Ag and Au NMs were recorded using Bruker-AXS: D8 DISCOVER with GADDS Powder X-ray diffractometer with Cu-Kα (λ = 1.54 Å) at 40 kV and 40 mA over a range of 2θ angle from 5 ° to 90 °. For sample preparation, Ag and Au NMs solutions were deposited onto cover glass (Marlenfeld GmbH) and dried in oven (70 ℃). The process was repeated several times to get a thick layer suitable for XRD analysis.

2.3.5 Surface plasmon resonance (SPR) properties

The surface plasmon resonance properties of nanomaterials were evaluated by their ultraviolet–visible **(**UV-Vis) measurements. The absorption spectra of nanomaterials aqueous solution were recorded on either UV-Vis-NIR spectrophotometer (Shimadzu UV-3600PC) or UV-Vis spectrophotometer (Shimadzu UV-1601PC). The measurements were conducted at room temperature.

2.3.6 Dynamic Light Scattering (DLS)

Dynamic light scattering (DLS) of nanomaterials aqueous solution were done using Malvern Zetasizer Nano-ZS90 at room temperature.

Colloidal stability of Ag NMs (Ag cube 1, cube 2 and nanowires) in different disperse solutions was measured. Ag NMs stock solution was diluted with water, Dulbecco's modified eagles medium (DMEM, HyClone) and DMEM with fetal bovine serum (FBS, GIBCO) (10%) to a final concentration 25 and 100 μg/mL and incubated for 24 hours before the analysis was performed. The DLS measurements were performed on Malvern Zetasizer Nano-ZS90. After a 30 seconds equilibration step at 25 ℃, each sample underwent three measurements. Intensity distribution data were considered for the analysis. Values were obtained by averaging the three measurements.

For Ag-PVP and Au-PVP nanoparticles, the aggregation and hydrodynamic size of nanoparticles in different solutions were measured by DLS. Ag nps stock solution were diluted with water, phosphate buffered saline (PBS, Biological Industries), serum free medium and medium with serum to a final concentration 50 μg/mL and incubated for 24 hours before the analysis was performed. The DLS measurements were performed on Malvern Zetasizer Nano-ZS90. After a 30 seconds equilibration step at 25 ℃, each sample underwent three measurements. Read number and duration for each measurement were set on 'automatic' on the Zetasizer control software. Only intensity distribution data were considered for the analysis. Values were obtained by averaging the three measurements.

Colloidal stability of Ag NMs (Ag cube 1, cube 2 and nanowires) in different disperse solutions was measured by DLS. Ag NMs stock solution was diluted with water, DMEM and DMEM with FBS (10%) to a final concentration 25 and 100 μg/mL and incubated for 24 hours before the analysis was performed. The DLS measurements were performed on Malvern Zetasizer Nano-ZS90. After a 30 seconds equilibration step at 25 ℃, each sample underwent three measurements. Intensity distribution data were considered for the analysis. Values were obtained by averaging the three measurements.

2.3.7 Surface charge of nanomaterials

Surface charge of nanomaterials was detected through zeta potential measurements performed on the Zetasizer Nano-ZS90 (Malvern Instruments).

Surface charge of Ag NMs (Ag cube 1, cube 2 and nanowires) in different disperse solutions was measured. Ag NMs were prepared using the similar procedures described above in DLS part and detected in triplicates after a 2 minutes equilibration step at 25 ℃.

For Ag-PVP and Au-PVP nanoparticles, nanoparticles stock solution was

diluted with water, PBS, serum-free media and media with serum to a final concentration 50 μg/mL. The measurements were conducted in triplicates on the Zetasizer Nano-ZS90 (Malvern Instruments). The sample was equilibrated at 25 ℃ for 2 minutes, and underwent measurements using the automatic measurement protocols recommended by Malvern.

For Ag NMs (Ag cube 1, cube 2 and nanowires), surface charge of Ag NMs in different solutions was checked using Malvern Zetasizer Nano-ZS90. Ag NMs stock solution was diluted with water, DMEM and DMEM with FBS (10%) to a final concentration 25 and 100 μg/mL and incubated for 24 hours before the analysis was performed. Ag NMs were detected in triplicates after a 2 minutes equilibration step at 25 ℃.

2.3.8 Silver ions release from Ag NMs

Ag NMs (Ag cube 1, cube 2 and nanowires) were dissolved in millipore water to prepare stock solution (2 mg/mL). Freshly prepared stock solutions (100 μL) were diluted with either water or cell culture medium (2 mL) to a final concentration (100 μg/mL). These solutions were kept at room temperature for 1 to 7 days. The resulting suspension was subjected to centrifugation at 10000 rpm for 1 h to remove the solid nanoparticles. The supernatant was filtered with Whatman filter, topped up to 10 mL with water before analysing silver content using ICP-OES (Dual-view Optima 5300 DV, PerkinElmer). The experiment for each group was performed in triplicates and average value is reported.

2.4 Cell culture

2.4.1 Human cancer cell line

Human cancer cell lines HeLa, HepG2 and MCF7 were purchased from commercial sources, American Type Culture Collection, USA. Cells were maintained in DMEM (HyClone) supplemented with 10% FBS (GIBCO) and 1% penicillin streptomycin (Gibco, Invitrogen). Cells were maintained in a 5%

carbon dioxide (CO_2) incubator at 37 ℃.

2.4.2 Human normal cell line

Normal human skin fibroblast cells (Department of Surgery, Yong Loo Lin School of Medicine, National University of Singapore, Singapore) and human dermal fibroblast (HDF, Gibco, Life technologies) were used in the study. Human normal cells were cultured in minimum essential medium (MEM, Gibco, Life technologies) supplemented with 10% FBS (Hyclone), 1% penicillin streptomycin (PAN Biotech GmbH), 1% MEM non-essential amino acids (100X, Gibco, Life technologies) and 1% MEM vitamin solution (100X, Gibco, Life technologies) and maintained in an incubator containing 5% CO_2 at 37 ℃.

2.4.3 Human cancer stem cell line

Human colon cancer stem cell line (colon CSCs) obtained from Celprogen. Cells were cultured in accordance with Celprogen specifications. In brief, cells were cultured in human colon cancer stem cell complete growth medium with the appropriate human colon cancer stem cell extra-cellular matrix (Celprogen) in a water-saturated atmosphere with 5% CO_2 at 37 ℃.

2.4.4 Human embryonic stem cell line

Human embryonic stem cells (HESCs) BG01V were obtained from American Type Culture Collection (ATCC, SCRC-2002), as a frozen stock. BG01V were cultured in a 6-well plate (Greiner Bio-One CELLSTAR) with mitomycin C-treated (mitomycin C, Sigma Aldrich) mouse embryonic fibroblasts (MEF) CF-1 (ATCC, SCRC-1040.2) feeder cells. Cells were cultured at 37℃, in a 5% CO2 atmosphere, in the HESC medium of 80% Dulbecco's Modified Eagle Medium **:** Nutrient Mixture F-12 (DMEM / F-12) (GIBCO, Life technologies), supplemented with 20% knockout serum replacement (GIBCO, Life technologies), 1% MEM non-essential amino acids (100X) (GIBCO, Invitrogen), 2 mmol L^{-1} L-glutamine (GIBCO, Life

technologies), 0.1 mmol·L^{-1} 2-mercaptoethanol (GIBCO, Invitrogen) and 4 ng·mL -1 basic fibroblast growth factor (FGF-basic-147, Cell guidance system). The cell medium were daily changed and cells were passaged every 6-7 days using collagenase Type IV (200 Units/mL) (GIBCO, Invitrogen).

2.4.5 Embryoid body (EB) formation

HESCs in culture were removed from feeder cells using collagenase IV. hESC clusters were transferred to 12-well plate (sterile non-treated, NUNC) and cultured in medium of 80% Dulbecco's Modified Eagle Medium: Nutrient Mixture F-12 (DMEM / F-12), supplemented with 20% knockout serum replacement, 1% MEM non-essential amino acids (100X), 2 mmol·L^{-1} L-glutamine and 0.1 mmol·L^{-1} 2-mercaptoethanol. The medium was changed every second day.

2.5 Preparation of stock solution and treatment

Stock solutions of nanomaterials (1 or 2 mg/mL) were prepared in sterile millipore water and diluted to the required concentrations (Ag nps: 0, 10, 25, 50 and 100 μg/mL; Ag cube1 cube 2 and nanowires: 0, 10, 25, 50, 100 and 200 μg/mL; AuNPs: 0, 25, 50, 100, 200 and 400 μg/mL) using cell culture medium. Cells were cultured in either 24 well plates or 96 well plates overnight. Appropriate concentration of stock solution was added to each well to obtain respective concentration of nanomaterials and incubated for 24 h to 72 h.

2.6 Microscopy

2.6.1 Light microscopy

Cells were plated in cell culture plates and treated with different concentration of nanomaterials. After incubation, cells were photographed to study the morphology changes under an inverted microscope (Olympus 1X71).

2.6.2. TEM of AuNPs treated cells

Ultrathin sections of the cells were analyzed using TEM to reveal the distribution of AuNPs. MCF7 cells (1.5 x 10^6 cells) were seeded in T25 flask (Griener Bio-one GmbH) with 5 mL medium overnight to allow cell proliferation. Thereafter cells were treated with AuNPs (50 μg/mL) in fresh medium for 24 h. At the end of the incubation period, cells were washed with PBS to remove excess unbound AuNPs. Cells were trypsinized, washed with PBS and fixed in 2.5% glutaraldehyde for 2 h. Fixed cells were washed with PBS and post-fixed with 1% osmium tetroxide for 1 h at room temperature. Cells were further washed, dehydrated using alcohol, treated with propylene oxide (30 min), propylene oxide-resin mixture (overnight) and pure resin (overnight) before embedding in beem capsules containing pure resin (70 ℃ for 2 days). Ultrathin sections were cut using Reichert Jung Ultracut, stained with 1% lead citrate and 0.5% uranyl acetate before analyzing with TEM (JEOL JEM 2010F). The presence of AuNPs inside the cells was confirmed using electron-dispersive x-ray analysis (EDX).

2.6.3 SEM observation of Ag NMs treated cells

For SEM imaging of Ag cube 1, cube 2 and nanowires treated cells, human skin fibroblast cells were seeded onto coverslips in a 24-well plate at a density of 10000/well and allowed to adhere and proliferate for 24 h. The cells were then treated with Ag NMs (100 μg/mL) and incubated for 24 h. Thereafter, the cells were washed with PBS several times and fixed in glutaraldehyde (5%) and formaldehyde (4%) in PBS buffer at 4 ℃ for 24 h. The fixed cells were washed 5 times in PBS and then dehydrated using 30%, 50%, 70%, 80%, 90%, 95% and 100% (2X) ethanol. The coverslips were dried, coated with platinum and further analyzed using JEOL JSM 6701F SEM.

2.6.4 Dark field microscopy

The morphology changes of cells treated with coffee, ginger and mint extracts were observed with dark field microscopy (Cyto Viva optical microscopy). Cells were seeded onto coverslips (Marlenfeld GmbH) of a 24-well plate (Greiner Bio-one, Cellstar) at a density of 6 x 10^3 cells per well and allowed to adhere and proliferate for 24 h. The coverslips were washed with 70% ethanol and soaked in sterile phosphate buffered saline (PBS, Vivantis) for 3-5 min before putting inside the 24-well plate. Spent media was removed the next day and replaced with fresh medium along with extracts (20 μg/mL) for 24 h. Untreated cells (control) were treated with medium only. The coverslip was removed from each well, rinsed with sterile PBS solution and placed face-down onto a clean glass slide for observation.

Changes in morphology of cells treated with Ag NMs (20 or 25 μg/mL) were checked with similar procedure as described above.

2.6.5 Confocal microscopy

The distribution of Ag NMs inside the cells was examined by Confocal microscope. Cells were seeded onto coverslips in a 24-well plate at a density of 10000 /well and allowed to adhere and proliferate for 24 h. The cells were then treated with Ag NMs at the concentration of 25 μg/mL and incubated for 24 h. Thereafter, the cells were washed with PBS several times, stained with CellMask™ Deep Red plasma membrane stain (2.5 μg/mL, Invitrogen) for 5 minute at 37 ℃. The staining solution was removed and the cells were fixed with warm 3.75% formaldehyde in PBS at 37℃ for 10 minute. The fixed cells were washed with PBS for 3 times and stained with DAPI (300 nM, Sigma Aldrich) at room temperature for 15 minutes. Thereafter, the coverslip was removed from each well, rinsed with sterile PBS solution and placed face-down onto a clean glass slide for observation under a confocal microscope (Olympus FV1000).

2.7 Cell viability assay

2.7.1 Measurement of ATP content

The viability of cells treated with Ag and Au NMs were measured using CellTiter-Glo luminescent cell viability assay (Promega) following manufacturer's instructions. This assay determines the number of viable cells in a cell culture based on quantification of the adenosine-5'-triphosphate (ATP) present, which signals the presence of metabolically active cells.[7] The assay is based on the conversion of luciferin to oxyluciferin by a recombinant luciferase in the presence of ATP. The observed luminescence is proportional to the quantity of ATP in cells.

The experiments were performed in 96-well plates (Corning, Costar). For the ATP assay, cells were plated in each well and incubated in 100 μL medium overnight for the cells to adhere to the bottom of the well. Spent medium was removed the next day and replaced with fresh medium and the cells were treated with different concentrations of nanomaterials (0, 10, 25, 50 and 100 μg/mL for Ag-coffee, Ag ginger and Ag-mint nanoparticles; 0, 10, 25, 50, 100 and 200 μg/mL for Ag cube 1, cube 2 and nanowires; 0, 25, 50, 100, 200 and 400 μg/mL for AuNPs) for 24 h or 24, 48 and 72 h. At respective time points, 100 μL of CellTiter-Glo viability assay pre-warmed to room temperature was added into each well and mixed properly. After 15 min, luminescence readings were measured using Tecan Infinite F200 microplate reader or BioTek microplate reader (Synergy 4). The dependence of toxicity on Ag nps was studied using mint, ginger and coffee extract stock solutions. Cells were treated with mint, ginger and coffee extracts (100 μg/mL) in 96-well plates for different incubation periods (24 h, 48 h and 72h) and then followed by CellTiter-Glo analysis.

The dependence of toxicity on purity of Ag NMs (Ag cube 1, cube 2 and nanowires) was studied using the supernatants from the centrifugation step.

The supernatant (20 mL) obtained after removing the nanomaterial pellet was concentrated by lyophilization and re-constituted in 1 mL of sterile water. Different volumes of the stock solution (0, 2.5, 5, 10, 15 and 20 μL) were dispensed in to 100 μL of medium in 96-well plates, incubated for 24 h and then followed by CellTiter-Glo analysis.

2.7.2 Mitochondrial function cell viability assay

Mitochondrial activity of cells with nanomaterials treatment was detected by a fluorimetric cell viability assay, CellTiter-Blue (Promega). This assay was used to measure the metabolically active cells in a culture by reducing resazurin in the reagent. Resazurin was reduced by the mitochondrial and microsomal enzymes to resorufin, a highly fluorescent molecule. Cells were seeded in 96-well plates at a density of 5 x 10^3 cells per well and incubated overnight for the cell proliferation. After incubation, cells were treated with different concentrations of nanomaterials (0, 10, 25, 50, 100 and 200 μg/mL for Ag cube 1, cube 2 and nanowires; 0, 25, 50, 100, 200 and 400 μg/mL for AuNPs; 0, 0.1, 0.5, 1.0, 2.5, 5 and 10 μg/mL for Ag-PVP and Au-PVP nanoparticles). Comparison study was conducted by treated cells with Ag and Au ions with similar metal amount as the nanoparticles (PVP capped nanoparticles) were used in the experiment based on elemental analysis results. After incubation, 20 μL of CellTiter-Blue cell viability assay pre-warmed to room temperature was added into each well. Cells were incubated in the dark at 37 ℃ for 2 h before detecting fluorescence using Tecan Infinite F200 microplate reader or BioTek microplate reader (Synergy 4) at 560/590 nm.

2.8 Intracellular reactive oxygen species (ROS) production

The generation of ROS was evaluated by employing 2', 7' - dichlorodihydrofluorescein diacetate (DCF-DA, Sigma Aldrich) staining.[8,9] During incubation, non-fluorescent and non-polar DCFH-DA could passively enter the cells and is deacetylated by cellular esterases to the non-fluorescent

but polar 2', 7'-diclorfluorescein (DCFH), which therefore trap inside the cells. In the presence of intracellular ROS, the non-fluorescent DCFH was converted to a highly florescent compound 2',7'-dichlorfluorescein (DCF). The ROS assay was performed using supplier's instructions. The ROS level can be measured through three different detection methods.

2.8.1 BioTek microplate reader

Approximately 5 x 10^3 cells incubated with Ag-coffee, Ag-ginger and Ag-mint nanoparticles (0, 10, 25, 50, and 100 μg/mL) for 24 h in 96-well plate were washed with PBS twice and incubated with 10 μM DCF-DA for 30 min at 37 ℃ in the dark. Then cells were washed twice with PBS and analyzed by microplate reader (BioTek, Synergy 4) at an excitation wavelength of 485 nm and an emission wavelength of 530 nm.[10]

2.8.2 Olympus microscope

Cells were seeded in 96-well plates at a density of 5 x 10^3 cells per well and incubated overnight to allow cells proliferation. After the cells were treated with nanomaterials at different concentrations (50 and 100 μg/mL for AuNPs; 0, 0.1, 1, and 10 µg/mL for Ag-PVP and Au-PVP nanoparticles) for 24 h, cells were washed twice with phosphate buffered saline (PBS, Vivantis) followed by incubation with 10 μM DCFH-DA at 37 ℃ for 30 min. Cells were then washed twice with PBS to remove the free DCFH-DA that did not enter the cells before observing under the inverted microscope (Olympus 1X71).

2.8.3 Flow cytometry

Approximately 4 x 10^5 cells were seeded in each well of a 6-well plate (Greiner Bio-one, Cellstar) and incubated with Ag NMs (25 μg/mL) for 24 h. Cells were washed twice with PBS followed by incubation with 10 μM DCF-DA for 30 min at 37 ℃ in dark. Cells were again washed twice with PBS to remove the free DCF-DA that did not enter the cells. Further

fluorescence of the cells was analyzed by flow cytometry (Epics Altra, Beckman and Coulter) at excitation wavelength of 488 nm and an emission wavelength of 530 nm. Data collected for 10000 cells were analyzed using Summit V4.3.02 software.

2.9 Cell cycle analysis

Cell cycle analysis was performed by staining DNA with propidium iodide (PI, Sigma Aldrich). Approximately 1 x 10^5 cancer cells and 3 x 10^5 skin fibroblast cells were seeded in each well of 6-well plate (Corning, Costar) and incubated at 37 ℃ overnight for cells to proliferate. Following cells treated with the nanomaterials at different concentrations (20 μg/mL for Ag-coffee, Ag-ginger, Ag-mint nanoparticles, 24h; 25 μg/mL for Ag cube1, cube 2 and nanowires, 24 h; 0, 0.1, 1 and 10 μg/mL for Ag-PVP and Au-PVP nanoparticles, 3 days), the cell medium was removed and stored. Cells were washed in PBS, trypsinized, harvested in the stored medium, and centrifuged. The pellet was washed twice in PBS, fixed in fresh prepared ice-cold ethanol (70%), and stored at -20 ℃ overnight. Thereafter, cells were washed in PBS, stained with PI in RNase (40 μg/mL PI and 100 μg/mL RNase A) at 37 ℃ for 30 min and followed by incubation at 4 ℃ until analysis. Flow cytometry analysis was performed at an excitation wavelength of 488 nm and emission wavelength of 610 nm (Epics Altra, Beckman and Coulter). Data collected for 1 x 10^4 cells for HepG2 cells and HeLa cells was analyzed using Summit V4.3.02 software.

2.10 Cell death

2.10.1 Morphological assessment of apoptotic cells by DAPI staining

Apoptotic nuclei in cells with Ag and Au NMs treatment were detected by a DNA-binding dye, 4', 6-diamidino-2-phenylindole (DAPI, Sigma Aldrich). Cells were seeded in a 24 well plate (1×10^4 cells/well) for 24 h to allow the cells to adhere to the bottom of the well. Cells were then treated with

nanomaterials at different concentrations (100 μg/mL for AuNPs; 0, 0.1, 1.0 and 10 μg/mL for Ag-PVP and Au-PVP nanoparticles) for 24 h. After incubation, cells were fixed with 2% paraformaldehyde at 4 ℃ for 30 min and then treated with absolute ethanol for 5 minutes. After washing with PBS twice, cells were stained with DAPI and observed under a fluoresce microscope (Olympus 1X71).

2.10.2 Annexin-V staining for apoptosis and necrosis

Annexin-V staining was performed to distinguish apoptosis and necrotic cell death induced by nanomaterials. Annexin-V, a family of calcium-dependent phospholipid-binding proteins, has a high affinity for phosphotidyl serine (PS). Upon initiation of apoptosis, PS is translocated from the inner to the outer leaflet of the plasma membrane, thus exposing PS to the external cellular environment. Its conjugation with the fluorescent probe FITC facilitates measurement for cells undergoing apoptosis using flow cytometric analysis. Use of propidium iodide (PI) staining helps to differentiate between apoptosis and necrosis, which is attributed to difference in permeability of PI through the cell membranes of live and damaged cells. Approximately 2.5 x 10^5 HepG2 and HeLa cells and 3 x 10^5 skin fibroblast cells were placed in 60 x 15 mm tissue culture dish (Falcon, Franklin Lakes), and then treated with nanomaterials at different concentrations (20 μg/mL for Ag nps; 25 μg/mL for Ag cube 1, cube 2 and nanowires) for 24 h. Treated cells were harvested and washed twice in dulbecco's phosphate buffered saline (DPBS, Sigma-Aldrich) and stained (annexin-V FITC apoptosis detection kit, Sigma-Aldrich) as manufacturer's instruction before detecting with flow cytometry (Epics Altra, Beckman and Coulter). Data was collected for 1 x 10^4 gated cells and analyzed using Summit V4.3.02 software.

2.11 Quantitation of cellular uptake of AuNPs

The nanoparticle uptake by the cells was quantified using inductively coupled

plasma-optical emission spectroscopy (ICP-OES, Perkin Elmer Optima 5300 DV). Cells were seeded at a density of 1.5×10^5 cells in T-75 flask and treated with Au nanoplates to achieve a final concentration of 100 µg/mL. Following incubation period, medium was removed and flasks were washed 5 times with PBS. Cells were harvested using trypsin, washed 3-4 times in PBS and resuspended in 10 mL PBS. The cell number in all tubes was adjusted to 2 million and one millilitre of the lysate was analysed after homogenization. Control, without silver nanoparticles treatment, was also sent for elemental analysis.

2.12 Gene expression profile using real time-reverse transcriptase-polymerase chain reaction (RT-PCR)

Colon CSCs (2×10^5 cells) were seeded in T25 flask for overnight and then treated with Ag and Au nps (0, 0.1, 1.0 and 10 µg/mL) for 3 days. The cells were washed once with PBS and the total RNAs were extracted from the cells using TRIzol® reagent (Life Technologies, Invitrogen) according to the manufacturer's protocol. The extracted RNA was dissolved with 70 µL DEPC (diethylpyrocarbonate) treated water. To verify the purity of the RNA and to determine the concentration, the extracted RNA was analyzed by the 260nm absorbance and the 260/280nm absorbance ratio on NanoDrop 1000 (Thermo Scientific), respectively. The extracted RNA was stored at -80 ℃. Afterwards, 2 mg of the extracted mRNA was reverse transcribed into complementary DNA (cDNA) with EZ-first strand cDNA synthesis kit (Biological industries). The cDNA was then stored at −20 °C.

Quantitative real-time polymerase chain reaction (RT-PCR) for cDNA was performed on an Applied Biosystems StepOnePlus™ Instrument using Taqman® Gene expression assays (Applied Biosystems, USA) according to the supplier's instructions.

Glyceraldehyde-3-phosphate dehydrogenase (GAPDH) was used as

control for normalization. The final reaction volume was 20 µL, containing 10 µL Taqman® Gene expression master mix (2X, Applied Biosystems, USA), 1.0 µL Taqman® Gene expression assay (20X, Applied Biosystems, USA), 1.0 µL cDNA template and 8 µL RNase-free water. Cycling conditions were as follows: a 2 min incubation at 50 ℃ step for optimal UDG enzyme activity, and a 95 ℃ AmpliTaq Gold® enzyme activation for 10 min, followed by 40 cycles of 95 ℃ denaturation for 15 s and 60 ℃ anneal/extension for 1 min.

Each measurement was conducted in triplicate, and negative controls with no cDNA template were included for each assay. After PCR, a dissociation curve analysis was done. Relative gene expression was calculated using the $2^{-\Delta\Delta CT}$ method with pooled cDNA from all samples as a reference.[11]

2.13 Statistical analysis

Statistical analyses of data for all experiments are expressed as mean and standard deviation. The data were analyzed using Student's t-test (Microsoft Excel, Microscoft Corporation). Differences were considered as statistically significant when P value <0.05.

2.14 References

(1) Vallhov, H.; Qin, J.; Johansson, S. M.; Ahlborg, N.; Muhammed, M. A.; Scheynius, A.; Gabrielsson, S. *Nano Lett*. **2006**, *6*, 1682.

(2) Nadagouda, M. N.; Varma, R. S. *Green Chem*. **2008**, *10*, 859.

(3) Kumar, K. P.; Paul, W.; Sharma, C. P. *Process Biochem*. **2011**, *46*, 2007.

(4) Sun, Y.; Xia, Y. *Science* **2002**, *298*, 2176.

(5) Wiley, B.; Sun, Y. G.; Mayers, B.; Xia, Y. N. *Chem-Eur. J.* **2005**, *11*, 454.

(6) Seo, D.; Park, J. C.; Song, H. *J. Am. Chem. Soc.* **2006**, *128*, 14863.

(7) Wang, P. W.; Henning, S. M.; Heber, D. *Plos One* **2010**, *5*.

(8) Qiu, Y.; Liu, Y.; Wang, L. M.; Xu, L. G.; Bai, R.; Ji, Y. L.; Wu, X. C.;

Zhao, Y. L.; Li, Y. F.; Chen, C. Y. *Biomaterials* **2010**, *31*, 7606.

(9) Oh, W. K.; Kim, S.; Choi, M.; Kim, C.; Jeong, Y. S.; Cho, B. R.; Hahn, J. S.; Jang, J. *ACS Nano* **2010**, *4*, 5301.

(10) Hussain, S. M.; Hess, K. L.; Gearhart, J. M.; Geiss, K. T.; Schlager, J. J. *Toxicol. in Vitro* **2005**, *19*, 975.

(11) Livak, K. J.; Schmittgen, T. D. *Methods* **2001**, *25*, 402.

CHAPTER 3

BIOCAPPING AGENT EFFECTS ON SILVER NANOPARTICLES TOXICITY

Publication from this chapter:

Wang Chunyan and Suresh Valiyaveettil, "Correlation of biocapping agents and cytotoxic effects of silver nanoparticles on human tumor cells", RSC Advances, 2013, 3, 14329-14338

3.1 Introduction

Owing to the antimicrobial activity, silver (Ag) nanoparticles have been used in a wide range of consumer products ranging from cosmetics, household products and medical applications including imaging, drug delivery and disinfection. Ag nps impregnated catheters[1] and wound dressings[2] are used in therapeutic applications. However, previous studies have indicated that nanoparticles have a size-, time- and dose-dependent cytotoxicity, where smaller particles with longer exposure time at higher concentrations showed the highest toxicity.[3,4] A possible mechanism of cytotoxicity of Ag nps involves disruption of the mitochondrial respiratory chain, increase of reactive oxygen species (ROS) production and interruption of adenosine-5'-triphosphate (ATP) synthesis, which in turn cause deoxyribonucleic acid (DNA) damage.[4] An organic capping agent with functional groups is used to fine-tune solubility, stability, surface charges, and interactions of nanoparticles with other molecules. The nature of capping agent influences both the physicochemical properties and biological properties of nanoparticles.[3,5-8] To our knowledge, little is known on the influence of capping agents on the bioactivity of Ag nps.[9,10] Recently, there has been growing interests in developing environmentally friendly and multifunctional biomaterials as capping agents for nanoparticles to reduce toxicity.[11-16]

Green approaches have been employed for the synthesis of nanoparticles where plant extracts were used as reducing agent and capping agent.[17-21] Here, we use common ginger,[22] mint and coffee[23] extracts as reducing and capping agents to control the size and surface functional groups for the synthesis of water soluble Ag nps. Ag nps were characterized with multiple techniques and their cytotoxic effects in cell lines (hepatocellular liver carcinoma cells, HepG2 and human cervical cancer cells, HeLa) were investigated by using the following experimental methods which were described in detail in Chapter 2 (Materials and Methods):

1. Synthesis, purification and characterization of Ag-coffee, Ag-ginger and Ag-mint nanoparticles;
2. Dark field microscopy (CytoViva) – cell morphology and Ag nps uptake;
3. ATP assay (CellTiter-Glo) – cell viability;
4. Cell cycle assay – cell proliferation;
5. ROS production – mechanism of Ag nps cytotoxicity;
6. Apoptosis assay – mechanism of cell death.

3.2 Results and discussion

The separation and identification of various components in coffee, ginger and mint extracts were reported in literature.[22-30] The extracts from the above materials contain polyphenols,[31-33] which can form complexes with silver ions in solution and reduce them to Ag nps.[17] Some other compounds existed in the extracts may also help to stabilize Ag nps in solution, which include caffeine, sucrose and amino acids in coffee extract;[34] ascorbic acid in both ginger and mint extracts.[29,35] All Ag nps capped with plant extracts were synthesized at room temperature, purified by repeated centrifuging and washing. These Ag nps were stable at room temperature for long periods of 6 months or more. Ag-mint, Ag-ginger and Ag-coffee nanoparticles showed good solubility in water with bluish yellow, brownish yellow and light brownish yellow color, respectively (**Figure 3.1A**). From the elemental analysis of the lyophilized particles, it appears that Ag-mint has a slightly higher Ag content (48.76 wt%) than Ag-ginger (41.33 wt%) and Ag-coffee (41.46 wt%). Ag nps exhibit unique surface plasmon resonance (SPR) properties, which could be detected by UV-Vis spectroscopy (**Figure 3.1B).** A characteristic absorbance band of Ag nps is dependent on the size of nanoparticles. Ag-mint nanoparticles showed a maximum absorbance at 460 nm, while Ag-coffee nanoparticles and Ag-ginger nanoparticles showed absorption maxima at 442 nm and 424 nm, respectively (**Table 3.1**).

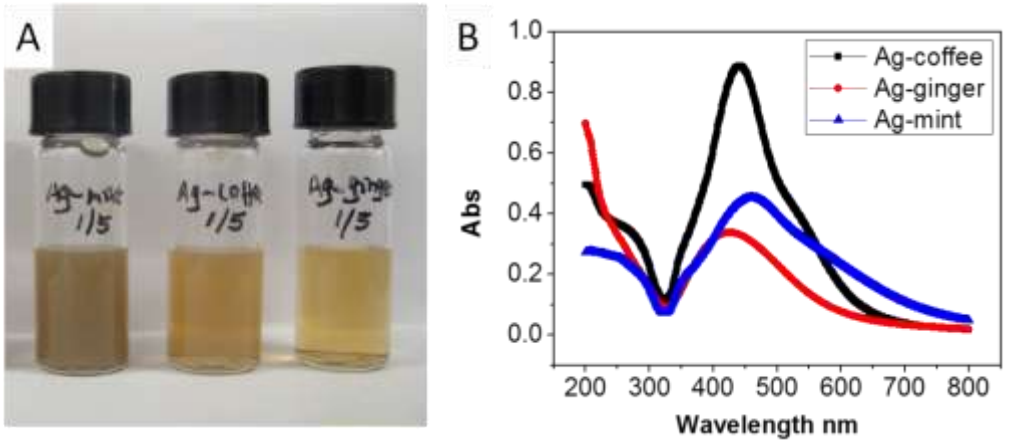

Figure 3.1: Optical images (A) and UV-Vis spectra (B) of Ag-mint, Ag-coffee and Ag-ginger nanoparticles solution. The concentration of solution in (A) is 0.1 mg/mL.

3.2.1 TEM analysis of Ag nps

TEM images showed that Ag nps are present in varying size formed by using different natural material extracts (**Figure 3.2A-C**). For Ag-mint nanoparticles, the size distribution was in the range of 5 to10 nm with a few larger nanoparticles with the size of 50 nm (**Figure 3.2A**); for Ag-ginger nanoparticles, nanoparticles were distributed in the range of 5 to10 nm along with some large particles range from 30 to 40 nm (**Figure 3.2B**); while for Ag-coffee nanoparticles, the majority was in the range of 30 to 40 nm (**Figure 3.2C**). The calculated size distribution histograms are shown in **Figure 3.2D-F**.

The size of Ag nps depends on the efficiency of the reducing agent and the binding ability of the capping agent. Smaller Ag nps could be obtained through slow reduction,[36] or in presence of strong capping agent.[37] In our experiment, mint, ginger and coffee extracts were acted as both reducing agent and capping agent. Among the three Ag nps prepared under similar conditions, Ag-mint nanoparticles are smaller than both Ag-ginger and Ag-coffee nanoparticles (**Figure 3.2**), indicating that the mint extracts are more active towards reduction of Ag^+ ions and capping to nanoparticles.

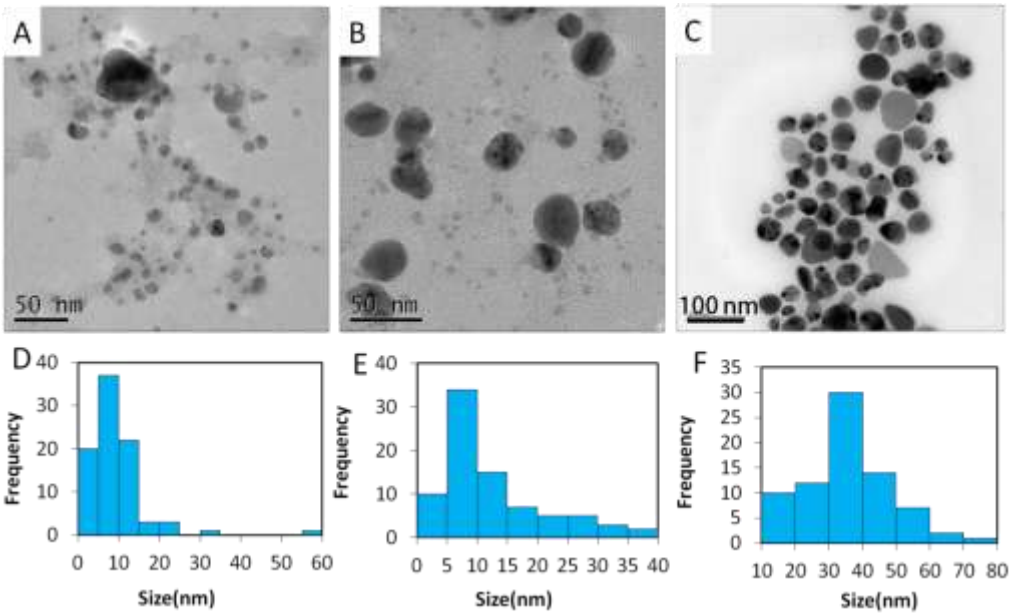

Figure 3.2: Typical TEM image of Ag-mint (A), Ag-ginger (B) and Ag-coffee (C) nanoparticles and the size distribution histogram of Ag-mint (D), Ag-ginger (E) and Ag-coffee (F) generated using image (A-C) captured with JEOL JSM 2010F.

3.2.2 DLS and zeta potential measurements

The hydrodynamic diameter of the Ag nps was determined using Malvern Zetasizer Nano System. All Ag nps are dispersible in water owing to the hydrophilic capping agents which can prevent individual particle from aggregating. The histograms of hydrodynamic size distributions of Ag-mint. Ag-ginger and Ag-coffee nanoparticles were showed in **Figure 3.3.** DLS measurements showed that Ag-mint, Ag-ginger and Ag-coffee nanoparticles showed two major size distributions in the water solution, indicating the aggregation of Ag nps in the solution. TEM images gave the diameter of nanoparticles at dry state, while DLS offers the hydrodynamic size distribution which includes the core particle, its organic layers (capping agents) and the hydration shell.[38] The zeta potential values of Ag-mint and Ag-ginger nanoparticles were at -10.1 mV and -10.2 mV while that of Ag-coffee nanoparticles was at -27.1 mV (**Table 3.1**). The high negative charge of Ag-coffee nanoparticles could enhance the stabilization, which led to smaller hydrodynamic diameters compared to the other two nanoparticles.

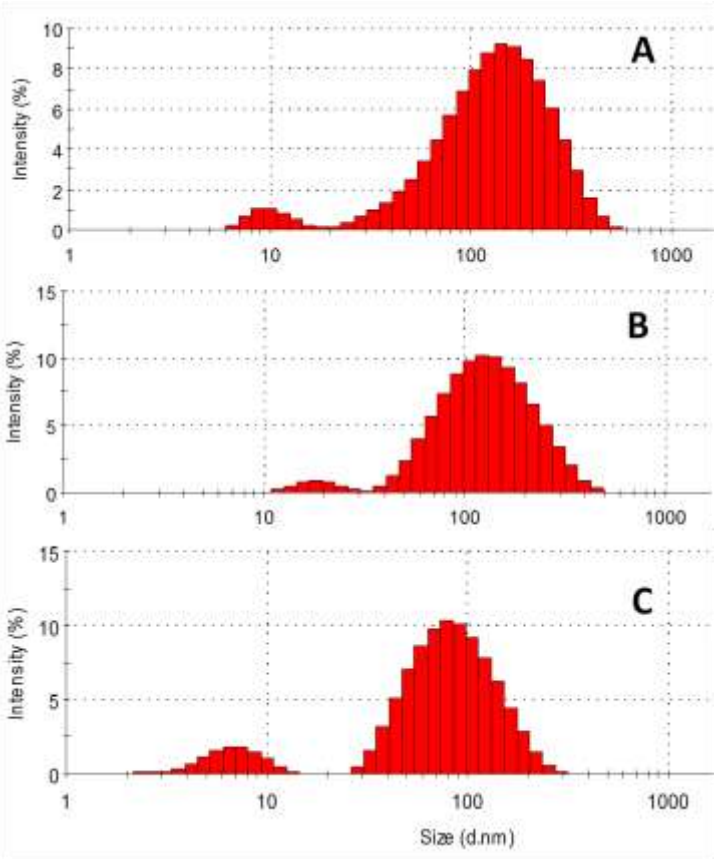

Figure 3.3: Histograms of hydrodynamic size of Ag-coffee (A), Ag-ginger (B) and Ag-mint nps (C) detected by DLS measurement.

Table 3.1: Chemical composition (in wt%), zeta potential and SPR peaks of Ag-mint, Ag-coffee and Ag-ginger nps.

Element	Ag	C	H	N	O (estimate)	Zeta potential mV	SPR peak nm
Ag-mint	48.76	10.45	1.45	2.38	36.96	-10.1	460
Ag-coffee	41.46	37.04	3.23	5.63	12.64	-27.1	442
Ag-ginger	41.33	19.31	3.35	5.43	30.58	-10.2	424

3.2.3 Elemental analysis

As can be seen in **Table 3.1**, it is apparent that the ratio of capping agent to silver in Ag-coffee is high. On the contrary, lowest carbon content was observed for Ag-mint nanoparticles. Silver content (48.8%, 41.3% vs. 41.5%) of all three samples were comparable which enables a fair comparison

between these three nanoparticles in cell viability testing. Oxygen content of Ag-mint nanoparticles was found to be higher than expected due to its hygroscopic nature.

3.2.4 Dark field microscopy

The first readily noticeable effect seen after exposure of cells to toxic materials is the alteration in cell shape or morphology. The experiment was first performed by treating HepG2 cells with mint, coffee and ginger extracts alone for 24 h and compared with the untreated cells which served as control. As can be seen in **Figure 3.4**, the plasma membrane, nuclear envelopes, cellular contents and organelles of all the cells could be observed in dark field microscopy. However, untreated cells showed much clearer plasma membrane compared to those treated with mint, coffee and ginger extracts which become less distinct from each other, although they still appear to maintain their structural integrity as the membranes remained intact.

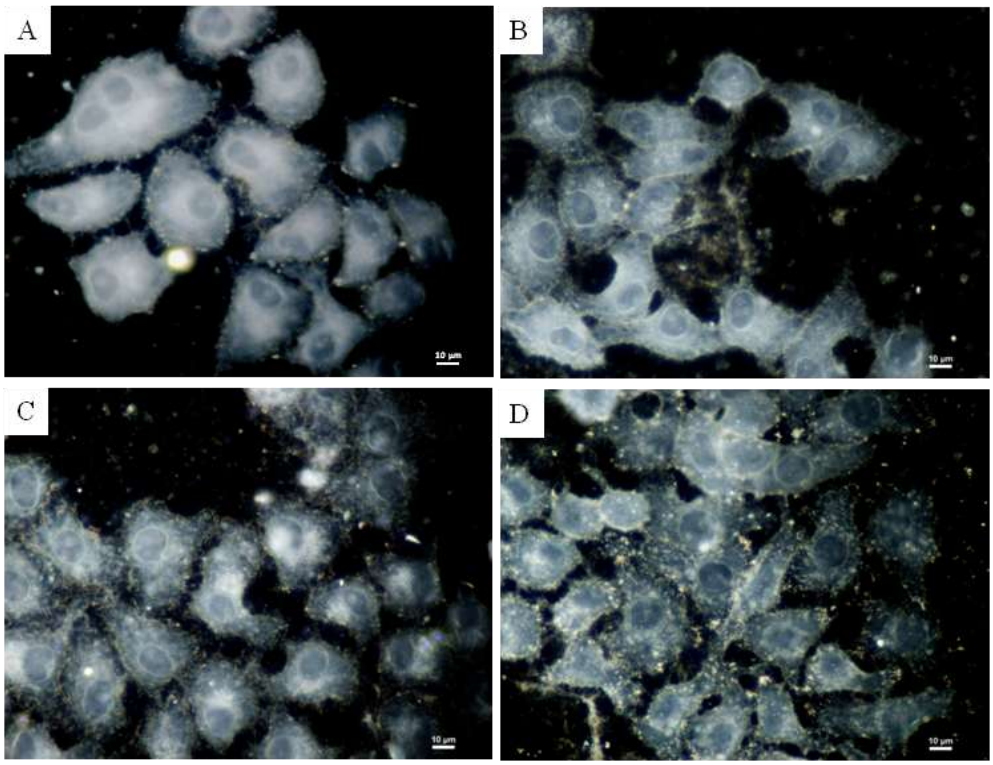

Figure 3.4: Low magnification (40X) dark field images of HepG2 cells untreated (A) and treated with mint extracts (B), coffee extracts (C) and ginger

extracts (D). Concentration of extracts = 20 μg/mL

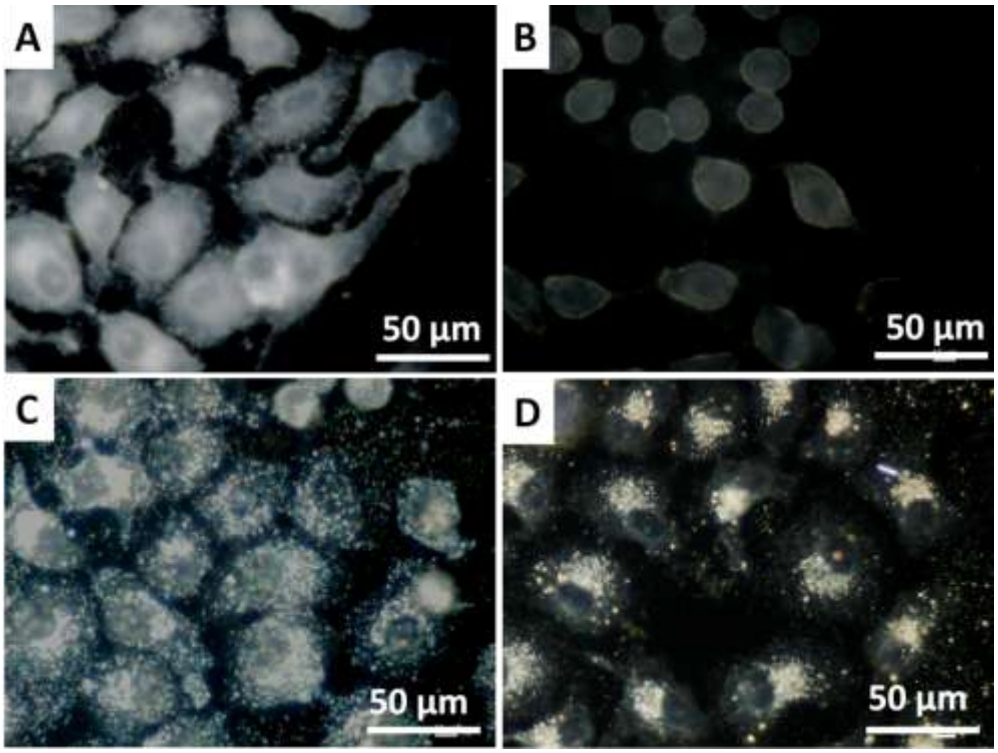

Figure 3.5: Low magnification (40X) dark field images of HepG2 cells untreated (A) and treated with Ag-mint (B), Ag-coffee (C) and Ag-ginger (D) nanoparticles. Concentration of Ag nps = 20 μg/mL.

The morphology changes of HepG2 cells treated with Ag nps (20 μg/mL, 24 h) were also compared with untreated cells (**Figure 3.5**). Low magnification dark image (40X) of HepG2 cells with Ag-mint treatment showed significant morphological changes as compared to untreated cells. Cells treated with Ag-ginger and Ag-mint nanoparticles showed that Ag nps were concentrated in cells. High magnification (100X) images were further captured by dark field microscopy to observe the detailed cell changes with Ag nps treatment (**Figure 3.6**). Images of treated cells showed distinct morphological changes indicating unhealthy cells, whereas the control cells appeared normal. Ag-mint nanoparticles treated cells appeared to be slightly elongated as compared to the untreated cells. This could be due to the disturbances in cytoskeletal framework as a consequence of nanoparticles treatment. Untreated cells showed a small number of bright, round shape of spots distributed throughout the cells. These bright specks (green arrows)

could be transport vesicles (endosomes) or organelles which contain high concentrations of ions and proteins (**Figure 3.6A**). Such bright specks should not be mistaken for Ag nps aggregates (yellow arrows) which are randomly-shaped. Ag nps are so small that they could not be observed directly under an optical microscope. Therefore, the bright objects seen in these images should be considered as scattered light from nanoparticles. It is also clearly found that Ag nps entered the cytoplasm but not the nucleus, which is consistent with literature findings.[39] Ag-mint treated cells showed more sparkling specks with visible cell morphology changes indicating that they could penetrate the cell membrane more efficiently (**Figure 3.6B**) owing to their smaller size. In contrast, cells treated with Ag-coffee nanoparticles and Ag-ginger nanoparticles showed no morphology changes along with sparking specks inside the cells (**Figure 3.6C and 3.6D**) which can be interpreted that such Ag nps are less toxic than Ag-mint nanoparticles. Similar results were also observed for Ag nps treated HeLa cells (**Figure 3.7**).

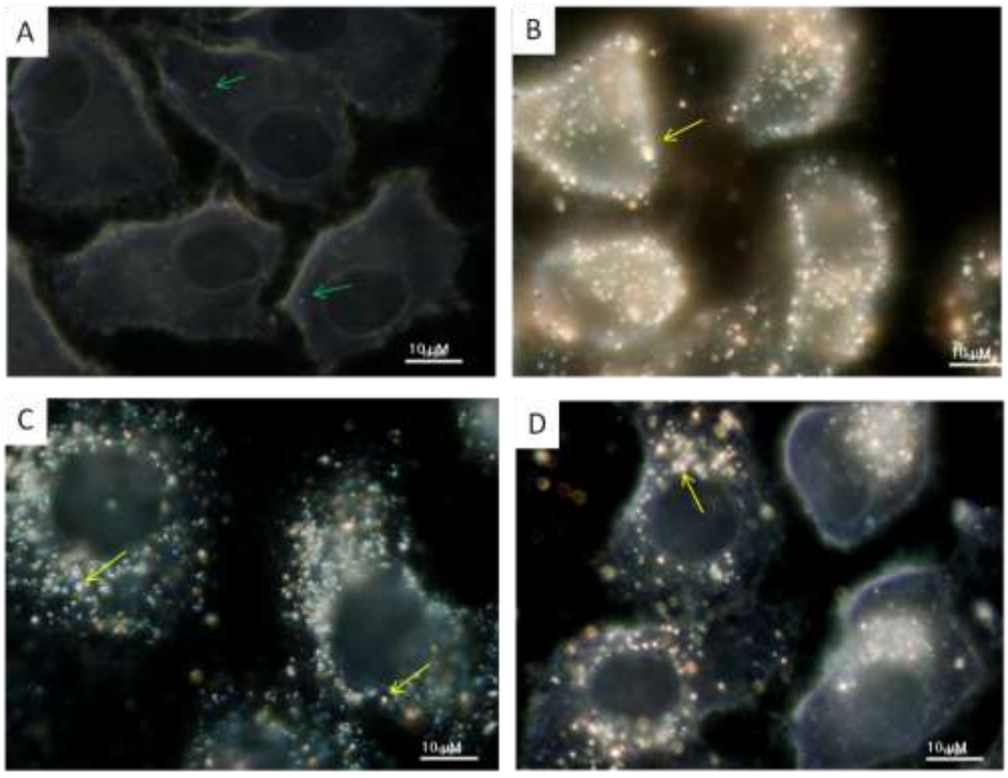

Figure 3.6: High magnification (100X) dark field images of HepG2 cells untreated (A) and treated with Ag-mint (B), Ag-coffee (C) and Ag-ginger (D)

nanoparticles. Concentration of Ag nps = 20 μg/mL. Green arrows point to cellular components such as endosomes and lysosomes, while yellow arrows point to big Ag nanoparticle aggregates.

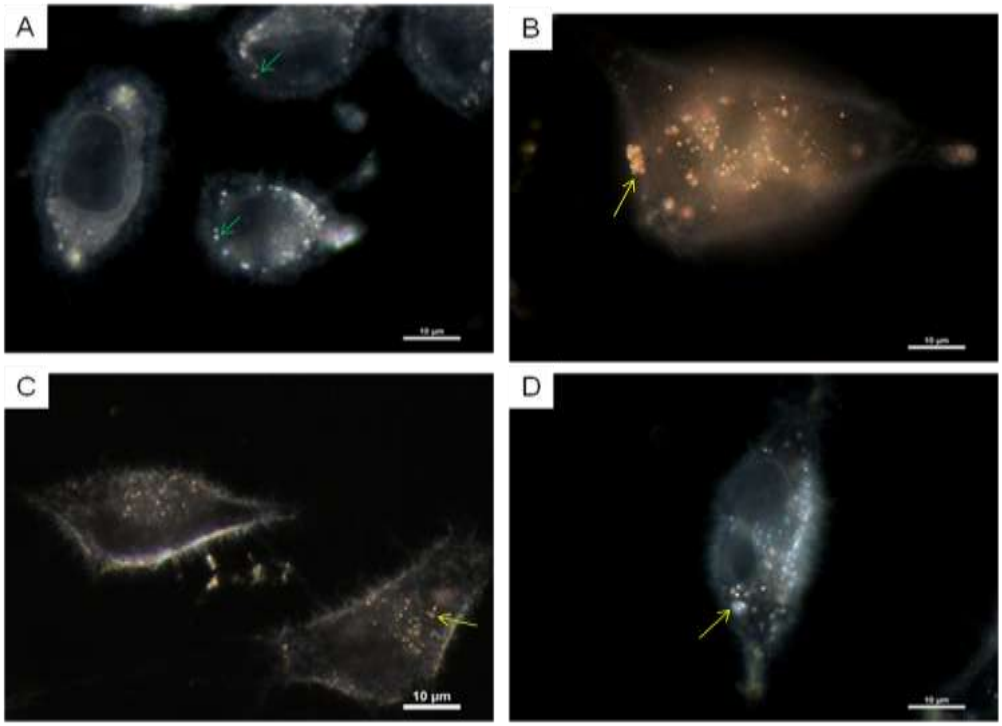

Figure 3.7: High magnification (100X) dark field images of HeLa cells untreated (A) and treated with Ag-mint (B), Ag-coffee (C) and Ag-ginger (D) nanoparticles. Concentration of Ag nps = 20 μg/mL. Green arrows point to cellular components such as endosomes and lysosomes, while yellow arrows point to big Ag nanoparticle aggregates.

Many papers from different laboratories have reported that uptake of nanoparticles was size-dependent.[3,40,41] It showed that optimal nanoparticle radius for endocytosis is in the order of 25–30 nm.[40] Smaller particles (< 10 nm) are known to pass through various pores on the cell membrane. The cellular uptake of nanoparticles was also dependent on the nature of the capping agent.[5] Generally, the smaller water soluble nanoparticles with targeting groups (e.g. transferrin, folic acid, galactose) are absorbed faster into the cell as compared to those capped with nontargeting capping agents such as PVP and PEG.[42-44] Dark filed images also shown that Au nps could be selectively delivered into the cell nucleus by using RGD (arginine-glycine-aspartic acid) and nuclear location sequence (NLS) peptides

or the cytoplasm region using RGD alone, while the PEG conjugated Au nps did not enter into the cells.[45] Further the cellular uptake of nanoparticles was also dependent on the cell lines.[46] Recently, we have shown that platinum nanoparticles capped with PVP showed higher cellular uptake in HeLa cells than in MCF7 and IMR90 cells.[44] The strong reflection from Ag nps observed in our study could be attributed to many factors, such as size or capping agents. Moreover, similar results were also found in Ag nps capped with tea extract.[9] Ag nps capped with epicatechin alone showed minimal interaction with human keratinocyte cells (HaCaT) while Ag nps capped with tea extract showed extensive interaction (at the 1:1 ratio of water to tea extract).[9] Further, the interaction between cells with Ag nps decreased when decreasing concentrations of tea extract.

3.2.5 Viability assay

Viability assays are important for identifying toxicity that indicates the cellular response to a toxic chemical and gives information on cell death, survival and metabolic activities. A concentration- and time-dependent study was performed to find out the effect of Ag nps on cell viability. Commonly used viability assays such as MTT or MTS assay were used to study the viability and the proliferation of cells through monitoring the absorbance of a formazan product formed in living cells. However, nanomaterials which show similar optical properties of a formazan product caused errors during the quantitative analysis. In our experiments, Ag nps solution which showed distinct UV-Vis absorption peaks gave inaccurate results when MTT or MTS assays were used. Such absorbance-based methods are considered not suitable for Ag nps treated cells. The Cell Titer-Glo luminescent cell viability assay was used in our experiment which could monitor cytotoxicity as well as cell proliferation (Procedure details refer to Page 66, section 2.7.1). This assay measures the amount of ATP present in the culture medium, which is proportional to the number of viable cells. It is more sensitive with short

waiting time (minutes) as compared to other assays such as resazurin assay and MTS (1 to 4 h or more).[47]

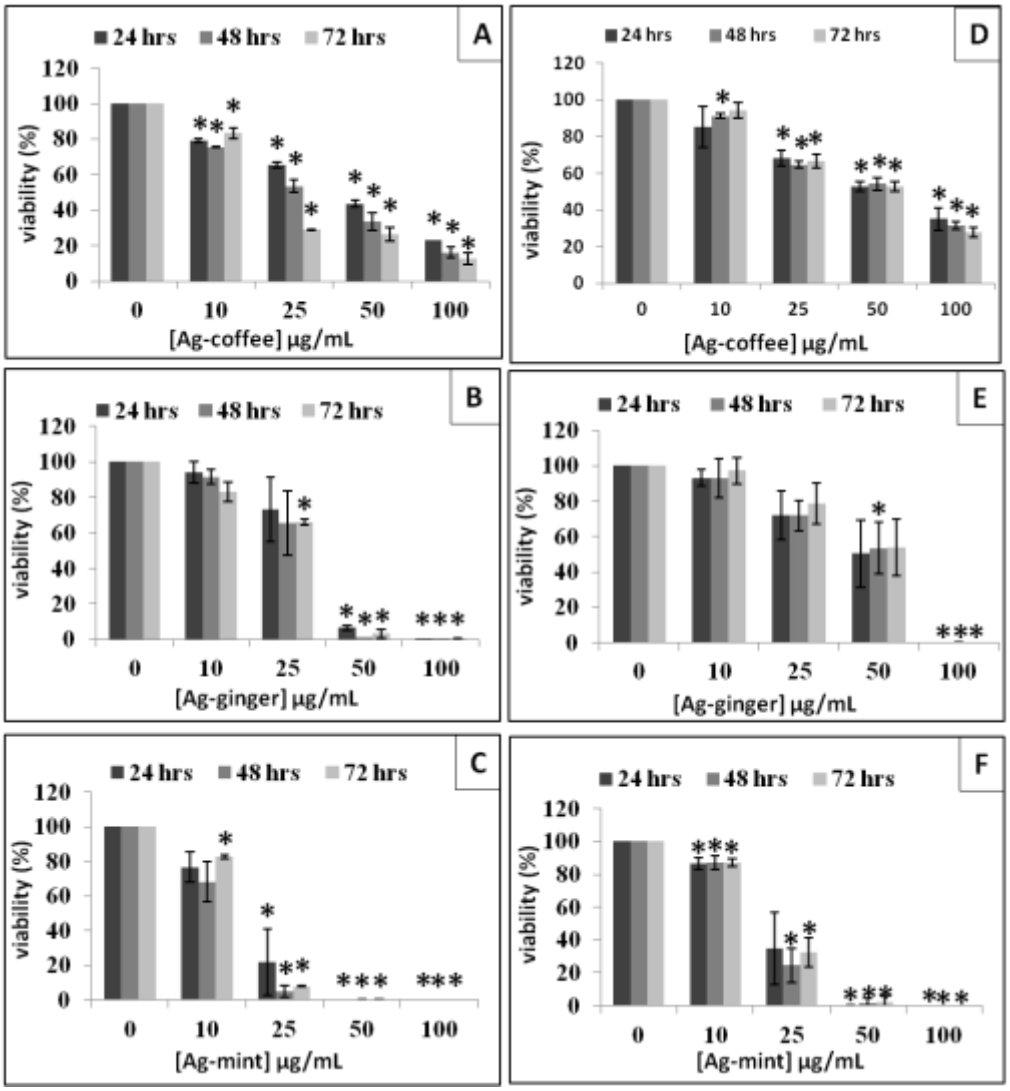

Figure 3.8: Viability of HepG2 cells treated with Ag-coffee nanoparticles (A), Ag-ginger nanoparticles (B), Ag-mint nanoparticles (C) and HeLa cells treated with Ag-coffee (D), Ag-ginger (E), Ag-mint (F) nanoparticles at different concentrations, * represents $P < 0.05$.

The viability trends of Ag-mint, Ag-ginger and Ag-coffee treated cells were similar across different cell types. Generally, the viability of cells decreased with an increase in the concentration of Ag nps and with exposure time from 24 h to 72 h (**Figure 3.8**). HepG2 cells showed high ATP content (> 70%) when treated with all three Ag nps at a lower dosage (10 *µ*g/mL), however, ATP level decreased more significantly for cells treated with higher

concentration of Ag-mint nanoparticles than the others. HepG2 cells treated with Ag-mint nanoparticles showed low ATP content (20% or even less) at the dosage 25 μg/mL or higher. Ag-ginger treated cells showed ATP depletion nearly 0% at the concentration of 50 μg/mL or higher. However, for cells treated with Ag-coffee nanoparticles, ATP was nearly 50% and 30% at concentration of 50 μg/mL and 100 μg/mL, respectively. This observation suggests that among all the three nanoparticles screened, Ag-mint nanoparticles are found to be the most toxic, followed by Ag-ginger nanoparticles and Ag-coffee nanoparticles showed least toxicity. Compared to HepG2 cells, HeLa cells treated with Ag nps seem to have higher viability at the same concentration, indicating that Ag nps showed different toxicity to different cell lines.

The cytotoxicity of Ag nps with different capping agents was also explored on human normal cell line: human dermal fibroblast (HDF, Gibco, Life Technologies) cells (**Figure 3.9**). Similar results were also observed in HDF cells. After exposure to Ag nps for 24 h, the toxicity of all three Ag nps to the cells was dependent on the dose. Furthermore, of all three Ag nps, Ag-mint nanoparticles were the most toxic, followed by Ag-ginger nanoparticles and then Ag-coffee nanoparticles. All data put together suggest that change in the capping agents of Ag nps not only produce change in the extent of toxicity in human cancer cells but also in normal cells. When plant material extracts alone were used as control, it showed no significant cytotoxicity in HepG2 cells even at high concentration (100 μg/mL, **Figure 3.10A**). However, coffee and ginger extracts were relatively more toxic to HeLa cells at 72 h (**Figure 3.10B**). A low ATP value does not always represent cell death and it could be due to the inhibition of metabolic processes in cells. No significant cell death was observed in the presence of Ag nps at low concentrations. Absence of large number of floating cells in the culture medium implies a possibility for metabolic arrest. Hence, it is of great

importance to analyze the cell cycle to interpret the viability data fully.

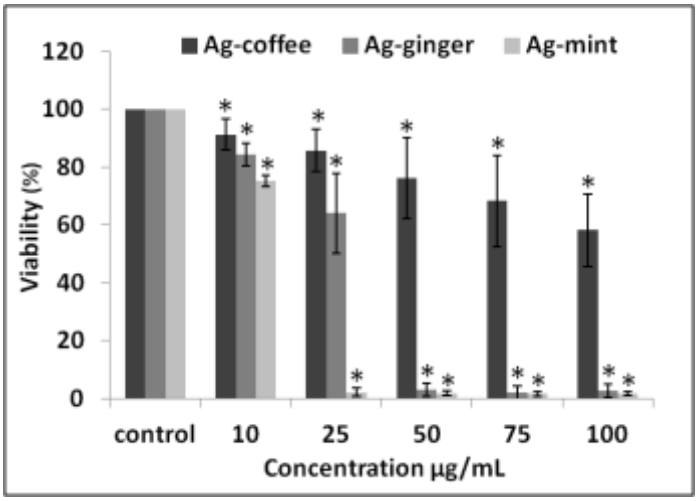

Figure 3.9: Viability of HDF cells treated with Ag-coffee, Ag-ginger and Ag-mint nanoparticles at different concentrations for 24h, * represents $P < 0.05$.

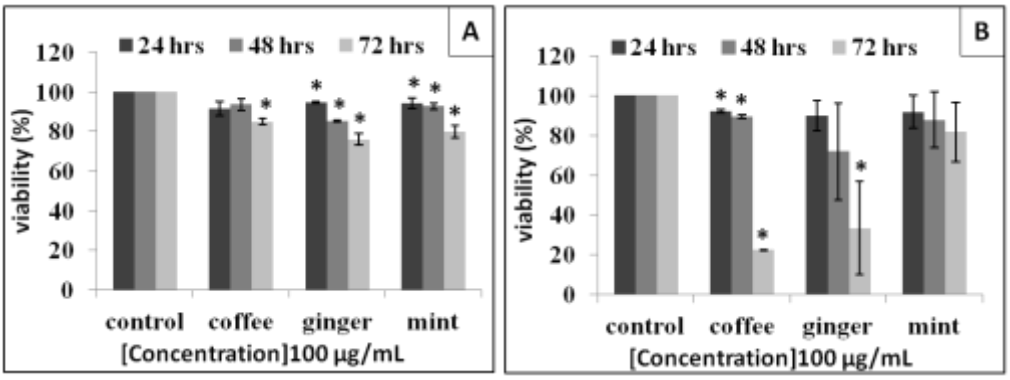

Figure 3.10: Comparison of viability of HepG2 (A) and HeLa (B) cells treated with coffee, ginger and mint extracts (100 μg/mL), * represents $P < 0.05$.

3.2.6 Intracellular ROS level

Oxidative stress was reported to play an important role in nanoparticle toxicity.[48] It is known that a small size and large surface area of nanoparticles could generate ROS. Oxidative stress represents an imbalance between the production and manifestation of ROS, which has specific effects in the cells such as oxidative damage to protein, lipids and DNA.[49] All three extracts used in our experiments were reported to have antioxidant components.[28,50,51] The antioxidant components of coffee extracts were polyphenols and

melanoidins.[52] The major constituents of mint leaves extract include terpenes (α-menthol, neomenthol) and flavonoids (quercetin, eugenol).[53] Similarly, the ginger extracts contain gingerols, shogaols and some related phenolic ketone derivatives.[50] Ginger extracts is reported to possess antioxidant characteristics and known to scavenge superoxide anion and hydroxyl radicals.[54] To check the effect of capping agents on the surface of Ag nps in the production of ROS, DCF-DA staining methods were conducted in HepG2 and HeLa cells (Procedure details, refer to Page 68, section 2.8). In the presence of ROS, DCF-DA is promptly oxidized to 2′-, 7′- dichlorodihydrofluorescein (DCF), which is highly fluorescent.[4] However, no significant increase was observed when cells were treated with different Ag nps (**Figure 3.11**). On the contrary, the analysis showed a decrease of ROS in both cell lines, which is proportional to concentration of Ag nps. Even at a low concentration of 10 μg/mL, the ROS level was less than 20% as compared to the control cells for all three Ag nps. For Ag-mint and Ag-ginger treated cells, the ROS level decreased drastically as the concentration of nanoparticles increased. For Ag-mint nanoparticles (100 μg/mL) treated cells, the ROS concentration of HepG2 cells was less than 20% while 30% of ROS was observed in HeLa cells. For Ag-ginger nanoparticles (100 μg/mL) treated cells, an approximately 60% reduction of ROS was observed in both cell lines.

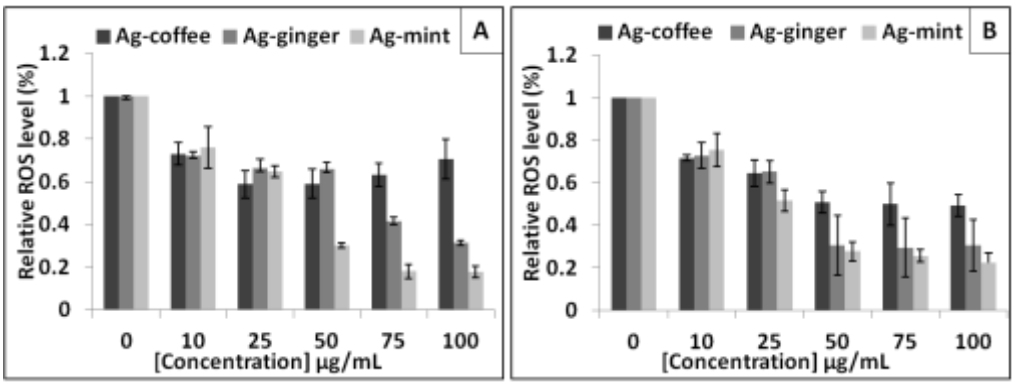

Figure 3.11: ROS production from DCF-DA staining of HepG2 (A) and HeLa (B) cells treated with Ag-coffee, Ag-ginger and Ag-mint nanoparticles for 24 h. Untreated cells were negative control. All the data are significance different

from the control, as all the $P < 0.05$.

The ROS data shows that Ag-mint nanoparticles have highest antioxidant capacity, followed by Ag-ginger nanoparticles. ROS production was reported to be dependent on the nanoparticles surface functionalization.[55] Ag nps with other capping agents such as PVP, starch, citrate or tannic acid were reported to induce cytotoxicity through ROS production.[4,56-59] The decreased ROS in cells treated with our Ag nps could be attributed to antioxidant effect of the capping agents.

3.2.7 Mechanism of toxicity

The differences in toxicity of Ag-mint, Ag-ginger and Ag-coffee nanoparticles could be due to many factors such as size of nanoparticles, silver content and nature of capping agent. Small nanoparticles showed high toxicity due to enhanced uptake into the cells and large surface area for interaction with biological molecules[60] or generation of ROS.[61] Majority of Ag-mint and Ag-ginger nanoparticles are in the range of 5 to 10 nm while Ag-coffee nanoparticles are in the range of 30 to 40 nm. The silver content of Ag-mint is higher (49%) as compared to that in Ag-coffee (42%) and Ag-ginger (41%). Under slightly acidic conditions, Ag^{o} can be converted to Ag^{+}, which is believed to be responsible for ROS production and cause of the cell damage.[58,62]

ROS was reported to have the potential to inhibit or promote cell proliferation by modulating the cell signaling pathways.[63] ROS is produced in response to variety of extracellular and intracellular stimuli, whose reactivity and regulation could be controlled by antioxidants.[64] Zhang et al.[65] has reported that apoferritin-encapsulated platinum nanoparticles can improve the viability of the cells by decreasing the H_2O_2-induced intracellular ROS level. However, ROS is also a normal product of cellular metabolism, which is an indispensible component in cell signaling and homeostasis.[66] The cell signaling pathways can be disturbed at low levels of ROS, which in turn cause

the cell damage and ultimately to cell death.[66] In our study, the ROS level decreased drastically when cells were treated with all three Ag nps, especially for Ag-ginger and Ag-mint nanoparticles. The viability data is consistent with the decreased ROS levels in cells, which is attributed to the antioxidant effect of the capping agents.

3.2.8 Apoptosis and necrosis

Apoptosis and necrosis, the most preferred responses for cell death among various mechanisms,[41,67] are investigated to access the extent and mode of cell death upon exposure to Ag nps. Annexin V-FITC was used as a marker for apoptosis while PI was utilized to detect plasma membrane integrity to recognize necrotic cell death. Statistical data were acquired from the dot plots, based on the percentages of unstained cells (viable cells), and those stained with PI (necrotic cells), FITC (apoptotic cells), and dual stained cells (late apoptosis).

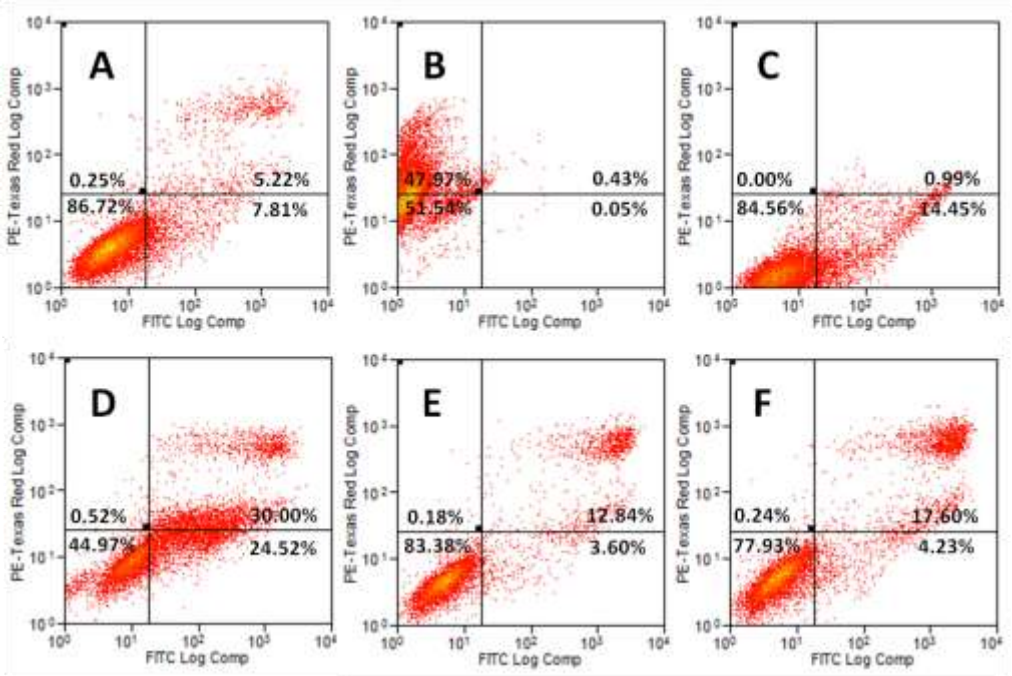

Figure 3.12: Dot plots from Annexin- FITC staining of HepG2 cells. Untreated cells (A) are used to calculate % of change in population. Cells accumulating at lower left window represent live cells. (B) shows necrosis positive controls (H_2O_2 treated) which accumulate on upper left window for

red fluorescent cells.(C) shows apoptosis positive controls (Staurosporine treated) accumulating on lower right window. Late apoptotic cells will accumulate in upper right window. (D) shows cell population for cells treated with Ag-mint (E) represents cells treated with Ag-ginger and (F) represents cells treated with Ag-coffee NPs (20 µg/mL). The % of cells under each category (live, early and late apoptosis, necrosis) is represented in respective windows.

The above mentioned results of HepG2 cells with Ag nps treatment are shown in **Figure 3.12**. For Ag-ginger and Ag-coffee nanoparticles treated HepG2 cells, a decrease in the percentage of viable cells (3-8%) and early apoptosis cells (3-4%) was observed as compared to control cells. Moreover, 7-12% increase was found in the percentage of late apoptosis cells, indicating that Ag-ginger and Ag-coffee nanoparticles were only slightly toxic to HepG2 cells at a concentration of 20 μg/mL. However, a significant decrease in the percentage of live cells (42%) was observed for Ag-mint nanoparticles treated cells, accompanied by an increase in both early apoptosis (17%) and late apoptosis (25%) stages. It confirmed that Ag-mint nanoparticles are the most toxic, which is consistent with cell viability results.

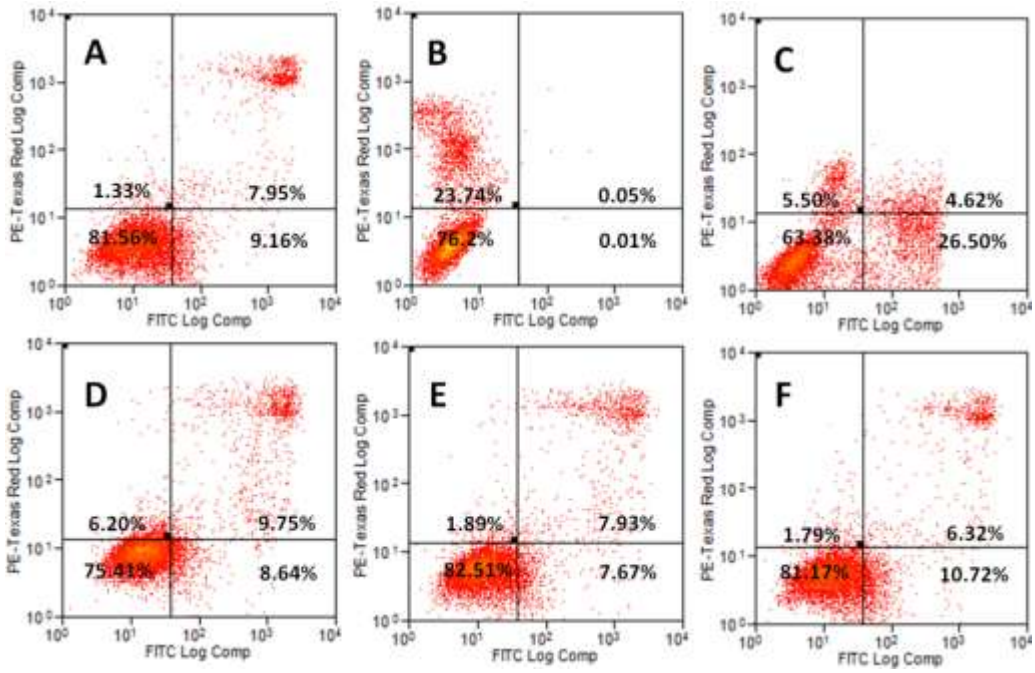

Figure 3.13: Dot plots from Annexin- FITC staining of HeLa cells. Untreated cells (A) are used to calculate % of change in population. Cells accumulating

at lower left window represent live cells. (B) shows necrosis positive controls (H_2O_2 treated) which accumulate on upper left window for red fluorescent cells.(C) shows apoptosis positive controls (Staurosporine treated) accumulating on lower right window. Late apoptotic cells will accumulate in upper right window. (D) shows cell population for cells treated with Ag-mint (E) represents cells treated with Ag-ginger and (F) represents cells treated with Ag-coffee NPs (20 µg/mL). The % of cells under each category (live, early and late apoptosis, necrosis) is represented in respective windows.

The response of HeLa cells to Ag nps was quite similar to HepG2 cells (**Figure 3.13**). Decrease in the percentage of live cells along with increase in the percentage of apoptosis cells was observed for all three Ag nps treated HeLa cells. Only small changes were observed on both Ag-ginger and Ag-coffee nanoparticles treated cells, indicating that these two nanoparticles were less toxic at low concentrations. Around 2% increase in late apoptosis cells along with 6% decrease in live cells were observed for Ag-mint nanoparticles treated cells, which indicate that Ag-mint nanoparticles were toxic to cells at a low concentration. Significant increase of necrotic cells (5%) was observed in Ag-mint treated HeLa cell.

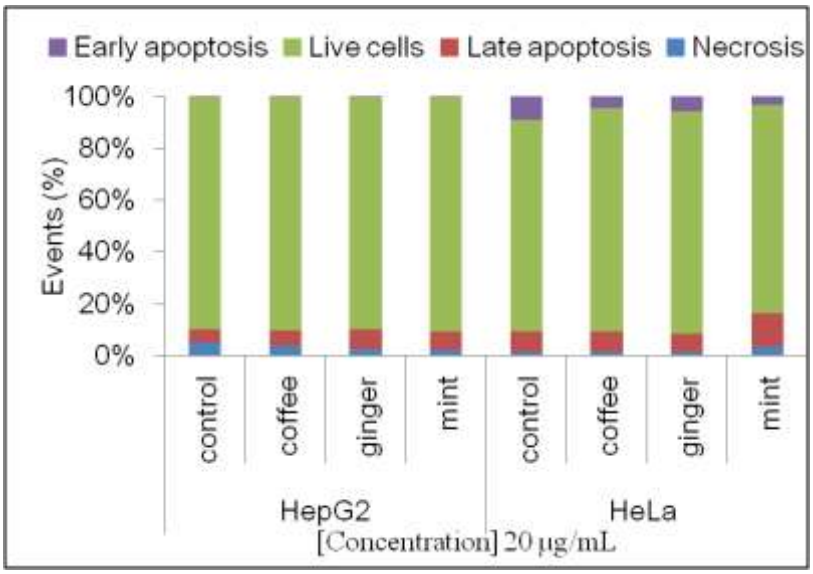

Figure 3.14: Apoptosis and necrosis mode of HepG2 and HeLa cells with ginger, coffee or mint extracts treatment (100 µg/mL, 24 h) by using Annexin-FITC staining. The percentage of cells stained with PI alone is represented as necrotic cells, whereas percentage of cells stained with FITC alone represents early apoptosis. Cells at final stages of apoptosis take up both stains. The percentage of cells under each area was generated using Summit V4.3.02

software.

To check the cellular response of plant extracts on cells, HepG2 and HeLa cells, were treated with plant extracts (100 μg/mL, 24 h) and investigated the response. As can be seen from **Figure 3.14**, plant extracts treated cells did not induce significant cell death from neither apoptosis nor necrosis.

Necrosis is usually related to loss of lysosomal membrane integrity and uncontrolled release of inflammatory cellular contents,[68] while apoptosis is associated with the generation of ROS and JNK activation,[69] mitochondrial fusion/fission machinery,[70] caspase activation,[71] calcium overload[72] or caused by death-inducing signals.[73] Oh et al.[41] reported that the apoptosis and necrosis observed among silica-titania hollow nanoparticles internalized macrophages were size-dependent and surface functionality-dependent, which agrees with other experimental results.[61] Small changes in particle size and functional groups on the surface affect the mechanism of cell death. Furthermore, these factors may also have significant influence on the nanoparticle and membrane interaction, nanoparticle internalization and degradation within cells.

3.2.9 Effects of Ag nps on cell cycle

Earlier reports have emphasized a bidirectional effect of ROS on genomic stability.[74] High intracellular ROS levels in CTAB-coated Au nanorods treated cells induced mitochondrial damage which led to changes of cell cycle and increased apoptosis.[75] Intracellular ROS levels can be decreased dramatically by the addition of high-dose of antioxidants. Furthermore, DNA damage from low level ROS in stem cells treated with antioxidants was reported to be concentration dependent.[74] Moreover, the early effect of DNA damage was seen in cell cycle progression. Cells with damaged DNA accumulated in gap1 (G1), DNA synthesis (S), or in gap2/mitosis (G2/M) phase while cells with irreversible damage accumulated in subG1 phase.[76] By detecting parameters such as apoptosis, cell cycle arrest and evidence of DNA damage, the toxicity of Ag nps on the cells is established.

A

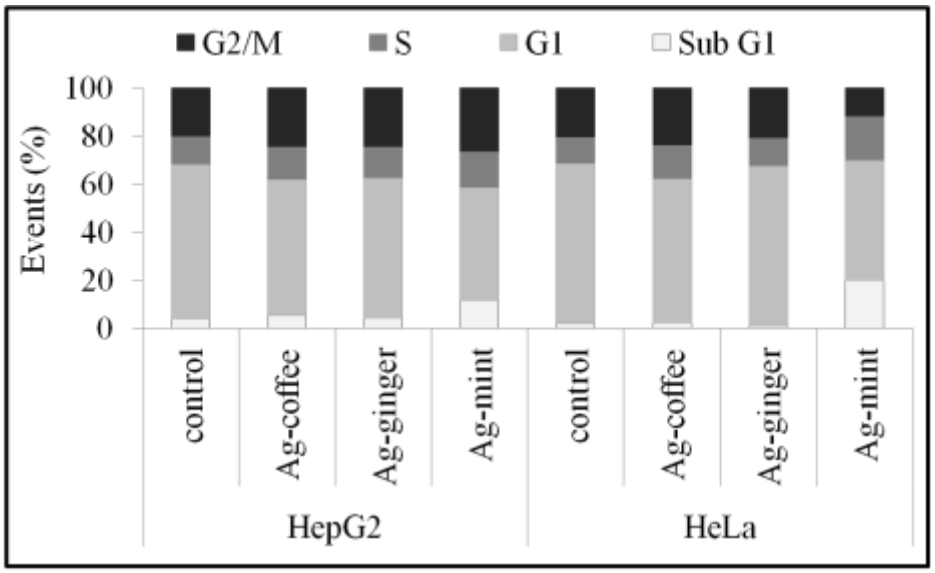

B

Cells	Sample	Sub G1 %	G1 %	S %	G2/M %
HepG2	Control	3.9	64.3	11.7	20.1
	Ag-coffee	5.3	56.6	13.5	24.6
	Ag-ginger	4.2	58.2	13.2	24.3
	Ag-mint	11.5	47.0	15.1	26.6
HeLa	Control	2.1	66.3	11.0	20.7
	Ag-coffee	2.3	59.8	14.2	23.8
	Ag-ginger	1.1	66.6	11.4	21.0
	Ag-mint	19.9	49.9	18.4	12.5

Figure 3.15: Cell cycle graph (A) and data (B) of HeLa and HepG2 treated with 20 μg/mL Ag nps for 24h to detect the DNA damage of cells. Markers were set at regions of interest (sub G1, G1, S, and G_2/M), and the percent of cells (events) under each area was generated using Summit V4.3.02 software through **Figure 3.16**.

The influence of Ag nps on the percentage of cells in each phase of the cell cycle was analyzed (**Figure 3.15**). Both HeLa and HepG2 cell lines showed a decrease in G1 phase. Ag nps treated HepG2 cells showed significant increase in both S and G2/M stages, while Ag-mint treated HepG2 cells also showed significant increase in subG1 stage. For Ag nps treated HeLa cells, Ag-coffee induced significant increase in both S and G2/M stages and Ag-ginger induced only G2/M arrest. However, Ag-mint nps caused a significant increase in both subG1 and S stages. The significant increase in subG1 stage for Ag-mint treated cells indicated that cells were seriously

damaged as a result of an irreversible DNA damage while G2/M or S arrest revealed reversible DNA damage. Only small increases in subG1 stage of HepG2 cells with Ag-ginger and Ag-coffee treatment were observed while no changes were found in HeLa cells. The absence of changes in number of cells in subG1 of HeLa cells indicates no significant cell death via apoptosis occurred when cells were treated with Ag-ginger or Ag-coffee nps. In other words, both Ag-ginger and Ag-coffee treated cells only showed reversible DNA damage with G2/M and S arrest.

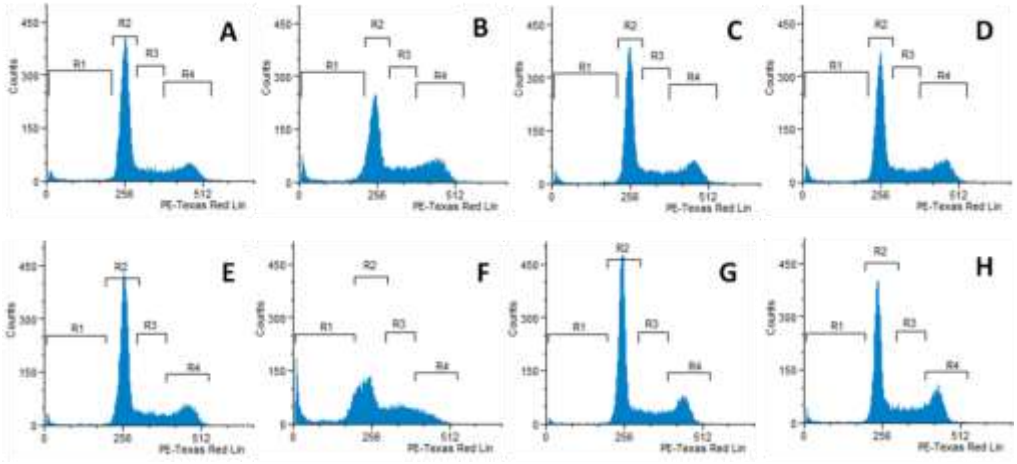

Figure 3.16: Histograms representing cell cycle analysis of HepG2 (A-D) and HeLa (E-H) cells. The control showed normal distribution of sub G1, G1, S and G2/M (A and E). The cells treated with 20 µg/mL Ag mint (B and F), Ag-ginger (C and G) and Ag-coffee (D and H) showed increases in S/G2 population indicating S/G2 arrest while the presence subG1 population of cells treated Ag mint (B and F) indicates cell death through apoptosis. Markers were drawn on regions of interest (R1-subG1, R2-G1, R3-S and R4-G2/M) to generate statistics of cells under each region. Corresponding statistics were generated using Summit V4.3.02 software.

Several reports suggest that Ag nps could induce cell cycle arrest in G2/M phase and enhance apoptosis.[4,77,78] Absence of massive apoptosis and necrosis for Ag-ginger and Ag-coffee nanoparticles treated cells accompanied by G2/M arrest (**Figure 3.15**) indicates a retarded cell proliferation, allowing cells extra time to repair DNA damage prior to segregation of chromosomes. However, the DNA repair could be affected by the reduction of ATP content (**Figure 3.8**) after Ag nps treatment, as ATP played multiple roles in the repair of DNA

damage.[79-81] Excessive ROS production was reported to be harmful to DNA, while low levels of ROS affect cell signaling particularly at the level of redox modulation.[82] Relatively low level of ROS was observed to promote cell proliferation rather than cell degeneration or death.[65,83] Low levels of ROS was also reported to induce DNA damage in cells[74] and similar results were observed in our study.

3.3 Conclusion

In this study, a green synthesis of Ag nps using mint, ginger, and coffee extracts as a reducing and capping agents was explored. The cellular uptake and toxicity of Ag nps was determined using the changes in cell morphology, cell viability and oxidative stress. Ag-mint, Ag-ginger and Ag coffee nanoparticles were found to be more toxic to HepG2 than to HeLa cells. Among all the Ag nps, Ag-mint were the most toxic, followed by Ag-ginger and Ag-coffee were the least toxic. Morphology changes and cellular uptake observed among Ag nps treated cells were considered as the first indication of toxicity. Significant decrease in cell viability was observed as a result of reduction in ATP. Surprisingly, bioextracts capped Ag nps did not increase but decreased the production of ROS in a dose dependent manner, which can be attributed to the antioxidant activity of biomaterial extracts on the surface. The low levels of ROS are believed to be the trigger for DNA damage. No massive apoptosis or necrosis and G2/M arrested cells were observed for the cells exposed with Ag-ginger and Ag-coffee nanoparticles, suggesting an active DNA repair pathway operating inside the damaged cells. On the other hand, significant increase in apoptosis and arrest in subG1 stage was observed for Ag-mint nanoparticles treated cells, indicating an irreversible DNA damage. The higher toxicity of Ag-mint nanoparticles to cancer cells could be further explored for evaluating their potential use in cancer therapy.

In summary, the results indicate that cytotoxicity of Ag nps was strongly related to their compositions and capping agents. Among three Ag nps

investigated, Ag-mint nanoparticles were much more toxic compared to Ag-ginger and Ag-coffee nanoparticles. Exposure of cells to Ag nps led to low levels of ROS which caused DNA damage followed by cell arrest in G2/M stage and eventually cell death through apoptosis. However, complete elimination of toxicity, especially at higher concentration is not yet achieved and need further studies.

3.4 References

(1) Samuel, U.; Guggenbichler, *J. P. Int. J. Antimicrob. Ag.* **2004**, *23*, S75.

(2) Chen, J.; Han, C.; Lin, X.; Tang, Z.; Su, S. *Zhonghua Wai Ke. Za Zhi* **2006**, 50.

(3) Oh, E.; Delehanty, J. B.; Sapsford, K. E.; Susumu, K.; Goswami, R.; Blanco-Canosa, J. B.; Dawson, P. E.; Granek, J.; Shoff, M.; Zhang, Q.; Goering, P. L.; Huston, A.; Medintz, I. L. *ACS Nano* **2011**, *5*, 6434.

(4) AshaRani, P. V.; Mun, G. L. K.; Hande, M. P.; Valiyaveettil, S. *ACS Nano* **2009**, *3*, 279.

(5) Moros, M.; Hernáez, B.; Garet, E.; Dias, J. T.; Sáez, B.; Grazú, V.; González-Fernández, Á.; Alonso, C.; de la Fuente, J. M. *ACS Nano* **2012**, *6*, 1565.

(6) Cheng, J.; Fernando, K. A. S.; Veca, L. M.; Sun, Y.-P.; Lamond, A. I.; Lam, Y. W.; Cheng, S. H. *ACS Nano* **2008**, *2*, 2085.

(7) Yuan, H.; Fales, A. M.; Vo-Dinh, T. *J. Am. Chem. Soc.* **2012**, *134*, 11358.

(8) Perry, J. L.; Reuter, K. G.; Kai, M. P.; Herlihy, K. P.; Jones, S. W.; Luft, J. C.; Napier, M.; Bear, J. E.; DeSimone, J. M. *Nano Lett.* **2012**, *12*, 5304.

(9) Moulton, M. C.; Braydich-Stolle, L. K.; Nadagouda, M. N.; Kunzelman, S.; Hussain, S. M.; Varma, R. S. *Nanoscale* **2010**, *2*, 763.

(10) Kumar, K. P.; Paul, W.; Sharma, C. P. *Process Biochem.* **2011**, *46*,

2007.

(11) Vigneshwaran, N.; Nachane, R. P.; Balasubramanya, R. H.; Varadarajan, P. V. *Carbohyd. Res.* **2006**, *341*, 2012.

(12) Dwivedi, A. D.; Gopal, K. *Colloid Surf. A-Physicochem. Eng. Asp.* **2010,** *369*, 27.

(13) Philip, D. *Spectrochim Acta A* **2009**, 73, 650.

(14) Philip, D. *Spectrochim Acta A* **2010**, *75*, 1078.

(15) Vasileva, P.; Donkova, B.; Karadjova, I.; Dushkin, C. *Colloid Surf. A-Physicochem. Eng. Asp.* **2011**, *382*, 203.

(16) Venu, R.; Ramulu, T. S.; Anandakumar, S.; Rani, V. S.; Kim, C. G. *Colloid Surf. A-Physicochem. Eng. Asp.* **2011**, *384*, 733.

(17) Nadagouda, M. N.; Varma, R. S. *Green Chem.* **2008**, *10*, 859.

(18) Bar, H.; Bhui, D. K.; Sahoo, G. P.; Sarkar, P.; De, S. P.; Misra, A. *Colloid Surf. A-Physicochem. Eng. Asp.* **2009**, *339*, 134.

(19) Dubey, S. P.; Lahtinen, M.; Sillanpää, M. *Colloid Surf. A-Physicochem. Eng. Asp.* **2010**, *364*, 34.

(20) Dubey, S. P.; Lahtinen, M.; Sillanpää, M. *Process Biochem.* **2010**, *45*, 1065.

(21) Kouvaris, P.; Delimitis, A.; Zaspalis, V.; Papadopoulos, D.; Tsipas, S. A.; Michailidis, N. *Mater. Lett.* **2012**, *76*, 18.

(22) Ghayur, M. N.; Gilani, A. H.; Afridi, M. B.; Houghton, P. J. *Vascul. Pharmacol.* **2005**, *43*, 234.

(23) Jagetia, G. C.; Baliga, M. S. *Strahlentherapie Und Onkologie* **2002**, *178*, 91.

(24) Goya, L.; Delgado-Andrade, C.; Rufian-Henares, J. A.; Bravo, L.; Morales, F. J. *Mol. Nutr. Food Res.* **2007**, *51*, 536.

(25) Ali, B. H.; Blunden, G.; Tanira, M. O.; Nemmar, A. *Food Chem. Toxicol.* **2008**, *46*, 409.

(26) Shati, A. A.; Elsaid, F. G. *Food Chem. Toxicol.* **2009**, *47*, 1945.

(27) Shukla, Y.; Singh, M. *Food Chem. Toxicol.* **2007**, *45*, 683.

(28) Policegoudra, R. S.; Abiraj, K.; Gowda, D. C.; Aradhya, S. M. J. *Chromatogr. B* **2007**, *852*, 40.

(29) Sazhina, N.; Misin, V.; Korotkova, E. *Chemistry & Chemical Technology* **2011**, *5*, 13.

(30) Grigoleit, H. G.; Grigoleit, P. *Phytomedicine* **2005**, *12*, 612.

(31) Gao, J. H.; Xu, B. *Nano Today* **2009**, *4*, 37.

(32) Rahath Kubra, I.; Ramalakshmi, K.; Rao, L. J. M. E-J. *Chem*. **2011**, *8*, 721.

(33) She, G. M.; Xu, C.; Liu, B.; Shi, R. B. *J. Food Sci.* **2010**, *75*, C359.

(34) del Castillo, M. D.; Ames, J. M.; Gordon, M. H. *J. Agr. Food Chem*. **2002**, *50*, 3698.

(35) Shirin, A.; Prakash, *J. Health Environ. Res. Online* **2010**, *4*, 2674.

(36) Shervani, Z.; Ikushima, Y.; Sato, M.; Kawanami, H.; Hakuta, Y.; Yokoyama, T.; Nagase, T.; Kuneida, H.; Aramaki, K. *Colloid Polym. Sci.* **2008**, *286*, 403.

(37) Seo, D.; Park, J. C.; Song, H. *J. Am. Chem. Soc.* **2006**, *128*, 14863.

(38) Barth, B. M.; Sharma, R.; Altinoglu, E. I.; Morgan, T. T.; Shanmugavelandy, S. S.; Kaiser, J. M.; McGovern, C.; Matters, G. L.; Smith, J. P.; Kester, M.; Adair, J. H. *ACS Nano* **2010**, *4*, 1279.

(39) Komatsu, T.; Tabata, M.; Kubo-Irie, M.; Shimizu, T.; Suzuki, K.; Nihei, Y.; Takeda, K. *Toxicol. in Vitro* **2008**, *22*, 1825.

(40) Zhang, S.; Li, J.; Lykotrafitis, G.; Bao, G.; Suresh, S. *Adv. Mater.* **2009**, *21*, 419.

(41) Miranda, A.; Malheiro, E.; Skiba, E.; Quaresma, P.; Carvalho, P. A.; Eaton, P.; de Castro, B.; Shelnutt, J. A.; Pereira, E. *Nanoscale* **2010,** *2,* 2209.

(42) Hu, R.; Yong, K.-T.; Roy, I.; Ding, H.; He, S.; Prasad, P. N. *J. Phys. Chem. C* **2009**, *113*, 2676.

(43) Ding, H.; Yong, K.-T.; Roy, I.; Pudavar, H. E.; Law, W. C.; Bergey, E. J.; Prasad, P. N. *J. Phys. Chem. C* **2007**, *111*, 12552.

(44) Teow, Y.; Valiyaveettil, S. *Nanoscale* **2010**, *2*, 2607.

(45) Qian, W.; Huang, X.; Kang, B.; El-Sayed, M. A. *J. Biomed. Opt*. **2010,** *15*, 046025.

(46) dos Santos, T.; Varela, J.; Lynch, I.; Salvati, A.; Dawson, K. A. *Small* **2011**, *7*, 3341.

(47) Mueller, H.; Kassack, M. U.; Wiese, M. J. *Biomol. Screen* **2004**, *9*, 506.

(48) Xia, T.; Kovochich, M.; Brant, J.; Hotze, M.; Sempf, J.; Oberley, T.; Sioutas, C.; Yeh, J. I.; Wiesner, M. R.; Nel, A. E. *Nano Lett*. **2006**, *6*, 1794.

(49) Zhang, Y. Y.; Hu, L.; Yu, D. H.; Gao, C. Y. *Biomaterials* **2010**, *31*, 8465.

(50) Fuhrman, B.; Rosenblat, M.; Hayek, T.; Coleman, R.; Aviram, M. J. *Nutr*. **2000**, *130*, 1124.

(51) Chan, E. W. C.; Lim, Y. Y.; Chong, K. L.; Tan, J. B. L.; Wong, S. K. J. *Food Comp. Anal*. **2010**, *23*, 185.

(52) Nestle http://www.nestle.com.au/Products/Categories/Hot-Cold-Beverages/Coffee/Nescafe/Soluble/Rich-Roast.

(53) Almeida, P. P.; Mezzomo, N.; Ferreira, S. R. S. *Food Bioprocess Tech.* **2012**, *5*, 548.

(54) Krishnakantha, T. P.; Lokesh, B. R. *Indian J. Biochem. Bio*. **1993**, *30*, 133.

(55) Chompoosor, A.; Saha, K.; Ghosh, P. S.; Macarthy, D. J.; Miranda, O. R.; Zhu, Z.-J.; Arcaro, K. F.; Rotello, V. M. *Small* **2010**, *6*, 2246.

(56) Foldbjerg, R.; Olesen, P.; Hougaard, M.; Dang, D. A.; Hoffmann, H. J.; Autrup, H. *Toxicology Letters* **2009**, *190*, 156.

(57) Sanpui, P.; Chattopadhyay, A.; Ghosh, S. S. *ACS Appl. Mater. Interfaces* **2011**, *3*, 218.

(58) Piao, M. J.; Kang, K. A.; Lee, I. K.; Kim, H. S.; Kim, S.; Choi, J. Y.; Choi, J.; Hyun, J. W. *Toxicol. Lett*. **2011**, *201*, 92.

(59) He, W.; Zhou, Y.-T.; Wamer, W. G.; Boudreau, M. D.; Yin, J.-J.

Biomaterials **2012**, *33*, 7547.

(60) Jin, Y.; Lohstreter, S.; Zhao, J. X. In Nanotechnologies for the Life Sciences; Wiley-VCH Verlag GmbH & Co. KGaA: **2007**.

(61) Pan, Y.; Neuss, S.; Leifert, A.; Fischler, M.; Wen, F.; Simon, U.; Schmid, G.; Brandau, W.; Jahnen-Dechent, W. *Small* **2007**, *3*, 1941.

(62) Foldbjerg, R.; Olesen, P.; Hougaard, M.; Dang, D. A.; Hoffmann, H. J.; Autrup, H. *Toxicol. Lett*. **2009,** *190*, 156.

(63) Levonen, A. L.; Patel, R. P.; Brookes, P.; Go, Y. M.; Jo, H.; Parthasarathy, S.; Anderson, P. G.; Darley-Usmar, V. M. *Antioxid. Redox Signal*. **2001**, *3*, 215.

(64) Burch, P. M.; Heintz, N. H. *Antioxid. Redox Signal.* **2005**, *7*, 741.

(65) Zhang, L. B.; Laug, L.; Munchgesang, W.; Pippel, E.; Gosele, U.; Brandsch, M.; Knez, M. *Nano Lett*. **2010**, *10*, 219.

(66) Burhans, W. C.; Heintz, N. H. *Free Radical Bio. Med*. **2009**, *47*, 1282.

(67) Jin, Y.; Kannan, S.; Wu, M.; Zhao, J. X. *Chem. Res. Toxicol.* **2007**, *20*, 1126.

(68) Fink, S. L.; Cookson, B. T. *Infect. Immun*. **2005**, *73*, 1907.

(69) Hsin, Y. H.; Chena, C. F.; Huang, S.; Shih, T. S.; Lai, P. S.; Chueh, P. J. *Toxicol. Lett*. **2008**, *179*, 130.

(70) Jahani-Asl, A.; Germain, M.; Slack, R. S. *BBA-Mol. Basis Dis.* **2010**, *1802*, 162.

(71) Park, E.-J.; Yi, J.; Chung, K.-H.; Ryu, D.-Y.; Choi, J.; Park, K. *Toxicol. Lett*. **2008**, *180*, 222.

(72) Ozaki, T.; Yamashita, T.; Ishiguro, S.-i. *BBA-Mol. Cell Res.* **2009**, *1793*, 1848.

(73) Chipuk, J. E.; Green, D. R. *Nat. Rev. Mol. Cell Biol.* **2005**, *6*, 268.

(74) Li, T.-S.; Marbán, E. *Stem Cells* **2010**, *28*, 1178.

(75) Qiu, Y.; Liu, Y.; Wang, L. M.; Xu, L. G.; Bai, R.; Ji, Y. L.; Wu, X. C.; Zhao, Y. L.; Li, Y. F.; Chen, C. Y. *Biomaterials* **2010**, *31*, 7606.

(76) Ishikawa, K.; Ishii, H.; Saito, T. DNA and Cell Biol. 2006, 25, 406.

(77) Eom, H.-J.; Choi, J. *Environ. Sci. Technol.* **2010**, *44*, 8337.

(78) Liu, L. K.; Ni, F.; Zhang, J. C.; Jiang, X. L.; Lu, X. A.; Guo, Z. R.; Xu, R. Z. *Acta Bioch. Bioph. Sin.* **2011**, *43*, 316.

(79) Costelloe, T.; FitzGerald, J.; Murphy, N. J.; Flaus, A.; Lowndes, N. F. *Exp. Cell Res.* **2006**, *312*, 2677.

(80) Seki, S.; Mori, S.; Nakashima, A.; Oda, T. *Carcinogenesis* **1987**, *8*, 1391.

(81) Citterio, E.; Van Den Boom, V.; Schnitzler, G.; Kanaar, R.; Bonte, E.; Kingston, R. E.; Hoeijmakers, J. H. J.; Vermeulen, W. *Mol. Cell Biol.* **2000**, *20*, 7643.

(82) Martin, K. R.; Barrett, J. C. *Hum. Exp. Toxicol.* **2002**, *21*, 71.

(83) Finkel, T. *Febs Lett.* **2000**, *476*, 52.

CHAPTER 4

SHAPE SENSITIVE TOXICITY OF SILVER NANOMATERIALS

Publication from this chapter:

Chunyan Wang, Jitendra Kumar, Thang Toan Pham and Suresh Valiyaveettil, "Shape Selective Toxicity of Silver Nanomaterials on Human Skin Fibroblast Cells", submitted

4.1 Introduction

In the last few decades, many consumer products incorporated with nanomaterials have reached the market and nanomaterials have already been employed to create new analytical tools or imaging agents for biotechnology and life sciences.[1,2] Notably, silver nanomaterials (Ag NMs) are at the forefront in terms of commercialization due to their antibacterial and wound healing properties.[3] Recently, Ag NMs have also attracted much attention for their use in biomedical imaging and photothermal therapy owing to their surface plasmon resonances (SPR) in the visible spectral range.[4] Further, the plasmon properties of Ag NMs can be tailored with great versatility by controlling their shapes during synthesis.[5-7] Comparison of plasmonic properties of Ag and gold (Au) nanorods revealed that Ag nanorods showed two times higher sensitivity in the spectral range of 600 - 700 nm and about 10 to 20% in 700 - 900 nm region than Au nanorods.[8] Ag NMs also have the lowest plasmonic losses among other metallic nanomaterials in the UV-visible spectrum.[9] Furthermore, a rich variety of dipolar and higher order plasmon resonances have been illustrated for nanocubes and nanoparallelepipeds of Ag, in contrast to the simple dipolar modes found on Ag nanospheres or nanorods,[10] and they seems to be more toxic to surrounding healthy tissues.[11-13] However, toxicity of Ag NMs could be reduced through surface modifications.[9,14,15] Until now, there are limited studies on the cytotoxicity of Ag NMs with different morphologies, such as nanocubes and nanowires.[16] Therefore, it is important to evaluate the potential biological impact of different morphologies of Ag NMs to understand the shape sensitive interaction of such NMs with living organisms.

Toxicity of spherical Ag NMs has been established by many research groups using various models which also include results published from our lab.[17-19] In this chapter, response of human skin fibroblast cells on exposure to Ag nanocubes (Ag cube 1), truncated nanocubes (cube 2) and nanowires was

investigated. The experimental methods were described in detail in Chapter 2 (Materials and Methods):

1. Synthesis and purification of Ag cube1, cube 2 and nanowires;
2. Characterization of Ag cube1, cube 2 and nanowires – SEM, DLS, XRD and UV-Vis spectroscopy;
3. Dark field microscope, SEM and confocal microscope of Ag NMs treated cells – cell morphology and uptake of Ag NMs;
4. ATP production and metabolic activity – cell viability;
5. ROS production – mechanism of cytotoxicity;
6. Cell cycle analysis – cell proliferation;
7. Apoptosis and necrosis – cell death.

4.2 Results and discussion

Ag NMs with different shapes were synthesized through a polymer-mediated polyol process and characterized using a range of techniques.[20] Different morphologies were obtained by changing the experimental parameters such as the sequence of adding reagents (e.g. $AgNO_3$ and PVP) and reaction time. Synthesized nanocubes, truncated nanocubes and nanowires of Ag were characterized using SEM. Ag nanocubes and Ag truncated nanocubes were referred as Ag cube 1 and Ag cube 2, respectively, throughout the manuscript. SEM images revealed that Ag cube 1 showed regular cubic morphology with an average edge size of around 152 $\pm$ 15 nm whereas Ag cube 2 showed truncated cubic structures with etched corners of a regular cubes with an edge size 176 $\pm$ 27 nm (**Figure 4.1**). Interestingly, the Ag nanowires showed different lengths (7.5 $\pm$4.1 μm) with diameter 272 $\pm$ 78 nm. Low magnification SEM images (**Figure 4.2**) of Ag NMs suggested that more than 95% of nanoparticles were with the desired shapes. Based on these images, the size distribution histograms of Ag NMs were generated

(**Figure 4.3**).

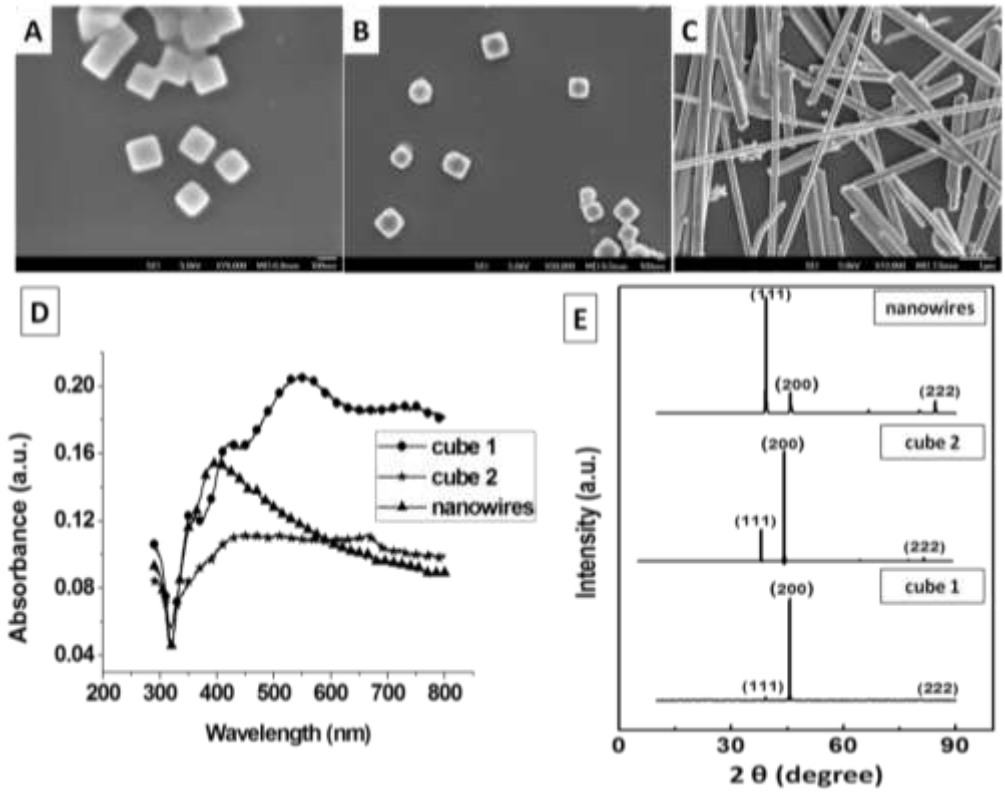

Figure 4.1: SEM images of cube 1 (A), cube 2 (B) and nanowires (C), UV-Vis spectra (D) and XRD patterns (E)of different Ag NMs.

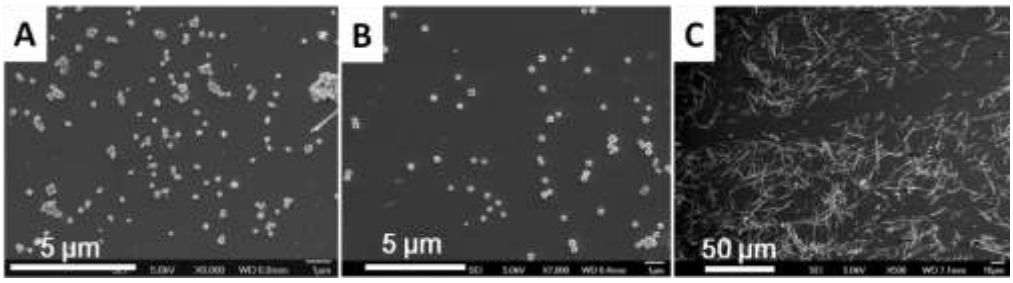

Figure 4.2: Low magnification SEM images of Ag cube 1(A), cube 2 (B) and nanowires.

The hydrodynamic size of Ag NMs in different media was measured using DLS to examine the stability with time. Ag NMs with desired concentrations (25 μg/mL and 100 μg/mL) were prepared in water, MEM or in cell medium and kept for 24 h at room temperature before measurement. The hydrodynamic size of Ag cube 1 was 214 ± 2 nm in water and 212 ± 1 nm in cell medium. However, their size significantly increased to 634 ± 104 nm in MEM medium (**Table 4.1**). Similar results were also observed for cube 2 in

different solvents (water: 317 ± 8 nm; cell medium: 290 ± 17 nm and MEM: 1564 ± 686 nm). Secondly, when increasing the concentrations of Ag NMs (cube 1 and cube 2) from 25 μg/mL to 100 μg/mL, no significant changes were observed in their hydrodynamic size (**Table 4.1**).

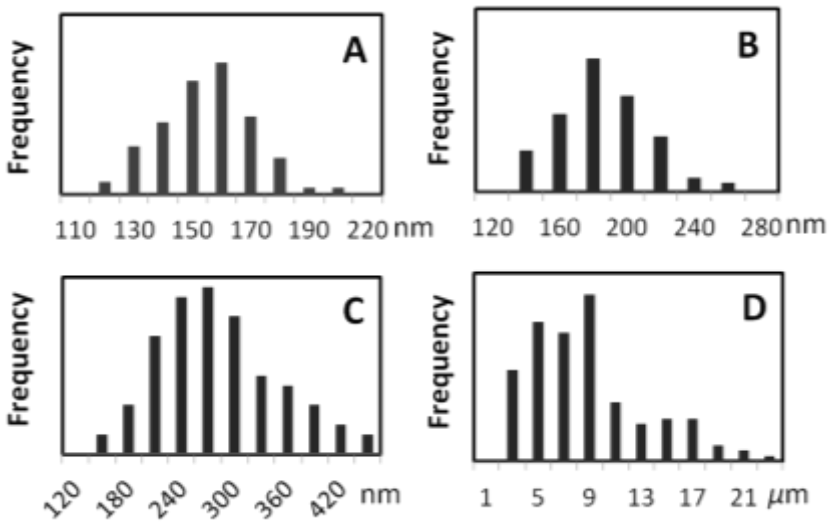

Figure 4.3: The size distribution histogram of Ag cube 1 (A), cube 2 (B), diameter (C) and length of Ag nanowires (D) generated using images captured with JEOL JSM 2010F (**Figure 4.2**).

Table 4.1: Hydrodynamic size of Ag NMs with different concentrations in different disperse solvents (water, MEM and cell medium).[a]

	SEM side length nm	Hydrodynamic size nm					
		Water		MEM		Cell medium	
		25 μg/mL	100 μg/mL	25 μg/mL	100 μg/mL	25 μg/mL	100 μg/mL
Ag cube 1	152 ± 15	214.5 ± 2.4	212.6 ± 1.0	634.2 ± 104.7	343.1 ± 7.7	212.4 ± 1.0	211.8 ± 6.0
Ag cube 2	176 ± 27	317.3 ± 8.1	306.8 ± 3.8	1564.0 ± 686.8	1024.0 ± 177.3	290.4 ± 13.0	298.0 ± 27.2
Ag nanowires	D: 272 ± 78 L: 7.5 ± 4.1 μm	1365.6 ± 120.6	1344.2 ± 214.2	1379.0 ± 251.2	2267.0 ± 254.6	1261.0 ± 417.7	1296.0 ± 551.6

[a]Each sample was detected in triplicates and the values were presented with mean ± standard deviation (SD). The large errors observed for Ag nanowires could be due to its high aspect ratio, as DLS is commonly used to detect the hydrodynamic size of spherical nanoparticles. The large errors for Ag cube1 and cube 2 in MEM medium could be attributed to their aggregation in this

medium.

Table 4.2: Zeta pontential of Ag NMs with different concentrations in different disperse solvents (water, MEM and cell medium).[a]

	Zeta mV					
	Water		**MEM**		**Cell medium**	
	25 μg/mL	**100 μg/mL**	**25 μg/mL**	**100 μg/mL**	**25 μg/mL**	**100 μg/mL**
Ag cube 1	-26.7 ± 0.6	-26.7 ± 0.7	-13.5 ± 0.8	-9.9 ± 0.9	-9.5 ± 0.2	-10.7 ± 1.0
Ag cube 2	-37.3 ± 0.5	-36.5 ± 0.6	-11.9 ± 0.7	-9.8 ± 1.3	-8.8 ± 0.2	-9.8 ± 0.3
Ag nanowires	-34.7 ± 1.4	-31.7 ± 2.2	-12.1 ± 0.9	-10.3 ± 0.2	-8.6 ± 1.1	-9.8 ± 0.7

[a]Each sample was detected in triplicates and the values were presented with mean ± standard deviation (SD).

Table 4.3: Ag ions release of Ag NMs in different disperse solvents (water and completed cell medium) at the concentration 100 μg/mL.[a]

	H_2O 100 μg/mL (Ag^+, ppm)		**Cell medium 100 μg/mL** (Ag^+, ppm)	
	1 day	**7 days**	**1 day**	**7 days**
Ag cube 1	0.363 ± 0.021	0.383 ± 0.015	0.640 ± 0.017	2.790 ± 0.062
Ag cube 2	< 0.10	0.276 ± 0.005	0.187 ± 0.006	0.687 ± 0.021
Ag nanowires	< 0.10	0.113 ± 0.011	0.123 ± 0.015	0.160 ± 0.010

[a]Every experiment was performed in triplicates and the values were presented with mean ± standard deviation (SD).

Overall, the results indicate that the colloidal stability of Ag NMs was independent on their concentrations, but closely related to the nature of the medium. There is significant interaction between Ag NMs and components of MEM medium (without FBS) while the addition of FBS significantly enhanced the colloidal stability of Ag NMs in cell medium. The observed differences in size from SEM and DLS measurements are attributed to the state of the dry sample (SEM) and solvated sample (DLS) used for measurements.[21,22] The apparent high and somewhat inaccurate hydrodynamic

diameter of Ag nanowires is attributed to their long aspect ratios (**Table 4.1**).

The surface charge of Ag NMs in different solvents was measured by zeta potential measurements and the results were summarized in **Table 4.2**. The zeta potential of Ag cube 1 (25 μg/mL) was -26.7 ± 0.6 mV in water, -13.5 ± 0.8 mV in MEM and -9.5 ± 0.2 mV in completed cell medium, which indicates that surface charge of Ag cube 1 were strongly dependent on their disperse solvent. Further, slight changes were observed when increasing the concentration of Ag cube 1 from 25 μg/mL to 100 μg/mL, indicating that concentration of the particles is also a factor in determining the final surface charge. Similar results were also found for Ag cube 2 and Ag nanowires in different solvents at different concentrations. Overall, the results indicate that the nature and composition of the solvents are the dominant factor for determining the surface charge of Ag NMs in solutions.

Silver ion (Ag^+) release form Ag NMs is one of the important factors which affect the toxic effects of Ag NMs to cells. Freshly prepared Ag NMs purified by centrifuge were suspend in water and cell medium(MEM with FBS) and kept in room temperature for 1 day and 7 days before performing the elemental analysis measurements. The experiments were performed in triplicates and the results were summarized in **Table 4.3**. After 24 h, Ag^+ in Ag cube 1 water solutions showed 0.363 ± 0.021 ppm (part per million) while both Ag cube 2 and Ag nanowires water solutions showed minimal release of Ag^+ with less than 0.10 ppm. However, increased release of Ag^+ from Ag NMs in cell medium was observed after 24 h. Ag^+ in Ag cube 1 showed 0.640 ± 0.017 ppm while those in Ag cube 2 and Ag nanowires were 0.187 ± 0.006 ppm and 0.123 ± 0.015 ppm, respectively. The results indicates that the release of Ag^+ from Ag NMs were dependent on both the morphology of Ag NMs and their disperse solvent. The release of Ag^+ was the fastest for Ag cube 1 in cell medium. Further, significant increase of Ag^+ from Ag NMs were observed in both water solution and cell medium after 7 days, indicating that the release of

Ag^+ was also strongly time-dependent.

Surface plasmon resonance (SPR) properties of Ag NMs with different morphologies were measured by UV-Vis-NIR spectrophotometer. The UV-visible absorption spectra of three aqueous dispersions that contained Ag cube 1, Ag cube 2, and Ag nanowires are shown in Figure 4.1D. The number of SPR peaks is dependent on the symmetry of particles: spherical particles showed one peak, while multiple peaks are often observed for cubic or triangular nanoparticles.[20] Ag cube 1 displayed three SPR peaks located at 352, 420, and 550 nm and can be attributed to the possibility of several distinct symmetries for dipole resonance.[23,24] Ag cube 2 exhibited two SPR peaks at 432 and 665 nm, which is in accordance with the reported values.[24,25] McLellan et al.[25] reported that Ag nanocubes with large size (100 nm) exhibited much broader SPR bands with a red-shift as compared to those with smaller size (60 nm), similar results were also observed for truncated Ag nanocubes. The extremely broad peaks observed in our study could be attributed to their large size distribution (150-180 nm). Ag nanowires showed two absorption peaks at 352 and 392 nm, which should be attributed to the out-of-plane quadrupole resonance and out-of-plane dipole resonance of the Ag nanowires, respectively.[9,26,27] The longitudinal mode of the Ag nanowires is absent here probably due to the high aspect ratio.[28]

In order to examine the crystalline structure of the resulting Ag NMs, XRD measurements were carried out (Figure 4.1E). Strong intensity of the (200) peak of Ag cube 1 in the XRD pattern indicated a predominance of oriented (100) facets.[6,29] A slight increase in intensity of the (111) peak of Ag cube 2 suggests the etching edge of sharp corner of nanocube.[30] Ag nanowires showed three strong peaks which were assigned to the diffraction of (111), (200) and (222) planes of metallic silver, which are in agreement with standard value for the face-centered cubic (fcc) structure of silver lattice (JCPDS card no. 04-0783).[9,31]

4.2.1 Cellular uptake of Ag NMs

As commented earlier, the purpose of preparation Ag NMs in this study was to check their shape-dependent bioactivity to human skin dermal fibroblast cells. The changes in cell morphology and cellular uptake of Ag cube 1, Ag cube 2 and Ag nanowires were measured by dark field optical microscopy. After cells were exposed to Ag NMs for 24 h, no significant increase in the number of floating cells was observed (**Figure 4.4**), indicating that absence of massive cell death through apoptosis or necrosis. Intact cell membrane and clear nucleus could be observed in untreated cells (**Figure 4.5A**), while cellular uptake of Ag cube 1, cube 2 and nanowires were clearly observed in the cells (**Figure 4.5B-D**).

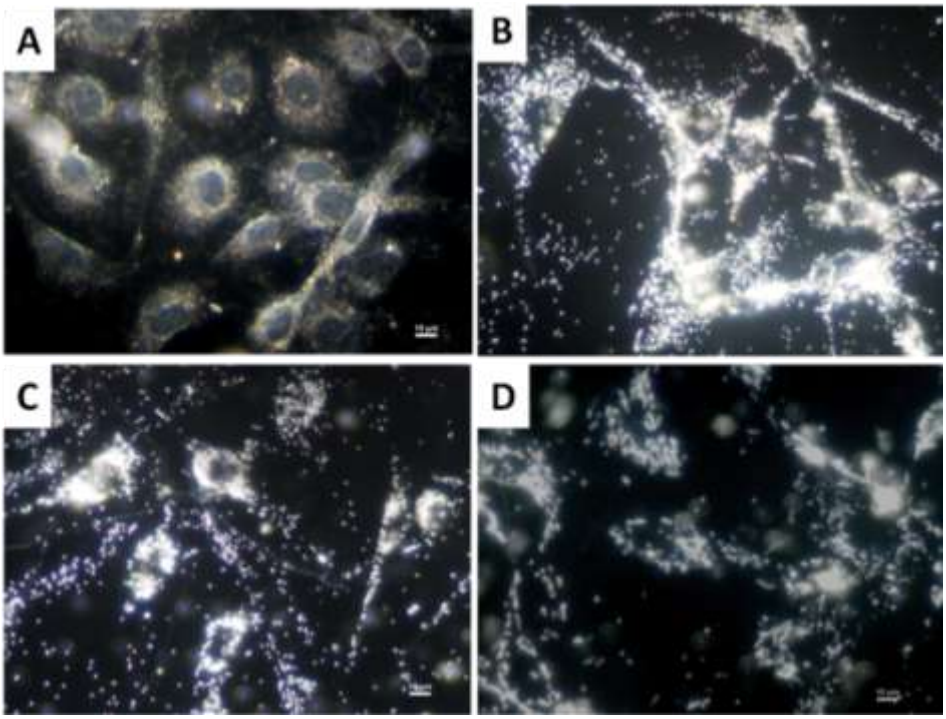

Figure 4.4: Dark field optical images of human skin fibroblast cells untreated (A) and treated with Ag nanocubes (B), Ag truncated nanocubes (C) and Ag nanowires (D). Concentration of Ag NMs = 25 μg/mL and Scale bar= 10 μm

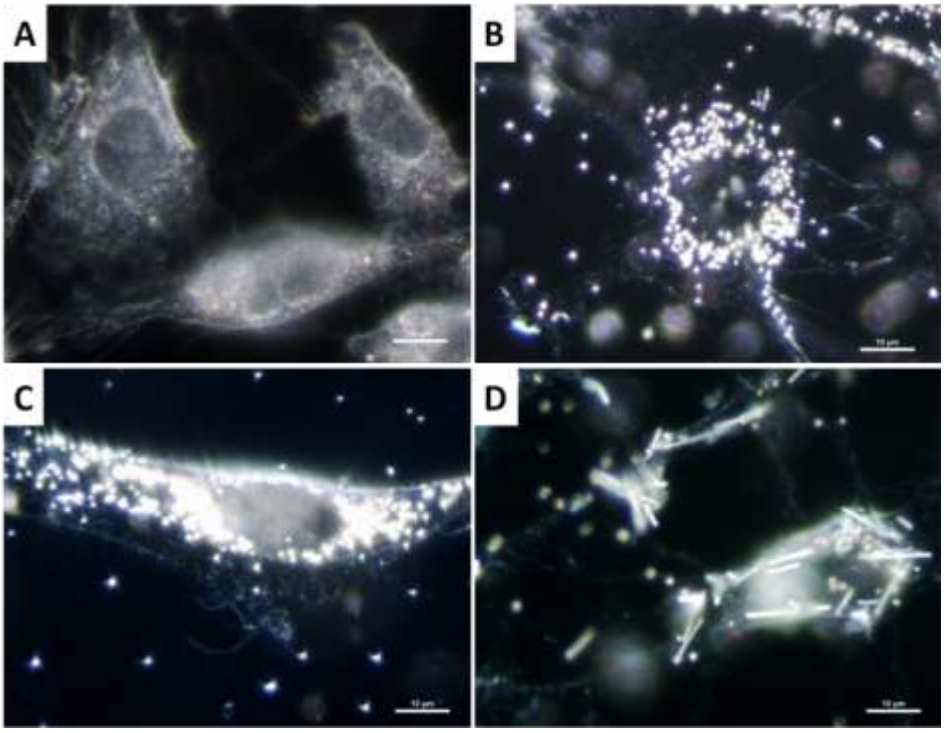

Figure 4.5: High magnification optical microscope images of cells (Passage 7) untreated (A) and treated with cube 1 (B), cube 2 (C) and nanowires (D) of Ag NMs. Concentration of Ag NMs = 25 μg/mL, scale bar is 10 μm

To confirm whether Ag NMs were only attached on the surface of cell membrane or penetrate inside the cells, human skin dermal fibroblast cells with Ag NMs (25 μg/mL, 24 h) treatment were analyzed using SEM. In order to remove the unattached Ag NMs, cells were washed several times with PBS solution before fixation. No significant morphology changes were observed while bright dots/wires were found on the cell surface for cells treated with Ag NMs (**Figure 4.6**). High magnification SEM images were taken to confirm the presence of Ag NMs on the cell surface (**Figure 4.7**). Ag cube 1 and Ag cube 2 were found to be displayed both on the surface of cell membrane and inside the cells (**Figure 4.7B and 4.7C**). Owing to the high aspect ratio, the Ag nanowires were observed to partially penetrate the cells (**Figure 4.7D**).

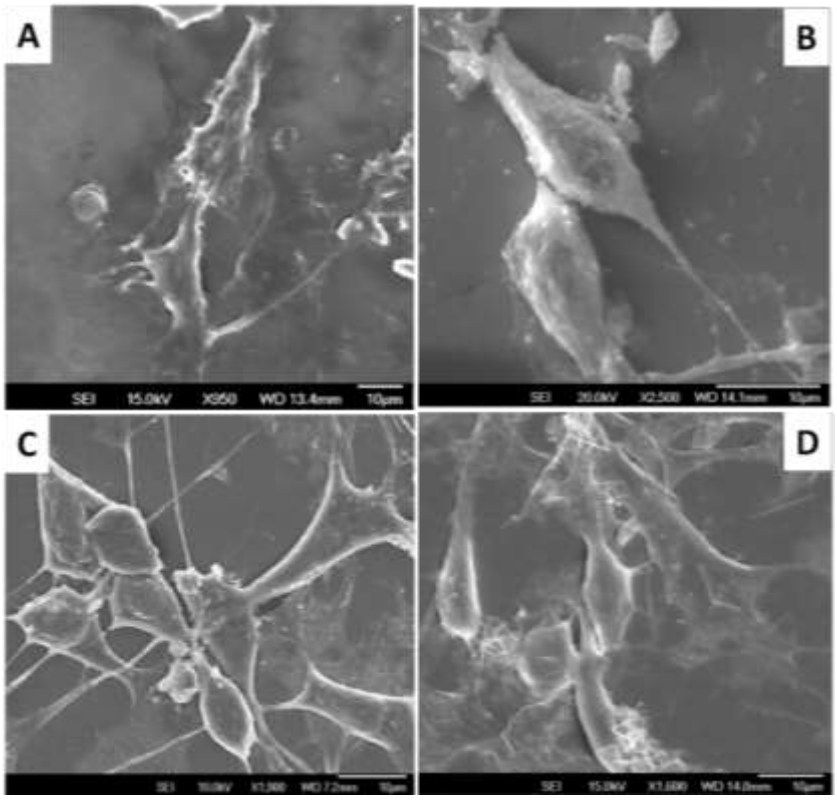

Figure 4.6: Low magnification SEM images of human skin fibroblast cells untreated (A) and treated with Ag nanocubes (B), Ag truncated nanocubes (C) and Ag nanowires (D). Concentration of Ag NMs = 25 μg/mL

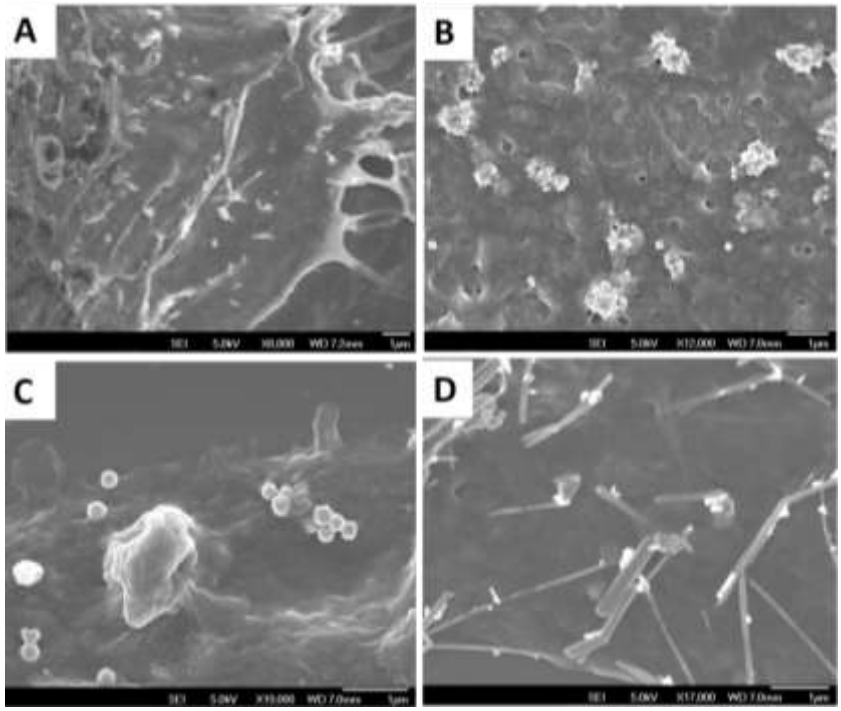

Figure 4.7: High magnification SEM images of cells untreated (A) and treated with Ag cube 1 (B), Ag cube 2 (C) and Ag nanowires (D). Concentration of Ag NMs = 25 μg/mL

In order to further establish the presence of Ag NMs inside the cells, energy-dispersive X-ray spectroscopy (EDX) analysis was performed. Cells treated with Ag cube 1 were chosen as an example for EDX analysis. The gray spots were selected to provide comprehensive evidence on the presence of Ag NMs underneath the cell membrane (**Figure 4.8**). Gray spots displayed on the cells (**Figure 4.8A**) were analyzed and the Ag peaks shown in EDX analysis confirmed the presence of silver (**Figure 4.8B**). Similar data were obtained from other gray spots on the surface. As a control, the dark area on the cell membrane (**Figure 4.8C**) was also analyzed. The EDX pattern was different from gray spots and did not show any Ag peaks (**Figure 4.8D**).

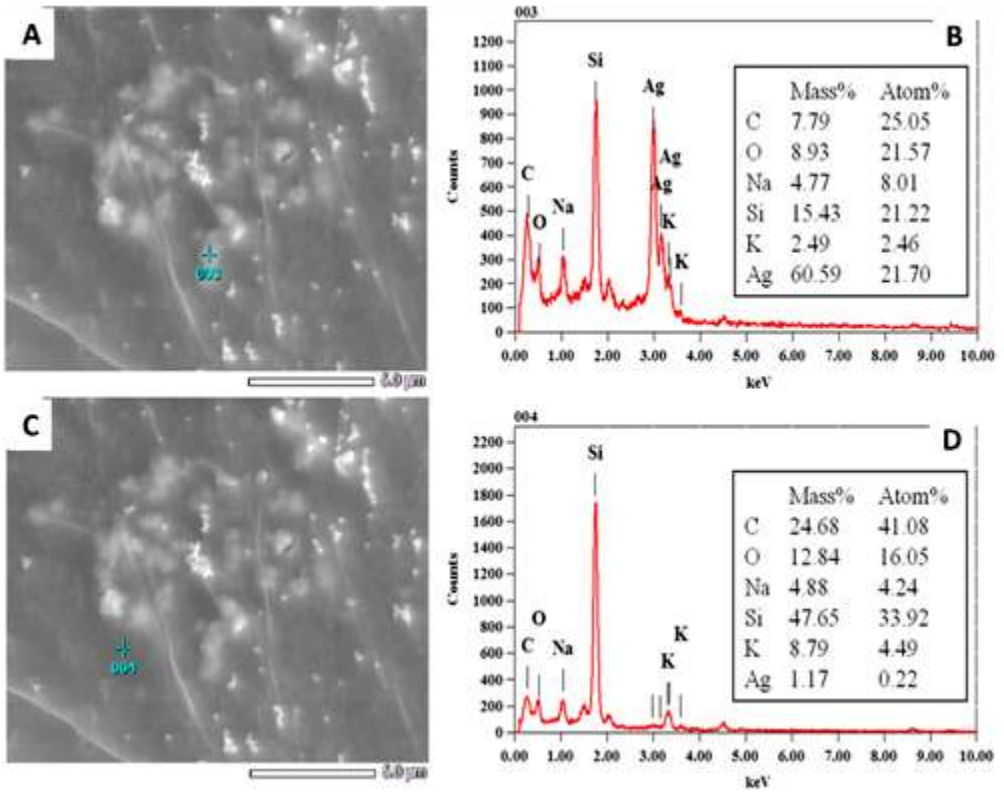

Figure 4.8: SEM images and EDS analysis at marked places on cells (Passage 7) treated with Ag cube 1 to confirm the cellular uptake. The images in the right panel correspond to the analysis of the marked places in the images on the left panel. Concentration of Ag cube 1 = 25 μg/mL

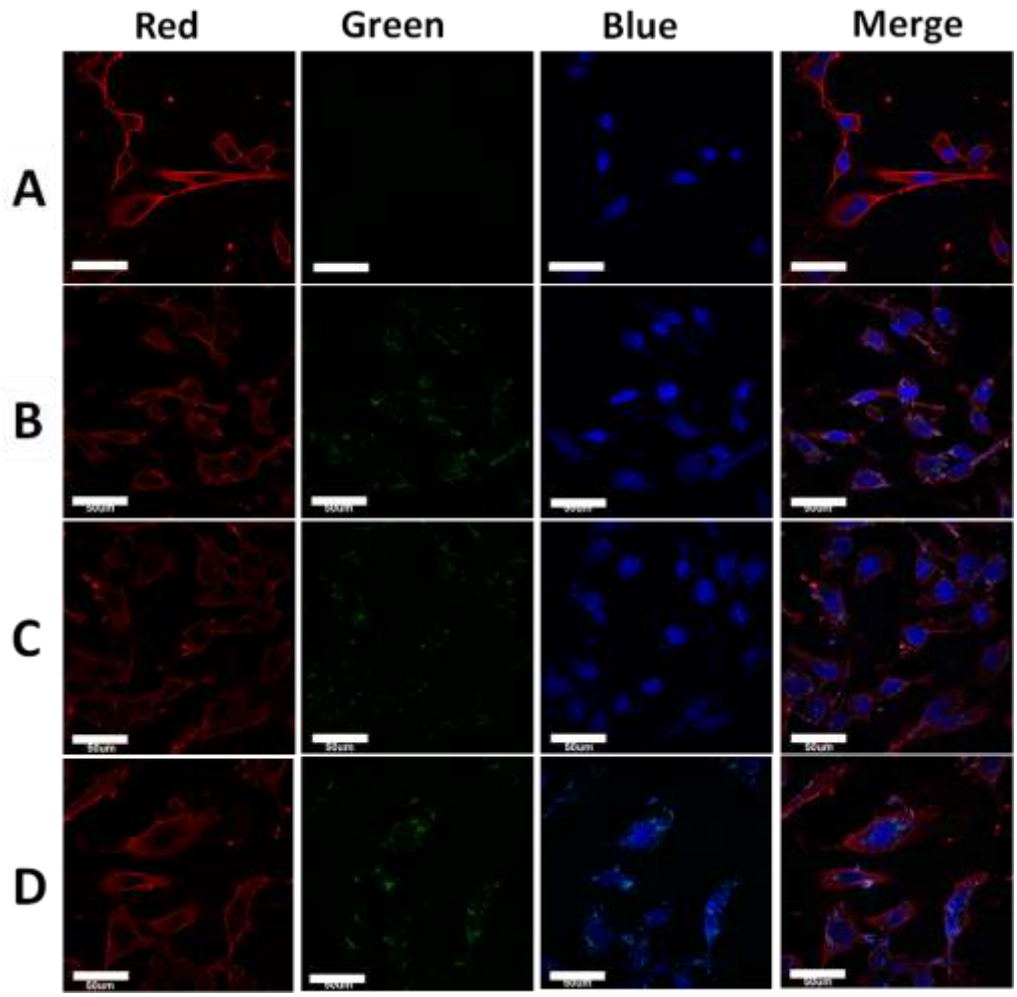

Figure 4.9: Confocal microscope images of cells stained with Cellmask deep red and DAPI. Cellmask stained the cell membrane showed red color while DAPI stained cells showed blue nucleus. Due to their SPR effect, Ag cube 1, cube 2 and nanowires exhibited both blue and green color in the images. Images A are untreated cells, B cells with Ag cube 1 treatment, C with Ag cube 2 treatment and D are cells with Ag nanowires treatment. Concentration of Ag NMs = 25 μg/mL

The distribution of Ag NMs inside the cells was also examined using a confocal microscope (**Figure 4.9**). After treatment with Ag NMs (25 μg/mL, 24 h), cells were stained with both Cellmask Deep Red (Invitrogen) and 4',6-diamidino-2-phenylindole (DAPI, Sigma Aldrich) to distinguish the cell membrane and nucleus. Owing to their small size and special SPR effects, Ag cube 1, cube 2 and nanowires exhibited photoluminescence after excitation at 405 and 473 nm. Klein et al. reported that Au nps with the size from 15 to 80 nm exhibited similar effects after excitation with light at 543 and 633 nm.[32] As

seen in **Figure 4.9**, clear cell membrane (Red) and nucleus (Blue) were observed in control cells (untreated cells). Ag NMs treated cells showed both blue and green fluorescence in the confocal images (**Figure 4.9**), confirming their presence inside the cells after treatment. Z-stack images captured by confocal microscope (**Figure 4.10**) suggest that Ag NMs were not only present on the surface of cell membrane but also penetrated inside the cells, which is consistent with earlier reports.[33]

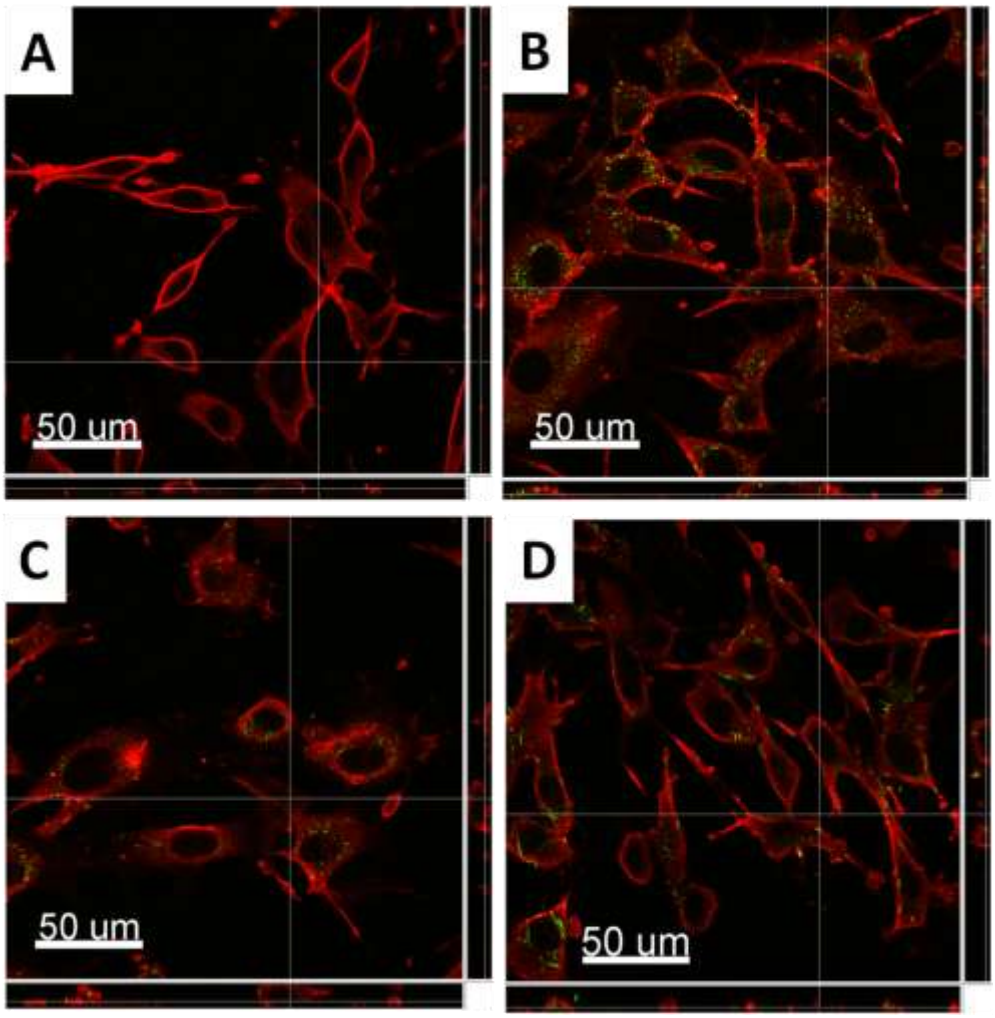

Figure 4.10: Z-stack confocal images of untreated cells (A), Ag nanocubes (B), truncated nanocubes (C) and nanowires (D) exposed cells are given. A, B, C and D are merge images of cells treated with Cellmask (A) and Cellmask plus Ag NMs (B-D). The cell membrane showed red color and green dots represent the Ag NMs (25 μg/mL, 24 h).

4.2.2 Cellular responses of Ag NMs

The cellular responses of Ag NMs were further explored using viability assays, which were designed to measure activities related to cellular growth and viability. Normally, viability assays include monitoring the level of metabolic biomarkers such as mitochondrial reductase potential and ATP.[34]

Since the viability of cells could be measured by detecting reduced potential in mitochondria, resazurin, one of the most commonly used assays, was chosen to detect the metabolic activity of the Ag NMs treated cells.[35] The metabolic activity decreased for cells treated with Ag cube 1 with an increase in the concentration of nanomaterials (**Figure 4.11**), indicating a dose-dependent toxicity. Unlike the cells treated with Ag cube 1, metabolic activity of cells exposed to Ag cube 2 and Ag nanowires treatment were less affected and no significant decrease was observed even at high concentrations 200 μg/mL (**Figure 4.11**).

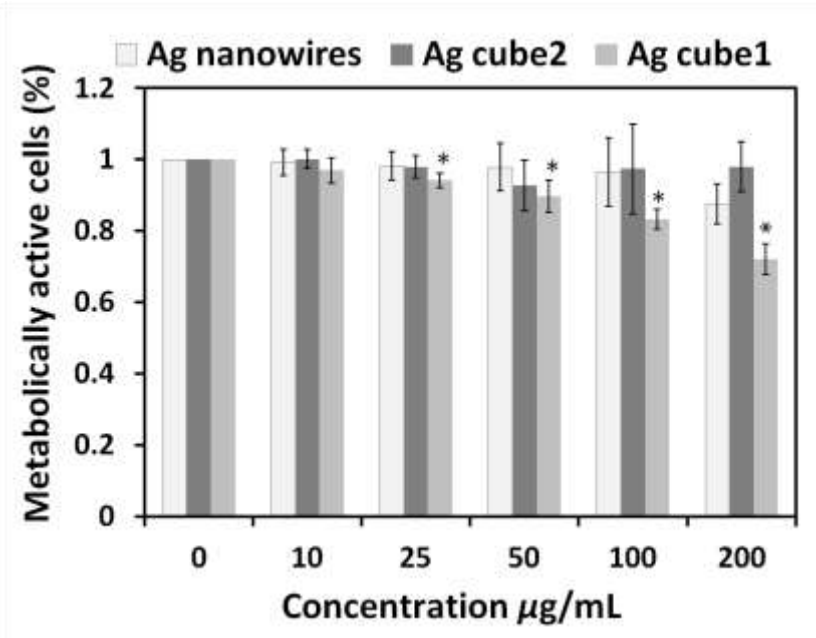

Figure 4.11: Mitochondrial activity of cells (Passage 7-9) after exposure to various concentrations of Ag cube 1, Ag cube 2 and Ag nanowires for 24 h. The *y*-axis represents the percentage of metabolically active cells which relates to viable cells present in the treated sample after 24 h and the *x*-axis represents the concentrations of Ag NMs. The values represent the mean ± standard deviation of three independent experiments; * denotes $P < 0.05$ with respect to

untreated cells using Student's t test.

The viability of cells was further detected using a widely accepted, rapid and sensitive ATP assay.[36-38] ATP contents of cells treated with Ag NMs were less affected at low concentrations whereas significant decrease was shown at high concentrations (**Figure 4.12**), indicating a concentration dependent toxicity. Among all three Ag NMs, Ag cube 1 was the most toxic, followed by Ag cube 2 and Ag nanowires. Higher ATP content was observed in cells treated with Ag nanowires as compared to that treated with Ag cube 1 or Ag cube 2 at high concentrations (100 and 200 μg/mL). To check the presence of any toxic materials left over from the synthesis, toxicity studies were done using the supernatant liquid obtained after centrifugation of Ag NMs solution, which is expected to contain excess of reagents, if any. Our results showed no evidence of toxicity for this supernatant liquid (**Figure 4.13**). The cell viability in all the wells was comparable to that of control.

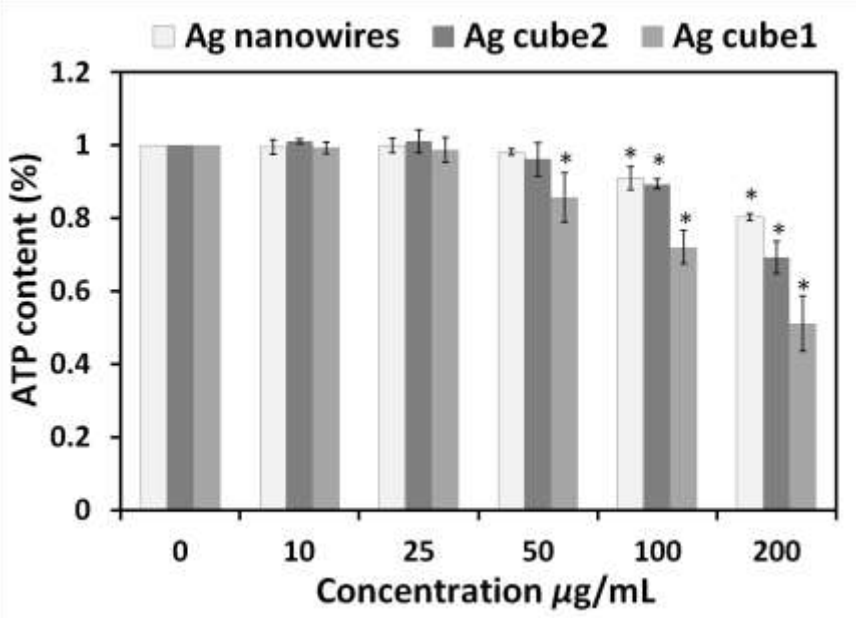

Figure 4.12: ATP content of cells (Passage 7-9) after exposure to various concentrations of Ag cube 1, Ag cube 2 and Ag nanowires for 24 h. The *y*-axis represents the percentage of ATP content which relates to viable cells present in the treated sample after 24 h whereas the *x*-axis represents Ag NMs with different concentrations. The values represent the mean ± standard deviation of three independent experiments; * denotes $P < 0.05$ with respect to untreated cells using Student's t test.

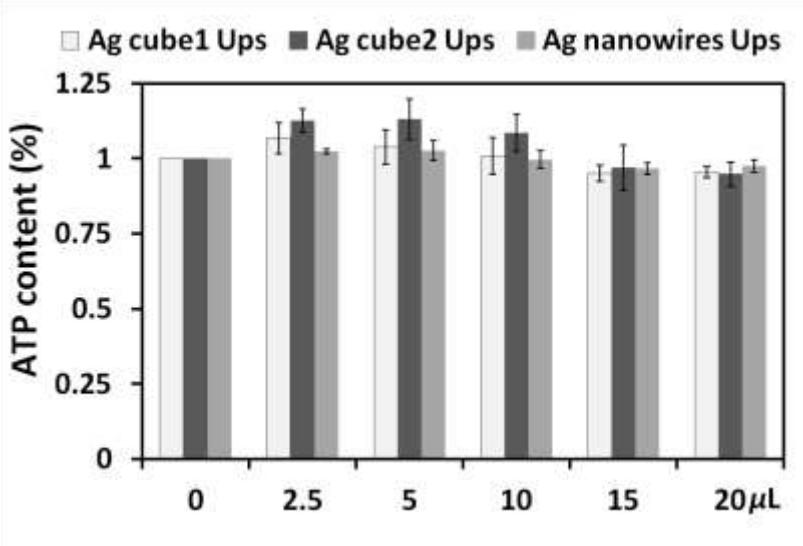

Figure 4.13: Toxicity studies of the supernatant liquid obtained after centrifugation of Ag NMs solution were investigated using ATP assay. ATP content of cells exposed to various volumes (0, 2.5, 5, 10, 15 and 20 μL) of centrifuge supernatant liquid of Ag cube 1, Ag cube 2 and Ag nanowires for 24 h. The values represent the mean ± standard deviation of three independent experiments.

The viability data suggested that Ag cube 1 nanoparticles seems to be more toxic, while Ag cube 2 and Ag nanowires were relatively less toxic. Toxicity of nanomaterials is believed to be multifactorial, where size, morphology, composition, surface charge, surface functionalization, concentration and potential to release the corresponding metal ions could play significant roles in living systems.[2,39-43] Earlier reports showed that spherical Ag nanoparticels exhibited size-dependent toxicity.[16] Nanoparticles with smaller size are reported to be more toxic than those with the larger size due to their higher penetration rate into cells and increase in reactive surface area for interaction with biomolecules.[16,39,44,45] PVP coated Ag nps were more toxic to zebrafish embryos than citrate coated ones at the same particle core size (110 nm).[46] Cytotoxicity studies of Ag spherical nanoparticles (100 - 200 nm) showed they could induce cell damage at very low concentrations 10 μg/mL, or even less (5 μg/mL).[47-50] In our study, Ag NMs with different morphologies were less toxic as compared to reported Ag sphere nanoparticles. Ag nanocubes caused mitochondrial damage at a concentration of 25 μg/mL,

while Ag truncated nanocubes and nanowires induced ATP decrease at a higher concentration (100 μg/mL) and showed no mitochondrial damage even at 200 μg/mL. The relationship of morphology and toxicity of Ag NMs were explored, as our Ag NMs are all PVP-capped. The different toxicities of Ag NMs could be explained using several factors. First, the size of Ag cube 1 was the smallest (150 nm), while Ag cube 2 (180 nm) and Ag nanowires (2 -10 μm) were slightly larger. Second, different morphologies are expected to induce different degree of toxicities to cells.[51,52] Relatively sharp edges of Ag cube 1 may lead to instability of NMs due their high chemical potential, which enable particles to penetrate cell membrane and then decompose inside cells much more easily, as compared to the other two Ag NMs.

4.2.3 Mechanism of cytotoxicity

Oxidative stress has been reported to play an important role in the NMs toxicity, which could induce oxidative damage to protein and DNA.[53-56] To explore the role of oxidative stress toward toxicity of Ag NMs, reactive oxygen species (ROS) production of cells with Ag NMs treatment were measured by 2', 7' - dichlorohydrofluorescein diacetate (DCF-DA, Invitrogen) staining. After exposure to the cell, DCF-DA was first deacetylated by cellular esterases to a non-fluorescent compound. In the presence of ROS, it could be oxidized into a highly fluorescent compound 2', 7' - dichlorofluorescin (DCF). Fluorescent intensity of the cells treated with Ag NMs and stained with DCFH-DA was increased. Unstained cells were used as a negative control to detect the autofluorescence from cells. Untreated cells (control) were used as standards to calculate the extent of ROS production in Ag NMs treated cells by measuring the percentage increase in fluorescence intensity (**Figure 4.14**). Cells treated with Ag NMs (25 μg/mL) showed increase in percentage of gated cells with high ROS production as compared to control cells. Cells treated with Ag NMs showed increase in fluorescent intensity – Ag nanowires (9.7%); Ag cube 2 (12.6%) and Ag cube 1 (17.6%).

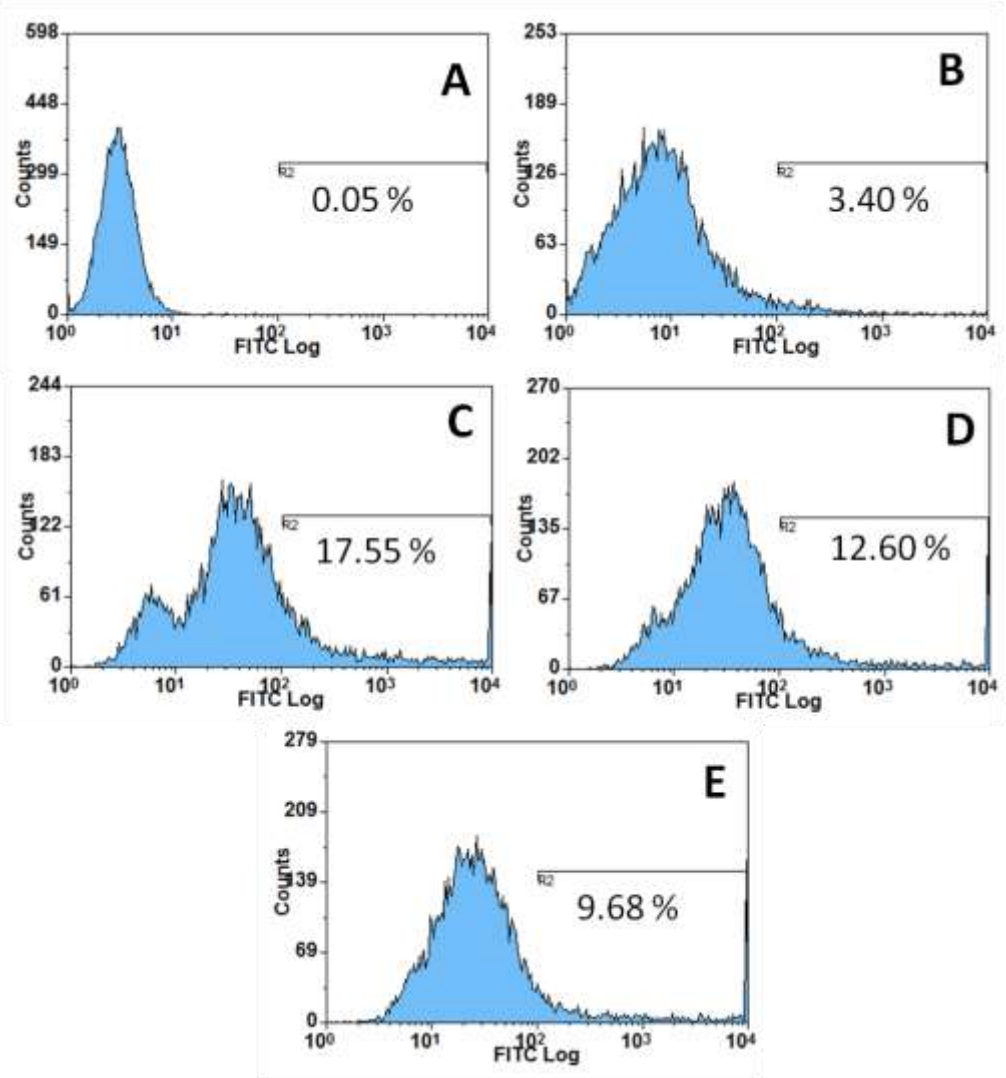

Figure 4.14: The graphs of ROS production in cells without (A and B) or with Ag cube 1 (C), cube 2 (D) and nanowires (E) treatment (25 μg/mL, 24h) by flow cytometry. The graph represents the percentage of gated cells among the Ag NMs exposed cells. Untreated cells were considered as control (B). Cells without DCF-DA staining (negative control) were used to detect the autofluorescence of cells (A). The percentage of cells with high fluorescent intensity (FITC $\geq 10^2$) was considered as gated cells and totally 10000 cells were calculated in each graph.

The early sign of the DNA damage inside the cells caused by NMs could be seen in the cell progression. Cells with reversible DNA damage will accumulate in gap1 (G1), DNA synthesis (S) or in gap2/mitosis (G2/M) phase, while cells with irreversible DNA damage will undergo apoptosis, and then accumulate in subG1 phase. Thus toxicity studies of Ag NMs were further extended to cell cycle analysis through detecting parameters such as apoptosis

and cell cycle arrest to confirm DNA damage. The influence of Ag NMs on the cell cycle was analyzed by detecting DNA content using a fluorescent DNA-selective dye PI, which exhibits emission signals proportional to the content of DNA. Compared to untreated cells (control), an increase of cell population in G2/M phase (9% for Ag cube 1, 7% for Ag cube 2 and 11% for Ag nanowires, respectively) was observed (**Figure 4.15**), indicating that all Ag NMs could induce G2 arrest. For control cells, major cell population was observed in G1 phase, whereas in cells treated with Ag cube 1, a decrease in G1 population was observed which was accompanied by an increase in G2/M and S population. For the cells treated with Ag cube 2 and Ag nanowires, the proportion of cells in S phase was less affected as compared to the G2/M population. Absence of cells in subG1 was observed for all Ag NMs treated cells, indicating that no significant apoptosis or necrosis had occurred.

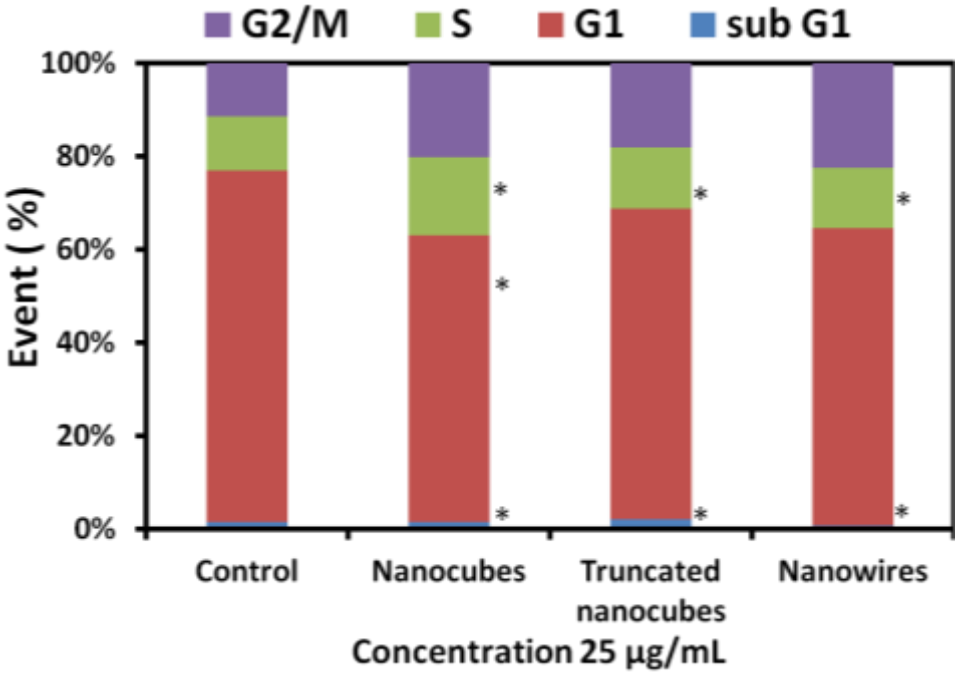

Figure 4.15: Ag cube 1 treated cells showed an increase in the S/G2 population, and Ag cube 2 and Ag nanowires treated cells showed G2/M arrest. Markers were set at regions of interest (subG0, G1, S, and G2/M), and the percentage of cells (events) under each area was generated using Summit V4.3.02 software; * represents $P < 0.05$. Histograms are included in **Figure 4.16**.

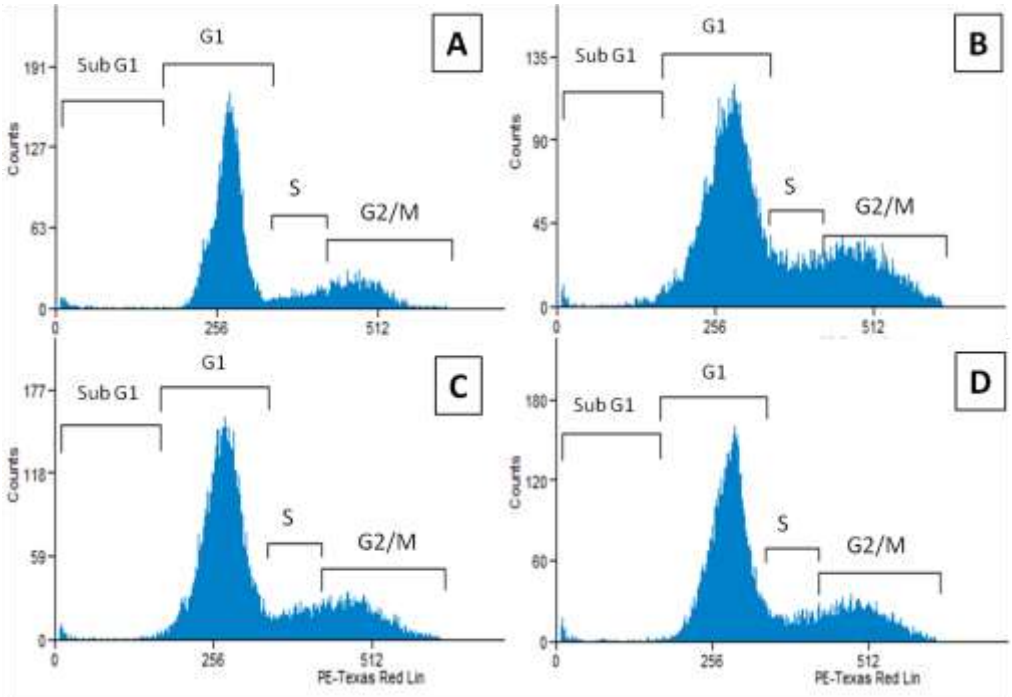

Figure 4.16: Histograms represent cell cycle analysis of human skin fibroblast cells. The control showed normal distribution of sub G1, G1, S and G2/M (A). The cells treated with 25 μg/mL Ag nanocubes (B), truncated nanocubes (C) and nanowires (D) showed increases in S/G2 population indicating S/G2 arrest. Markers were drawn on regions of interest (subG1, G1, S and G2/M) to generate statistics of cells under each region. Corresponding statistics were generated using Summit V4.3.02 software.

Mechanism of cytotoxicity of Ag NMs was explored by investigating the relationships of ATP content, mitochondrial activity, oxidative stress and DNA damage. The decreased cellular ATP content could be caused by the damage of the mitochondrial respiratory chain. The mitochondrial dysfunction and damage could be attributed to two possible reasons: oxidative stress induced by ROS production and mechanical injury caused by nanoparticle depositions in mitochondria. Oxidative stress is considered as a common mechanism for cell damage induced by nanomaterials.[53] Deposition of nanomaterials inside mitochondria can induce mitochondrial dysfunction by disrupting electron transport chain and ultimately result in increase of ROS, low ATP yield and even apoptosis.[17,57] Many nanomaterials such as titanium dioxide, zinc oxide, silicon dioxide and multi-wall carbon nanotubes were known to exert toxicity through oxidative stress.[58-60] ROS is also believed to be the major reason of

spontaneous damage to DNA and genotoxicity observed among cells treated with metal oxide nanoparticles.[58] In eukaryotic cells, DNA damage causes cell cycle arrest at the G2/M and/or S boundary, allowing cells extra time to repair damages before replication.[61] The reduction in ATP content after Ag NMs treatment could affect the DNA repair, as ATP is required in the repair process.[62,63] Cell cycle data indicates reversible DNA damage, as cells arrested in the G2/M and S phase after exposure to Ag NMs, which enable them to have enough time for the cells to repair the damaged DNA. The level of cell cycle arrest is dependent on the shape of NMs where a drastic increase in cell population was observed in the G2/M and S phase for Ag cube 1.

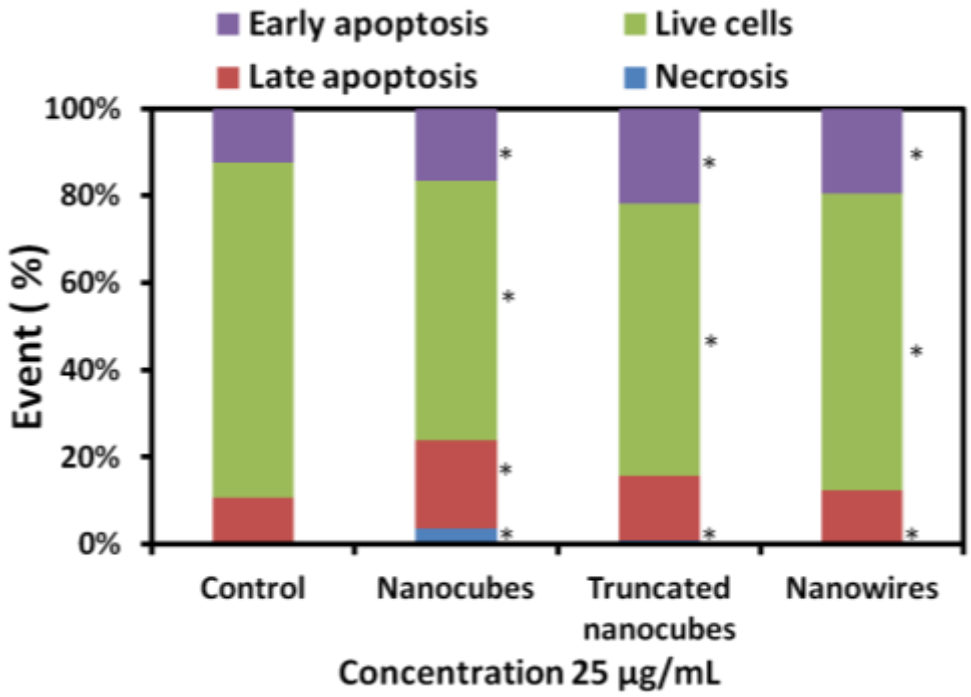

Figure 4.17: Apoptosis and necrosis of cells with Ag nanocubes, truncated nanocubes and nanowires treatement. Ag nanocubes treated cells showed an increase of cell population in both apoptosis (early and late) and necrosis death mode, while Ag truncated nanocubes and nanowires induced cell death mainly through apoptosis. The percentage of cells under each area was generated using Summit V4.3.02 software * represents $P < 0.05$.

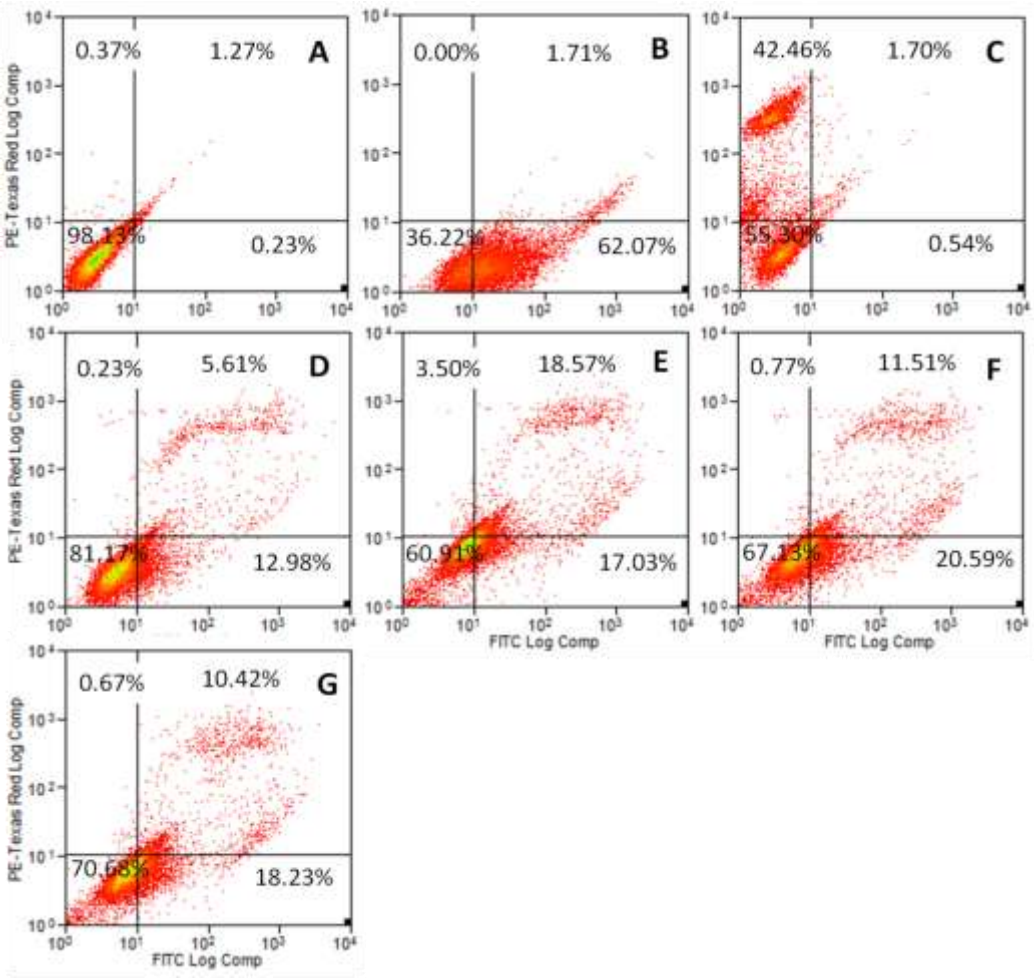

Figure 4.18: Dot plots from Annexin-FITC staining of human skin fibroblast cells. Untreated cells (A) are used to calculate % of change in population. Cells accumulating at lower left window represent live cells. Apoptosis positive controls (Staurosporine treated) accumulating on lower right window (B). Necrosis positive controls (H_2O_2 treated) which accumulate on upper left window for red fluorescent cells (C). Late apoptotic cells will accumulate in upper right window. (D) shows cell population for cells treated with Ag nanocubes, (E) represents cells treated with truncated nanocubes and (F) represents cells treated with Ag nanowires (25 μg/mL). The % of cells under each category (live, early and late apoptosis, necrosis) is represented in respective windows.

4.2.4 Apoptosis and necrosis

Apoptosis and necrosis are two general modes of cell death.[64] Flow cytometry and Annexin V assays were used to study both processes using cells treated with Ag NMs (**Figure 4.17**). Statistical data were acquired from the dot plots (**Figure 4.18**). Viable cells are negative for both PI and Annexin staining

whereas necrotic cells are PI positive and Annexin negative. Early apoptotic cells are PI negative and Annexin positive, whereas later apoptotic cells are positive for both PI and Annexin V staining. For untreated cells (control), no significant cell death (late apoptosis) was observed, and major cell population remained viable (**Figure 4.17**). Compared to untreated cells, a significant increase in early apoptosis was observed among Ag NMs treated cells. Cells treated with Ag cube 1, cube 2 and nanowires showed a small increase in necrosis; however, apoptosis was the dominant process. Ag cube 1 induced a significant increase of cell population in late apoptosis (20%) and a slightly increase in early apoptosis stage (16%). However, Ag cube 2 and nanowires caused significant increases of cell population in early apoptosis (cube 2: 22% and nanowires: 20%) other than late apoptosis (cube 2: 15% and nanowires: 12%). The results demonstrated that cells treated with Ag cube 1 became unhealthier as compared to those treated with cube 2 and nanowires.

4.3 Conclusion

Ag NMs with different morphologies showed interesting optical properties, which offer opportunities for potential applications. Furthermore, they also showed different levels of toxicity to cells. Among three Ag NMs discussed in the paper, Ag cube 1 was the most toxic, while Ag cube 2 and Ag nanowires were relatively less toxic. Cellular uptake revealed that all Ag NMs could penetrate inside the cells, irrespective of their shapes. Oxidative stress was believed to be the reason for toxicity, which could induce DNA damage shown by cell cycle arrest. Cells exposed to Ag NMs showed G2/M or S stage cell cycle arrest, indicating a reversible DNA damage, which could either be repaired in cell cycle or undergone apoptosis. Only Ag cube 1 treated cells showed a significant increase in later apoptosis, which is consistent with viability data. In viability test, Ag cube 1 treated skin fibroblast cells showed mitochondrial damage (25 μg/ml), while Ag cube 2 and nanowires caused ATP decrease (100 μg/ml) in cells and showed no mitochondrial damage even at

200 μg/ml. The low toxicity of Ag cube 2 and Ag nanowires make them potential candidates for applications in drug delivery or bioimaging in the future.

4.4 References

(1) Wu, J.; Wang, C.; Sun, J.; Xue, Y. *ACS Nano* **2011**, *5*, 4476.

(2) Oh, E.; Delehanty, J. B.; Sapsford, K. E.; Susumu, K.; Goswami, R.; Blanco-Canosa, J. B.; Dawson, P. E.; Granek, J.; Shoff, M.; Zhang, Q.; Goering, P. L.; Huston, A.; Medintz, I. L. *ACS Nano* **2011**, *5*, 6434.

(3) Ahamed, M.; Karns, M.; Goodson, M.; Rowe, J.; Hussain, S. M.; Schlager, J. J.; Hong, Y. L. *Toxicol. Appl. Pharm.* **2008**, *233*, 404.

(4) Damm, C.; Segets, D.; Yang, G. A.; Vieweg, B. F.; Spiecker, E.; Peukert, W. *Small* **2011**, *7*, 147.

(5) Zeng, J.; Zheng, Y. Q.; Rycenga, M.; Tao, J.; Li, Z. Y.; Zhang, Q. A.; Zhu, Y. M.; Xia, Y. N. *J. Am. Chem. Soc.* **2010**, *132*, 8552.

(6) Im, S. H.; Lee, Y. T.; Wiley, B.; Xia, Y. N. *Angew. Chem. Int. Edit.* **2005**, *44*, 2154.

(7) Uchida, S.; Taguchi, A.; Mitani, M.; Ichimura, T.; Kawata, S.; Yamamura, K.; Zettsu, N. *J. Nanosci. Nanotechnol.* **2011**, *11*, 2890.

(8) Jakab, A.; Rosman, C.; Khalavka, Y.; Becker, J.; Trugler, A.; Hohenester, U.; Sonnichsen, C. *ACS Nano* **2011**, *5*, 6880.

(9) Ramasamy, P.; Seo, D. M.; Kim, S. H.; Kim, J. *J. Mater. Chem.* **2012**, *22*, 11651.

(10) Cortie, M. B.; Liu, F. G.; Arnold, M. D.; Niidome, Y. *Langmuir* **2012**, *28*, 9103.

(11) Park, M.; Neigh, A. M.; Vermeulen, J. P.; de la Fonteyne, L. J. J.; Verharen, H. W.; Briede, J. J.; van Loveren, H.; de Jong, W. H. *Biomaterials* **2011**, *32*, 9810.

(12) Panyala, N. R.; Pena-Mendez, E. M.; Havel, J. *J. Appl. Biomech.* **2008**, *6*, 117.

(13) Yeo, M. K.; Kang, M. *B. Kor. Chem. Soc.* **2008**, *29*, 1179.

(14) Moulton, M. C.; Braydich-Stolle, L. K.; Nadagouda, M. N.; Kunzelman, S.; Hussain, S. M.; Varma, R. S. *Nanoscale* **2010**, *2*, 763.

(15) Sur, I.; Cam, D.; Kahraman, M.; Baysal, A.; Culha, M. *Nanotechnology* **2010**, *21*.

(16) George, S.; Lin, S.; Ji, Z.; Thomas, C. R.; Li, L.; Mecklenburg, M.; Meng, H.; Wang, X.; Zhang, H.; Xia, T.; Hohman, J. N.; Lin, S.; Zink, J. I.; Weiss, P. S.; Nel, A. E. *ACS Nano* **2012**, *6*, 3745.

(17) AshaRani, P. V.; Low Kah Mun, G.; Hande, M. P.; Valiyaveettil, S. *ACS Nano* **2008**, *3*, 279.

(18) AshaRani, P.; Hande, M. P.; Valiyaveettil, S. *BMC Cell Biol.* **2009**, *10*, 65.

(19) Asharani, P. V.; Sethu, S.; Vadukumpully, S.; Zhong, S.; Lim, C. T.; Hande, M. P.; Valiyaveettil, S. *Adv. Funct. Mater.* **2010**, *20*, 1233.

(20) Wiley, B.; Sun, Y. G.; Mayers, B.; Xia, Y. N. *Chem-Eur. J.* **2005**, *11*, 454.

(21) Barth, B. M.; Sharma, R.; Altinoglu, E. I.; Morgan, T. T.; Shanmugavelandy, S. S.; Kaiser, J. M.; McGovern, C.; Matters, G. L.; Smith, J. P.; Kester, M.; Adair, J. H. *ACS Nano* **2010**, *4*, 1279.

(22) Kittler, S.; Greulich, C.; Gebauer, J. S.; Diendorf, J.; Treuel, L.; Ruiz, L.; Gonzalez-Calbet, J. M.; Vallet-Regi, M.; Zellner, R.; Koller, M.; Epple, M. *J. Mater. Chem.* **2010**, *20*, 512.

(23) Rycenga, M.; McLellan, J. M.; Xia, Y. N. *Chem. Phys. Lett.* **2008**, *463*, 166.

(24) Xiong, Y. *Chem. Commun.* **2011**, *47*, 1580.

(25) McLellan, J. M.; Siekkinen, A.; Chen, J. Y.; Xia, Y. N. *Chem. Phys. Lett.* **2006**, *427*, 122.

(26) Bi, Y.; Hu, H.; Lu, G. *Chem. Commun.* **2010**, *46*, 598.

(27) Zhu, J.-J.; Kan, C.-X.; Wan, J.-G.; Han, M.; Wang, G.-H. *J. Nanomaterials.* **2011**, DOI: 10.1155/2011/982547.

(28) Gao, Y.; Song, L.; Jiang, P.; Liu, L. F.; Yan, X. Q.; Zhou, Z. P.; Liu, D. F.; Wang, J. X.; Yuan, H. J.; Zhang, Z. X.; Zhao, X. W.; Dou, X. Y.; Zhou, W. Y.; Wang, G.; Xie, S. S.; Chen, H. Y.; Li, J. Q. *J. Cryst. Growth* **2005**, *276*, 606.

(29) Gagner, J. E.; Qian, X.; Lopez, M. M.; Dordick, J. S.; Siegel, R. W. *Biomaterials* **2012**, *33*, 8503.

(30) Wiley, B.; Herricks, T.; Sun, Y. G.; Xia, Y. N. *Nano Lett.* **2004**, *4*, 2057.

(31) Lu, Y. Z.; Wang, Y. C.; Chen, W. *J. Power Sources* **2011**, *196*, 3033.

(32) Klein, S.; Petersen, S.; Taylor, U.; Barcikowski, S.; Rath, D. *J. Biomed. Optics* **2010**, *15*, 036015.

(33) Komatsu, T.; Tabata, M.; Kubo-Irie, M.; Shimizu, T.; Suzuki, K.; Nihei, Y.; Takeda, K. *Toxic. in Vitro* **2008**, *22*, 1825.

(34) Niles, A. L.; Moravec, R. A.; Riss, T. L. *Expert Opin. Drug Discov.* **2008**, *3*, 655.

(35) Niles, A. L.; Moravec, R. A.; Riss, T. L. *Curr. Chem. Genomics* **2009**, *3*, 33.

(36) Teow, Y.; Valiyaveettil, S. *Nanoscale* **2010**, *2*, 2607.

(37) Slater, K. *Curr. Opin. Biotechnol.* **2001**, *12*, 70.

(38) Crouch S, K. R., Slater K *J. Immunol. Methods* **1993**, *160*, 81.

(39) Yen, H. J.; Hsu, S. H.; Tsai, C. L. *Small* **2009**, *5*, 1553.

(40) Zhang, Y.; Xu, D.; Li, W.; Yu, J.; Chen, Y. *J. Nano Mat.* **2012**, *2012*, 7.

(41) Moros, M.; Hernáez, B.; Garet, E.; Dias, J. T.; Sáez, B.; Grazú, V.; González-Fernández, Á.; Alonso, C.; de la Fuente, J. M. *ACS Nano* **2012**, *6*, 1565.

(42) Wang, S.; Lu, W.; Tovmachenko, O.; Rai, U. S.; Yu, H.; Ray, P. C. *Chem. Phys. Lett.* **2008**, *463*, 145.

(43) Pan, Y.; Neuss, S.; Leifert, A.; Fischler, M.; Wen, F.; Simon, U.; Schmid, G.; Brandau, W.; Jahnen-Dechent, W. *Small* **2007**, *3*, 1941.

(44) Liu, W.; Wu, Y.; Wang, C.; Li, H. C.; Wang, T.; Liao, C. Y.; Cui, L.; Zhou, Q. F.; Yan, B.; Jiang, G. B. *Nanotoxicology* **2010**, *4*, 319.

(45) Peng, H.; Zhang, X.; Wei, Y.; Liu, W.; Li, S.; Yu, G.; Fu, X.; Cao, T.; Deng, X. *J. Nano Mat.* **2012**, *2012*, 9.

(46) Kim Kt Fau - Truong, L.; Truong L Fau - Wehmas, L.; Wehmas L Fau - Tanguay, R. L.; Tanguay, R. L. *Nanotechnology* **2013**, *24*, 1.

(47) Asare, N.; Instanes, C.; Sandberg, W. J.; Refsnes, M.; Schwarze, P.; Kruszewski, M.; Brunborg, G. *Toxicology* **2012**, *291*, 65.

(48) Hussain, S. M.; Hess, K. L.; Gearhart, J. M.; Geiss, K. T.; Schlager, J. J. *Toxicol. in Vitro* **2005**, *19*, 975.

(49) Kim, T.-H.; Kim, M.; Park, H.-S.; Shin, U. S.; Gong, M.-S.; Kim, H.-W. *J. Biomed. Mater. Res.* **2012**, *100A*, 1033.

(50) Soto, K.; Garza, K. M.; Murr, L. E. *Acta Biomater.* **2007**, *3*, 351.

(51) Wang, S. G.; Lu, W. T.; Tovmachenko, O.; Rai, U. S.; Yu, H. T.; Ray, P. C. *Chem. Phys. Lett.* **2008**, *463*, 145.

(52) Huang, X. L.; Li, L. L.; Liu, T. L.; Hao, N. J.; Liu, H. Y.; Chen, D.; Tang, F. Q. *ACS Nano* **2011**, *5*, 5390.

(53) Xia, T.; Kovochich, M.; Brant, J.; Hotze, M.; Sempf, J.; Oberley, T.; Sioutas, C.; Yeh, J. I.; Wiesner, M. R.; Nel, A. E. *Nano Lett.* **2006**, *6*, 1794.

(54) Zhang, Y. Y.; Hu, L.; Yu, D. H.; Gao, C. Y. *Biomaterials* **2010**, *31*, 8465.

(55) Qiu, Y.; Liu, Y.; Wang, L. M.; Xu, L. G.; Bai, R.; Ji, Y. L.; Wu, X. C.; Zhao, Y. L.; Li, Y. F.; Chen, C. Y. *Biomaterials* **2010**, *31*, 7606.

(56) Martin, K. R.; Barrett, J. C. *Human Exper. Toxico.* **2002**, *21*, 71.

(57) Li, J.-h.; Liu, X.-r.; Zhang, Y.; Tian, F.-f.; Zhao, G.-y.; Yu, Q.-l.-y.; Jiang, F.-l.; Liu, Y. *Toxicol. Res.* **2012**, *1*, 137.

(58) Yang, H.; Liu, C.; Yang, D. F.; Zhang, H. S.; Xi, Z. G. *J. Appl. Toxicol.* **2009**, *29*, 69.

(59) Sohaebuddin, S.; Thevenot, P.; Baker, D.; Eaton, J.; Tang, L. *Part. Fibre Toxicol.* **2010**, *7*, 22.

(60) Liu, S. C.; Xu, L. J.; Zhang, T.; Ren, G. G.; Yang, Z. *Toxicology* **2010**, *267*, 172.

(61) Papamichos-Chronakis, M.; Krebs, J. E.; Peterson, C. L. *Genes Dev.* **2006**, *20*, 2437.

(62) Huang, J.; Liang, B.; Qiu, J. J.; Laurent, B. C. *Cell Cycle* **2005**, *4*, 1713.

(63) Xu, Y.; Price, B. D. *Cell Cycle* **2011**, *10*, 261.

(64) Butler, R. E.; Brodin, P.; Jang, J.; Jang, M.-S.; Robertson, B. D.; Gicquel, B.; Stewart, G. R. *PLoS ONE* **2012**, *7*, e47573.

CHAPTER 5

SHAPE SENSITIVE TOXICITY OF GOLD NANOPLATES

Publication from this chapter:

Chunyan Wang, Yoshikazu Ito, Bindu Pradeep and Suresh Valiyaveettil, "Shape sensitivity of gold nanoplates on human breast cancer cells", submitted to Journal

5.1 Introduction

Gold nanomaterials (Au NMs) have been explored in a wide range of applications including catalysis,[1,2] photoelectronic devices,[3,4] biosensing[5,6] and nanomedicines[7-9] owing to their unique chemical and physical properties that are distinctly different from bulk materials.[10] The rapid increase of Au NMs applications has attracted researchers' attention on their health and environmental safety concerns. However, until now, no conclusive information on Au NMs cytotoxicity is available. A recent review summarized that cellular uptake and toxicity of Au NMs were very complex, which were affected by many factors such as size, surface functionalization, animal and cell models, doses applied, the type of Au NMs administration, time of examination and assays for evaluating Au NMs toxicity.[11] Au NMs were reported to show a size-dependent toxicity as size of Au NMs is an important physical parameter that controls endocytosis effectiveness.[11] Furthermore, the toxicity of Au NMs was also dependent on their concentrations and surface functionalizations, and Au NMs were more toxic at higher concentrations or with toxic capping agents such as cetyltrimethylammonium bromide (CTAB).[11] However, very few studies have examined the shape effect of Au NMs on their toxic responses. Shape of nanoparticles is expected to play a significant role towards interaction with biomacromolecules such as proteins and therefore influence the final outcome of exposure. Small nanoparticles enter the cells through endocytosis or via pores in the cell membrane. The shape of the particle may play significant roles in both nanoparticles endocytosis and transport through pores. In addition, interaction and complexation of nanoparticles with different proteins may also depend on shape. This is the main reason for the shape sensitive toxicity and more investigations are needed to understand the mechanism in detail.

Recently metallic nanoplates have attracted great interests as they could

exhibit a strong plasmon band in the near-infrared region (NIR),[12] which could be used in cell imaging and photothermal therapy. Gold nanoplates (AuNPs) were reported to show an intensive and enhanced Raman scattering during surface-enhanced Raman scattering study.[13-15] Au nanoplate surfaces exhibit unique electro-catalytic activities which could be used for oxygen reduction and glucose oxidation.[16] Triangle nanoplates showed higher catalytic efficiency in the oxidation of small organic substrates as compared to nanospheres or nanowires from the same metal.[17]

Although a number of studies have examined the cellular and toxicity of Au NMs, very few concentrated specifically on their shape effect on cellular uptake and cytotoxicity of Au NMs. Since Au NMs are being extensively used in various biomedical applications,[18] there is still a need for a more detailed evaluation of their toxic effect. The current study aims to explore the shape, dose and incubation time effects of AuNPs on their cellular uptake and toxicity in human breast cancer cell line (MCF7). Au hexagon nanoplates (HAuNPs), pentagon nanoplates (PAuNPs) and triangle nanoplates (TAuNPs) were synthesized in the presence of calcium ions and fully characterized with multiple techniques. Cellular responses of such AuNPs on MCF7 cell lines were evaluated by cell viability and reactive oxygen species (ROS) generation. Cellular uptake and biodistribution of AuNPs were investigated using transmission electron microscopy (TEM). The details of experimental methods are described in Chapter 2 (Materials and Methods).

1. Synthesis, purification and characterization of HAuNPs, PAuNPs and TAuNPs;
2. Light microscopy – cell morphology changes with AuNPs treatment;
3. ATP production – cell viability;
4. ROS production – mechanism of cytotoxicity;
5. DAPI staining of apoptotic nuclei – cell death;

6. Cell cycle analysis;
7. TEM of AuNPs treated cells – cellular uptake and biodistribution of AuNPs.

5.2 Results

5.2.1 Synthesis and characterization of AuNPs

A one pot synthesis of AuNPs was developed in this study. Calcium ions were used to facilitate the growth of nanoplates. Different morphologies could be obtained by changing the gold to calcium ion concentration ratios during the synthesis. As the calcium concentration decreases, the morphology changes from hexagon to pentagon and to triangles. TEM images showed clear morphologies of Au hexagons, pentagons and triangles (**Figure 5.1**).

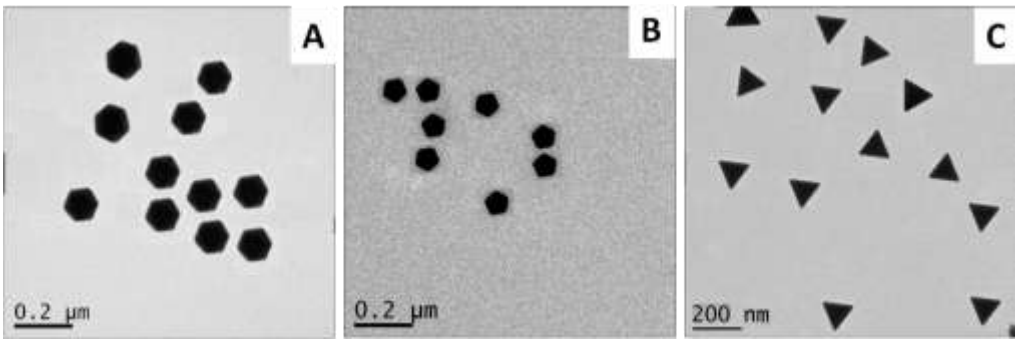

Figure 5.1: TEM images of AuNPs grown in the presence of different concentrations of Ca^{2+} ions: HAuNPs (A), PAuNPs (B) and TAuNPs (C).

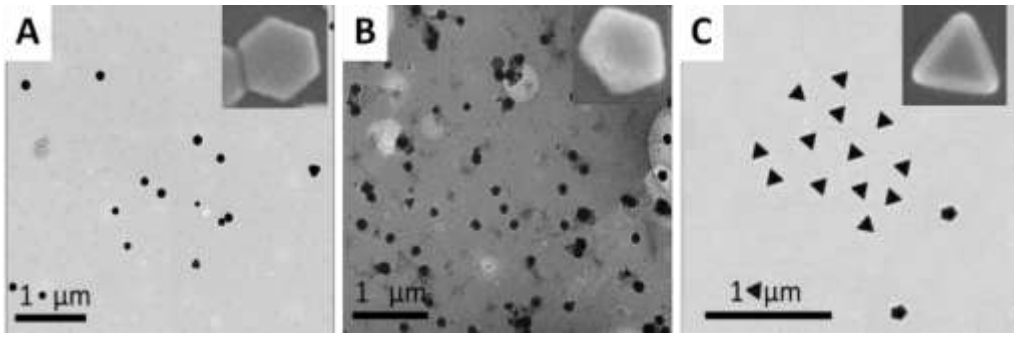

Figure 5.2: Low magnification TEM images of HAuNPs (A), PAuNPs (B) and TAuNPs (C). SEM images of AuNPs were present in the right corner of each TEM image.

The relation between the morphology of AuNPs and the change in

concentrations of Au/Ca cations are summarized in **Table 5.1**. Low magnification TEM images indicated that Au hexagons, pentagons and triangles were monodispersed (**Figure 5.2**). The shape distribution of AuNPs was showed in **Table 5.2**. More than 85% of the desired nanoplate shape was observed, and these nanoplates were further used to for the toxicology studies.

Table 5.1: Characterization of shape-dependent AuNPs*

AuNPs	Concentration of Au/Ca	Shape	Side length (nm)	Surface area (nm^2)	Volume (nm^3)
HAuNPS	200/1	Hexagon	60 - 65	3.0×10^4	2.2×10^5
PAuNPs	400/1	Pentagon	50 - 55	1.5×10^4	9.5×10^4
TAuNPs	800/1	Triangle	120 - 130	2.1×10^4	1.4×10^5

*Additional SEM images of AuNPs are included in **Figure 5.2**.

Table 5.2: Ratio of the calcium and Au salt concentrations and observed percentage of compositions based on low magnification TEM images.

	Concentration of Au/Ca		
	200/1	400/1	800/1
Shape	Hexagon 85% Truncated triangle 10% Polyhedron 5%	Pentagon 80% Hexagon &Triangle 10% Polyhedron 10%	Triangle 85% Pentagon 10% Polyhedron 5%

The average surface area and volume of AuNPs were calculated based on shape, side length and thickness of AuNPs and summarized in **Table 5.3**. As expected, the average volume and surface area are different based on their size, shape and edge length. The hydrodynamic sizes of HAuNPs, PAuNPs and TAuNPs in water were 156 nm, 106 nm and 94 nm, respectively, which indicate the size of hydrated nanoplates (**Table 5.3**). The core size of AuNPs was determined by TEM and their hydrodynamic size distribution was investigated by DLS. The hydrodynamic size of AuNPs includes its solid cores, its organic layers (capping agents) and the hydration shell.[19,20]

Table 5.3: Surface charge and aggregate state of AuNPs in water and cell exposure media (100 μg/mL) for 24 h*

AuNPs	H_2O (100 μg/mL)		Cell medium (100 μg/mL)	
	Size (nm)	Zeta (mV)	Size (nm)	Zeta (mV)
HAuNPS	156.0 ± 3.1	-34.5 ± 0.4	176.9 ± 4.2	-8.3 ± 0.2
PAuNPs	106.4 ± 0.7	-25.0 ± 0.5	121.0 ± 1.1	-6.0 ± 0.4
TAuNPs	94.3 ± 0.3	-25.0 ± 1.1	103.5 ± 0.6	-7.0 ± 0.7

*Hydrodynamic size and zeta potential results were measured after 24 hrs of incubation in corresponding solvents in triplicates and the average values are presented with mean ± standard deviation (SD).

Aggregation of AuNPs was checked by dispersing nanoplates in cell exposure media for 24 h. The hydrodynamic size of nanoplates did not change significantly in cell medium as compared to water, which indicated that AuNPs were stable in cell culture media and did not aggregate. The differences in size of nanoplates in disperse media can be attributed to the different thicknesses of their hydration shells due to potential adsorption of various components of cell medium on nanoplate surface and not due to aggregation. In addition, HAuNPs, PAuNPs and TAuNPs showed high negative surface charges in water, which decreased in cell exposure media owing to high ionic strength. Decrease in surface charges in cell medium also highlights the adsorption of ions from the medium to the nanoplate surface. Similar results were reported for neutral and hydrophilic polymer PVP stabilized AuNPs.[21]

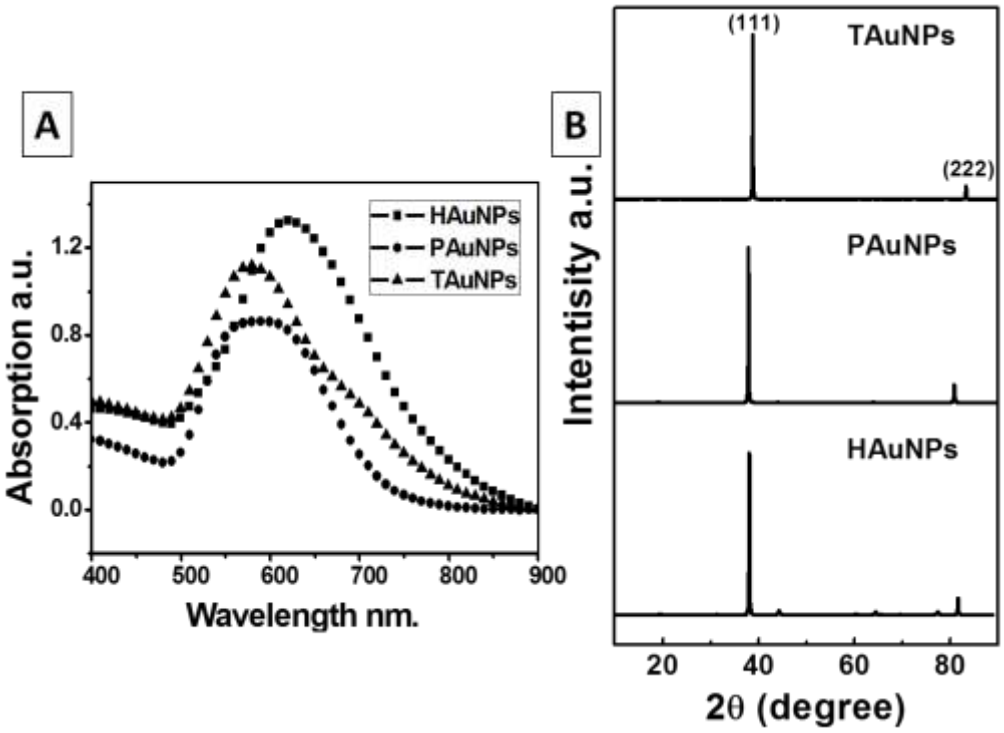

Figure 5.3: UV-Vis absorption spectra (A) of HAuNPs, PAuNPs and TAuNPs in aqueous solution and their XRD patterns (B).

Surface plasmon resonance (SPR) properties of AuNPs were examined by UV-Vis spectroscopy (**Figure 5.3A**). The maximum absorption wavelength showed a red shift as the number of edges in the AuNPs increased from 3 to 6 (Triangle to Hexagon). The SPR peaks gradually shifted from 574 nm for TAuNPs to 585 nm for PAuNPs and 620 nm for HAuNPs, indicating that AuNPs exhibit shape-dependent optical properties. The crystalline structures of AuNPs were examined using XRD measurements (**Figure 5.3B**). The XRD patterns of HAuNPs, PAuNPs and TAuNPs are all dominated by the (111) and (222) peaks, indicating that all AuNPs are mainly bound by the (111) planes, which are consistent with earlier reports.[22]

5.2.2 Morphology changes of cells with AuNPs treatment

Morphological changes of cells treated with AuNPs were considered as the first noticeable phenomenon of cellular responses. Cell morphology of AuNPs treated cells was observed under an optical microscope and compared with untreated cells, which served as a control. Microscopic observations of

AuNPs treated cells showed dose dependent morphological changes indicating unhealthy cells, whereas the control cells appeared normal. Only small changes in cell morphologies were observed in cells exposed to HAuNPs and PAuNPs at a concentration of 50 μg/mL (**Figure 5.4B and 5.4C**). Moreover, TAuNPs treated cells showed significant number of spherical cells with restricted proliferation (**Figure 5.4D**). HAuNPs did not induce significant morphological changes to cells even at a higher concentration of 100 μg/mL (**Figure 5.4F**). However, PAuNPs and TAuNPs treated cells became unhealthier at higher concentration (100 μg/mL), and majority (80%) of the cells showed spherical morphologies (**Figure 5.4G and 5.4H**). Even after repeated washings, dark orange patches were seen on the cell surface of AuNPs treated cells, which is due to the penetration of nanoplates into the cells. Moreover, very few floating cells or cellular debris were observed under the microscope (**Figure 5.4**), indicating that no widespread cell death occurred through necrosis owing to the treatment.

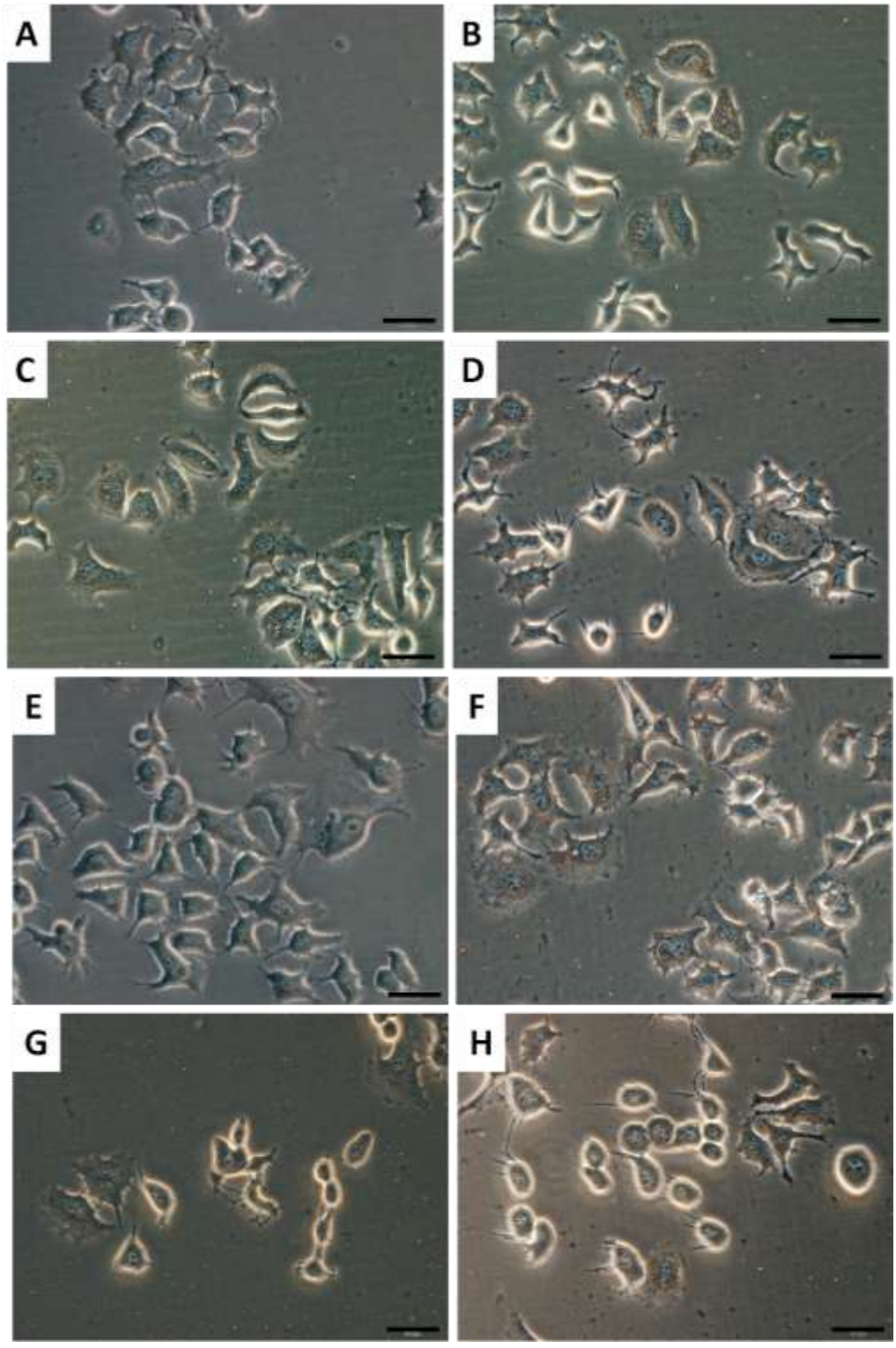

Figure 5.4: Optical images of cell morphology of MCF7 cells with or without AuNPs treatment: untreated cells (A, E), MCF7 cells exposed with 50 μg/mL of HAuNPs (B), PAuNPs (C), TAuNPs (D) treatment and MCF7 cells exposed with 100 μg/mL of HAuNPs (F), PAuNPs (G), TAuNPs (H) treatment. Scale bar = 50 μm

5.2.3 Cell viability with AuNPs treatment

Viability assays are vital steps to explain the cellular response to nanomaterials. In addition, they also give information on cell death, survival, and metabolic activities. The effect of AuNPs on MCF7 cells was studied by using both luminescence-based assay and fluorescent based assay. ATP assessment of toxicity of AuNPs (**Figure 5.5**) showed a concentration-dependent drop in luminescence intensity in MCF7 cells, signifying a dose-dependent toxicity. No significant changes in ATP content of cells in the presence of AuNPs were observed with an increase in exposure time from 24 h to 72 h, indicating that cell damage caused by AuNPs occurred within 24 h. At the same concentration and incubation time, TAuNPs were the most toxic, followed by PAuNPs and HAuNPs.

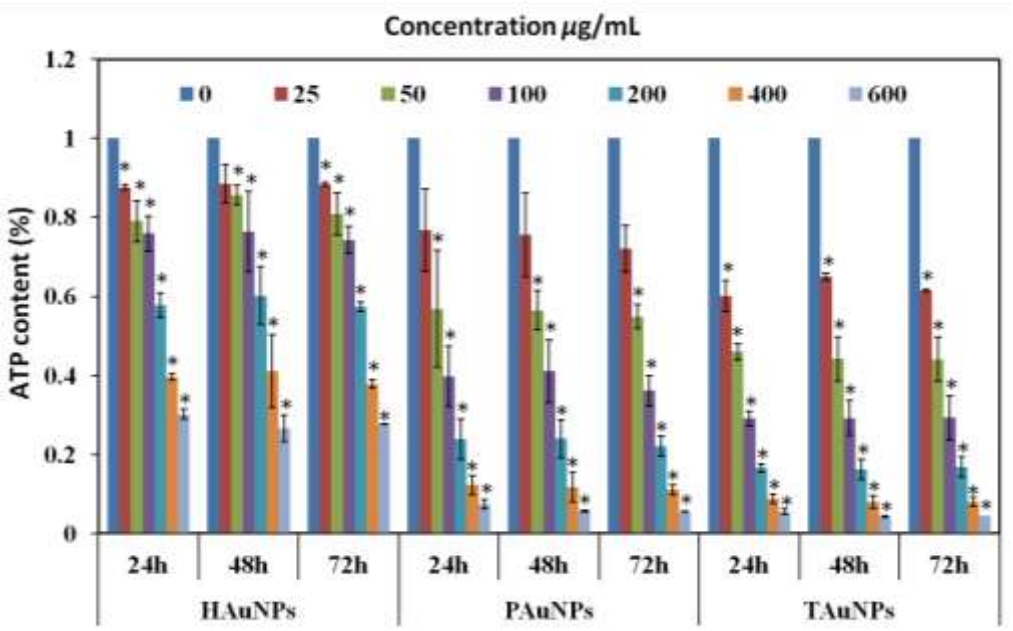

Figure 5.5: Cell viability assays of MCF7 after exposure to various concentrations of HAuNPs, PAuNPs and TAuNPs after 24, 48 and 72 h using CellTiter-Glo assay. The *y*-axis represents the percentage of ATP content which relates to viable cells present in the treated sample after a certain time and the *x*-axis represents AuNPs with different exposure time. The values represent the mean ± standard deviation of three independent experiments; * denotes $P < 0.05$ with respect to the control group using Student's t test.

To check the presence of any toxic materials left over from the AuNPs

synthesis, toxicity studies were done using the supernatant liquid obtained after centrifugation of AuNPs solution. The results showed no evidence of toxicity for supernatant liquid (**Figure 5.6**). The viability of cells exposed to supernatant liquid was comparable to that of control.

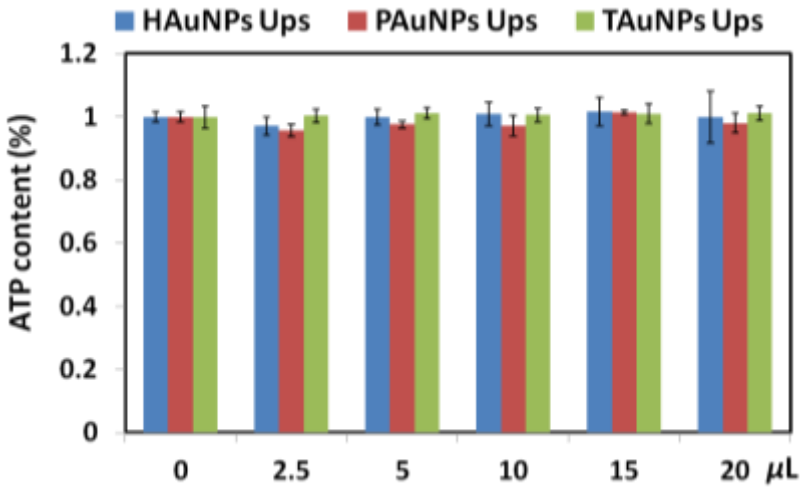

Figure 5.6: Intracellular ATP content of MCF7 cells treated with supernatant solution of AuNPs (0, 2.5, 5, 10, 15 and 20 μL). The data show no toxicity after 24 h incubation.

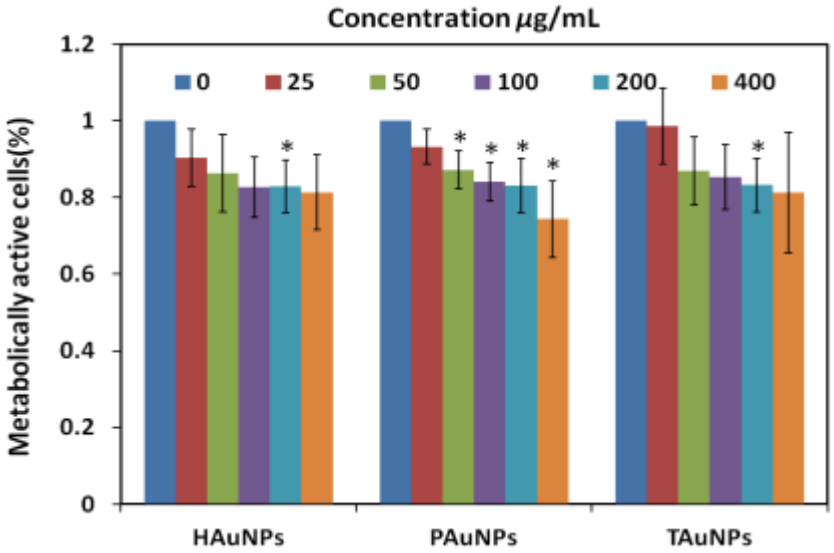

Figure 5.7: Cell viability assays of MCF7 after exposure to HAuNPs, PAuNPs and TAuNPs with various concentrations after 24 h of exposure using CellTiter-Blue assay. The values represent the mean ± standard deviation of three independent experiments; * denotes $P < 0.05$ with respect to the control group using Student's t test.

No significant cell death was observed after exposing to AuNPs. Since the

cell damage was caused by AuNPs within the first 24 h, the metabolic activity studies were conducted using CTB assay. The results from CTB assay were similar to ATP content analysis, a small drop (15%) in mitochondrial activity was observed with increase in concentration of AuNPs to 50 μg/mL (**Figure 5.7**). However, the effect of AuNPs to mitochondrial activity was not as significant as to ATP depletion at a high concentration (400 µg/mL).

5.2.4 Detection of cellular oxidative stress

Intracellular ROS production induced by AuNPs was detected by applying the fluorescent DCFH-DA assay as a measure for oxidative stress. DCFH-DA, a cellular membrane permeable non-fluorescent probe, can be irreversibly oxidized by intracellular ROS into a green fluorescent molecule, dichlorofluorescein (DCF).[23,24] It is clearly shown that AuNPs induced intracellular ROS generation in a dose-dependent fashion (**Figure 5.8**). Untreated cells (control) showed low fluorescence while green fluorescent cells were observed under the microscope when exposed to AuNPs (50 and 100 μg/mL), indicating increase in ROS production in the AuNPs treated cells.

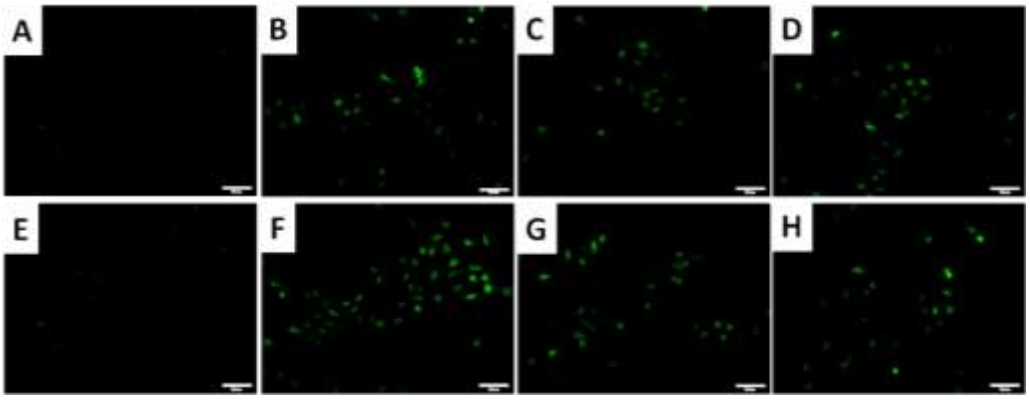

Figure 5.8: Fluorescence images (DCF-DA staining) of MCF7 cells with or without AuNPs treatment: untreated cells (A and E), MCF7 cells exposed with 50 μg/mL of HAuNPs (B), PAuNPs (C), TAuNPs (D) and MCF7 cells exposed with 100 μg/mL of HAuNPs (F), PAuNPs (G), TAuNPs (H). Scale bar = 50 μm

5.2.5 Morphological changes in cell nucleus

Morphological assessment of apoptotic cells induced by AuNPs was

detected by DAPI staining of cell nucleus. Cell shrinkage or nuclear fragmentation with condensed chromatin indicates cells undergoing apoptosis.[25,26] Moreover, chromosomes remain condensed throughout mitosis. Under a fluorescent microscope, control cells were stained uniformly with blue and few condensed or fragmented nuclei were observed (**Figure 5.9A**). However, cells treated with HAuNPs, PAuNPs and TAuNPs for 24 h, significant numbers of condensed or fragmented nuclei were observed (**Figure 5.9B, 5.9C and 5.9D**, yellow arrows). Morphological changes in cell nucleus indicated that all three AuNPs either induced cell apoptosis or arrested in cell division. In addition, more condensed or fragmented nuclei were observed in cells exposed to TAuNPs, as compared to cells treated with HAuNPs and PAuNPs.

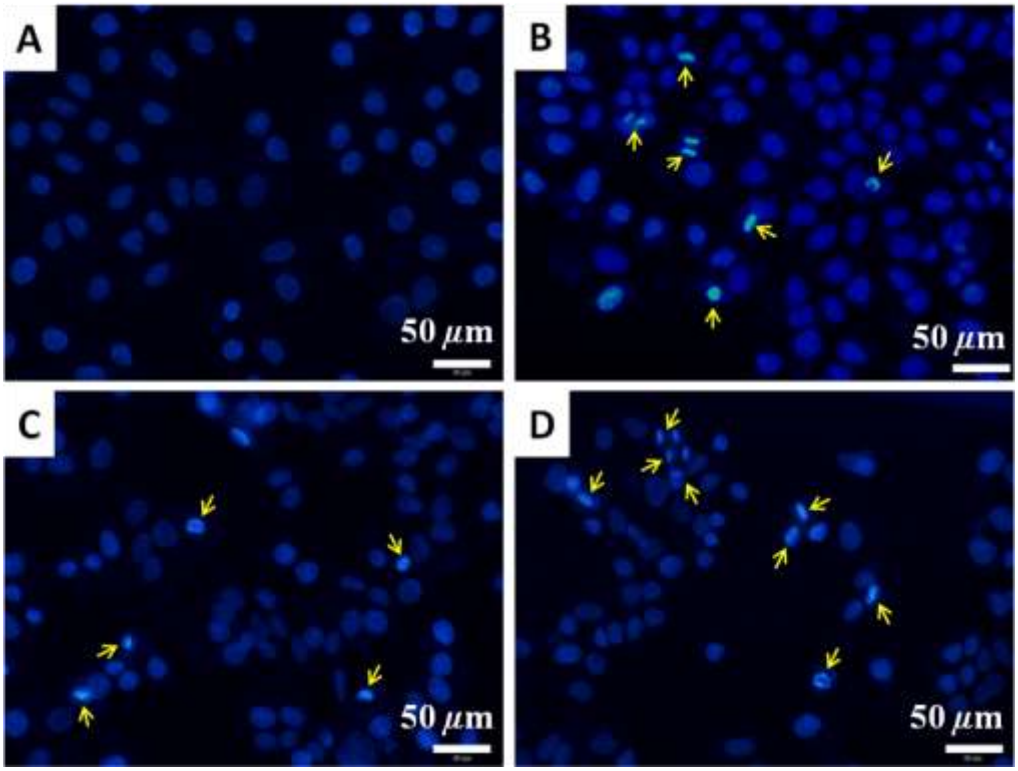

Figure 5.9: DAPI staining of untreated MCF7 cells (A) and cells exposed to HAuNPs (B), PAuNPs (C) and TAuNPs (D). Concentration of AuNPs = 100 μg/mL, yellow arrows represent condensed or fragmented nuclei.

5.2.6 Cell cycle arrest

Cell cycle analysis was further conducted to examine DNA damage inside cells caused by AuNPs in the cell progression. Cells with reversible DNA damage will accumulate in gap1 (G1), DNA synthesis (S) or in gap2/mitosis (G2/M) phase, while cells with irreversible DNA damage will undergo apoptosis, and then accumulate in subG1 phase. Thus toxicity studies of AuNPs were further extended to cell cycle analysis through detecting parameters such as apoptosis and cell cycle arrest to confirm DNA damage.

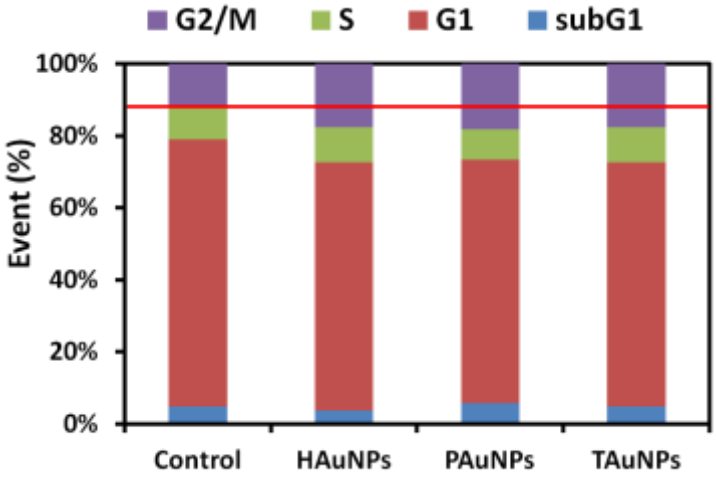

Figure 5.10: Cell cycle arrest of MCF7 cells with HAuNPs, PAuNPs and TAuNPs treatment. AuNPs treated cells showed a significant increase in the G2/M population as compared to the control cells. Markers were set at regions of interest (subG0, G1, S, and G2/M), and the percentage of cells (events) under each area was generated using Summit V4.3.02 software. The red line represents the percentage of cells in the G2/M stage for control cells.

The influence of AuNPs on the cell cycle was analyzed by detecting DNA content using a fluorescent DNA-selective dye PI, which exhibits emission signals proportional to the concentration of DNA. As compared to control, an increase of cell population in G2/M phase (5% for HAuNPs, 6% for PAuNPs and 5% for TAuNPs) was observed (**Figure 5.10**), indicating that all AuNPs induced a reversible DNA damage with G2/M arrest. For control cells, major cell population was observed in G1 phase. No significant increase of cell

population in the SubG1 stage was observed in cells exposed to AuNPs. This implies that AuNPs did not induce significant cell death. Therefore, the condensed or fragmented nuclei in DAPI staining represented that cells were arrested in the cell division stage rather than dying through apoptosis.

5.2.7 Cellular uptake of AuNPs

The extent of AuNPs uptake and cellular distribution within MCF7 cells was explored through TEM images of ultrathin sections of cells. Representative images illustrated that AuNPs were readily internalized following 24 h cellular exposure (**Figure 5.11**). Any morphological abnormalities of cells exposed to AuNPs were compared with controls. Untreated MCF7 cells (control) displayed circular nuclei, a prominent nucleolus (**Figure 5.11A**) while AuNPs treated cells exhibit relatively small oblong nuclei (**Figure 5.11B**, **5.11E** and **5.11H**). Small agglomerates of Au hexagon were observed at low magnification within both cytoplasmic vacuoles and nuclei of MCF7 (**Figure 5.11B**). High magnification images confirmed the presence of HAuNPs, and some were still maintaining the hexagonal shape while others showed slight round shape or large aggregate (**Figure 5.11C** and **5.11D**). Similarly, PAuNPs were seen in small agglomerates within vacuoles along the periphery of the nucleus (**Figure 5.11E**). High magnification images confirmed numerous PAuNPs aggregate within the vacuoles and some maintained their pentagonal shapes (**Figure 5.11F**). Furthermore, a small percentage of PAuNPs had already penetrated into the nuclei within 24 h (**Figure 5.11G**). Majority of TAuNPs were degraded into small nanoparticles and distributed evenly inside the cells, including the nuclei (**Figure 5.11H**). Only a small percentage of TAuNPs were still maintaining their shapes (**Figure 5.11I**). EDX of the cells exposed to AuNPs showed high concentration of gold inside the cells (Figure 11A). Quantitation of cellular uptake of AuNPs in MCF7 cells was conducted by

ICP-OES (Figure 11B). MCF7 cells not exposed to AuNPs were used as control, which showed no gold inside the cells. The highest amount of gold content was observed in TAuNPs treated cells (0.40 ppm) while the least amount was found in HAuNPs treated cells (0.29 ppm).

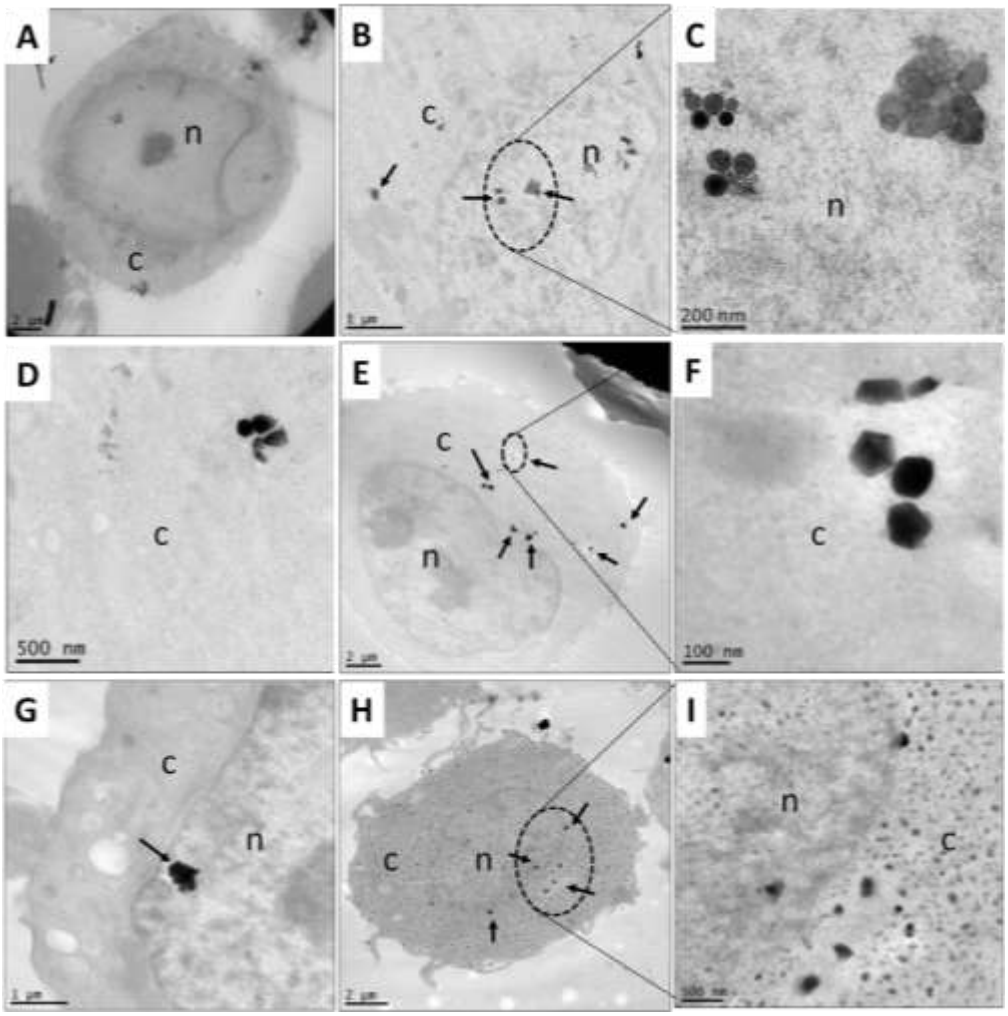

Figure 5.11: TEM images of untreated MCF7 cells (A) and MCF7 exposed with 50 μg/ml AuNPs for 24 h: MCF7 cells treated with HAuNPs (B – low magnification), magnified image of particles in nucleus (C), and cytoplasm (D); PAuNPs exposed cells – (E – low magnification), high magnification image of particles in cytoplasm (F), inside nucleus (G) and TAuNPs exposed cells with low magnification (H) and high magnification (I) images. The symbol ***n*** represents nuclei while ***c*** represents cytoplasm.

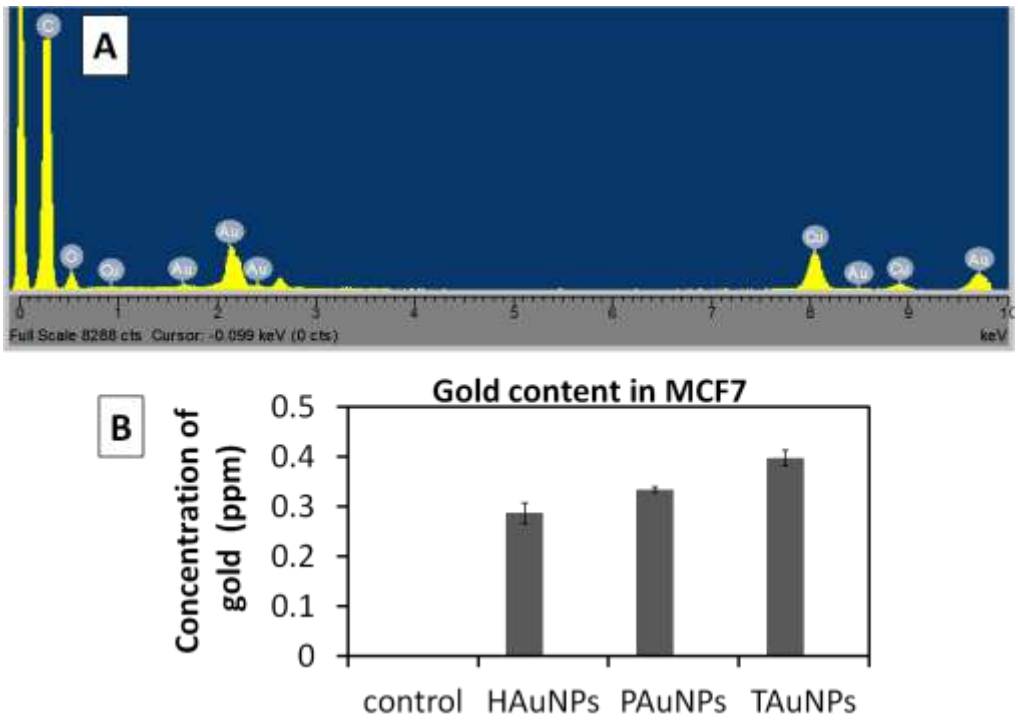

Figure 5.12: EDX of TAuNPs treated cells (A) and concentration of gold in cells with AuNPs treatment (B) estimated using ICP-OES. Cells were treated with HAuNPs, PAuNPs and TAuNPs at the concentrations 100 μg/mL for 24 h, before ICP-OES measurement. The values represent the mean ± standard deviation of three independent experiments. The amount of gold concentration in control cells without AuNPs treatment was undetectable.

5.3 Discussion

Au NMs have been widely used in medical field such as drug delivery, bioimaging or phototherapy owing to low toxicity, easy surface modifications and interesting optical properties.[7] A deeper understanding of the cytotoxicity of Au NMs including the mechanism is essential before extending their use in different biomedical sectors. The toxicity of Au NMs could be influenced by many factors such as size,[9,27] shape,[28] surface charge and functionalization.[29-31] However, majority of the published reports were focused on either spherical nanoparticles or rods with different aspect ratios.[32-34] The current study establishes the shape sensitivity of AuNPs on cellular toxicity. The cytotoxicity of Au nanospheres was dependent on their size; smaller nanoparticles (< 10 nm) were more toxic than larger nanoparticles (> 50

nm).[27, 35] Further, the cellular uptake and cytotoxicity of Au nanospheres were influenced by their surface functionalization,[36] charge[30] and the hydrophobicity.[31] In addition, the cytotoxicity of Au NMs were also affected by their shapes – Au nanorods induced apoptosis in human keratinocyte cell line (HaCaT) while Au nanospheres did not show such detrimental effects to cells.[28] Detailed studies of shape effects on cytotoxicity of AuNPs in MCF7 cells were explored in this study. AuNPs exhibited a dose- and shape-dependent toxicity to MCF7 cells with a reduction in ATP content and mitochondrial damages inside the cells. When the concentration of AuNPs with different shapes was increased from 25 μg/mL to 400 μg/mL, ATP amount inside the cell was significantly decreased (HAuNPs: from 88% to 40%; PAuNPs: 76% to 12% and TAuNPs: 60% to 8%). TAuNPs showed the highest toxicity to MCF7 cells, followed by PAuNPs and then HAuNPs. Further, toxicity of AuNPs did not show any changes with increase in the incubation time from 24 h to 48 h, or 72 h. This indicates that toxicity response of AuNPs occurs within 24 h. Oxidative stress has been reported to be reason for toxicity of Au nanospheres, which could cause oxidative damage to protein and DNA.[37, 38] Since ROS plays an important role in various pathogenic processes, it has been recognized as an early indicator for cytotoxic events and cellular disorders. Early studies indicated that exposure to Au nps induced the endogenous ROS production.[31] This oxidative stress could initiate the autophagic process to protect the cells,[39] which then destroys foreign molecules.[31] Since Au nps are not easy to be digested or removed from cells, a dose-dependent oxidative stress (**Figure 5.8**), inside the cells lead to DNA damage. Condensed or fragmented nuclei were observed in DAPI stained cells treated with AuNPs (**Figure 5.9**). G2/M arrest induced by AuNPs in the cell cycle analysis showed a reversible DNA damage (**Figure 5.10**), indicating retarded cell proliferation. It allowed cells extra time to repair DNA damage prior to segregation of chromosomes. However, the reduction of ATP content (**Figure 5.5**) induced by AuNPs may affect the DNA repair, as ATP plays

multiple roles in the repair of DNA damage.[40,41]

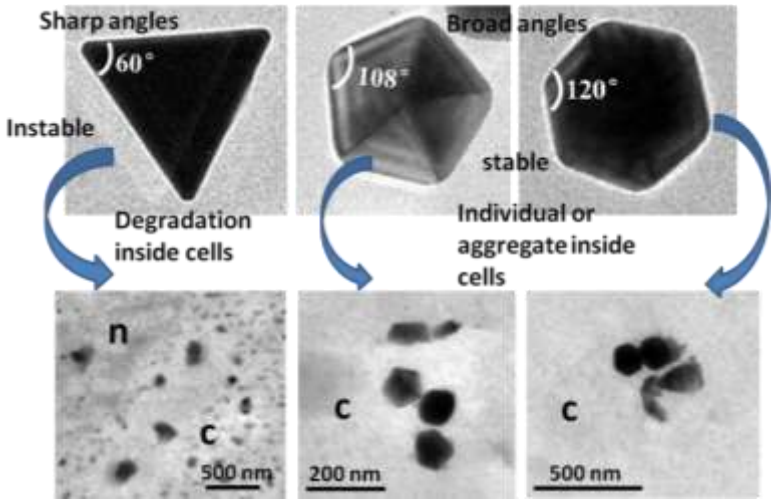

Figure 5.13: Interior angles and stability of AuNPs with different shapes. Interior angles of TAuNPs, PAuNPs and HAuNPs are 60 °, 108 ° and 120 °, respectively. The sharper of the angles, the higher surface energy of the vertices' atoms, as it interact with less number Au atoms. Instability of Au atoms at the vertices inside the cells: Triangle > Pentagon ≈ Hexagon. TEM images of ultrathin sections of TAuNPs treated cells confirmed their degradation inside the cytoplasm. Only individual or aggregate of AuNPs were observed inside the cells with HAuNPs and PAuNPs treatment. Symbol n represent nucleus and c represents cytoplasm.

The stability of AuNPs also plays significant effect in their physical translocation inside the cell and cytotxoic effects. Interior angles of TAuNPs, PAuNPs and HAuNPs are 60 °, 108 ° and 120 °, respectively (**Figure 5.13**). The number of Au atoms exist at the vertices is proportional to the sharpness of edges and value of interior angles of Au nanoplates. The atoms at the edges have minimum interaction with those in the lattice of the particles and thus show higher reactivity. TEM images of cells with Au nanoplates treatment showed that both HAuNPs and PAuNPs were remained in their original shape (**Figure 5.11**). However, TAuNPs were degraded into small nanoparticles (**Figure 5.11**) which were evidenced from EDX data (**Figure 5.12A**). Moreover, the sharper angle of Au nanoplates, the easier for them to penetrate inside the cells. ICP-OES data of cells with Au nanoplates treatment indicated that TAuNPs showed the maximum cell permeability within 24 h (**Figure**

5.12B), which amplifies the toxicity. All data presented in this paper suggest that the cytotoxicity of Au nanoplates was shape - and dose - dependent. A recent study showed that spherical Au nps affected the epidermal growth factor signal transduction in human epithelial cells even at a nontoxic dose (5 and 25 μg/ml).[42] Therefore, further studies are necessary to explain a complete mechanism of cell damage caused by AuNPs before applying them in future applications.

5.4 Conclusion

Three AuNPs (HAuNPs, PAuNPs and TAuNPs) were synthesized using alkaline earth cations (Ca^{2+}), characterized with various techniques and evaluated for their cellular responses using a commercial cancer cell line MCF7. This study demonstrated that Au NMs exhibited a dose- and shape-dependent toxicity to MCF7 cells, which could be resulted from oxidative stress caused by ROS production with AuNPs treatment. The shape effects of AuNPs on their toxicity are closely related to the sharp angle and the high cell permeability of nanoplates. Therefore, TAuNPs with sharp angle (60 °) showed the most toxicity as compared to PAuNPs and HAuNPs. Similar results were also observed in human dermal fibroblast cells. Therefore, special attention should be given and further studies are needed to perform to explore the cellular responses of AuNPs more deeply before incorporating them into bioapplications.

5.5 References

(1) Zhang, Y.; Cui, X.; Shi, F.; Deng, Y. *Chem. Rev.* **2011**, *112*, 2467.

(2) Yin, A.-X.; Min, X.-Q.; Zhang, Y.-W.; Yan, C.-H. *J. Am. Chem. Soc.* **2011**, *133*, 3816.

(3) Li, H.; Jo, J.; Wang, J.; Zhang, L.; Kim, I. *Cryst. Growth Des.* **2010**, *10*, 5319.

(4) Yusa, S.-i.; Fukuda, K.; Yamamoto, T.; Iwasaki, Y.; Watanabe, A.; Akiyoshi, K.; Morishima, Y. *Langmuir* **2007**, *23*, 12842.

(5) Dondapati, S. K.; Sau, T. K.; Hrelescu, C.; Klar, T. A.; Stefani, F. D.; Feldmann, J. *ACS Nano* **2010**, *4*, 6318.

(6) Beeram, S. R.; Zamborini, F. P. *ACS Nano* **2010**, *4*, 3633.

(7) Wang, F.; Wang, Y.-C.; Dou, S.; Xiong, M.-H.; Sun, T.-M.; Wang, J. *ACS Nano* **2011**, *5*, 3679.

(8) Gao, L.; Fei, J.; Zhao, J.; Li, H.; Cui, Y.; Li, J. *ACS Nano* **2012**, *6*, 8030.

(9) Huang, K.; Ma, H.; Liu, J.; Huo, S.; Kumar, A.; Wei, T.; Zhang, X.; Jin, S.; Gan, Y.; Wang, P. C.; He, S.; Zhang, X.; Liang, X.-J. *ACS Nano* **2012**, *6*, 4483.

(10) Zhang, Y.; Chang, G.; Liu, S.; Lu, W.; Tian, J.; Sun, X. *Biosens. Bioelectron.* **2011**, *28*, 344.

(11) Khlebtsov, N.; Dykman, L. *Chemical Society Reviews* **2011**, *40*, 1647.

(12) Wang, C.; Kan, C.; Zhu, J.; Zeng, X.; Wang, X.; Li, H.; Shi, D. *J. Nano Mat.* **2010**, *2010*, 1.

(13) Xia, Y.; Xiao, H. *J. Raman Spectrosc.* **2012**, *43*, 469.

(14) Bi, L.; Rao, Y.; Tao, Q.; Dong, J.; Su, T.; Liu, F.; Qian, W. *Biosens. Bioelectron.* **2013**, *43*, 193.

(15) Sun, J.; Guan, M.; Shang, T.; Gao, C.; Xu, Z. *Sci. China Chem.* **2010**, *53*, 2033.

(16) Seo, B.; Choi, S.; Kim, J. *ACS Appl. Mater. Interfaces.* **2011**, *3*, 441.

(17) Miranda, A.; Malheiro, E.; Skiba, E.; Quaresma, P.; Carvalho, P. A.; Eaton, P.; de Castro, B.; Shelnutt, J. A.; Pereira, E. *Nanoscale* **2010**, *2*, 2209.

(18) Tiwari, P.; Vig, K.; Dennis, V.; Singh, S. *Nanomaterials* **2011**, *1*, 31.

(19) Barth, B. M.; Sharma, R.; Altinoglu, E. I.; Morgan, T. T.; Shanmugavelandy, S. S.; Kaiser, J. M.; McGovern, C.; Matters, G. L.; Smith, J. P.; Kester, M.; Adair, J. H. *ACS Nano* **2010**, *4*, 1279.

(20) Kittler, S.; Greulich, C.; Gebauer, J. S.; Diendorf, J.; Treuel, L.; Ruiz, L.; Gonzalez-Calbet, J. M.; Vallet-Regi, M.; Zellner, R.; Koller, M.; Epple, M.

J. Mater. Chem. **2010**, *20*, 512.

(21) Teow, Y.; Valiyaveettil, S. *Nanoscale* **2010**, *2*, 2607.

(22) Chu, H.-C.; Kuo, C.-H.; Huang, M. H. *Inorg. Chem.* **2005**, *45*, 808.

(23) Chen, X.; Zhong, Z.; Xu, Z.; Chen, L.; Wang, Y. *Free Radical Res.* **2010**, *44*, 587.

(24) Pelka J Fau; Gehrke, H.; Gehrke H Fau - Rechel, A.; Rechel A Fau - Kappes, M.; Kappes M Fau - Hennrich, F.; Hennrich F Fau - Hartinger, C. G.; Hartinger Cg Fau - Marko, D.; Marko, D. *Nanotoxicology* **2013**, *7*, 2.

(25) Li, G.-L.; Jiang, W.; Xia, Q.; Chen, S.-H.; Ge, X.-R.; Gui, S.-Q.; Xu, C.-J. *J. Ethnopharmacol.* **2010**, *132*, 56.

(26) Park, K.; Lee, G.; Park, R.-W.; Kim, I.-S.; Kim, S.; Byun, Y. *Pharmaceut. Res.* **2008**, *25*, 268.

(27) Pan, Y.; Neuss, S.; Leifert, A.; Fischler, M.; Wen, F.; Simon, U.; Schmid, G.; Brandau, W.; Jahnen-Dechent, W. *Small* **2007**, *3*, 1941.

(28) Schaeublin, N. M.; Braydich-Stolle, L. K.; Maurer, E. I.; Park, K.; MacCuspie, R. I.; Afrooz, A. R. M. N.; Vaia, R. A.; Saleh, N. B.; Hussain, S. M. *Langmuir* **2012**, *28*, 3248.

(29) Nativo, P.; Prior, I. A.; Brust, M. *ACS Nano* **2008**, *2*, 1639.

(30) Schaeublin, N. M.; Braydich-Stolle, L. K.; Schrand, A. M.; Miller, J. M.; Hutchison, J.; Schlager, J. J.; Hussain, S. M. *Nanoscale* **2011**, *3*, 410.

(31) Chompoosor, A.; Saha, K.; Ghosh, P. S.; Macarthy, D. J.; Miranda, O. R.; Zhu, Z.-J.; Arcaro, K. F.; Rotello, V. M. *Small* **2010**, *6*, 2246.

(32) Chithrani, B. D.; Ghazani, A. A.; Chan, W. C. W. *Nano Lett.* **2006**, *6*, 662.

(33) Chithrani, B. D.; Chan, W. C. W. *Nano Lett.* **2007**, *7*, 1542.

(34) Albanese, A.; Sykes, E. A.; Chan, W. C. W. *ACS Nano* **2010**, *4*, 2490.

(35) Yen, H.-J.; Hsu, S.-h.; Tsai, C.-L. *Small* **2009**, *5*, 1553.

(36) Cho, E. C.; Au, L.; Zhang, Q.; Xia, Y. *Small* **2010**, *6*, 517.

(37) Nabeshi, H.; Yoshikawa, T.; Matsuyama, K.; Nakazato, Y.; Tochigi, S.; Kondoh, S.; Hirai, T.; Akase, T.; Nagano, K.; Abe, Y.; Yoshioka, Y.;

Kamada, H.; Itoh, N.; Tsunoda, S.-i.; Tsutsumi, Y. *Part. Fibre Toxicol.* **2011**, *8*, 1.

(38) Khaing Oo, M. K.; Yang, Y.; Hu, Y.; Gomez, M.; Du, H.; Wang, H. *ACS Nano* **2012**, *6*, 1939.

(39) Scherz-Shouval, R.; Shvets, E.; Fass, E.; Shorer, H.; Gil, L.; Elazar, Z. *Embo J.* **2007**, *26*, 1749.

(40) Costelloe, T.; FitzGerald, J.; Murphy, N. J.; Flaus, A.; Lowndes, N. F. *Exp. Cell Res.* **2006**, *312*, 2677.

(41) Citterio, E.; Van Den Boom, V.; Schnitzler, G.; Kanaar, R.; Bonte, E.; Kingston, R. E.; Hoeijmakers, J. H. J.; Vermeulen, W. *Mol. Cell Biol.* **2000**, *20*, 7643.

(42) Comfort, K. K.; Maurer, E. I.; Braydich-Stolle, L. K.; Hussain, S. M. *ACS Nano* **2011**, *5*, 10000.

CHAPTER 6

INVESTIGATION OF NANOTOXICITY OF SILVER AND GOLD NANOPARTICLES ON STEM CELLS

Publication from this chapter:

Chunyan Wang, Gwendoline Goh, Mark Richard and Suresh Valiyaveettil, "Investigation of Nanotoxicity on Stem Cells Exposed to Silver and Gold Nanoparticles", submitted to Journal

Chunyan Wang, Gwendoline Goh, Mark Richard and Suresh Valiyaveettil, "Genotoxicity of Silver Nanoparticles in Human Embryonic Stem Cells", under prepare

6.1 Introduction

Nanotechnology nanomaterials have been used in many areas such as electronics, engineering, pollutant remediation, therapeutics, diagnostic devices and personal care products.[1-5] Cancer, including colon cancer, has been widely accepted by the scientific community as a "stem cell disease".[6-9] Cancer stem cells (CSCs), isolated from a variety of tumor types, are the cell populations responsible for the development of tumor and have important role in cancer recurrences. Therefore, these cells are of particular importance to explore innovative cancer therapies.[10]

The mechanism of toxicity of the nanomaterials is not yet fully elucidated, previous studies have indicated that the physico-chemical properties of nanomaterials (size, shape, surface charge, chemical composition and solubility) play vital roles in the induced biological responses.[13-19] Earlier studies have indicated that silver nanoparticles (Ag nps) could cause morphological changes, damage to cell membrane, disruption of the mitochondrial respiratory chain, interruption of ATP synthesis, reactive oxygen species (ROS) generation, and further induce cell cycle arrest and cell apoptosis.[20,21] A recent review reported that toxic effects of Au nps are dependent on both cell types and capping agents used for stabilizing the nanoparticles.[22] The formation of ROS within cells exposed to nanoparticles is considered to be a major contributor to their toxicological effects.[23-25] Even at nontoxic doses, Ag and Au nps reduced cathepsin activity in Vero cells,[26] indicating their potential to impact a host's immune system. In addition, the introduction of Ag and Au nps (at low doses) within the human epithelial cells (A-431) was reported to impair their epidermal growth factor signal transduction.[4] However, few studies have been explored for the potential disturbance induced by Ag and Au nps at low doses to colon CSCs with no toxic response.

Normal stem cells, including embryonic stem cells (ESCs) and adult stem cells, have attracted particular attention in the field of regenerative medicine because of their pluripotency. Several groups have already explored the possibilities of using embryonic and fetal stem cells to produce dopaminergic cells for curing Parkinson's disease.[27] Mesenchymal stem cells could be implanted locally to promote or augment repair or regeneration of a fractured or osteoporotic bone.[28] Skin stem cells can not only provide hope for the functional repair of the skin itself but also offer a potential source of adult stem cells for the cell-based therapy of injuries and diseases throughout the body.[29] Various reports have shown that nano based materials can facilitate stem cell therapy for bone engineering[30] and wound healing.[31] Directed differentiation of stem cells into certain types of cells is one of the most important issues in ESCs research, which represent not only theoretical interest, but also show potential application on cell or tissue therapy for curing serious human diseases.[32] Human ESCs (HESCs) can differentiate into cardiomyocytes under low serum concentration supplemented with bone morphogenetic protein-2,[33] otherwise they may differentiate into hepatic cells in serum-free medium with both fibroblast growth factor-4 and bone morphogenetic protein-2.[34] Besides growth factors and specific genes, numerous microenvironmental cues such as soluble chemicals and adhesive contexts can also affect physiologically relevant differentiation responses of stem cells. Au nps can promote the differentiation of mesenchymal stem cells toward osteoblast cells over adipocyte cells through p38 MAPK Pathway.[35] Furthermore, Laura A. Smith et al.[36] proposed that nano-fibrous architecture could enhance the osteogenic differentiation of the HESCs compared to more traditional scaffolding architectures. Even C. Greulich et al.[37] found that Ag nps exert cytotoxic effects on human mesenchymal stem cells at high concentrations but also induce cell activation (as analyzed by the release of IL-8) at high but nontoxic concentrations of nanosilver. Both in vitro and in vivo, studies have already unveiled evidences of significant toxicity associated

with Ag nps.[38,39] However, until now, little is understood about the effects and mechanisms of Ag nps on HESCs.

The first part of the present study investigates the cellular responses of Ag and Au nps with similar size and morphology, but with different composition, to colon CSCs. The study was carried out with special emphasis on the toxicological effects of nanoparticles at relative low doses and their effects on gene expressions. Moreover, nanoparticles were characterized using electron microscopy (TEM), dynamic light scattering (DLS), element analysis, UV-Vis absorption and X-ray diffraction (XRD). The cellular responses of colon CSCs treated with Ag and Au nps at low doses are evaluated by changes in viability, ROS generation, morphological changes of nuclei, cell cycle arrest and changes in gene expression. The second part of the study focuses on the effect of Ag nps to undifferentiated HESCs and the embryoid body (EB, differentiation state) at relatively low doses.

6.2 Results and discussion

6.2.1 Characteristics of Ag and Au nps

Synthesized Ag and Au nps were characterized with a combination of analytical techniques in order to measure their primary physical and chemical properties. TEM images revealed that Ag and Au nps form homogeneous colloids in water with no signs of agglomeration (**Figure 6.1**). The size of Ag nps is in the range of 6 to 18 nm, while that of Au nps was in a narrower range from 2 to 14 nm. Both Ag and Au are water dispersible owing to their hydrophilic capping agents. PVP was selected as the capping agent also due to its high compatibility with biological systems.[40]

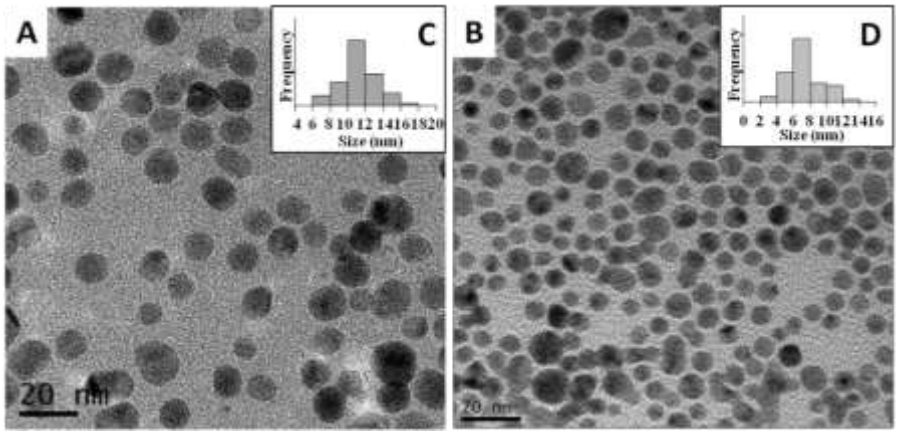

Figure 6.1: TEM images of Ag (A) and Au (B) nanoparticles and the histogram of size distribution of these two nanoparticles based on their TEM images.

The hydrodynamic size of Ag and Au nps suspensions in water, PBS, serum free media and media with serum were detected to check their agglomeration in different dispersants (**Table 6.1**). DLS measurements showed that the average hydrodynamic diameters of Ag (109.8 nm) and Au nps (86.7 nm) in water were larger than their TEM size. This could be attributed to the fact that the hydrodynamic size of nanoparticles includes not only the core particles but also their organic layers and the hydration shell.[41] The average hydrodynamic size of Ag and Au nps in PBS is 82.7 nm and 93.7 nm, which are similar to the size in water. Significant increase of hydrodynamic size of Ag (1083.7 nm) and Au nps (3399.5 nm) were observed in serum free media indicating pronounced agglomeration of Ag and Ag nps. The dispersal of nanoparticles in media was improved by the addition of serum, the average hydrodynamic size of Ag (50.8 nm) and Au (32.7 nm) nanoparticles in media with serum decreased. The surface charge of these nanoparticles was determined by measurement of their zeta potential (**Table 6.1**), indicating that the surface charge of nanoparticles were dependent on their dispersant. The negative surface charge of Ag nps (-24.5 mV) decreased when dispersed them in media with or without serum (-11.3 and -10.1 mV), similar results were also found for Au nps.

Table 6.1: Hydrodynamic diameter size and zeta potential of Ag and Au nps in H_2O, PBS, serum free media and media with serum*

	Hydrodynamic diameter nm			
	H_2O	**PBS**	**serum free media**	**media with serum**
Ag nps	109.8 ± 1.4	82.7 ± 1.9	1083.7 ± 6.7	50.8 ± 1.9
Au nps	86.7 ± 3.3	93.7 ± 8.4	3399.5 ± 202.9	32.7 ± 8.4
	Zeta potential mV			
	H_2O	**PBS**	**serum free media**	**media with serum**
Ag nps	-24.5 ± 0.3	-9.2 ± 0.8	-11.3 ± 0.8	-10.1 ± 0.2
Au nps	-29.0 ± 1.1	-12.2 ± 1.4	-8.7 ± 0.8	-8.3 ± 0.6

*The average hydrodynamic size and zeta potential of Ag and Au nps suspended in water, PBS, media without serum and media with serum. The working concentration of nanoparticles suspensions were prepared by mixing 20 μl of the original nanoaprticles solution (stock concentration of 1 mg/mL) to 1 mL of water, PBS or media with/without serum and kept at room temperature overnight. All measurements were done in triplicates, and the values were shown in average ± SD.

Table 6.2: Chemical composition (in wt%) of Ag and Au nps.

Element	**C wt%**	**H wt%**	**N wt%**	**M wt%**	**O wt% (estimate)**	**C/Ag or C/Au atom ratio**
Ag nps	7.95	1.24	2.33	Ag 52.88	35.60	1.35
Au nps	7.07	1.05	1.66	Au 65.74	24.48	1.76

The chemical composition of Ag and Au nps were measured using elemental analysis, the summarized data were shown in **Table 6.2**. It is clearly showed that the ratio of capping agent to gold in Au nps is high (high carbon to gold ratio 1.76). On the contrary, low carbon to silver was observed for Ag nps (1.35). Oxygen contents of both Ag and Au nps were found to be higher than expected due to their hygroscopic nature.

The crystalline structure of Ag and Au nps were detected by XRD. The XRD peaks of Ag nps at 2θ degrees of 38°, 44°, 64°, 77°and 81° can be attributed to the 111, 200, 220, 311 and 222 crystalline planes of the face centered cubic (fcc) structure of silver (JCPDS file No. 00–004–0783).[42] Similarly, the XRD peaks of Au nps can also be attributed to 111, 200, 220 and

311 crystalline structure of the face centered cubic (fcc) structure of gold (JCPDS file No. 00–004–0784). Surface plasmon resonance (SPR) properties of Ag and Au nps in water were characterized using UV-Vis-NIR spectrophotometer. The number of SPR peaks of nanoparticles was dependent on their symmetry: spherical nanoparticles showed one peak while multiple peaks were often observed for cubic structures or triangular nanoplates.[43] Single SPR peaks of Ag (400 nm) and Au (550 nm) nanoparticles confirmed their spherical shape (**Figure 6.2**).

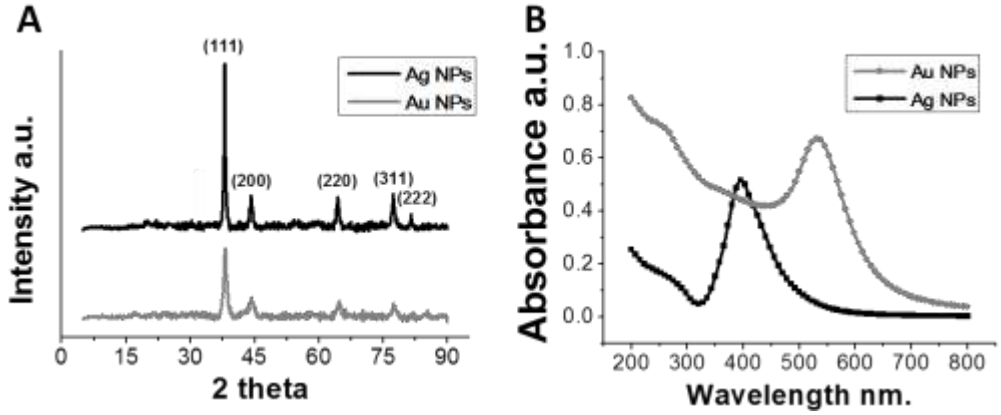

Figure 6.2: XRD (A) pattern and UV-Vis absorption (B) of Ag and Au nps.

6.2.2 Ag and Au nps to colon CSCs

6.2.2.1 Viability

The viability of colon CSCs treated with Ag and Au nps at low concentrations were measured with resaruzin assay (**Figure 6.3A**). No toxicity of Ag nps were found at the concentration 2.5 μg/mL or less, and viability of cell was around 90% for cells treated with fresh prepared Ag nps at 5 and 10 μg/mL, indicating Ag nps showed high biocompatibility at low concentrations. Similar results were observed in colon CSCs treated with Au nps. Au nps showed no toxicity to colon CSCs at 5 μg/mL or less, and caused 10% cell death at a concentration of 10 μg/mL. Further we also examined the toxic effect Ag and Au ions with similar amount of metal as nanoparticles used based on their elemental analysis results (Ag: 52.88 wt%; Au: 65.74 wt%). It

is clearly showed that Ag ions were more toxic than Ag nps (**Figure 6.3B**). Ag ions killed almost 90% cells at the concentration 2.6 and 5.3 μg/mL (equal to 5 and 10 μg/mL for Ag nps). On the contrary, Au ions showed low toxicity to cells at a concentration of 6.6 μg/mL (equal to 10 μg/mL for Au nps) with around 90% viability (**Figure 6.3C**).

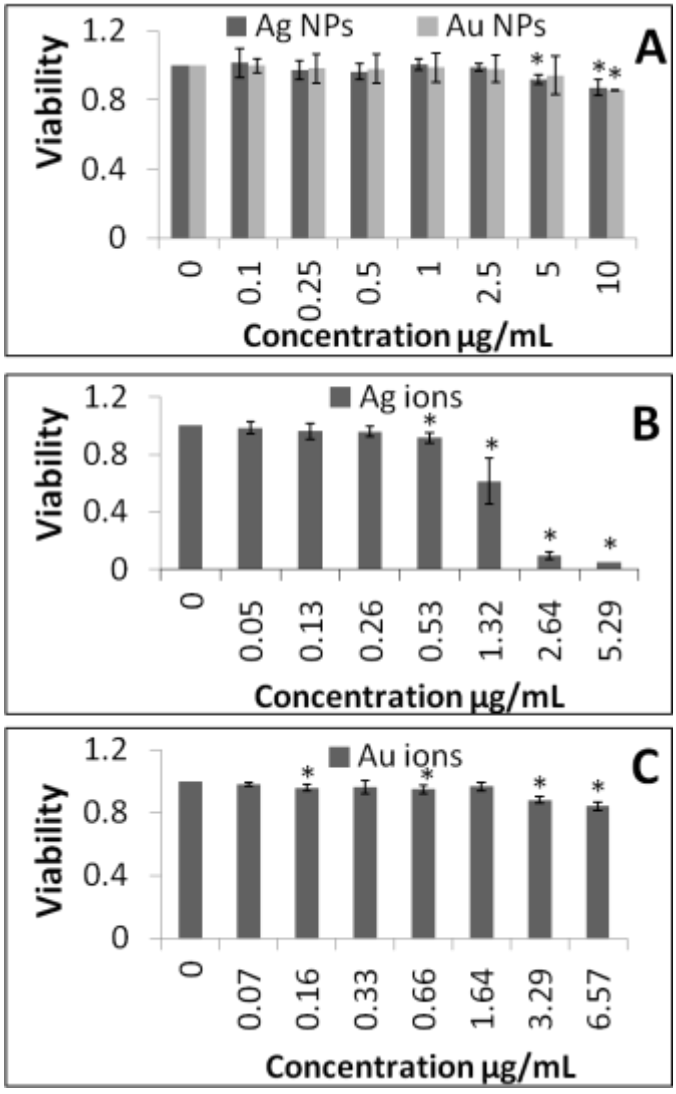

Figure 6.3: Viability of colon CSCs treated with Ag and Au nps (A), Ag ions (B) and Au ions (C) at different concentrations for 3 days. The concentrations for Ag and Au nps were 0, 0.1, 0.25, 0.5, 1, 2.5, 5, 10 μg/mL. And the concentration of Ag and Au ions used in this experiment were calculated based on their elemental analysis results.

6.2.2.2 Intracellular ROS generation

The introduction of ROS was generally used as a measure for oxidative

stress.[44] The intracellular ROS production induced by Ag and Au nps in colon CSCs was detected by applying the fluorescent DCF-DA assay (**Figure 6.4**). After 24 h incubation, no morphology changes could be observed from optical microscope images. Further, no green fluorescence was observed in control (untreated cells) while green fluorescence was observed in Ag and Au nps treated cells. The images also indicated a dose-dependent increase in ROS production. Both Ag and Au nps were found to significantly induce ROS production in concentrations ≥ 0.1 mg/ml. The fluorescence intensity of cells increased as the concentration of nanoparticles increased from 0.1 μg/mL to 10 μg/mL. Moreover, ROS production of cells treated with Ag nps is more sensitive as compared to Au nps treated ones. Almost all cells treated with Ag nps showed fluorescence at a concentration of 0.1 μg/mL, while very few cells showed fluorescence with Au treatment at the same concentration (0.1 μg/mL).

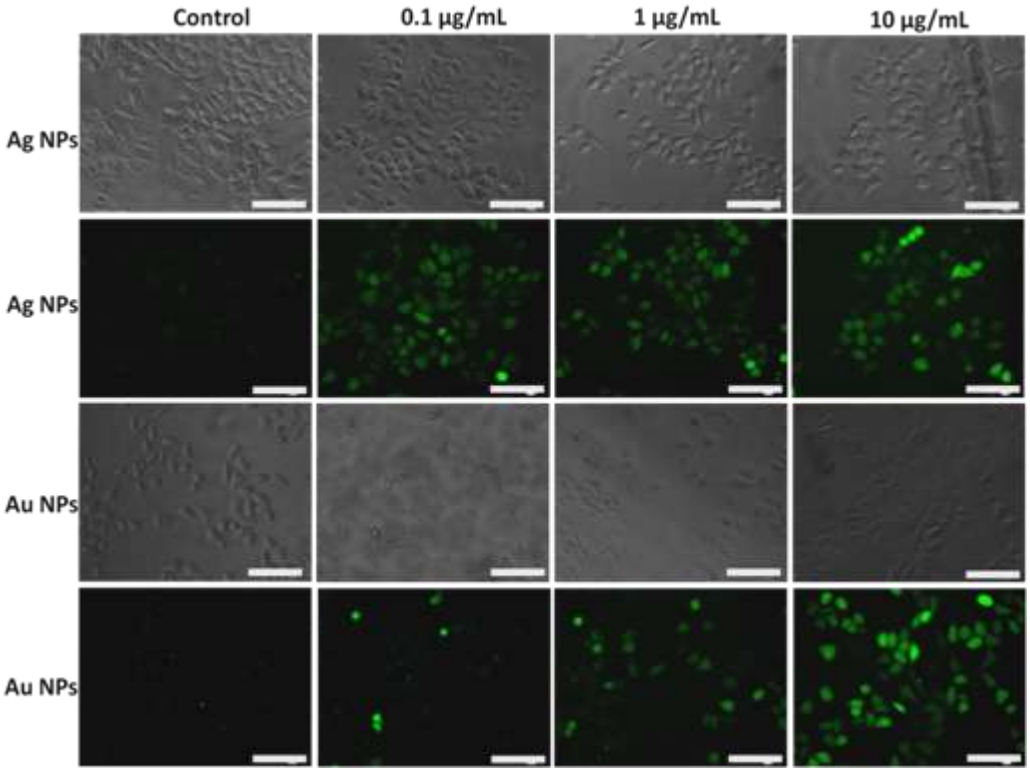

Figure 6.4: Phase contrast images (A and C) and DCF-DA staining (B and D) images of colon CSCs treated with Ag and Au nps at different concentrations (0, 0.1, 1, and 10 μg/mL) for 24 h.

6.2.2.3 Cell cycle analysis

To check DNA damage of colon CSCs treated with Ag and Au nps, cell cycle analysis was performed using fluorescence PI staining. Cells with reversible DNA damage usually accumulate in gap1 (G1), DNA synthesis (S), or in gap2/mitosis (G2/M) phase while cells with irreversible DNA damage will accumulate in subG1 phase. Our cell cycle analysis showed that Ag and Au nps exert little influence on the cell cycle progression at low concentrations (0.1, 1 and 10 μg/mL) during a period of 3 days (**Figure 6.5**).

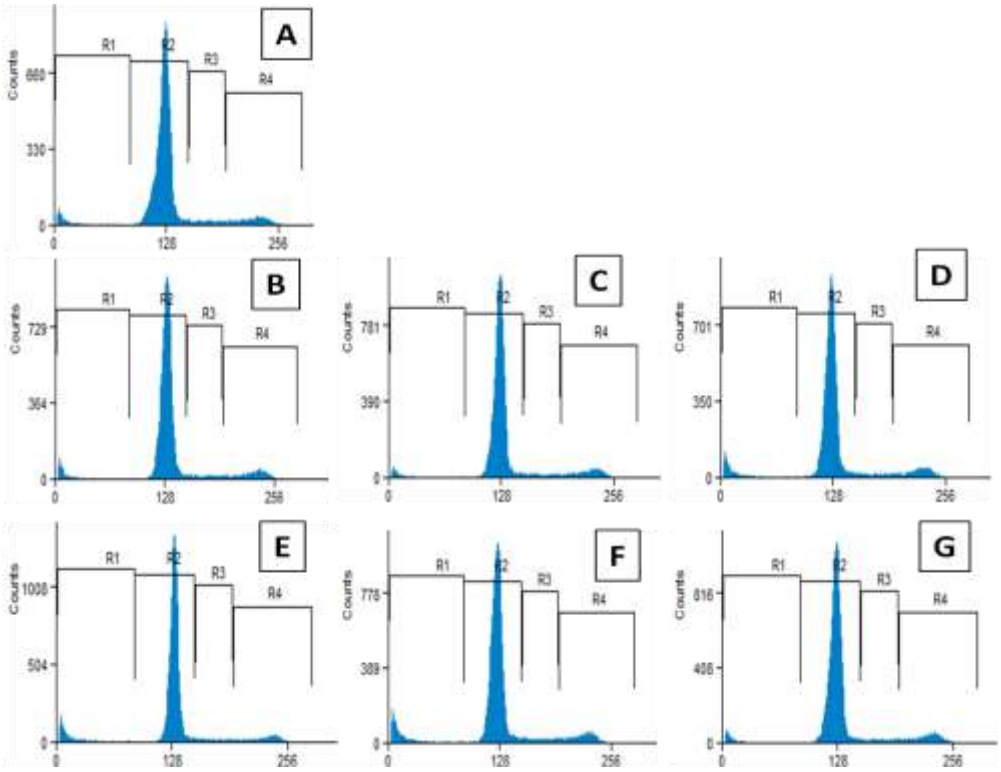

Figure 6.5: Cell cycle of colon CSCs untreated (A) and treated with Ag nps 0.1 μg/mL (B), 1 μg/mL (C), 10 μg/mL (D) and Au nps 0.1 μg/mL (E), 1 μg/mL (F) and 10 μg/mL (G) for 3 days. Cell cycle analysis was divided into four phases: SubG1 (R1), G1 (R2), S (R3) and G2/M (R4).

6.2.2.4 DAPI staining

Morphological changes of cell nuclei induced by nanoparticles were detected by DAPI staining (**Figure 6.6**). Cell shrinkage, fragmented or condensed nuclei indicates cells either undergoing apoptosis or arrest in cell division.[45,46] Majority of control cells showed uniformly stained nuclei. A

small increase in condensed or fragmented nuclei was observed for Ag and Au nps treated cells at concentrations of 0.1 and 1 μg/mL. However, more condensed and fragmented nuclei were observed in cells treated with higher concentrations (10 μg/mL) of Ag and Au nps.

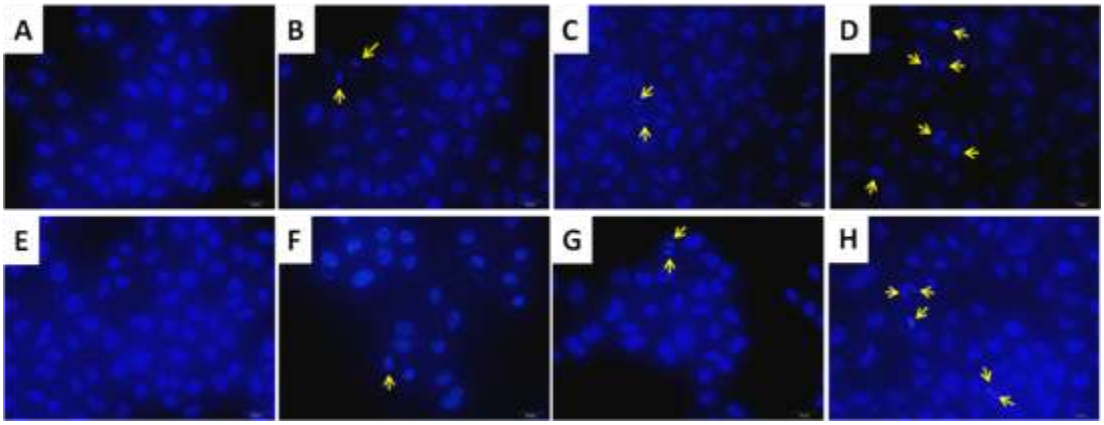

Figure 6.6: Nanoparticles induced nuclear morphology changes in colon CSCs stained with DAPI: A and E control cells (untreated cells), B Ag nps (0.1 μg/mL), C Ag nps (1 μg/mL), D Ag nps (10 μg/mL), F Au nps (0.1 μg/mL), G Au nps (1 μg/mL) and H Au nps (10 μg/mL).

6.2.2.5 Real-time RT-PCR analysis

To investigate the impact of Ag and Au nps exposure to colon CSCs at lower concentrations (0.1, 1 and 10 μg/mL), gene expression changes of cell treated with nanoparticles for 3 days were analyzed by real-time PCR. Several key members of the MAPK-Jnk pathway (MAPK9, NFATC3, and TP53), which are known to be induced by stress and often leads to cellular apoptosis, were detected in our experiments. The epidermal growth factor receptor (EGFR) signaling pathway is one of the most important pathways which regulate growth, survival, proliferation, and differentiation in mammalian cells.[47] Changes on EGFR and EPS8 gene were also analyzed after Ag and Au nps treatment. The activation of EGFR could induce a specific pathway for the Ras/Erk cascades, several genes (BRAF, an upstream kinase of Erk; DUSP1 and DUSP6, the negative regulation of the Ras/Erk cascade) were further examined in our study. As can be seen in **Table 6.3**, Ag and Au nps induced changes in gene expression at a low concentration of 1 μg/mL and no

interference of gene expression was observed at extremely low concentration (0.1 μg/mL). Up-regulated MAPK9 together with down-regulated NFATC3 observed with Ag nps treatment (10 μg/mL) were antagonized by a concurrent decrease in TP53, indicating low cell apoptosis response. Further, the up-regulated DUSP1 and DUSP6 together with down-regulated EGFR, and EPS8 suggest a suppression of Ras/Erk cascade by Ag nps. Interestingly, Au nps attempted to enhance cellular proliferation evidenced by the gene expression data. Au nps induced down-regulation of MAPK9 and NFATC3, suggesting that Au nps showed a tendency toward enhanced cell survival. Moreover, the down-regulated DUSP6 induced by Au nps treatment may antagonize the negative effects on Ras/Erk cascade caused by the decreased B-Raf, EGFR and EPS8.

Table 6.3: Gene expression changes of colon CSCs treated with Ag and Au nps.

		fold regulation (*vs* control)[a]					
		Ag nps			**Au nanoparticles**		
Gene symbol	**Gene function**	**0.1 μg/mL**	**1 μg/mL**	**10 μg/mL**	**0.1 μg/mL**	**1 μg/mL**	**10 μg/mL**
MAPK9	stress induced MAPK that induces apoptosis	-	-	1.56 *	-	-	-2.26*
NFATC3	transcription complex downstream of Jnk	-	-1.27 *	-1.28 *	-	-1.71*	-3.41*
TP53	inhibit proliferation, cause apoptosis	-	-	-1.32 *	-	-	-
BRAF	proto-oncogene involved in Ras/Erk signaling	-	-	-	-	-1.47*	-3.06*
DUSP1	negatively regulator for Erk	-	-	-	-	-1.65*	-3.66*
DUSP6	negatively regulator for Erk	-	1.35 *	2.21 *	-	-	-2.37*
EGFR	epidermal growth factor receptor (EGFR)	-	-	-1.28 *	-	-1.43*	-3.19*

EPS8	part of the EGFR pathway with unknown role	-	-1.30 *	-1.67 *	-	-	-3.35*

[a]Genes checked in our experiments. "*" denotes $p < 0.05$ and "-" indicates that no statistically significant change occurred.

Ag and Au nps are two of the most commonly used nanomaterials incorporated into commercial products. For in vitro studies, researches were focus on various cell lines which include both cancer and normal cell lines. However, limited work has done on cancer stem cells (CSCs) which exhibit vital importance in exploring innovative cancer therapies.[9,10] Ag and Au nps used in this study showed varied colloid stability in different solvent. Agglomeration of nanoparticles was observed in serum free media with a 24 h incubation period. Addition of serum in the cell media enhances the stability of Ag and Au nps which exhibited remarkable stability in the cell media. No agglomeration and precipitation were observed throughout the test period. Nanoparticle stability is a major concern in nanotoxicology, which may affect the test interpretations as unstable nanoparticles precipitate to metal clumps during experiments. In the case of water-insoluble nanoparticles the carrier solvents may cause toxic effects to cells. Therefore, it would be ideal to use water as a carrier solvent to test nanoparticle toxicity. The water-insoluble nanoparticles might be less affective to cells due to phase separation. PVP is a biocompatible agent which possesses the advantages of being non-toxic and good water-soluble stabilizing agents for nanoparticles.

Our results suggest that Ag and Au nps showed a concentration-dependent toxicity to colon CSCs, they were nontoxic at low concentrations ($\leq$ 2.5 μg/mL) and started to cause cell damage at higher concentrations (5 and 10 μg/mL). Indication of toxicity was observed by the drop in cell viability. As compared to Ag nps, Ag ions were much more toxic which caused cell death at much lower concentration (0.53 μg/mL, which contains same amount of silver equals to 1 μg/mL for Ag nps) and killed almost all the cells at 2.64 μg/mL (equals to 5 μg/mL for Ag nps). However, similar toxic effects were observed

for both Au ions and Au nps at concentrations which contained same amount of gold. An earlier report showed that the toxicity of Ag nps increased during long storage due to slow dissolution under release of Ag ions,[48] so freshly prepared Ag and Au nps were used in our experiments. Due to their low toxicity at low concentrations, no significant cell cycle arrest was observed for cells with Ag and Au nps treatment. Intracellular ROS production showed that nanoparticles induced oxidative stress to cells even at low concentrations. Earlier reports showed that oxidative stress induced by nanoparticles was considered as the trigger for DNA damage which may further induce cell apoptosis.[49-51] TiO_2 nanoparticles induced significant oxidative DNA damage and caused apoptosis in HepG2 cells at very low concentrations (1 μg/mL).[3] DAPI staining results in our study indicates that Ag and Au nps exhibited cell-dependent morphological changes of cell nuclei, which is consistent with our viability data. RT-PCR results showed that they also affected the gene expressions at low concentrations. Slight impact on gene transcription was observed in cells with Ag nps treatment indicates that it may not the leading cause for silver nanotoxicity, but it may work in conjunction with ROS production to increase cell damage. Gene interference was also observed for Au nps at low concentrations, which may attract much more concerns. Over the past decades, Au nps have been extensively studied for biological and medical applications such as drug delivery,[52] cancer imaging[53] and cancer therapies.[54] Careful design and synthesis of Au nps and their implementation in gene expression might be useful in the development of cancer therapy.

6.2.3 Ag nps effects to HESCs

6.2.3.1 Viability of HESCs with Ag nps treatment

The toxic effects of Ag nps to undifferentiated HESCs cells or embryoid body (EB) were detected with rezarurin assay. Undifferentiated HESCs cells and EB were prepared, treated with Ag nps with different concentrations (0, 0.1, 1 and 10 μg/mL) of Ag nps and incubated at 37 °C for 3 days. Ag nps did

not cause any toxic effect to the undifferentiated HESCs at low concentrations (**Figure 6.7A**). Similar results were observed in EB with Ag nps treatment (**Figure 6.7B**).

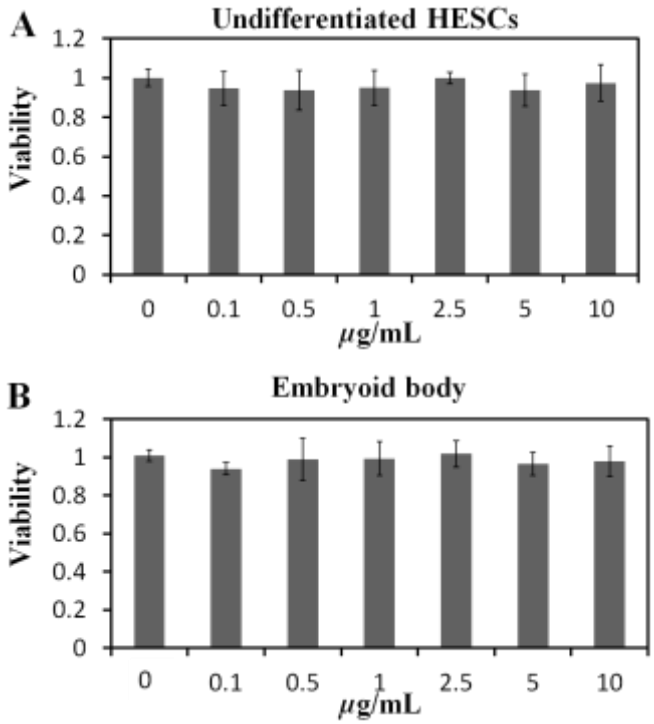

Figure 6.7: Viability of undifferentiated HESCs and EB treated with Ag nps (0, 0.1, 0.5, 1, 2.5, 5 and 10 μg/mL) for 3 days.

6.2.3.2 Morphological changes of HESCs treated with Ag nps

As we already known that Ag nps did not cause any damage to the HESCs at low concentrations, their effect to HESCs cell morphological changes was further investigated. Morphological changes of undifferentiated HESCs treated with Ag nps (0, 1 and 10 μg/mL) were observed under an inverted microscope at different incubation time (1 day, 3 days and 5 days). As can be seen from **Figure 6.8**, slight differences of HESCs colony were only observed to cells treated with relatively high concentration of Ag nps (10 μg/mL) for 1 day. When the incubation time increases, significant differences were clearly shown indicating the effect of Ag nps to HESCs at the concentration 10 μg/mL. After 5 days treatment, slight differences were also found in HESCs colony with Ag nps at 1 μg/mL.

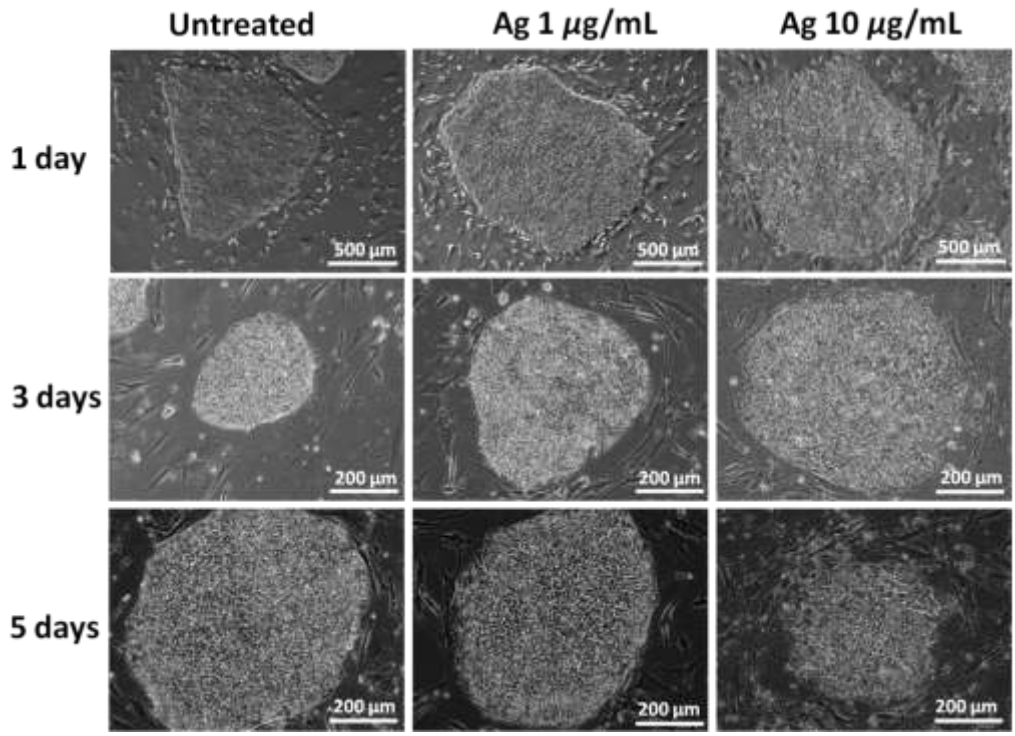

Figure 6.8: Morphological changes of undifferentiated HESCs colony treated with Ag nps (0, 1 and 10 μg/mL) for 1 day, 3 days and 5 days.

6.2.3.3 Morphological changes of EB treated with Ag nps

Morphological changes of EB with Ag nps treatment were further examined by the inverted microscope. EB were prepared through culture HESCs colony in untreated cell culture plates to form 3 dimensional cell colonies. EB were treated with different concentrations (0, 1 and 10 μg/mL) of Ag nps and incubated for different periods. As can be seen from **Figure 6.9**, Ag nps caused the morphology changes of EBs as compared to untreated cells. The higher the concentration of Ag nps and the longer incubation time, the more significant morphological cell changes were observed in the images. Moreover, the black dots and objectives observed in EBs with 10 μg/ml Ag nps treatment were considered as the aggregate of Ag nps.

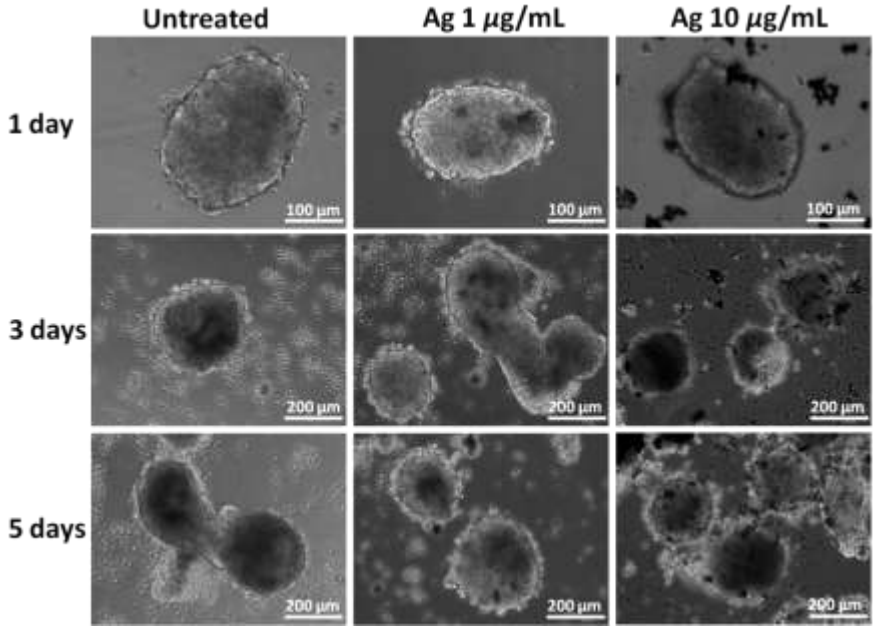

Figure 6.9: Morphological changes of EB treated with Ag nps (0, 1 and 10 μg/mL) for 1 day, 3 days and 5 days.

The cellular responses of HESCs to Ag nps were investigated and the results showed Ag nps did not cause much adverse effect to both the undifferentiated and differentiated HESCs cells at low concentrations. Moreover, the cell morphological changes were observed in cells with Ag nps treatment. The higher the concentration of Ag nps and the longer the incubation time, the higher morphological differences by Ag nps were observed. HESCs have the ability to differentiate into different cell lines, which plays significant roles in stem cell therapies and tissue implanting. The effect of Ag nps to the differentiation of HESCs was planed to expolore through the gene expressions. The whole human genome of HESCs with Ag nps treatment is examined through microarray analysis by Origen Lab (Origen Laboratories Pte Ltd, Singapore). The microarray data analysis is in process and the results will be discussed in our future work.

6.3 Conclusion

The present study investigates the cytotoxicity and genotoxicity of Ag and Au nps on human colon cancer stem cells (CSCs). The size and shape of both Ag and Au nps were kept the same throughout the study. The viability results

suggest that both Ag and Au nps were relatively nontoxic to colon CSCs and more than 80% cells were still alive even at the concentration 10 μg/mL. Although the intracellular ROS generation suggests that Ag and Au nps induced oxidative stress to CSCs, no interference on cell cycle progression was observed with Ag and Au nps treatment, even at the high concentration (10 μg/mL). Gene expression interference observed in the RT-PCR results clearly showed that both Ag and Au nps induced genotoxicity on CSCs even at relatively low doses (1 and 10 μg/mL). Future studies on their effects on whole human genome are still needed to fully understand their potential toxicity to humans due to the increasingly prevalence of Ag and Au nps in everyday products and medical procedures.

The cellular responses of Ag nps to HESCs were also examined in our study. Ag nps exhibited induced cell morphological changes to HESCs at low concentrations without causing any adverse effect to the cell viability. Carefully design to control the differentiation of HESCs into special cell lines will play vital roles in stem cell therapies and tissue implanting in the future.

6.4 References

(1) Wijnhoven, S. W. P.; Peijnenburg, W. J. G. M.; Herberts, C. A.; Hagens, W. I.; Oomen, A. G.; Heugens, E. H. W.; Roszek, B.; Bisschops, J.; Gosens, I.; Van De Meent, D.; Dekkers, S.; De Jong, W. H.; van Zijverden, M.; Sips, A. J. A. M.; Geertsma, R. E. *Nanotoxicology* **2009**, *3*, 109.

(2) Lewinski, N.; Colvin, V.; Drezek, R. *Small* **2008**, *4*, 26.

(3) Shukla, R. K.; Kumar, A.; Gurbani, D.; Pandey, A. K.; Singh, S.; Dhawan, A. *Nanotoxicology* **2013**, *7*, 48.

(4) Comfort, K. K.; Maurer, E. I.; Braydich-Stolle, L. K.; Hussain, S. M. *ACS Nano* **2011**, *5*, 10000.

(5) Chen, R.; Ratnikova, T. A.; Stone, M. B.; Lin, S.; Lard, M.; Huang, G.; Hudson, J. S.; Ke, P. C. *Small* **2010**, *6*, 612.

(6) Fau, T. M.; D'Asaro, M.; Caccamo, N.; Iovino, F.; Francipane, M. G.;

Meraviglia, S. M.; Orlando, V.; Mendola, C.; Gulotta, G.; Salerno, A.; Dieli, F.; Stassi, G. *J. Immun.* **2009**, *182*, 7287.

(7) Vinicius Kannen; Hintzsche, H.; Zanette, D. L.; Wilson A. Silva, J.; Garcia, S. B.; Waaga-Gasser, A. M.; Stopper, H. *PLoS One* **2012**, *7*, e50043.

(8) O/'Brien, C. A.; Pollett, A.; Gallinger, S.; Dick, J. E. *Nature* **2007**, *445*, 106.

(9) Di Franco, S.; Mancuso, P.; Benfante, A.; Spina, M.; Iovino, F.; Dieli, F.; Stassi, G.; Todaro, M. *Cancers* **2011**, *3*, 1957.

(10) Todaro, M.; Francipane, M. G.; Medema, J. P.; Stassi, G. *Gastroenterology* **2010**, *138*, 2151.

(11) Botchkina, G. *Cancer Lett*. **2012**.

(12) Neuzil, J.; Stantic, M.; Zobalova, R.; Chladova, J.; Wang, X.; Prochazka, L.; Dong, L.; Andera, L.; Ralph, S. J. *Biochem. Biophys. Res. Commu.***2007**, *355*, 855.

(13) Pan, Y.; Neuss, S.; Leifert, A.; Fischler, M.; Wen, F.; Simon, U.; Schmid, G.; Brandau, W.; Jahnen-Dechent, W. *Small* **2007**, *3*, 1941.

(14) Nativo, P.; Prior, I. A.; Brust, M. *Acs Nano* **2008**, *2*, 1639.

(15) Moros, M.; Hernáez, B.; Garet, E.; Dias, J. T.; Sáez, B.; Grazú, V.; González-Fernández, Á.; Alonso, C.; de la Fuente, J. M. *ACS Nano* **2012**, *6*, 1565.

(16) Wang, S.; Lu, W.; Tovmachenko, O.; Rai, U. S.; Yu, H.; Ray, P. C. *Chem. Phys. Lett*. **2008**, *463*, 145.

(17) Yen, H. J.; Hsu, S. H.; Tsai, C. L. *Small* **2009**, *5*, 1553.

(18) Sohaebuddin, S.; Thevenot, P.; Baker, D.; Eaton, J.; Tang, L. *Part. Fibre Toxicol.* **2010**, *7*, 22.

(19) Schaeublin, N. M.; Braydich-Stolle, L. K.; Schrand, A. M.; Miller, J. M.; Hutchison, J.; Schlager, J. J.; Hussain, S. M. *Nanoscale* **2011**, *3*, 410.

(20) AshaRani, P. V.; Mun, G. L. K.; Hande, M. P.; Valiyaveettil, S. *ACS Nano* **2009**, *3*, 279.

(21) Liu, W.; Wu, Y.; Wang, C.; Li, H. C.; Wang, T.; Liao, C. Y.; Cui, L.;

Zhou, Q. F.; Yan, B.; Jiang, G. B. *Nanotoxicology* **2010**, *4*, 319.

(22) Khlebtsov, N.; Dykman, L. *Chem. Soc. Rev.* **2011**, *40*, 1647.

(23) Chompoosor, A.; Saha, K.; Ghosh, P. S.; Macarthy, D. J.; Miranda, O. R.; Zhu, Z.-J.; Arcaro, K. F.; Rotello, V. M. *Small* **2010**, *6*, 2246.

(24) Foldbjerg, R.; Dang, D. A.; Autrup, H. *Arch. Toxico.* **2011**, *85*, 743.

(25) Hsin, Y.; Chen, C.; Huang, S.; Shih, T.; Lai, P.; Chueh, P. J. *Toxicol Lett* **2008**.

(26) Speshock, J.; Braydich-Stolle, L.; Szymanski, E.; Hussain, S. *Nanoscale Res. Lett*. **2011**, *6*, 17.

(27) Brodhun, M.; Bauer, R.; Patt, S. *Experimental and Toxicologic Pathology* **2004**, *56*, 103.

(28) Tarantino, U.; Cerocchi, I.; Celi, M.; Scialdoni, A.; Saturnino, L.; Gasbarra, E. *Clin. Cases Miner Bone Metab*. **2009**, *6*, 144.

(29) Shi, C.; Zhu, Y.; Su, Y.; Cheng, T. *Trends biotech.* **2006**, *24*, 48.

(30) Ilie, I.; Ilie, R.; Mocan, T.; Bartos, D.; Mocan, L. *Int. J. Nanomedicine* **2012**, *7*, 2211.

(31) Mohamed, A.; Xing, M. M. *Int J Burns Trauma* **2012**, *2*, 29.

(32) Grivennikov, I. A. *Biochemistry Moscow* **2008**, *73*, 1438.

(33) Pal, R.; Khanna, A. *Differentiation* **2007**, *75*, 112.

(34) Cai, J.; Zhao, Y.; Liu, Y.; Ye, F.; Song, Z.; Qin, H.; Meng, S.; Chen, Y.; Zhou, R.; Song, X.; Guo, Y.; Ding, M.; Deng, H. *Hepatology* **2007**, *45*, 1229.

(35) Yi, C.; Liu, D.; Fong, C.-C.; Zhang, J.; Yang, M. *ACS Nano* **2010**, *4*, 6439.

(36) Smith, L. A.; Liu, X.; Hu, J.; Ma, P. X. *Biomaterials* **2010**, *31*, 5526.

(37) Greulich, C.; Kittler, S.; Epple, M.; Muhr, G.; Köller, M. *Langenbecks Arch. Surg.* **2009**, *394*, 495.

(38) Shin, S.-H.; Ye, M.-K. *Clin. Exp. Otorhinolaryngol* **2012**, *5*, 222.

(39) Park, J.; Lim, D.-H.; Lim, H.-J.; Kwon, T.; Choi, J.-s.; Jeong, S.; Choi, I.-H.; Cheon, J. *Chem. Commun.* **2011**, *47*, 4382.

(40) Giri, N.; Natarajan, R. K.; Gunasekaran, S.; Shreemathi, S. *Arch. Appl.*

Sci. Res. **2011**, *3*, 624.

(41) Teow, Y.; Valiyaveettil, S. *Nanoscale* **2010**, *2*, 2607.

(42) Shameli, K.; Ahmad, M.; Jazayeri, S.; Shabanzadeh, P.; Sangpour, P.; Jahangirian, H.; Gharayebi, Y. *Chem. Central J.* **2012**, *6*, 73.

(43) Wiley, B.; Sun, Y. G.; Mayers, B.; Xia, Y. N. *Chem-Eur. J.* **2005**, *11*, 454.

(44) Pelka, J.; Gehrke, H.; Rechel, A.; Kappes, M.; Hennrich, F.; Hartinger, C. G.; Marko, D. *Nanotoxicology* **2013**, *7*, 2.

(45) Li, G.-L.; Jiang, W.; Xia, Q.; Chen, S.-H.; Ge, X.-R.; Gui, S.-Q.; Xu, C.-J. *J. Ethnopharmacol.* **2010**, *132*, 56.

(46) Park, K.; Lee, G.; Park, R.-W.; Kim, I.-S.; Kim, S.; Byun, Y. *Pharmaceut. Res.* **2008**, *25*, 268.

(47) Oda, K.; Matsuoka, Y.; Funahashi, A.; Kitano, H. *Mol. Syst. Biol.* **2005**, *1*.

(48) Kittler, S.; Greulich, C.; Diendorf, J.; Köller, M.; Epple, M. *Chem. Mat.* **2010**, *22*, 4548.

(49) Park, E.-J.; Yi, J.; Chung, K.-H.; Ryu, D.-Y.; Choi, J.; Park, K. *Toxicol. Lett.* **2008**, *180*, 222.

(50) Cheng, X.; Zhang, W.; Ji, Y.; Meng, J.; Guo, H.; Liu, J.; Wu, X.; Xu, H. *RSC Advances* **2013**, *3*, 2296.

(51) AshaRani, P. V.; Low Kah Mun, G.; Hande, M. P.; Valiyaveettil, S. *ACS Nano* **2008**, *3*, 279.

(52) Wang, F.; Wang, Y.-C.; Dou, S.; Xiong, M.-H.; Sun, T.-M.; Wang, J. *ACS Nano* **2011**, *5*, 3679.

(53) Boisselier, E.; Astruc, D. *Chem. Soc. Rev.* **2009**, *38*, 1759.

(54) Wu, X.; Ming, T.; Wang, X.; Wang, P.; Wang, J.; Chen, J. *ACS Nano* **2009**, *4*, 113.

CHAPTER 7

CONCLUSIONS

The primary objectives of this study were to investigate cytotoxicity of Ag and Au NMs with different surface functional groups and shapes. It was found that nanomaterials with different characteristics showed diverse toxicity to cells. The toxicity results indicate that the toxicity of novel nanomaterials with different properties could not be deduced from earlier knowledge and results, as a very small difference of the properties of nanomaterials could induce huge changes in toxicity. Further, cell cycle and gene expression of cells, the mechanism of nanotoxicity of Ag and Au NMs was explored through the examination of changes of mitochondria activity.

Cytotoxicity of Ag nps with different functional groups was examined (Chapter 3), especially for those with plant extracts as functional groups. Among three plant extracts capped Ag nps, Ag-mint were the most toxic, followed by Ag-ginger, and then by Ag-coffee. In addition, it was found that the toxicity of Ag nps was not caused by oxidative stress, as the ROS of Ag nps treated cells did not increase but actually decreased. This can be adequately explained by the high antioxidant activity of plant extracts. Moreover, the cell cycle study showed that Ag-ginger and Ag-coffee nps induced cell arrest in S and G2/M stage, indicating a reversible DNA damage. However, Ag-mint nps were believed to cause cell death through apoptosis, which was confirmed by cell arrest in Sub G1 stage. In conclusion, the results demonstrated that Ag nps with different capping agents induced different toxicities in human tumor cells.

Cytotoxicity of Ag and Au NMs with different morphologies was discussed in Chapter 4 and 5. Nanomaterials with different morphologies showed different properties, which may further cause different toxicities to cells. Among the three Ag NMs (Ag nanocube, Ag truncated nanocube and Ag nanowire), Ag nanocubes were the most toxic, which could be attributed to their relatively sharp edges and high instability. The high dissolution effect of Ag nanocubes was confirmed by the silver ion release experiment. Similarly,

among the three AuNPs (HAuNPs, PAuNPs and TAuNPs), TAuNPs were the most toxic. The relatively sharp angles and high surface potential energy of TAuNPs enabled them to penetrate cell membrane and degrade inside the cells more easily. Furthermore, cellular uptake of Ag NMs examined by SEM and confocal microscope showed that Ag NMs were only penetrated inside the cytoplasm but not the nucleus of cells. Nevertheless, cellular uptake of Au NMs examined by TEM showed that Au NMs could penetrate and be distributed in both cytoplasm and nucleus part of cells. This is especially for the case of TAuNPs, as TAuNPs were evenly distributed throughout the whole area of cells. The ROS resulted indicate that oxidative stress could be the possible reason to cause cell toxicity, which further induced DNA damage. All the data put together indicated that the toxicity of nanomaterials is very sensitive, which could be influenced by many factors such as the components, the surface group, the size, the shape and the chemical potential energy of nanomaterials. The results also showed that the level of ROS which was either too high or too low could induce DNA damage and then cause cell damage.

Last but not the least, cytotoxicity and genotoxicity of Ag and Au nps on stem cells were reported in Chapter 6. The results of cell morphology changes and cell viability showed that Ag and Au nps did not cause cytotoxicity to colon cancer stem cells at low concentrations. However, gene expression interference observed in the RT-PCR results clearly showed that Ag and Au nps induced genotoxicity to CSCs even at relatively low doses (1 and 10 μg/mL). Moreover, Ag nps exhibited induced cell morphological changes to HESCs at low concentrations without causing any adverse effect to the cell viability. HESCs have the ability to differentiate into different cell lines, which plays significant roles in stem cell therapies and tissue implanting. The effect of Ag nps to the differtiation of HESCs is planed to explore and report in the near future. At the meantime, long-term chronic toxicity of Ag NMs will also need to be carefully investigated in the future.